



BİNGÖL  
ÜNİVERSİTESİ

e-ISSN 2149-6366

Cilt 12, Sayı 2, Haziran 2023

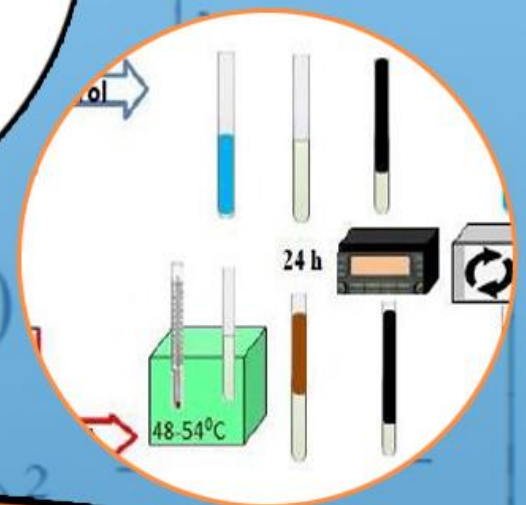
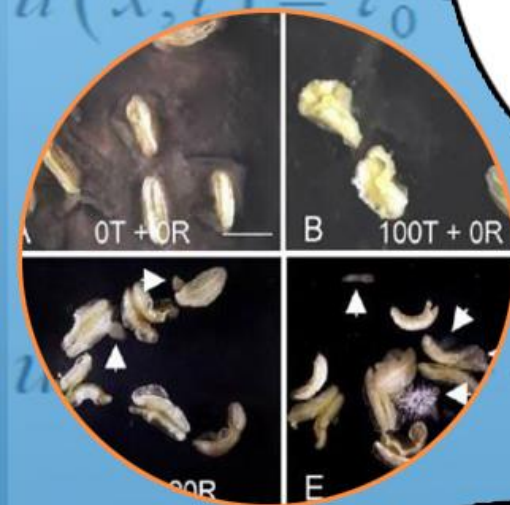
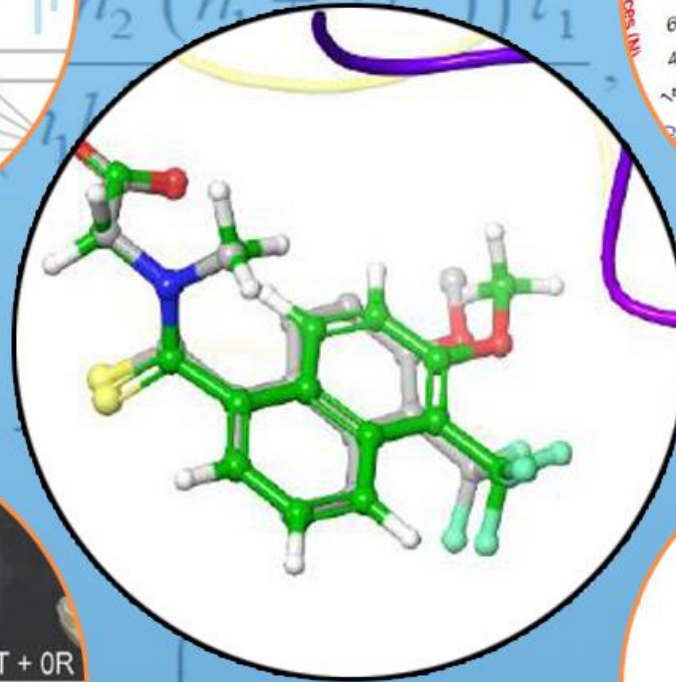
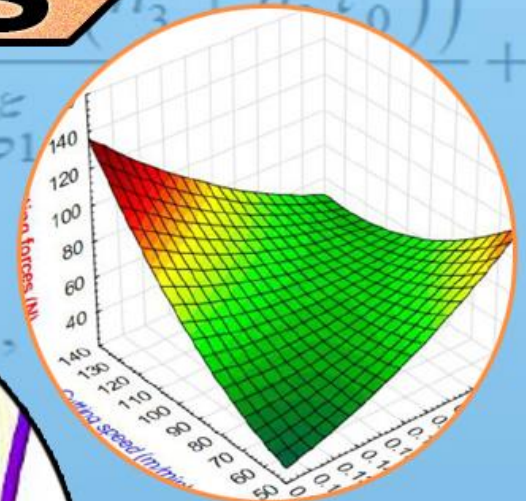
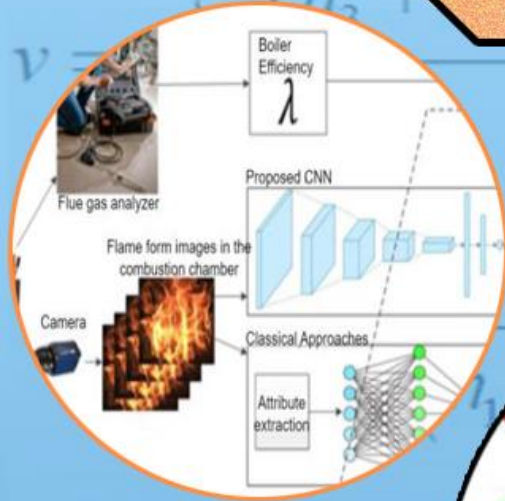
Volume 12, Issue 2, June 2023

**TDFD**

**TÜRK DOĞA ve FEN DERGİSİ**

TURKISH JOURNAL OF NATURE AND SCIENCE

**TJNS**



[www.dergipark.gov.tr/tdfd](http://www.dergipark.gov.tr/tdfd)

Bingöl Üniversitesi Fen Bilimleri Enstitüsü tarafından  
yayımlanmaktadır.

Published by Bingöl University Institute of Science

ULAKBİM

**TRDİZİN**

# TÜRK DOĞA VE FEN DERGİSİ

## Amaç

Türk Doğa ve Fen Dergisi, Dergipark tarafından yayınlanan Bingöl Üniversitesi Fen Bilimleri Enstitüsüne ait ulusal ve hakemli bir dergidir. Türk Doğa ve Fen Dergisi, Türkiye ve dünyanın her yerinden gelen doğa ve fen bilimlerinin her alanında özgün, yayımlanmamış, yayımlanmak üzere başka yere gönderilmemiş makale, derleme ve sempozyum değerlendirmesi gibi çalışmaların bilim alemine sunulması amacıyla kurulmuştur.

## Kapsam

Türk Doğa ve Fen Dergisinde Mühendislik, Ziraat, Veterinerlik, Fen ve Doğa Bilimleri alanlarından olmak üzere Türkçe ve İngilizce hazırlanmış orijinal makale, derleme ve sempozyum değerlendirmesi gibi çalışmalar yayımlanır. Türk Doğa ve Fen Dergisi sadece online sistemde yayımlanmakta olup ayrıca kağıt baskısı bulunmamaktadır.

## Merhaba...

Türk Doğa ve Fen Dergisi, Dergipark tarafından yayımlanmakta olup Bingöl Üniversitesi Fen Bilimleri Enstitüsüne aittir. Bahar ve güz dönemi olmak üzere yılda iki defa çıkarılan ulusal hakemli bir dergi olarak ilk sayısını 2012 bahar döneminde yayımlamıştır. Türk Doğa ve Fen Dergisi, Türkiye ve dünyanın her yerinden gelen doğa ve fen bilimlerinin her alanında özgün, yayımlanmamış, yayımlanmak üzere başka yere gönderilmemiş makale, derleme ve sempozyum değerlendirmesi gibi çalışmaların bilim alemine sunulması amacıyla kurulmuştur. İlk sayısından bugüne kesintisiz olarak faaliyetlerini sürdürmektedir.

Türk Doğa ve Fen Dergisi sadece online sistemde yayımlanmakta olup ayrıca kağıt baskısı bulunmamaktadır. Dergimize gelen her çalışma öncelikle Turnitin intihal programında taranmaktadır. Dergimizde editörlerin, hakemlerin ve yazarların, uluslararası yayım etik kurallarına uyması ve makalelerin yazım kurallarına uyumlu olması zorunluluğu vardır.

Yazarlar yayımlanmak üzere dergimize gönderdikleri çalışmalarını ile ilgili telif haklarını zorunlu olarak Bingöl Üniversitesi Türk Doğa ve Fen Dergisi'ne devretmiş sayılırlar. Yazarlardan herhangi bir ücret talep edilmemektedir. Yazarların değerlendirmeleri, dergimizin resmi görüşü olarak kabul edilemez. Çalışmaların her türlü sorumluluğu yazarlarına aittir. Araştırma ürünleri için etik kurul raporu gerekli ise, çalışma üzerinde bu raporun alınmış olduğu belirtilmeli ve kurul raporu sisteme kaydedilmelidir. Araştırma ile ilgili intihal, atıf manipülasyonu, sahte veri uydurma vb. suistimallerin tespit edilmesi halinde yayım ve etik ilkelerine göre davranılır. Bu durumda çalışmanın yayımlanmasını önlemek, yayımdan kaldırmak ya da başka işlemler yapmak için gerekli işlemler takip edilmektedir.

Dergimizde, kaynak gösteriminde uluslararası Vancouver sistemine geçilmiştir. Ayrıca dergimiz, Creative Commons ile lisanslanmak suretiyle dergimizde yayımlanan makalelerin paylaşımı, kaynak gösterimi ve yayımlanmasında dergi ve yazar haklarını korumaya almıştır. 2018 yılı güz döneminden itibaren makaleler, uluslararası yazar kimlik numarası ORCID No'su ile yayımlanmaktadır.

Dergi ekibi, dergimizin ulusal ve uluslararası indekslerce taranan bir dergi olması yönünde çalışmalarını titizlikle sürdürmektedir. Dergimize gösterilen ilgi bu yönde bizleri teşvik etmeye devam edecektir.

Bingöl Üniversitesi Fen Bilimleri Enstitüsü tarafından yayımlanmaktadır

## EDİTÖRLER (YAYIN) KURULU

### BAŞEDİTÖR

**Doç. Dr. Ekrem DARENDELİOĞLU**

Bingöl Üniversitesi, Fen-Edebiyat Fakültesi, Moleküler Biyoloji ve Genetik  
Bölümü

E-Mail: [edarendelioglu@bingol.edu.tr](mailto:edarendelioglu@bingol.edu.tr)

### EDİTÖR YARDIMCILARI

**Doç. Dr. Adnan AYNA**

Bingöl Üniversitesi, Fen-Edebiyat Fakültesi, Kimya Bölümü

E-Mail: [aayna@bingol.edu.tr](mailto:aayna@bingol.edu.tr)

**Dr. Öğr. Üyesi Mücahit ÇALIŞAN**

Bingöl Üniversitesi, Mühendislik-Mimarlık Fakültesi, Bilgisayar Mühendisliği

E-Mail: [mcalisan@bingol.edu.tr](mailto:mcalisan@bingol.edu.tr)

### EDİTÖRLER

#### Fen ve Doğa Bilimleri

**Doç. Dr. İkram ORAK**

Bingöl Üniversitesi, Sağlık Hizmetleri Meslek Yüksekokulu, Tıbbi Hizmetler ve  
Teknikler

E-Mail: [iorak@bingol.edu.tr](mailto:iorak@bingol.edu.tr)

**Prof. Dr. Selami SELVİ**

Balıkesir Üniversitesi, Altınoluk Meslek Yüksekokulu, Bitkisel ve Hayvansal  
Üretim Bölümü

E-Mail: [sselvi2000@yahoo.com](mailto:sselvi2000@yahoo.com)

**Prof. Dr. Refik KESKİN**

Sakarya Üniversitesi, Fen-Edebiyat Fakültesi, Matematik Bölümü

E-Mail: [rkeskin@sakarya.edu.tr](mailto:rkeskin@sakarya.edu.tr)

**Prof. Dr. Halim ÖZDEMİR**

Sakarya Üniversitesi, Fen-Edebiyat Fakültesi, Matematik Bölümü

E-Mail: [hozdemir@sakarya.edu.tr](mailto:hozdemir@sakarya.edu.tr)

**Prof. Dr. Zafer ŞİAR**

Bingöl Üniversitesi, Fen-Edebiyat Fakültesi, Matematik Bölümü  
E-Mail: [zsiar@bingol.edu.tr](mailto:zsiar@bingol.edu.tr)

**Prof. Dr. Uğur ÇAKILCIOĞLU**

Munzur Üniversitesi, Pertek Sakine Genç Meslek Yüksekokulu, Bitki Morfolojisi  
ve Anatomisi Bölümü  
E-Mail: [ucakilcioglu@yahoo.com](mailto:ucakilcioglu@yahoo.com)

**Doç. Dr. Kamuran DİLSİZ**

Bingöl Üniversitesi, Fen-Edebiyat Fakültesi, Fizik Bölümü  
E-Mail: [kdilsiz@bingol.edu.tr](mailto:kdilsiz@bingol.edu.tr)

**Doç. Dr. Şükran KONCA**

Bakırçay Üniversitesi, Mühendislik ve Mimarlık Fakültesi, Temel Bilimler,  
Matematik Bölümü  
E-Mail: [sukran.konca@bakircay.edu.tr](mailto:sukran.konca@bakircay.edu.tr)

**Doç. Dr. İdris YAZGAN**

Kastamonu Üniversitesi, Fen Edebiyat Fakültesi, Biyoloji  
E-Mail: [idrisyazgan@gmail.com](mailto:idrisyazgan@gmail.com)

**Doç. Dr. Abdulcabbar YAVUZ**

Gaziantep Üniversitesi, Mühendislik Fakültesi, Metalurji ve Malzeme Mühendisliği  
E-Mail: [ayavuz@gantep.edu.tr](mailto:ayavuz@gantep.edu.tr)

**Doç. Dr. Bünyamin ALIM**

Bayburt Üniversitesi, Teknik Bilimler Meslek Yüksekokulu, Elektrik ve Enerji  
Bölümü  
E-Mail: [balim@bayburt.edu.tr](mailto:balim@bayburt.edu.tr)

**Dr. Öğr. Üyesi Mustafa Şükrü KURT**

Erzurum Teknik Üniversitesi, Fen Fakültesi, Temel Bilimler  
E-Mail: [mustafa.kurt@erzurum.edu.tr](mailto:mustafa.kurt@erzurum.edu.tr)

**Dr. Öğr. Üyesi Sinan SAĞIR**

Karamanoğlu Mehmetbey Üniversitesi, Fizik  
E-Mail: [sinansagir@kmu.edu.tr](mailto:sinansagir@kmu.edu.tr) / [sinan.sagir@cern.ch](mailto:sinan.sagir@cern.ch)

**Doç. Dr. Murat AYDEMİR**

Erzurum Teknik Üniversitesi, Fen Fakültesi, Temel Bilimler

E-Mail: [murat.aydemir@erzurum.edu.tr](mailto:murat.aydemir@erzurum.edu.tr)

**Mühendislik Bilimleri**

**Doç. Dr. Özgür ÖZGÜN**

Bingöl Üniversitesi, Sağlık Bilimleri Fakültesi, İş Sağlığı ve Güvenliği Bölümü

E-Mail: [oozgun@bingol.edu.tr](mailto:oozgun@bingol.edu.tr)

**Prof. Dr. Figen KOREL**

İzmir Yüksek Teknoloji Enstitüsü, Gıda Mühendisliği Bölümü

E-Mail: [figenkorel@iyte.edu.tr](mailto:figenkorel@iyte.edu.tr)

**Prof. Dr. Kubilay ASLANTAŞ**

Afyon Kocatepe Üniversitesi, Teknoloji Fakültesi, Makine Mühendisliği Bölümü

E-Mail: [aslantas@aku.edu.tr](mailto:aslantas@aku.edu.tr)

**Prof. Dr. Hamit Özkan GÜLSOY**

Marmara Üniversitesi, Teknoloji Fakültesi, Metalurji ve Malzeme Mühendisliği  
Bölümü

E-Mail: [ogulsoy@marmara.edu.tr](mailto:ogulsoy@marmara.edu.tr)

**Prof. Dr. Ali Adnan HAYALOĞLU**

İnönü Üniversitesi, Mühendislik Fakültesi, Gıda Mühendisliği Bölümü

E-Mail: [adnan.hayaloglu@inonu.edu.tr](mailto:adnan.hayaloglu@inonu.edu.tr)

**Prof. Dr. Barbara SAWICKA**

University of Life Sciences in Lublin, Department of Plant Production Technology  
and Commodities Sciences

E-Mail: [barbara.sawicka@gmail.com](mailto:barbara.sawicka@gmail.com)

**Prof. Dr. İbrahim GÜNEŞ**

Giresun Üniversitesi, Mühendislik Fakültesi, İnşaat Mühendisliği Bölümü

E-Mail: [ibrahim.gunes@giresun.edu.tr](mailto:ibrahim.gunes@giresun.edu.tr)

**Doç. Dr. Sırma YEĞİN**

Ege Üniversitesi, Mühendislik Fakültesi, Gıda Mühendisliği Bölümü  
E-Mail: [sirma.yegin@ege.edu.tr](mailto:sirma.yegin@ege.edu.tr)

**Doç. Dr. Hasan OĞUL**

Sinop Üniversitesi, Mimarlık ve Mühendislik Fakültesi, Nükleer Enerji  
Mühendisliği  
E-Mail: [hogul@sinop.edu.tr](mailto:hogul@sinop.edu.tr)

**Doç. Dr. Murat YILMAZTEKİN**

İnönü Üniversitesi, Mühendislik Fakültesi, Gıda Mühendisliği Bölümü  
E-Mail: [murat.yilmaztekin@inonu.edu.tr](mailto:murat.yilmaztekin@inonu.edu.tr)

**Doç. Dr. Ferhat AYDIN**

Sakarya Uygulamalı Bilimler Üniversitesi, Teknoloji Fakültesi, İnşaat  
Mühendisliği Bölümü  
E-Mail: [ferhata@subu.edu.tr](mailto:ferhata@subu.edu.tr)

**Dr. Öğr. Üyesi Nurullah DEMİR**

Bingöl Üniversitesi, Mühendislik ve Mimarlık Fakültesi, Gıda Mühendisliği  
Bölümü  
E-Mail: [ndemir@bingol.edu.tr](mailto:ndemir@bingol.edu.tr)

**Dr. Öğr. Üyesi Ahmet GÜNER**

Bingöl Üniversitesi, Mühendislik ve Mimarlık Fakültesi, Elektrik ve Elektronik  
Mühendisliği Bölümü  
E-Mail: [aguner@bingol.edu.tr](mailto:aguner@bingol.edu.tr)

**Dr. Öğr. Üyesi Tahir AKGÜL**

Sakarya Uygulamalı Bilimler Üniversitesi, Teknoloji Fakültesi, İnşaat  
Mühendisliği Bölümü  
E-Mail: [tahirakgul@subu.edu.tr](mailto:tahirakgul@subu.edu.tr)

**Dr. Erhan Sulejmani**

University of Tetova, Faculty of Food Technology and Nutrition  
E-Mail: [erhan.sulejmani@unite.edu.mk](mailto:erhan.sulejmani@unite.edu.mk)

**Dr. Hacène Medjoudj**

Larbi Ben M'Hidi University of Oum El Bouaghi, Food Science Department  
E-Mail: [medjoudjh@yahoo.com](mailto:medjoudjh@yahoo.com)

**Dr. Avinash Lakshmikanthan**

Nitte Meenakshi Institute of Technology, Department of Mechanical Engineering,  
Karnataka, India  
E-Mail: [avinash.laks01@gmail.com](mailto:avinash.laks01@gmail.com)

**Dr. Manjunath Patel GC**

PES Institute of Technology and Management, Department of Mechanical  
Engineering, Karnataka, India  
E-Mail: [manju09mpm05@gmail.com](mailto:manju09mpm05@gmail.com)

**Sağlık Bilimleri**

**Doç. Dr. Aydın Şükrü BENGÜ**

Bingöl Üniversitesi, Sağlık Hizmetleri Meslek Yüksekokulu, Tıbbi Hizmetler ve  
Teknikler  
E-Mail: [abengu@bingol.edu.tr](mailto:abengu@bingol.edu.tr)

**Dr. Öğr. Üyesi Dilhun Keriman ARSERİM UÇAR**

Bingöl Üniversitesi, Sağlık Bilimleri Fakültesi, Beslenme ve Diyetetik Bölümü  
E-Mail: [dkucar@bingol.edu.tr](mailto:dkucar@bingol.edu.tr)

**Dr. Öğr. Üyesi Abdullah TUNÇ**

Bingöl Üniversitesi, Sağlık Bilimleri Fakültesi, İş Sağlığı ve Güvenliği Bölümü  
E-Mail: [atunc@bingol.edu.tr](mailto:atunc@bingol.edu.tr)

**Dr. Öğr. Üyesi Ramazan GÜNDOĞDU**

Bingöl Üniversitesi, Sağlık Hizmetleri Meslek Yüksekokulu, Eczane Hizmetleri  
E-Mail: [rgundogdu@bingol.edu.tr](mailto:rgundogdu@bingol.edu.tr)

**Dr. Alexander HERGOVICH**

UCL Cancer Institute, Faculty of Medical Sciences, Department of Cancer Biology,  
UCL, London, UK  
E-Mail: [a.hergovich@uc.ac.uk](mailto:a.hergovich@uc.ac.uk)

**Dr. Valenti GOMEZ**

UCL Cancer Institute, Faculty of Medical Sciences, Department of Oncology,  
UCL, London, UK

E-Mail: [valentin.gomez@ucl.ac.uk](mailto:valentin.gomez@ucl.ac.uk)

**Veterinerlik Bilimleri**

**Doç. Dr. Cüneyt ÇAĞLAYAN**

Bilecik Şeyh Edebali Üniversitesi, Tıp Fakültesi, Temel Tıp Bilimleri Bölümü,  
Tıbbi Biyokimya Anabilim Dalı

E-Mail: [cuneyt.caglayan@bilecik.edu.tr](mailto:cuneyt.caglayan@bilecik.edu.tr)

**Prof. Dr. Fatih Mehmet KANDEMİR**

Atatürk Üniversitesi, Veteriner Fakültesi, Veteriner Hekimliği Temel Bilimler

E-Mail: [fmehmet.kandemir@atauni.edu.tr](mailto:fmehmet.kandemir@atauni.edu.tr)

**Doç. Dr. Akın KIRBAŞ**

Bozok Üniversitesi, Veteriner Fakültesi, Klinik Bilimler Bölümü

E-Mail: [akindahiliye55@yahoo.com](mailto:akindahiliye55@yahoo.com)

**Doç. Dr. Emrah Hicazi AKSU**

Atatürk Üniversitesi, Veteriner Fakültesi, Klinik Bilimler Bölümü

E-Mail: [emrahaksu@atauni.edu.tr](mailto:emrahaksu@atauni.edu.tr)

**Ziraat Bilimleri**

**Dr. Öğr. Üyesi Zeynep DUMANOĞLU**

Bingöl Üniversitesi, Ziraat Fakültesi, Biyosistem Mühendisliği Bölümü

E-Mail: [zdumanoglu@bingol.edu.tr](mailto:zdumanoglu@bingol.edu.tr)

**Prof. Dr. Kağan KÖKTEN**

Bingöl Üniversitesi, Ziraat Fakültesi, Tarla Bitkileri Bölümü

E-Mail: [kahafe1974@yahoo.com](mailto:kahafe1974@yahoo.com)

**Prof. Dr. Mustafa SÜR MEN**

Adnan Menderes Üniversitesi, Ziraat Fakültesi, Tarla Bitkileri Bölümü

E-Mail: [mustafa.surmen@adu.edu.tr](mailto:mustafa.surmen@adu.edu.tr)



**Prof. Dr. Banu YÜCEL**

Ege Üniversitesi, Ziraat Fakültesi, Hayvan Yetiştirme Anabilim Dalı, Zootekni  
Bölümü

E-Mail: [banu.yucel@ege.edu.tr](mailto:banu.yucel@ege.edu.tr)

**Doç. Dr. Hakan İNCİ**

Bingöl Üniversitesi, Ziraat Fakültesi, Zootekni Bölümü

E-Mail: [hinci@bingol.edu.tr](mailto:hinci@bingol.edu.tr)

**TEKNİK EDİTÖRLER**

**Dr. Nimetullah KORKUT**

Bingöl Üniversitesi, BİNÜZEM, Bilgisayar Teknolojileri

E-Mail: [nkorkut@bingol.edu.tr](mailto:nkorkut@bingol.edu.tr)

**Öğr. Gör. MEHMET VURAL**

Bingöl Üniversitesi, Genç Meslek Yüksek Okulu, Bilgisayar Teknolojileri

E-Mail: [mvural@bingol.edu.tr](mailto:mvural@bingol.edu.tr)






**DİL EDİTÖRÜ**

**Öğr. Gör. Dr. Ahmet KESMEZ**

Bingöl Üniversitesi, Yabancı Diller Yüksekokulu, İngilizce Bölümü








E-Mail: [akesmez@bingol.edu.tr](mailto:akesmez@bingol.edu.tr)









## İÇİNDEKİLER/CONTENTS

<p><b>The Role of Royal Jelly on Exhaustive Exercise-Induced Oxidative Stress</b></p> <p><b>Murat BAKIR<sup>1*</sup></b> , <b>Tülay ÖZHAN BAKIR<sup>2</sup></b> </p> <p><sup>1</sup> Bingöl University, The School of Physical Education and Sports Faculty, Sports Management Department, Bingöl, Türkiye <sup>2</sup> Bingöl University, The School of Physical Education and Sports Faculty, Coaching Education Department, Bingöl, Türkiye Murat BAKIR ORCID No: 0000-0003-0149-7162 Tülay ÖZHAN BAKIR ORCID No: 0000-0003-3526-0446</p> <p><i>*Corresponding author: muratbakir6@gmail.com</i></p> <p>(Received: 15.11.2022, Accepted: 07.04.2023, Online Publication: 22.06.2023)</p>	<p><b>1</b></p>
<p><b>Comparison of Central and Individual Heating Systems Used for Heating Housings</b></p> <p><b>Muhammed Arslan OMAR<sup>1*</sup></b> </p> <p><sup>1</sup> Kafkas University, Engineering and Architecture Faculty, Mechanical Engineering Department, Kars, Türkiye Muhammed Arslan OMAR ORCID No: 0000-0003-4258-8634</p> <p><i>*Corresponding author: m.arslanomar@gmail.com</i></p> <p>(Received: 16.01.2023, Accepted: 24.04.2023, Online Publication: 22.06.2023)</p>	<p><b>8</b></p>
<p><b>Investigation Of Relative Story Shifts In Buildings With Projection Irregularities At Different Ratios</b></p> <p><b>M. Zeki ÖZYURT<sup>1*</sup></b> , <b>Emir DEMİR<sup>2</sup></b> </p> <p><sup>1</sup> Sakarya University, Engineering Faculty, Civil Engineering Department, Sakarya, Türkiye <sup>2</sup> Sakarya University, Engineering Faculty, Civil Engineering Department, Sakarya, Türkiye M. Zeki ÖZYURT ORCID No: 0000-0002-1593-4581 Emir DEMİR ORCID No: 0000-0002-9252-9651</p> <p><i>*Corresponding author: ozyurt@sakarya.edu.tr</i></p> <p>(Received: 25.01.2023, Accepted: 24.04.2023, Online Publication: 22.06.2023)</p>	<p><b>17</b></p>

<p align="center"><b>Investigation of Some Biological Properties of Propolis in Hawthorn Vinegar Extract</b></p> <p align="center"><b>Büşra BILDIR<sup>1</sup>  , Zeynep DEMİRKAN<sup>2</sup>  , Bülent KAYA<sup>3*</sup>  Fatma CAF<sup>4</sup> </b></p> <p><sup>1</sup>Department of Nutrition and Dietetics, Faculty of Health Sciences, Bingöl University, Bingöl, Türkiye  <sup>2</sup> Department of Bee and Bee Products, Institute of Sciences, Bingöl University, Bingöl, Türkiye  <sup>3</sup> Department of Molecular Biology and Genetics, Faculty of Sciences and Arts, Bingol University, Bingöl, Türkiye  <sup>4</sup> Department of Veterinary, Vocational School of Food, Agriculture and Livestock, Bingöl University, Bingöl, Türkiye</p> <p align="center">Büşra BILDIR ORCID No: 0000-0002-5631-1946  Zeynep DEMİRKAN ORCID No: 0000-0002-8101-8194  Bülent KAYA ORCID No: 0000-0002-1216-6441  Fatma CAF ORCID No: 0000-0002-0363-4848</p> <p align="center"><i>*Corresponding author: bkaya@bingol.edu.tr</i></p> <p align="center">(Received: 8.12.2022, Accepted: 25.04.2023, Online Publication: 22.06.2023)</p>	<b>24</b>
<p align="center"><b>Classifying RNA Strands with A Novel Graph Representation Based on the Sequence Free Energy</b></p> <p align="center"><b>Enes ALGÜL<sup>1*</sup> </b></p> <p><sup>1</sup> Bingol University, Engineering and Architecture Faculty, Department of Computer Engineering, Bingöl, Türkiye  Enes ALGÜL ORCID No: 0000-0001-6597-4242  <i>*Corresponding author: ealgul@bingol.edu.tr</i></p> <p align="center">(Received: 20.01.2023, Accepted: 05.05.2023, Online Publication: 22.06.2023)</p>	<b>32</b>
<p align="center"><b>Epidemic Spread Analysis in Social Communication Networks With Sir Model</b></p> <p align="center"><b>Yiğit Alisan<sup>1*</sup>  , Nagehan İlhan<sup>2</sup> </b></p> <p><sup>1</sup> Adana Alparslan Türkeş Science and Technology University, Department of Information Technology Adana, Türkiye  <sup>2</sup> Harran University, Engineering Faculty, Computer Engineering Department, Şanlıurfa, Türkiye  Yiğit Alisan ORCID No: 0000-0003-2943-7743  Nagehan İlhan ORCID No: 0000-0002-1367-9230</p> <p align="center"><i>*Corresponding author: yalisan@atu.edu.tr</i></p> <p align="center">(Received: 20.01.2023, Accepted: 16.05.2023, Online Publication: 22.06.2023)</p>	<b>40</b>
<p align="center"><b>Parameter Analysis of Convolutional Neural Network Operated on Embedded Platform for Estimation of Combustion Efficiency in Coal Burners</b></p> <p align="center"><b>Veysel GÜNDÜZALP<sup>1*</sup>  , Gaffari ÇELİK<sup>2</sup>  , Muhammed Fatih TALU<sup>3</sup>  , Cem ONAT<sup>4</sup> </b></p> <p><sup>1,3</sup> Inonu University, Faculty of Engineering, Department of Computer Engineering, Malatya, Türkiye  <sup>2</sup> Agri Ibrahim Cecen University, Vocational School, Department of Computer Technology, Ağrı, Türkiye  <sup>4</sup> Adiyaman University, Faculty of Engineering, Department of Mechanical Engineering, Adiyaman, Türkiye</p> <p align="center">Veysel GÜNDÜZALP ORCID No: 0000-0002-9199-5749  Gaffari ÇELİK ORCID No: 0000-0001-5658-9529  Muhammed Fatih TALU ORCID No: 0000-0003-1166-8404  Cem ONAT ORCID No: 0000-0002-4295-4860</p> <p align="center"><i>*Corresponding author: vgunduzalp@gmail.com</i></p> <p align="center">(Received: 17.10.2022, Accepted: 16.05.2023, Online Publication: 22.06.2023)</p>	<b>48</b>

<p align="center"><b>Evaluation of Machining Parameters Affecting Cutting Forces in Dry Turning of GGG50 Ductile Cast Iron</b></p> <p align="center"><b>Rüstem BİNALİ<sup>1*</sup>  , Mustafa KUNTOĞLU<sup>1</sup> </b></p> <p><sup>1</sup> Selcuk University, Technology Faculty, Mechanical Engineering Department, Konya, Türkiye Rüstem BİNALİ ORCID No: 0000-0003-0775-3817 Mustafa KUNTOĞLU ORCID No: 0000-0002-7291-9468</p> <p align="center"><i>*Corresponding author: rustem.binali@selcuk.edu.tr</i></p> <p align="center">(Received: 25.11.2022, Accepted: 16.05.2023, Online Publication: 22.06.2023)</p>	<b>55</b>
<p align="center"><b>Evaluation of Benzaldehyde Derivatives as being Bovine Kidney Aldose Reductase Inhibitors</b></p> <p align="center"><b>Bülent ŞENGÜL<sup>1*</sup> </b></p> <p><sup>1</sup> Department of Health Care Services, Vocational School of Health Services, Bayburt University, Bayburt, Türkiye</p> <p align="center">Bülent ŞENGÜL ORCID No: 0000-0002-9998-6564</p> <p align="center"><i>*Corresponding author: bulentsengul@bayburt.edu.tr</i></p> <p align="center">(Received: 14.11.2022, Accepted: 16.05.2023, Online Publication: 22.06.2023)</p>	<b>61</b>
<p align="center"><b>Experimental Investigation of Photovoltaic Panel Performance in Bingöl Province for Different Parameters</b></p> <p align="center"><b>Sinem KILIÇKAP IŞIK<sup>1*</sup>  , Perihan ÇULUN<sup>2</sup> </b></p> <p><sup>1,2</sup> Bingöl University, Faculty of Engineering and Architecture, Mechanical Engineering Department, Bingöl, Türkiye Sinem KILIÇKAP IŞIK ORCID No: 0000-0002-1044-5092 Perihan ÇULUN ORCID No: 0000-0002-1797-9695</p> <p align="center"><i>*Corresponding author: sinemisik@bingol.edu.tr</i></p> <p align="center">(Received: 24.02.2023, Accepted: 22.05.2023, Online Publication: 22.06.2023)</p>	<b>68</b>
<p align="center"><b>Investigation of The Effect of Creamed Honey Production Process on The Sugar Profile of Honey</b></p> <p align="center"><b>Davut KARAHAN<sup>1*</sup>  , Bayram YURT<sup>2</sup>  , Esra ÇAPANOĞLU GÜVEN<sup>3</sup> </b></p> <p><sup>1</sup>Bingöl University, Honey Bee and Natural Products R&amp;D and P&amp;D Center, Bingöl, Türkiye <sup>2</sup>Bingöl University, Faculty of Engineering and Architecture, Department of Food Engineering, Bingöl, Türkiye <sup>3</sup>Istanbul Technical University, Faculty of Chemical and Metallurgical Engineering, Department of Food Engineering, Istanbul, Türkiye</p> <p align="center">Davut KARAHAN ORCID No: 0000-0003-4571-1095 Bayram YURT ORCID No: 0000-0001-5447-1586 Esra ÇAPANOĞLU GÜVEN ORCID No: 0000-0003-0335-9433</p> <p align="center"><i>*Corresponding author: dkarahan@bingol.edu.tr</i></p> <p align="center">(Received: 03.12.2022, Accepted: 24.05.2023, Online Publication: 22.06.2023)</p>	<b>76</b>

<p style="text-align: center;"><b>The Effects of Water/Cement Ratio and Cement Dosage Variables on the Performance of Shotcrete: Compressive Strength and Drying Shrinkage Perspective</b></p> <p style="text-align: center;"><b>Hasan POLAT<sup>1*</sup> , Cengiz ÖZEL<sup>2</sup> </b></p> <p><sup>1</sup> Bingöl University, Vocational School of Technical Sciences, Department of Architecture and Urban Planning, 12000, Bingöl, Turkey</p> <p><sup>2</sup> Isparta University of Applied Sciences, Faculty of Technology, Department of Civil Engineering, 32260, Isparta, Turkey</p> <p>Hasan POLAT ORCID No: 0000-0003-1521-0695 Cengiz ÖZEL ORCID No: 0000-0002-2715-1680</p> <p style="text-align: center;"><i>*Corresponding author: hpolat@bingol.edu.tr</i></p> <p style="text-align: center;">(Received: 02.05.2023, Accepted: 02.06.2023, Online Publication: 22.06.2023)</p>	<b>82</b>
<p style="text-align: center;"><b>Rough Groups Over Rough Sets</b></p> <p style="text-align: center;"><b>Ramazan YAŞAR<sup>1*</sup> </b></p> <p><sup>1</sup> Hacettepe University, Hacettepe-ASO 1.OSB Vocational School, Sincan, Ankara, Türkiye</p> <p>Ramazan YAŞAR ORCID No: 0000-0001-6775-1069</p> <p style="text-align: center;"><i>*Corresponding author: ryasar@hacettepe.edu.tr</i></p> <p style="text-align: center;">(Received: 30.01.2023, Accepted: 02.02.2023, Online Publication: 22.06.2023)</p>	<b>88</b>
<p style="text-align: center;"><b>Geotechnical Inspections and Applications in Underground Rail System Constructions: Halkalı - İstanbul Airport Metro Line Example</b></p> <p style="text-align: center;"><b>Rabia KELEŞ<sup>1*</sup> , İsa VURAL<sup>2</sup> </b></p> <p><sup>1</sup> Sakarya University of Applied Sciences, Faculty of Technology, Department of Civil Engineering, Sakarya, Türkiye</p> <p><sup>2</sup> Sakarya University of Applied Sciences, Faculty of Technology, Department of Civil Engineering, Sakarya, Türkiye</p> <p>Rabia KELEŞ ORCID No: 0000-0002-6689-4217 İsa VURAL ORCID No: 0000-0003-2370-7597</p> <p style="text-align: center;"><i>*Corresponding author: y18007009@subu.edu.tr</i></p> <p style="text-align: center;">(Received: 15.11.2022, Accepted: 08.06.2023, Online Publication: 22.06.2023)</p>	<b>93</b>
<p style="text-align: center;"><b>Investigation of Arginine Deiminase Activity in <i>Bacillus cereus</i> and <i>Ralstonia eutropha</i> Under Minimal Conditions</b></p> <p style="text-align: center;"><b>Cennet Canan KARADERİ<sup>1*</sup> , Hüseyin KAHRAMAN<sup>2</sup> </b></p> <p><sup>1</sup> İnönü Üniversitesi, Fen Bilimleri Enstitüsü, Biyoloji Bölümü, Malatya, Türkiye</p> <p><sup>2</sup> İnönü Üniversitesi, Fen Edebiyat Fakültesi, Biyoloji Bölümü, Malatya, Türkiye</p> <p>Cennet Canan KARADERİ ORCID No: 0000-0002-4841-4435 Hüseyin KAHRAMAN ORCID No: 0000-0001-6235-5497</p> <p style="text-align: center;"><i>*Corresponding author: ckaraderi@gmail.com</i></p> <p style="text-align: center;">(Received: 18.01.2023, Accepted: 12.06.2023, Online Publication: 22.06.2023)</p>	<b>99</b>

<p style="text-align: center;"><b>Amoebicidal Effect of Fluconazole and Verapamil Together Against Trophozoites and Cysts of <i>Acanthamoeba castellanii</i></b></p> <p style="text-align: center;"><b>Mehmet AYKUR<sup>1*</sup></b> </p> <p><sup>1</sup> Tokat Gaziosmanpasa University, Medicine Faculty, Parasitology Department, Tokat, Türkiye Mehmet AYKUR ORCID No: 0000-0002-6100-1037</p> <p style="text-align: center;"><i>*Corresponding author: mehmetaykur@gmail.com</i></p> <p style="text-align: center;">(Received: 02.03.2023, Accepted: 12.06.2023, Online Publication: 22.06.2023)</p>	<b>104</b>
<p style="text-align: center;"><b>Investigation of Vegetative High Temperature Tolerance of Some Cotton (<i>Gossypium hirsutum</i> L.) Varieties</b></p> <p style="text-align: center;"><b>Yusuf Güzel DEMİRAY<sup>1</sup></b> , <b>Remzi EKİNCİ<sup>2*</sup></b> , <b>Adem BARDAK<sup>3</sup></b> </p> <p><sup>1</sup> GAP International Agricultural Research and Training Center, 21200, Diyarbakir, Turkey <sup>2</sup> Dicle University, Faculty of Agriculture, Department of Field Crops, 21280, Diyarbakir, Turkey <sup>3</sup> Kahramanmaraş Sütcü Imam University, Faculty of Agriculture, Department of Agricultural Biotechnology, Kahramanmaraş, Turkey</p> <p style="text-align: center;">Yusuf Güzel DEMİRAY ORCID No: 0000-0002-4113-5855 Remzi EKİNCİ ORCID No: 0000-0003-4165-6631 Adem BARDAK ORCID No: 0000-0002-5715-302X</p> <p style="text-align: center;"><i>*Corresponding author: remzi.ekinci@dicle.edu.tr</i></p> <p style="text-align: center;">(Received: 26.04.2023, Accepted: 13.06.2023, Online Publication: 22.06.2023)</p>	<b>111</b>
<p style="text-align: center;"><b>Determination of Ground-Based Structural Problems in the Historical Four-Legged Minaret with Ground Penetration Radar</b></p> <p style="text-align: center;"><b>Süleyman İPEK<sup>1*</sup></b> , <b>Nursen İŞİK<sup>2</sup></b> , <b>Fatma Meral HALİFEOĞLU<sup>3</sup></b> </p> <p><sup>1</sup> Bingöl University, Engineering and Architecture Faculty, Architecture Department, Bingöl, Türkiye <sup>2</sup> Dicle University, Architecture Faculty, Architecture Department, Diyarbakır, Türkiye <sup>3</sup> Dicle University, Architecture Faculty, Architecture Department, Diyarbakır, Türkiye</p> <p style="text-align: center;">Süleyman İPEK ORCID No: 0000-0001-8891-949X Nursen İŞİK ORCID No: 0000-0002-6125-1896 Fatma Meral HALİFEOĞLU ORCID No: 0000-0003-2032-3774</p> <p style="text-align: center;"><i>*Corresponding author: sipek@bingol.edu.tr</i></p> <p style="text-align: center;">(Received: 25.12.2022, Accepted: 14.06.2023, Online Publication: 22.06.2023)</p>	<b>119</b>
<p style="text-align: center;"><b>Carvacrol Ameliorates Sodium Arsenite-Induced Intestinal Toxicity</b></p> <p style="text-align: center;"><b>Mustafa İLERİTÜRK<sup>1*</sup></b> , <b>Özge KANDEMİR<sup>2</sup></b> </p> <p><sup>1</sup> Ataturk University, Horasan Vocational College, Department of Animal Science, Erzurum, Türkiye <sup>2</sup> Aksaray University, Aksaray Technical Sciences Vocational School, Aksaray, Türkiye</p> <p style="text-align: center;">Mustafa İLERİTÜRK ORCID No: 0000-0002-4581-4492 Özge KANDEMİR ORCID No: 0000-0001-8884-4168</p> <p style="text-align: center;"><i>*Corresponding author: m.ileriturk@atauni.edu.tr</i></p> <p style="text-align: center;">(Received: 10.05.2023, Accepted: 15.06.2023, Online Publication: 22.06.2023)</p>	<b>132</b>

**Antioxidant, Antiinflammatory, and Antiapoptotic Effects of Rutin in Spleen Toxicity Induced by Sodium Valproate in Rats**

Nurhan AKARAS<sup>1\*</sup> , Fatih Mehmet KANDEMİR<sup>2</sup> , Hasan ŞİMŞEK<sup>3</sup> , Cihan GÜR<sup>4</sup> ,  
Serpil AYGÖRMEZ<sup>5</sup> 

<sup>1</sup> Aksaray University, Faculty of Medicine, Department of Histology and Embryology, Aksaray, Türkiye

<sup>2</sup> Aksaray University, Faculty of Medicine, Department of Medical Biochemistry, Aksaray, Türkiye

<sup>3</sup> Aksaray University, Faculty of Medicine, Department of Physiology, Aksaray, Türkiye

<sup>4</sup> Atatürk University, Faculty of Veterinary, Department of Veterinary Biochemistry, Erzurum, Türkiye

<sup>5</sup> Kafkas University, Faculty of Veterinary, Department of Veterinary Biochemistry, Kars, Türkiye

Nurhan AKARAS ORCID No: 0000-0002-8457-9448

Fatih Mehmet KANDEMİR ORCID No: 0000-0002-8490-2479

Hasan ŞİMŞEK ORCID No: 0000-0001-5573-4923

Cihan GÜR ORCID No: 0000-0001-6775-7858

Serpil AYGÖRMEZ ORCID No: 0000-0002-5675-5096

*\*Corresponding author: nurakaras@hotmail.com*

(Received: 20.05.2023, Accepted: 15.06.2023, Online Publication: 22.06.2023)

138

**A New Method for Obtaining Haploid Plant Shed-Microspore Culture**

Mevlûde TATAR<sup>1\*</sup> 

<sup>1</sup> Alata Horticultural Research Institute, 33740, Mersin, Türkiye

Mevlûde TATAR ORCID No: 0000-0002-3707-1721

*\* Corresponding author e-mail: mtatar65@hotmail.com*

(Received: 22.06.2022, Accepted: 12.06.2023, Online Publication: 22.06.2023)

145

## The Role of Royal Jelly on Exhaustive Exercise-Induced Oxidative Stress

Murat BAKIR<sup>1\*</sup> , Tülay ÖZHAN BAKIR<sup>2</sup> 

<sup>1</sup> Bingöl University, The School of Physical Education and Sports Faculty, Sports Management Department, Bingöl, Türkiye

<sup>2</sup> Bingöl University, The School of Physical Education and Sports Faculty, Coaching Education Department, Bingöl, Türkiye

Murat BAKIR ORCID No: 0000-0003-0149-7162

Tülay ÖZHAN BAKIR ORCID No: 0000-0003-3526-0446

\*Corresponding author: [muratbakir6@gmail.com](mailto:muratbakir6@gmail.com)

(Received: 15.11.2022, Accepted: 07.04.2023, Online Publication: 22.06.2023)

### Keywords

Royal Jelly,  
Liver,  
Kidney,  
Skeletal  
muscle,  
Exhaustive  
exercise,  
Antioxidant

**Abstract:** In this study, the effects of Royal Jelly (RJ) on oxidative stress caused by exhaustive swimming exercise in rat tissues were evaluated. Methods: Twenty four male Wistar albino rats were indiscriminately distributed into four experimental groups: Sedentary control (SC); SC with the administration of RJ (100 mg kg<sup>-1</sup>) (SC + RJ); Exhaustive swimming exercise (E); Exhaustive swimming exercise with the administration of RJ (100 mg kg<sup>-1</sup>) (E + RJ). 100 mg kg<sup>-1</sup> of RJ was dissolved in drinking water. Rats in the SC+RJ and E+RJ groups were supplemented with RJ (100 mg kg<sup>-1</sup>) orally once a day for two weeks. Rats in groups E and E+RJ were subjected to acute exhaustive swimming exercise on the 14th day of the study, then some biochemical parameters related to oxidative stress of all groups were measured. Results: The level of alanine aminotransferase (ALT), aspartate aminotransferase (AST), alkaline phosphatase (ALP), blood urea nitrogen (BUN), and creatinine (CRE) significantly increased in the exercised rats compared with the sedentary rats (P < 0.05). The decreased superoxide dismutase (SOD), glutathione peroxidase (GSHPx), and catalase (CAT) activities of muscular and hepatic tissues significantly increased and the high malondialdehyde (MDA) levels of muscular, hepatic, and kidney tissues significantly reduced in exercised rats treated with RJ (P < 0.05). Conclusion: In this study, protective effects of RJ against oxidative damage on tissues after exhaustive exercise were observed.

1

## Arı Sütünün Tüketici Egzersize Bağlı Oksidatif Stres Üzerindeki Rolü

### Anahtar Kelimeler

Arı sütü,  
Karaciğer,  
Böbrek,  
İskelet kası,  
Tüketici  
egzersiz,  
Antioksidan

**Öz:** Bu çalışmada, Arı Sütü (RJ)'nin sıçan dokularındaki tüketici yüzme egzersizinin neden olduğu oksidatif stres üzerindeki etkileri değerlendirildi. Metodlar: Yirmi dört adet erkek Wistar albino sıçan rastgele dört deney grubuna ayrıldı: Sedanter kontrol (SC); 100 mg kg<sup>-1</sup> RJ uygulanmış SC (SC + RJ); tüketici yüzme egzersiz grubu (E); 100 mg kg<sup>-1</sup> RJ uygulanmış tüketici yüzme egzersiz grubu (E + RJ). 100 mg kg<sup>-1</sup> RJ içme suyunda çözüldü. SC + RJ ve E + RJ gruplarındaki sıçanlara, iki hafta boyunca günde bir kez ağızdan RJ (100 mg kg<sup>-1</sup>) verildi. E ve E + RJ gruplarındaki sıçanlar çalışmanın 14. gününde akut tüketici yüzme egzersizine tabi tutulduktan sonra tüm grupların oksidatif stres ile ilgili bazı biyokimyasal parametreleri ölçüldü. Bulgular: Alanin aminotransferaz (ALT), aspartat aminotransferaz (AST), alkalik fosfataz (ALP), kan üre azotu (BUN) ve kreatinin (CRE) seviyeleri, egzersiz yapılan sıçanlarda, sedanter sıçanlara kıyasla önemli ölçüde artmıştır (P < 0.05). RJ ile beslenen sıçanlarda kas ve hepatik dokuların azalmış olan süperoksit dismutaz (SOD), glutatyon peroksidaz (GSHPx) ve katalaz (CAT) aktiviteleri önemli ölçüde artmış ve kas, hepatik ve böbrek dokularının yüksek malondialdehit (MDA) seviyeleri önemli ölçüde azalmıştır (P < 0.05). Sonuç: Sonuç olarak, bu çalışmada, tüketici egzersiz sonrası oluşan dokular üzerindeki oksidatif hasara karşı RJ'nin koruyucu etkileri gözlenmiştir.



## 1. INTRODUCTION

As it is known, the effects of regular physical exercise on health have been investigated for years. Studies have shown that regular physical exercise has preventive effects on cardiovascular diseases, obesity, type 2 diabetes, and cancer [1]. During exercise, the amount of oxygen needed by the body increases 10-20 times compared to resting conditions. This rate is even higher in actively working muscles (200 times). Molecular oxygen is reduced in the mitochondrial electron transport chain as a result of the large flow of oxygen to the mitochondria. As a result of this process, the amount of superoxide ( $O_2^-$ ) and the formation of hydroxyl radicals increase [2]. If the intensity of exercise is high, it causes oxidative stress and cell damage. It has been previously shown that acute exhaustive exercise increases the production of reactive oxygen species (ROS) that causes glutathione oxidation and lipid peroxidation. In addition, it increases the amount of oxidative stress markers [3, 4]. Aerobic organisms produce free radicals in certain amounts within their normal metabolic processes. Free radicals are produced in cells from oxygen or nitrogen sources. Free radicals generated from oxygen sources are called ROS, and produced from nitrogen sources are named reactive nitrogen types (RNS) [5]. Studies have shown that excessive and continuous production of ROS causes adverse effects on nucleic acids, proteins, and lipids, resulting in cellular death [6]. All aerobic organisms, including humans, have developed a system called antioxidant defense systems to keep free radical production within certain limits and to prevent the harmful effects of these molecules [4]. In cell metabolism, ROS production is kept in balance by antioxidant enzyme system [7]. Antioxidants, which have an important role in ending oxidative chain reactions by preventing the emergence of free radical intermediates, are called free radical scavengers [8]. These substances strengthen the immune mechanism and also try to minimize the risk of cancer and degenerative diseases by preventing and repairing the destruction caused by ROS and RNS [9]. These enzymatic antioxidants are SOD, CAT, GSHPx, and glutathione reductase (GR) [4].

Antioxidants can be produced from the body by endogenous sources and can be taken exogenously from food [9]. In some cases (such as radiation, exercise, smoking and alcohol use), the endogenous antioxidant defense system is inadequate in regulating the oxidation-reduction (redox) balance and so oxidative stress occurs. Oxidative stress can be defined as disruption of redox signaling and oxidation-reduction balance in favor of oxidants [10]. Oxidative stress is caused by an imbalance among the generation and accumulation of ROS in the organism and the ability of the antioxidant defense system to eliminate the harmful effects of these reactive products [11]. The imbalance between pro- and antioxidant species (oxidative stress) is responsible for the development of many diseases such as diabetes, cancer, atherosclerosis, obesity, and osteoporosis [12].

As mentioned above, antioxidants can be produced endogenously in the biological system or can be taken exogenously from natural compounds. However, the endogenous antioxidant defense mechanism may be insufficient during intense exercise, therefore, oxidative stress biomarkers can be eliminated with external antioxidant supplements [13].

RJ is made and secreted in the hypopharyngeal (mandibular) and mandibular glands of young worker bees. The queen bee fed with RJ has different physical and structural features than the working bees, and the longer life span has led to the idea that this product can also be beneficial for humans and it has become attractive to consume this product. RJ contains high amounts of sugars, lipids, proteins, vitamins, minerals and water. In addition phenolic compounds (PC) and flavonoids play an important role in the chemical structure of RJ [14]. RJ has been found to have biological activities such as antioxidant and antiinflammatory [15].

In a study, it was observed that Bingöl Royal Jelly (BRJ) contains some medium and short-chain fatty acids such as essential fatty acids linoleic acid and propionic acid, in addition to major flavonoids and phenolic compounds such as apigenin, quercetin, naringenin, gallic acid, caffeic acid, which increase antioxidant capacity in metabolism. In the same study, the antimicrobial activity of BRJ against pathogens was also demonstrated [16].

In an oxidative stress model by Asadi *et al.* [17] RJ has been shown to reduce oxidative stress by increasing antioxidant capacity in the experimental varicocele model in rats. They observed that SOD, CAT, and GPx values of RJ treated experimental varicocele group increased significantly ( $P < 0.05$ ) and MDA showed a significant ( $P < 0.05$ ) decrease compared to the experimental varicocele group. The antioxidant activity of RJ has been shown in a rat model by reducing liver and pancreas MDA levels and increasing both ferric-reducing antioxidant power (FRAP) and CAT levels in the pancreas and liver ( $P < 0.05$ ) [18]. These experimental findings appear to support the antioxidative effects of RJ on oxidative stress induced tissue damage.

It was previously stated that acute exhaustive exercise increases ROS production, which induces lipid peroxidation, glutathione oxidation, and increases oxidative stress markers. These effects of acute exhaustive exercise allow it to be used as a model that generates oxidative stress [3]. Therefore, many studies have emphasized on the recognition of natural compounds that inhibit high production of ROS and reduce oxidative stress through ROS capture properties. For this reason, the present study aimed to reveal oxidative stress biomarkers by applying the exhaustive swimming exercise model and to demonstrate the protective effects of RJ through biochemical methods. Thus, it was aimed to test whether RJ would be a protective supplement product against oxidative damage occurring in tissues.

## 2. MATERIAL AND METHOD

### 2.1. Animal Models and Royal Jelly Administration

The study was approved by the Animal Ethics Committee of Bingöl University (approval date and no: 26/06/2018, BÜHADYEK-2018-02). The authors confirm that all the experiments were performed under approved guidelines and regulations. The study was carried out at Bingöl University's Experimental Researches Center on the rats supplied by the same Center. A total of twenty four male Wistar-Albino-type rats (9 weeks old, weight  $230 \pm 20$  g) were used for all experiments. Rats were provided standard pelleted rat food and water than housed in a controlled room with a 12-h light-dark cycle at  $22 \text{ }^\circ\text{C}$ . Fresh Royal Jelly (RJ) was acquired from a commercial firm in Türkiye (Bingöl, Türkiye) and kept at  $-20 \text{ }^\circ\text{C}$  until use.  $100 \text{ mg kg}^{-1}$  of RJ was dissolved in drinking water and subjected orally for 14 consecutive days to RJ groups [19]. In addition, the last RJ was administered on the 14th day of study, 1 h prior to the induction of exhaustive exercise.

### 2.2 Experimental Desing and Exhaustive Exercise

The study registered 24 Wistar-Albino-type (9 weeks old, weight  $230 \pm 20$  g) male rats which were divided into four groups in equal numbers: a sedentary control group fed on a standard diet (SC,  $n = 6$ ), a sedentary control group fed on standard diet containing RJ ( $100 \text{ mg kg}^{-1}$ ) for 14 days (SC + RJ,  $n = 6$ ), an exhaustive exercise group fed on standart diet and subjected to acute exhaustive swimming exercise on the 14th of the study (E,  $n = 6$ ) and an exhaustive exercise group fed on standart diet containing RJ ( $100 \text{ mg kg}^{-1}$  body weight $^{-1}$ ) for 14 days and subjected to acute exhaustive swimming exercise on the 14th of the study (E + RJ,  $n = 6$ ). Exercised rats were exposed a single exhaustive swimming test in barrels (60 cm x 90 cm x 50 cm) at a temperature of  $35 \text{ }^\circ\text{C} \pm 0.5 \text{ }^\circ\text{C}$ . The rats exposed to exhaustive exercise were primarily adapted to a swimming training  $20 \text{ min day}^{-1}$  for 3 days. The rats were kept in shallow water for 20 min on the first day. On the second day, the rats started to swim at the level of water that would exceed the height for 20 min. On the third day, they started swimming in deep enough water for 20 min. Then the rats were forced to swim with a weight (3% of their body weight) bonded to the tail till exhaustion [20]. Exhaustion was described by the following situation: more than 10 s drowning down the surface and loss of a righting reflex when put on a flat

surface [21]. After 2 weeks all rats were anesthetized with intraperitoneal ketamine/xylazine ( $60 \text{ mg kg}^{-1}$  and  $6 \text{ mg kg}^{-1}$ , respectively) and euthanized by cervical dislocation immediately after the exhaustive swimming exercise, and samples were collected for analysis.

### 2.3. Biochemical Analyses

Blood was taken from the heart and the serums were obtained by centrifugation (4500 rpm,  $4 \text{ }^\circ\text{C}$ , 10 min) and preserved at  $-80 \text{ }^\circ\text{C}$ . The ALT (Sigma -MAK052A), AST (Sigma-MAK055A), and ALP (Sigma-MAK447A) enzyme activities, as a measure of hepatic tissue damage, were measured using the commercial kits by an automated biochemical analyzer (Olympus AU 2700) based on instructions provided from Sigma-Aldrich Chemicals Co., St. Louis, USA. The intensities of BUN (Cayman-700623) and CRE (Cayman-10005314) were analyzed in triplicates with a commercially available assay kit (Cayman Chemical, Michigan, USA) in accordance with the instructions. Liver, kidney and muscle tissues were removed and kept at  $-80 \text{ }^\circ\text{C}$  until use. Assay of SOD (Cayman-706005), CAT (Cayman-707011), GSHPx (Cayman-703114) activities and MDA (Cayman-10009202) level were analyzed in triplicates with a commercially available assay kit (Cayman chemical, Michigan, USA) by the instructions.

### 2.4. Statistical Analysis

SPSS 22.0 (SPSS Inc., Chicago, IL, USA) was used for statistical calculations. Results were expressed as means  $\pm$  SD. One-way ANOVA test was used to compare multiple groups. Distinctions were considered significant when  $P < 0.05$ .

## 3. RESULTS

Plasma levels of AST, ALT, ALP, BUN, and CRE levels in group E were all significantly elevated by 87.6%, 116%, 33.8%, 68.7%, and 75% respectively, compared to group SC ( $P < 0.05$ ) (Table 1). However, there were no differences between groups E and E + RJ in plasma levels of AST, ALT, ALP, BUN, and CRE. Rices in cytosolic enzymes such as AST, ALT, and ALP in the plasma are replies to exhaustive exercise and are frequently used as signs of hepatic injury. Furthermore, alters in the levels of CRE and BUN have previously been used as signs of renal damage.

**Table 1.** Effects of RJ supplementation on plasma parameters of rats after exhaustive exercise.

Parameter	Units	SC	SC + RJ	E	E + RJ
AST	(U L $^{-1}$ )	81 $\pm$ 6 <sup>a</sup>	107 $\pm$ 12 <sup>a</sup>	152 $\pm$ 13 <sup>b</sup>	134 $\pm$ 9 <sup>a,b</sup>
ALT	(U L $^{-1}$ )	25 $\pm$ 3 <sup>a</sup>	27 $\pm$ 5 <sup>a</sup>	54 $\pm$ 10 <sup>b</sup>	52 $\pm$ 7 <sup>b</sup>
ALP	(U L $^{-1}$ )	177 $\pm$ 21 <sup>a</sup>	181 $\pm$ 19 <sup>a</sup>	237 $\pm$ 28 <sup>b</sup>	203 $\pm$ 16 <sup>a,b</sup>
BUN	(mg dL $^{-1}$ )	16 $\pm$ 1 <sup>a</sup>	17 $\pm$ 1 <sup>a</sup>	27 $\pm$ 2 <sup>b</sup>	25 $\pm$ 2 <sup>b</sup>
CRE	(mg dL $^{-1}$ )	0.44 $\pm$ 0.01 <sup>a</sup>	0.46 $\pm$ 0.02 <sup>a</sup>	0.77 $\pm$ 0.06 <sup>b</sup>	0.66 $\pm$ 0.03 <sup>b</sup>

Data are the means  $\pm$  SEM ( $n = 6$ ). Values in the same row with different superscript letters are significantly different at  $P < 0.05$ . SC, sedentary control; RJ, royal jelly; E, exhaustive swimming exercise; AST, aspartate aminotransferase; ALT, alanine aminotransferase; ALP, alkaline phosphatase; BUN, blood urea nitrogen; CRE, creatinine.

Table 2 shows the antioxidant enzyme activities. In comparison with the control group, the antioxidant

enzyme activities of SOD, CAT, and GSHPx in the liver and skeletal muscles and the SOD, and GSHPx activity

in the kidney of the E group were all significantly lower ( $P < 0.05$ ). Compared to the exercise group, these antioxidant enzymes activities were all significantly higher in E + RJ group in the liver and skeletal muscles

( $P < 0.05$ ). But, there were no distinctions between the exercise group and E + RJ group in antioxidant enzyme activities in the kidney.

**Table 2.** Effects of RJ supplementation on antioxidant enzymes, SOD, CAT and GSHPx activities in tissues of rats after exhaustive exercise.

Measurements	Units	SC	SC + RJ	E	E + RJ
<b>Skeletal muscle</b>					
SOD	(U mg <sup>-1</sup> protein)	2.08 ± 0.15 <sup>a</sup>	2.03 ± 0.19 <sup>a</sup>	0.56 ± 0.13 <sup>b</sup>	2.20 ± 0.18 <sup>a</sup>
CAT	(U mg <sup>-1</sup> protein)	6.01 ± 1.24 <sup>a</sup>	6.22 ± 1.16 <sup>a</sup>	1.87 ± 0.12 <sup>b</sup>	6.10 ± 1.23 <sup>a</sup>
GSHPx	(U mg <sup>-1</sup> protein)	72.33 ± 5 <sup>a</sup>	68.62 ± 4 <sup>a</sup>	21.36 ± 2 <sup>b</sup>	53.19 ± 6 <sup>a</sup>
<b>Liver</b>					
SOD	(U mg <sup>-1</sup> protein)	2.80 ± 0.46 <sup>a</sup>	2.85 ± 0.66 <sup>a</sup>	1.05 ± 0.31 <sup>b</sup>	2.77 ± 0.62 <sup>a</sup>
CAT	(U mg <sup>-1</sup> protein)	17.72 ± 1.6 <sup>a</sup>	18.64 ± 1.9 <sup>a</sup>	9.15 ± 0.6 <sup>b</sup>	18.71 ± 1.4 <sup>a</sup>
GSHPx	(U mg <sup>-1</sup> protein)	75.46 ± 7 <sup>a</sup>	77.52 ± 4 <sup>a</sup>	38.63 ± 19 <sup>b</sup>	72.44 ± 31 <sup>a</sup>
<b>Kidney</b>					
SOD	(U mg <sup>-1</sup> protein)	1.43 ± 0.11 <sup>a</sup>	1.36 ± 0.25 <sup>a</sup>	0.40 ± 0.13 <sup>b</sup>	0.93 ± 0.16 <sup>a,b</sup>
CAT	(U mg <sup>-1</sup> protein)	13.69 ± 2.8 <sup>a</sup>	14.11 ± 2.7 <sup>a</sup>	12.46 ± 1.9 <sup>a</sup>	12.73 ± 1.5 <sup>a</sup>
GSHPx	(U mg <sup>-1</sup> protein)	21.64 ± 3.1 <sup>a</sup>	22.13 ± 2.7 <sup>a</sup>	13.49 ± 2.4 <sup>b</sup>	16.87 ± 1.9 <sup>a,b</sup>

Data are the means ± SEM (n = 6). Values in the same row with different superscript letters are significantly different at  $P < 0.05$ . SC, sedentary control; RJ, royal jelly; E, exhaustive swimming exercise.

MDA was measured in the liver, kidney, and skeletal muscles (Figure 1). MDA levels of the liver, skeletal muscles, and kidneys were all significantly higher in group E compared to group SC ( $P < 0.05$ ). However compared to group E, the MDA levels were significantly lower in group E + RJ ( $P < 0.05$ ).

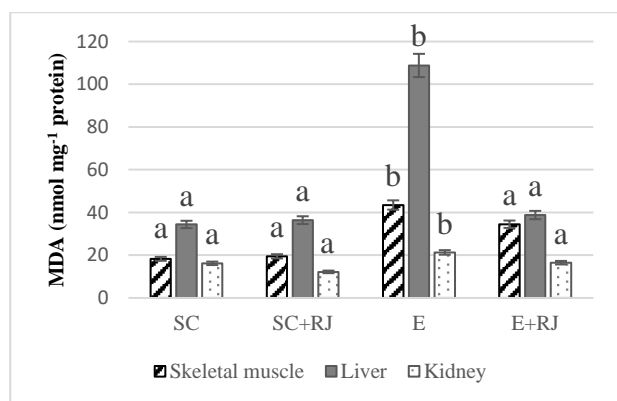


**Figure 1.** The effects of RJ on skeletal muscle, liver, and kidney MDA levels. The values are the means ± S.D. for groups of six rats, different letters are significantly different at  $P < 0.05$ . SC, sedentary control; RJ, royal jelly; E, exhaustive swimming

#### 4. DISCUSSION AND CONCLUSION

Exercise is a process that causes many physiological and biochemical changes that can alter the redox state. During exercise, oxygen consumption in the whole body and especially in skeletal muscle increases significantly. This process results in a drastic increase in ROS production. Whether exercise-induced ROS production is detrimental or beneficial probably depends on the balance between the levels of ROS produced during exercise and the competence of cellular antioxidant systems to protect cells against an oxidant challenge. Some recent studies have concluded that regular exercise does not lead to chronic oxidative stress in active muscles [22-26].

Low and moderate levels of exercise-induced ROS production play an important role in the exercise-induced adaptation of skeletal muscle. In contrast, high levels of ROS production cause muscle damage and a

decrease in physiological benefits associated with low and moderate ROS production [27]. This result is explained by the concept of exercise-induced hormesis. Hormesis is used to describe a biphasic dose-response curve in which a transient increase in low levels of a stressor produces a beneficial adaptive effect on cells, whereas a chronic high dose of a stressor causes damage to cells. Exercise-induced increases in ROS production in skeletal muscle have been found to play a necessary role in the adaptation of skeletal muscle to training. The bell-shaped hormesis curve predicts that exercise-induced increases in ROS production promote significant physiological benefits until an optimum level of ROS production is reached. However, if exercise leads to a true hormetic effect on the body, after this peak of physiological benefit is reached, any increase in exercise-induced ROS production will result in tissue damage and reduced exercise-induced adaptations [27]. Although short-term, low-intensity exercise does not appear to increase oxidative stress, it is well known that long-term, high-intensity endurance exercise increases oxidative stress. Prolonged and high-intensity endurance exercise causes increases in biomarkers of oxidative stress (eg, increased protein oxidation and lipid peroxidation) in both blood and active skeletal muscles in untrained humans and animals. The effect of ROS on muscle power production is biphasic and dependent on the level of ROS within the muscle fiber. Likewise, the main molecule in the ROS cascade is the superoxide radical dismutating to H<sub>2</sub>O<sub>2</sub>, and it seems likely that both O<sub>2</sub><sup>-</sup> and H<sub>2</sub>O<sub>2</sub> affect muscle contraction function. At rest, superoxide radicals are produced at low rates in skeletal muscle fibers. During exercise, the rate of O<sub>2</sub><sup>-</sup> production in the muscle increases markedly; the total amount of O<sub>2</sub><sup>-</sup> production in the muscle fiber depends on both the intensity and duration of the exercise and the temperature of the contracted muscle. In general, relatively high-intensity, prolonged aerobic exercise (ie 65%-75% VO<sub>2</sub>max) results in greater ROS production compared to low-intensity (ie <40% VO<sub>2</sub>max) short-term exercise. Also, increased muscle temperature results in higher ROS levels during contractions [28].

Increased ROS causes oxidative stress and lipid peroxidation, which have detrimental effects on the organism [29].

The current study focuses on determining the inhibitory effects of RJ against exhaustive swimming-induced oxidative stress. In this study, the antioxidant activity of royal jelly, which has different types of antioxidants, was tested. Exhaustive exercise causes oxidative stress, which is defined as the disruption of redox signaling and control [10]. Pending the performance of exhaustive exercise, different substances are made by the metabolic process, such as ROS [30]. Oxidative stress caused by increased ROS causes oxidative damage to tissues [4, 27]. When tissues such as muscle, kidney, and liver are damaged, various enzymes are released from these tissues into the bloodstream. Indicators of cellular damage can be observed in the blood after exhaustive exercise [31].

The previous studies demonstrated that exhaustive exercise raises AST, ALT CRE, and BUN levels in plasma and causes important skeletal muscle, kidney and, liver damage [32]. In this study compared to group SC, the CRE, AST, ALT ALP and BUN levels of group E were significantly higher ( $P < 0.05$ ). It is a remarkable protocol to try antioxidant food supplements to prevent the damage caused by exhausting exercise to the organism [32]. External antioxidant applications are frequently used to bring the increased enzyme levels to normal values. In the study of Ghanbari *et al.* [18], it has been reported that RJ treatment reduces liver injury by decreasing serum AST, ALT and, ALP levels. In another study, Kanbur, Eraslan [33] showed that RJ administration had protective effects against paracetamol-induced liver tissue damage. But Huang *et al.* [34] observed that the administration of L-arginine did not cause any changes in AST and ALT levels in rats exposed to exhaustive exercise. In the same vein, in the current study, rats in the RJ-supplemented group displayed no differences in AST, ALT, ALP, BUN, or CRE levels compared to group E (Table 1). No significant changes in AST, ALT, ALP, BUN, and CRE levels in RJ exercise groups show that RJ does not have beneficial effects on hepatocyte cells and kidney function.

Regarding lipid peroxidation, the traditional oxidative stress marker is MDA produced during fatty acid oxidation. This product is measured by the reaction of thiobarbituric acid, which generates thiobarbituric acid reactive substances (TBARS) in blood samples [27]. MDA levels were measured in the liver, kidney, and skeletal muscles (Figure 1). MDA is indicated as a substantial oxidative stress marker that can cause direct detriment to membrane structure, or indirect damage to other cellular ingredients via the production of reactive aldehydes [35]. In addition, MDA has been used as an indication of lipid peroxidation in exercise studies [36]. Previous studies have shown significant increases in lipid peroxidation products in the liver, kidney, and skeletal muscle as a result of exhaustive exercise ( $P < 0.05$ ) [36, 37]. MDA levels in our study are consistent

with the above-mentioned studies. In this study, the MDA levels in muscular, renal and hepatic tissues were significantly higher in group E compared to group SC ( $P < 0.05$ ). But, RJ supplementation substantially preserved the liver, skeletal muscles, and kidneys from ROS-mediated oxidative damage after exhaustive exercise. Oxygen consumption increases during exhaustive exercise, which can lead to an increase in ROS [37]. High amounts of ROS are potentially detrimental to the body if they are not rapidly deactivated [30]. It was previously showed that antioxidant enzymes are important in protecting the body against ROS. Antioxidant enzymes such as SOD, CAT and GSHPx inhibit ROS accumulation in the body [4, 36]. SOD catalyses the reduction of the superoxide to  $H_2O_2$  and  $H_2O$ ; GSHPx reduces  $H_2O_2$  to  $H_2O$ . Also, GSHPx can reduce lipid peroxides straight. CAT catalyzes the conversion of  $H_2O_2$  to  $H_2O$  [38]. The substantial reduction in the activities of SOD, GSHPx, and CAT in the skeletal muscle and liver tissues may be a sign of oxidative stress [4]. In the oxidative stress model developed by Asadi *et al.*, it has been shown that royal jelly reduces oxidative stress by increasing antioxidant capacity. They observed that SOD, CAT, and GPx values of the experimental varicocele group treated with RJ were significantly increased ( $P < 0.05$ ) and MDA was significantly decreased ( $P < 0.05$ ) compared to the experimental varicocele group [17]. Table 2 shows the antioxidant enzyme activities. In this study, a significant decrease in SOD, GSHPx, and CAT activities was observed after exhaustive exercise ( $P < 0.05$ ). The findings of this study are in accordance with some previous observations in the literature [37, 38]. In our study, the data also demonstrated that the GSHPx, SOD, and CAT activity values in the liver and skeletal muscles of RJ + E group were significantly higher than group E ( $P < 0.05$ ).

PCs in royal jelly are effective scavengers of free radicals and other non-radical ROS/RNS in vitro. The physiological ability of PCs to induce endogenous antioxidant gene expression, regulate ROS production by enzymes and redox-related transcription factors, causes PCs to be key reducers of OS and inflammation and protect lipids, proteins, and nucleic acid damage [39]. In this study, it is assumed that the functional hydroxyl group (OH) of PCs plays a key role in antioxidant defense. The results showed that RJ was able to restore antioxidant enzyme activities to control group levels, thereby protecting the tissues from oxidative stress caused by exhaustive swimming exercise.

In conclusion, the data demonstrated that RJ can increase SOD, GSHPx and CAT activities, but decrease the MDA levels. These effects might be due to its antioxidant feature. RJ treated as a good scavenger against free radical generation and thereby obstructs lipid peroxidation. These findings showed that RJ had protective effect against the oxidative stress caused by exhaustive exercise. The study shows that RJ can be used as a protective product against damages caused by oxidative stress that may occur for various reasons. The present study will provide a basis for subsequent similar studies.

## REFERENCES

- [1] Moore SC, Lee I-M, Weiderpass E, Campbell PT, Sampson JN, Kitahara CM, et al. Association of leisure-time physical activity with risk of 26 types of cancer in 1.44 million adults. *JAMA internal medicine*. 2016;176(6):816-25.
- [2] Morillas-Ruiz JM, Hernández-Sánchez P. Oxidative stress and antioxidant defenses induced by physical exercise. Basic principles and clinical significance of oxidative stress Rijeka: InTechOpen. 2015:221-41.
- [3] Malaguti M, Angeloni C, Garatachea N, Baldini M, Leoncini E, Collado PS, et al. Sulforaphane treatment protects skeletal muscle against damage induced by exhaustive exercise in rats. *Journal of Applied Physiology*. 2009;107(4):1028-36.
- [4] Powers SK, Jackson MJ. Exercise-induced oxidative stress: cellular mechanisms and impact on muscle force production. *Physiological reviews*. 2008;88(4):1243-76.
- [5] Halliwell B, Gutteridge JM. *Free radicals in biology and medicine*: Oxford university press, USA; 2015.
- [6] Liu Z, Ren Z, Zhang J, Chuang C-C, Kandaswamy E, Zhou T, et al. Role of ROS and nutritional antioxidants in human diseases. *Frontiers in physiology*. 2018;9:477.
- [7] Estruel-Amades S, Massot-Cladera M, Garcia-Cerdà P, Pérez-Cano FJ, Franch À, Castell M, et al. Protective effect of hesperidin on the oxidative stress induced by an exhausting exercise in intensively trained rats. *Nutrients*. 2019;11(4):783.
- [8] Gholamian-Dehkordi N, Luther T, Asadi-Samani M, Mahmoudian-Sani MR. An overview on natural antioxidants for oxidative stress reduction in cancers; a systematic review. *Immunopathologia Persa*. 2017;3(2):e12.
- [9] Chatterjee M, Saluja R, Kanneganti S, Chinta S, Dikshit M. Biochemical and molecular evaluation of neutrophil NOS in spontaneously hypertensive rats. *Cellular and Molecular Biology*. 2007;53(1):84-93.
- [10] Sies H. Oxidative stress: a concept in redox biology and medicine. *Redox biology*. 2015;4:180-3.
- [11] Pizzino G, Irrera N, Cucinotta M, Pallio G, Mannino F, Arcoraci V, et al. Oxidative stress: harms and benefits for human health. *Oxidative medicine and cellular longevity*. 2017;2017.
- [12] Liu Z, Zhou T, Ziegler AC, Dimitrion P, Zuo L. Oxidative stress in neurodegenerative diseases: from molecular mechanisms to clinical applications. *Oxidative medicine and cellular longevity*. 2017;2017.
- [13] Atashak S. The antioxidant role of artichoke (*Cynara scolymus* L.) extract against exhaustive exercise-induced oxidative stress in young athletes. *Journal of Medicinal Plants*. 2019;18(71):37-48.
- [14] Bărnuțiu LI, Mărghitaș LA, Dezmiorean DS, Mihai CM, Bobiș O. Chemical composition and antimicrobial activity of Royal Jelly-REVIEW. *Scientific Papers Animal Science and Biotechnologies*. 2011;44(2):67-72.
- [15] Kohno K, Okamoto I, Sano O, Arai N, Iwaki K, Ikeda M, et al. Royal jelly inhibits the production of proinflammatory cytokines by activated macrophages. *Bioscience, biotechnology, and biochemistry*. 2004;68(1):138-45.
- [16] Bengü AŞ, Adnan A, Özbolat S, Abdullah T, Aykutoğlu G, Çiftçi M, et al. Content and antimicrobial activities of bingol royal jelly. *Türk Tarım ve Doğa Bilimleri Dergisi*. 2020;7(2):480-6.
- [17] Asadi N, Kheradmand A, Gholami M, Saidi SH, Mirhadi SA. Effect of royal jelly on testicular antioxidant enzymes activity, MDA level and spermatogenesis in rat experimental Varicocele model. *Tissue and Cell*. 2019;57:70-7.
- [18] Ghanbari E, Nejati V, Khazaei M. Improvement in serum biochemical alterations and oxidative stress of liver and pancreas following use of royal jelly in streptozotocin-induced diabetic rats. *Cell Journal (Yakhteh)*. 2016;18(3):362.
- [19] Silici S, Ekmekcioglu O, Eraslan G, Demirtas A. Antioxidative effect of royal jelly in cisplatin-induced testes damage. *Urology*. 2009;74(3):545-51.
- [20] Zhang H, Liu M, Zhang Y, Li X. Trimetazidine attenuates exhaustive exercise-induced myocardial injury in rats via regulation of the Nrf2/NF-κB signaling pathway. *Frontiers in pharmacology*. 2019;10:175.
- [21] Thomas D, Marshall K. Effects of repeated exhaustive exercise on myocardial subcellular membrane structures. *International journal of sports medicine*. 1988;9(04):257-60.
- [22] Ji LL, Kang C, Zhang Y. Exercise-induced hormesis and skeletal muscle health. *Free Radical Biology and Medicine*. 2016;98:113-22.
- [23] de Sousa CV, Sales MM, Rosa TS, Lewis JE, de Andrade RV, Simões HG. The antioxidant effect of exercise: a systematic review and meta-analysis. *Sports medicine*. 2017;47:277-93.
- [24] Radak Z, Ishihara K, Tekus E, Varga C, Posa A, Balogh L, et al. Exercise, oxidants, and antioxidants change the shape of the bell-shaped hormesis curve. *Redox biology*. 2017;12:285-90.
- [25] Di Meo S, Napolitano G, Venditti P. Mediators of physical activity protection against ROS-linked skeletal muscle damage. *International journal of molecular sciences*. 2019;20(12):3024.
- [26] Nocella C, Cammisotto V, Pigozzi F, Borrione P, Fossati C, D'Amico A, et al. Impairment between oxidant and antioxidant systems: short-and long-term implications for athletes' health. *Nutrients*. 2019;11(6):1353.
- [27] Elejalde E, Villarán MC, Alonso RM. Grape polyphenols supplementation for exercise-induced oxidative stress. *Journal of the International Society of Sports Nutrition*. 2021;18(1):3.
- [28] Powers SK, Deminice R, Ozdemir M, Yoshihara T, Bomkamp MP, Hyatt H. Exercise-induced oxidative stress: Friend or foe? *Journal of sport and health science*. 2020;9(5):415-25.
- [29] Popovic LM, Mitic NR, Radic I, Miric D, Kisic B, Krdzic B, et al. The effect of exhaustive exercise on oxidative stress generation and antioxidant defense

- in guinea pigs. *Advances in Clinical and Experimental Medicine*. 2012;21(3):313-20.
- [30] Vale A, Ferreira H, Benetti E, Rebelo A, Figueiredo A, Barbosa E, et al. Antioxidant effect of the pequi oil (*Caryocar brasiliense*) on the hepatic tissue of rats trained by exhaustive swimming exercises. *Brazilian Journal of Biology*. 2018;79:257-62.
- [31] Huang Q, Ma S, Tominaga T, Suzuki K, Liu C. An 8-week, low carbohydrate, high fat, ketogenic diet enhanced exhaustive exercise capacity in mice part 2: effect on fatigue recovery, post-exercise biomarkers and anti-oxidation capacity. *Nutrients*. 2018;10(10):1339.
- [32] Huang K-C, Wu W-T, Yang F-L, Chiu Y-H, Peng T-C, Hsu B-G, et al. Effects of freshwater clam extract supplementation on time to exhaustion, muscle damage, pro/anti-inflammatory cytokines, and liver injury in rats after exhaustive exercise. *Molecules*. 2013;18(4):3825-38.
- [33] Kanbur M, Eraslan G, Beyaz L, Silici S, Liman BC, Altınordulu Ş, et al. The effects of royal jelly on liver damage induced by paracetamol in mice. *Experimental and Toxicologic Pathology*. 2009;61(2):123-32.
- [34] Huang C-C, Lin T-J, Lu Y-F, Chen C-C, Huang C-Y, Lin W-T. Protective effects of L-arginine supplementation against exhaustive exercise-induced oxidative stress in young rat tissues. *Chin J Physiol*. 2009;52(5):306-15.
- [35] Aksoy L, Aslan Z. Nephroprotective and antioxidative effects of royal jelly on ethylene glycol induced nephropathy in rats. *Ankara Üniversitesi Veteriner Fakültesi Dergisi*. 2017;64(4):241-8.
- [36] Yan F, Hao H. Effects of *Laminaria japonica* polysaccharides on exercise endurance and oxidative stress in forced swimming mouse model. *Journal of Biological Research-Thessaloniki*. 2016;23(1):1-7.
- [37] Yang Q, Jin W, Lv X, Dai P, Ao Y, Wu M, et al. Effects of macamides on endurance capacity and anti-fatigue property in prolonged swimming mice. *Pharmaceutical biology*. 2016;54(5):827-34.
- [38] Yan F, Wang B, Zhang Y. Polysaccharides from *Cordyceps sinensis* mycelium ameliorate exhaustive swimming exercise-induced oxidative stress. *Pharmaceutical Biology*. 2014;52(2):157-61.
- [39] Kruk J, Aboul-Enein BH, Duchnik E, Marchlewicz M. Antioxidative properties of phenolic compounds and their effect on oxidative stress induced by severe physical exercise. *The Journal of Physiological Sciences*. 2022;72(1):1-24.

## Comparison of Central and Individual Heating Systems Used for Heating Housings

Muhammed Arslan OMAR<sup>1\*</sup> 

<sup>1</sup> Kafkas University, Engineering and Architecture Faculty, Mechanical Engineering Department, Kars, Türkiye  
Muhammed Arslan OMAR ORCID No: 0000-0003-4258-8634

\*Corresponding author: [m.arslanomar@gmail.com](mailto:m.arslanomar@gmail.com)

(Received: 16.01.2023, Accepted: 24.04.2023, Online Publication: 22.06.2023)

### Keywords

Heating systems,  
Energy saving,  
Fuel  
consumption,  
Cost analysis

**Abstract:** Today, energy production based on fossil energy sources has become seriously questioned by societies due to both cost and environmental pollution. Fossil energy sources are mainly used for heating houses, which constitute a significant part of energy consumption. In this study, central heating systems, which are the most widely used methods to meet the heat energy needs of buildings and individual heating systems are examined and compared. In the study, the heat loss and energy need of a 5-story building consisting of 10 flats in Kars Center with a total heated area of 1080 m<sup>2</sup> were calculated using the TS 825 calculation method, accordingly, calculation of heater devices for both systems, determination of heating system elements, annual fuel consumption amount and cost calculation has been made. Natural gas was used as fuel in both systems to be compared for heating the building. According to the values obtained as a result of the study, it was seen that individual heating systems have higher costs than central heating systems in terms of both initial investment and heating cost. It has been determined that central heating systems are more advantageous in terms of initial investment cost, fuel consumption, and total cost. While the total cost was 441096 TL for the central heating system, it was 508825 TL for the individual heating system.

## Konutların Isıtılmasında Kullanılan Merkezi ve Bireysel Isıtma Sistemlerinin Karşılaştırılması

### Anahtar Kelimeler

Isıtma sistemleri,  
Enerji tasarrufu,  
Yakıt tüketimi,  
Maliyet analizi

**Öz:** Fosil enerji kaynaklarına dayalı enerji üretimi günümüzde hem maliyet hem de oluşturduğu çevre kirliliği nedeni ile toplumlar tarafından ciddi anlamda sorgulanır hale gelmiştir. Enerji tüketiminin önemli bir bölümünü oluşturan konutların ısıtılması için ağırlıklı olarak fosil enerji kaynakları kullanılmaktadır. Bu çalışmada, binaların ısı enerji ihtiyacının karşılanmasında en yaygın kullanılan yöntemlerden olan merkezi ısıtma sistemleri ve bireysel ısıtma sistemleri incelenerek karşılaştırılmıştır. Çalışmada Kars Merkezde 10 daireden oluşan toplam 1080 m<sup>2</sup> ısıtılan alana sahip olan 5 katlı bir binanın ısı kaybı ve enerji ihtiyacı TS 825 hesap metodu kullanılarak hesaplanmış buna göre her iki sistem için ısıtıcı cihazların hesaplanması, ısıtma sistemi elemanlarının belirlenmesi, yıllık yakıt tüketiminin miktarı ve maliyet hesabı yapılmıştır. Binanın ısıtılması için karşılaştırılacak her iki sistemde de yakıt olarak doğalgaz kullanılmıştır. Çalışma sonucunda elde edilen değerlere göre bireysel ısıtma sistemleri hem ilk yatırım hem de ısıtma maliyeti açısından merkezi ısıtma sistemlerine göre daha yüksek maliyete sahip olduğu görüldü. İlk yatırım maliyeti yakıt tüketimi ve toplam maliyet açısından merkezi ısıtma sistemlerinin daha avantajlı olduğu belirlenmiştir. Toplam maliyet merkezi ısıtma sisteminde 441096 TL olurken, bireysel ısıtma sisteminde ise 508825 TL bulunmuştur.

### 1. INTRODUCTION

Energy is one of the most important needs of humanity and has had a great impact on the development of humanity from its existence to the present [1]. Energy

costs are increasing daily due to international political crises, global economic crises, and wars. In addition, the use of fossil-based energy types is one of the most significant factors in environmental pollution and has led countries and states to search for the efficient use of fossil-based energy resources [2].

Due to the increase in energy use, there is a significant increase in the rate of carbon emissions in the atmosphere [3]. Emissions from the combustion of fossil fuels while creating a greenhouse effect in the atmosphere, natural balances are deteriorating and global disasters are increasing [4]. The majority of CO<sub>2</sub>, which is more effective in the increase of global warming compared to other emissions, occurs in energy production [5]. For these reasons, renewable, non-fossil sourced energy generation such as wind, solar, and hydrogen becomes important [6].

Fossil-based energy is widely used in residential heating systems. Houses constitute a large share of 40% of total energy consumption worldwide [7]. There are many systems used for heating houses. While these systems are grouped, they are named according to the place where the heat energy is obtained, the fluid in which the power is carried, and the way the heat energy is given to the volume. Heating systems according to the place where the heat energy is obtained; individual and central heating systems, according to the fluid in which the power is carried;

- Hot water heating system
- Steam heating system
- Hot water heating system
- Heating system with hot air

According to the way the heat energy is given to the volume;

- Heating system with heater
- Underfloor heating system
- Panel heating system
- Radiant heating system
- Heating system design with hot air

Central and individual heating systems are the most preferred systems for heating houses. The most important considerations in determining the system to be applied for heating the buildings are the comfort in the living area, the cost of the system to be applied, the compatibility of the heating system with the volume to be heated, the storability and cost of the fuel type to be used.

While 34% of the energy consumed in Turkey is used for heating and a large part of this heat energy is spent in residences [8]. For this reason, in this study, central heating systems and individual heating systems used for heating houses were examined and compared in terms of initial investment cost, fuel consumption amount, and fuel costs. There are many studies in the literature on the comparison of central and individual heating systems, the efficiency of these systems used in heating the houses, heat sharing, and measurement in the systems, some studies are given below.

Cockroft et al. (2017) examined the potential energy savings in meeting the zone-controlled independent volume with a standard central heating system. In their study, they evaluated and analyzed the savings that could

be achieved by taking into account the type, age, location, and number of people in the house. Annual simulations with dynamic models for thermal zones and airflow affecting the potential energy savings of zone-controlled and non-zone-controlled volumes were carried out. [9].

Meng et al. (2022) developed a model for heating control and comfortable energy saving of high-rise residential buildings with a central heating system. For the model, they analyzed the correlation between the temperature of the adjacent rooms and used it for the control of the heating elements in the boiler room, the optimization of the space temperature, and heat energy distribution. Compared to the central control method, they found that the energy consumption decreased by 14.28% and the efficiency of the heating elements in the boiler room increased. [10].

Yuruk et al. (2022) examined the cleaned installation of heating systems in houses in terms of efficient energy. In the study, they determined the energy loss caused by calcification and pollution in the heating systems with the measurements before and after the system cleaning. As a result of the study, they found a homogeneous temperature distribution and a decrease of 21.16% and 25% in natural gas consumption and harmful emissions, respectively, and an increase of 17.2% in convection heat transfer in the radiators in the lime and dirt-free system. [11]. Omar et al. (2015) developed and experimentally investigated a hemispherical porous metal matrix burner for boilers and combi boilers used as heating devices in central and individual heating systems. In the experimental study, the thermal and flow behavior of the burner in a combi unit used in heating systems were investigated. As a result of the improvements in the combustion processes in the device used in the heating systems in the study, they achieved a reduction in emission values by providing fuel and energy savings [12].

Tahir et al. (2022) evaluated a central energy system with an individual heating system using energy and exergy analysis. In this study, the energy and exergy analysis of individual heating systems in China according to the energy conservation laws of thermodynamics for an economically viable and carbon-free clean environment are examined. In the study, they proposed natural gas-fueled micro-combined heat-power, hydrogen-fueled micro-combined heat-power, and heat pump systems to meet different energy needs instead of fossil fuel boilers. [13].

Pavlovic et al. (2022) conducted a study to examine the situation of individual heating systems in Serbia. In the study, they found that the thermal insulation of the residences in Serbia was inadequate, and the heating systems were old and low-efficiency. In their studies, they emphasized that the effect of energy efficiency on climate change is important and this situation is significant for developing countries [14].



Zhang (2021) examined the measurement management system of individual heating in mass housing buildings with the central heating system. In the study, a pricing management system has been designed to ensure that the heating measurement is fair in the mass housing building and to solve the heat-sharing problem. He found that this measurement system is important in terms of energy optimization, energy saving, and emission values [15].

Cho et al. (2020) investigated the effect of hydraulic balancing of the heating system in buildings on energy saving and improving the thermal conditions of the volume. The methodology they developed consists of characterization, prediction, and scenario analysis for thermal comfort and energy savings through hydraulic balancing. They achieved energy saving between 2% and 14% by applying the study in Geneva, Switzerland [16]. Saba et al. (2017) experimentally investigated the heating cost distribution method for apartment buildings. In the study, they tried a new heat cost distribution method for apartments and compared this method with traditional heat cost distribution systems. Contrary to traditional methods, they have verified experimental study results by providing an estimation of the energy consumed without the need to measure the temperature of the heater radiators [17].

Terhan and Abak (2023) studied the optimization of insulation thickness in buildings using energy and exergy methods. For the study, they searched for optimum insulation thickness for exterior walls by taking the actual consumption values and dimensions of buildings in a campus in Turkey as a reference. They considered energy consumption, fuel Life Cycle Assessment, and payback periods to determine the optimum insulation thickness. They found the optimum insulation thickness as 2.3–10.0 cm for the outer wall according to different climatic regions. They determined that the fuel consumption of the insulated building decreased by 46.63%-53.46% compared to the uninsulated situation [18].

### 1.1. Central Heating Systems

Central heating systems are a system applied to meet the heating needs of buildings and living spaces. The heat energy produced by a common heating device is transferred to all volumes by one or more columns and heated to the radiators. As shown in Figure 1, these systems have types of multi-column central heating systems and single-column central heating systems according to the way they are applied.

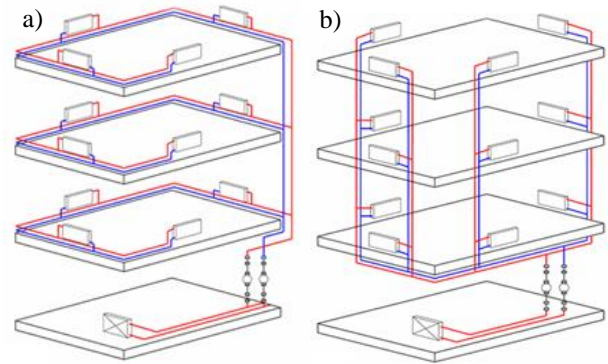


**Figure 1.** a) single column central heating system, b) multi-column central heating system [19]

According to the distribution type of water, which is the heat transfer fluid of central heating systems;

- Bottom-distribution-bottom-collection
- Top-distribution-bottom-collection
- Top-distribution-top-collection

It is examined in groups. Figure 2 shows the diagram of the central system with the bottom distribution-bottom collection and top distribution-bottom collection.

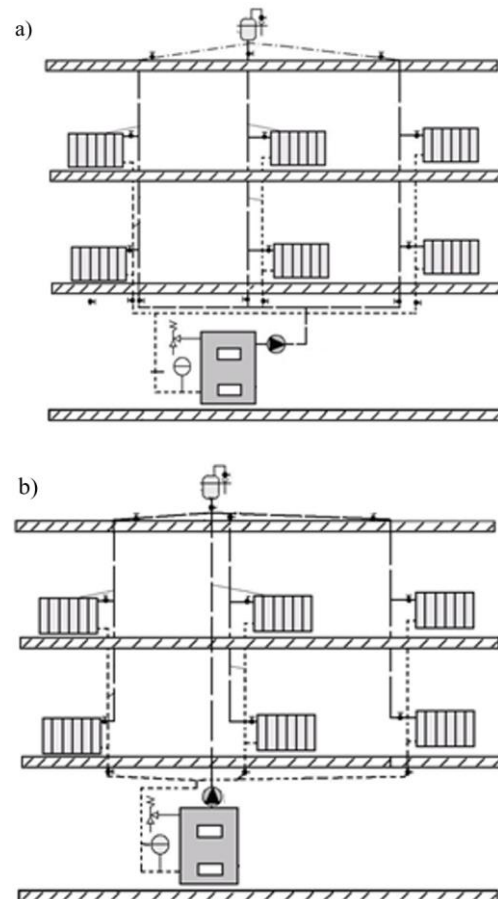


**Figure 2.** a) Bottom distribution-bottom collection, b) top distribution-bottom collection heating system [20]

### 1.2. Individual Heating Systems

Individual or individual heating systems are the type of heating system in which the heat energy of independent volumes is met separately. In Figure 3, floor heating and

combi boiler used in individual heating systems are shown. Individual heating systems are systems used for energy requirements below 40 kW [21]. These systems are the most used systems because of the easy measurability of the energy consumed in the houses.



**Figure 3.** Individual heating system devices a) Combi boiler [22], b) Floor heating [23]

Today, combi boilers are preferred instead of floor heating systems in individual heating systems. Combi boilers are classified as chimney combi boilers, hermetic combi boilers, semi-hermetic combi boilers, and condensing combi boilers. It is possible to save 17% on the fuel cost of the household by using a device that

works with condensation technology as the heating device in houses that are heated individually or with a combi boiler [24].

The advantages of combi boilers are that they can be used independently in houses, their emission values are low, they can meet both hot water and heating needs with the same device, and they are environmentally friendly. Combi boilers work in wide modulation ranges and prevent the stop-start problem that causes an increase in efficiency and a decrease in emissions. It can be adjusted by the electronic system of the combi boiler by determining the instantaneous energy needed and accordingly the air-fuel ratio. As a result of combustion with an optimum air-fuel ratio, high combustion efficiency, and low emission values can be obtained.

## 2. MATERIAL AND METHOD

In this study, the heat loss calculations of a building with a total heated area of 1080 m<sup>2</sup> were calculated by considering the temperature values of Kars province. The flats in the building are of standard type and consist of a living room, bedroom, living room, kitchen, children's room, and bathroom. The floor plan of the building is given in Figure 4.



**Figure 4.** Floor plan of the building

## 2.1. Features of the Building and the System to be Applied

The building examined in this study is located in the center of Kars and consists of 5 floors and 10 apartments, including the basement, ground, first and second floors. The floor height of each floor is 3m and the total height of the building excluding the basement is 10m. Condition and property information about the building is given in Table 1.

In the insulation of the building, extruded polyurethane foam (XPS) was used as 5 cm on the outer walls and 3 cm on the outside, between floors, and between independent sections. Considering Kars climatic conditions, -27 °C for Kars Center, windy zone, 3rd Climate Zone (TS 825) The building is a free-standing, reinforced concrete building in a windy zone.

**Table 1.** State property information of the building

City in which it is located	Kars, Center
TS825 zone of the building	Region 4
Outside temperature value	-27 °C
Building condition	Discrete order
Window type	Double glazed plastic joinery
Building height	12m
Floor height	3m
Number of floors	5 ( basement + 4 floors)

The building is insulated from the outside and the insulation material is 7cm extruded polystyrene foam (XPS). The outer walls are made of vertically perforated bricks in accordance with TS EN 771-1 with a thickness of 15 cm. The outer and inner surfaces are plaster made using 2 cm thick plaster. The cross-section of the outer walls of the building is shown in Figure 5. The heat transmission coefficients of the building components selected according to TS 825 are shown in Table 2.

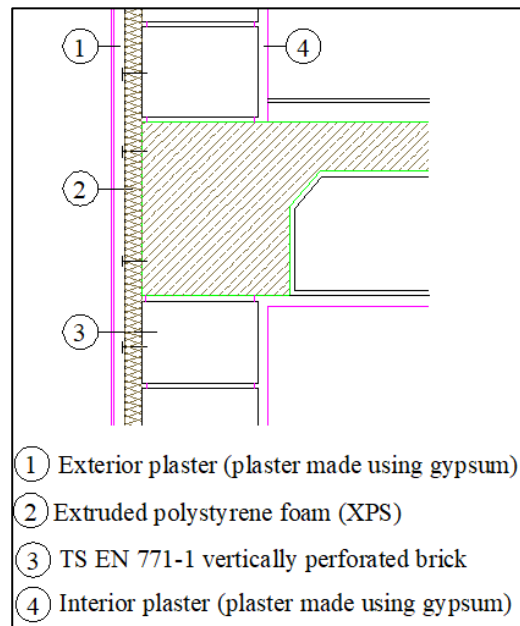


**Figure 5.** Cross section of the exterior walls of the building [25]

**Table 2.** Heat conduction of materials used in the exterior wall

Material	Thickness (m)	Heat Conduction coefficient (W/mK)	Density (kg/m <sup>3</sup> )
Interior plaster (plaster made using gypsum)	0.02	0.51	1200
TS EN 771-1 vertically perforated brick	0.15	0.5	1200
Extruded polystyrene foam (XPS)	0.07	0.03	25
Exterior plaster (plaster made using gypsum)	0.02	0.51	1200

Both the central heating system and the individual heating system have been applied as a system in the building. For the central heating system, a 90/70 °C hot water pump heating system with bottom distribution has been applied. The individual heating system, on the other hand, is provided by the energy produced by the combi boiler independently in each flat. Natural gas was used as fuel for both heating systems.

## 2.2. Calculation of Energy Need

TS 825 calculation method was used to calculate the heating load. The heat loss calculations are calculated by taking into account the heat losses on the walls, windows, doors, roof, and floor of the rooms of each flat, with the equations given in Equation 1 - 4 below, which consists of long calculation steps [26] It is shown in Table 3.

$$Q = q_i + q_s \quad (1)$$

$$q_i = q_o(1 + \%Z_D + \%Z_H) \quad (2)$$

$$q_o = kA\Delta T \quad (3)$$

$$q_s = \sum (al)RH\Delta T_e \quad (4)$$

Here,  $Q$  is the total heat loss,  $q_i$  is the incremental heat loss, and  $q_s$  is the air leakage heat loss.

In Equation 2,  $q_s$  non-increasing heat loss (W),  $Z_D$  combined increase coefficient (%),  $Z_H$  direction increase coefficient (%).

In Equation 3  $k$  heat transfer coefficient of building components (W/m<sup>2</sup> °C),

$A$  is the surface area of the building component (m<sup>2</sup>) and  $\Delta T$  is the indoor and outdoor temperature difference (°C). In Equation 4,  $l$  leakage gap perimeter (m),  $R$  the room feature (0.9),  $H$  is the layout status of the structure (Wh/m<sup>3</sup> °C) and  $Z$  shows the corner increment coefficient. Annual fuel consumption in heating systems is calculated using Equation 5 [27].

$$B_y = \frac{Q_{yul}}{H_u * \eta_k} \quad (5)$$

Here  $B_y$  is the annual fuel consumption amount ( $m^3$ ),  $Q_y$  annual heating energy requirement (kcal),  $H_u$  is the lower heating value of the fuel ( $kcal\ m^{-3}$ ),  $\eta_k$  is the boiler efficiency (%).

Annual fuel consumption cost is calculated using Equation 6 [28].

$$M_y = B_y * C_{yak} \quad (6)$$

Here,  $M_y$  shows the annual fuel cost (TL),  $B_y$  the amount of fuel consumed ( $m^3$ ) and the  $C_{yak}$  fuel unit price (TL/ $m^3$ ).

### 3. FINDINGS AND DISCUSSION

In addition to different heating methods, different heat sources are widely used for heating houses [29]. These are the central heating system and individual heating systems. In this study, these two types of heating, which are widely used in our country, were compared. For the study, considering Kars climatic conditions, heat loss calculation, heating energy need, calculation of heating devices, determination of heating system elements, calculation of annual fuel consumption, and cost calculation were made according to TS 825.

The heat losses of the building examined in the study, calculated according to the floors and flats of the building by Equations 1 - 4, are shown in Table 3.

**Table 3.** Heat loss of apartments

Floor	Home No	Calculated Heat Loss (W)	Selected Radiator Thermal Power (W)
Ground floor	Home 1	12643	12853
	Home 2	12483	12621
1st floor	Home 3	15710	16101
	Home 4	15779	16333
2nd floor	Home 5	15675	16217
	Home 6	15642	16333
3th floor	Home 7	15875	16333
	Home 8	15750	15985
Loft	Home 9	4663	4849
	Home 10	7112	7633

In order to meet the total energy requirement calculated according to the building's heat loss in Table 3, central and individual systems and system elements are examined separately. The comparison of the number of equipment to be used in each system, the capacities of the devices used, and the initial investment cost is shown in Table 4 and Table 5. In the cost calculation, the current prices of the devices are taken into account.

#### 3.1. Central System Elements and Device Selection

The hardware and equipment to be used in the central system were selected and determined according to the total energy requirement of the building. The properties, capacities, dimensions, and quantities of the system elements are shown in Table 4. In the cost calculation,

the current and real prices of the devices are taken into account.

**Table 4.** Equipment used in the central system

Device Name	Calculated Value	Calculated Device	Selected Device
Boiler (W)	135256	155544	197200
Expansion tank (L)	205	205	250
Chimney ( $cm^2$ )	1025.46	1025.46	1026
Circulation pump ( $m^3/h$ )	7.25	7.25	7.25
Patent black pipe, Aluminum foil pipe ins.	in various sizes	in various sizes	in various sizes
Strainer, Non-return valve			
Chimney valve, ball valve			
Radiator, Corner rad. valve, Rad. union			

#### 3.2. Individual System Device Selection

The equipment and equipment to be used in the individual system, which is another option to be used for the heating of the building, are also determined according to the total energy requirement. The properties, capacities, dimensions, and quantities of the system elements are shown in Table 5. In the cost calculation, the current and real prices of the devices are taken into account.

**Table 5.** Equipment used in the individual system

Device Name	Calculated Value	Calculated Device	Selected Device
Combi boiler (W)	13108-17284	13108-17284	24.000
Pex pipe	15mm	15mm	15mm
Pex pipe fittings	15mm	15mm	15mm
Flat collector	in various sizes	in various sizes	in various sizes
Radiator, corner rad. valve., Rad. union			

#### 3.3. Annual Fuel Consumption and Cost Calculation

Natural gas will be used as fuel in both systems to be compared for the heating of the building. Considering the annual total heating energy need, the annual fuel consumption was determined using Equation 5. The annual fuel consumption and annual fuel cost according to the annual heating energy requirement in the central system are shown in Table 6, and in the individual system, the annual fuel consumption and annual fuel cost according to the annual heating energy requirement per flat in the individual system are shown in Table 7.

Depending on the annual heating energy need of the building, the annual natural gas and annual fuel costs are calculated by considering Equation 5 and Equation 6, respectively.

**Table 6.** Annual fuel consumption and annual fuel cost according to the annual heating energy requirement in the central system

Annual Heating Max. Need, (W)	Annual Fuel Consumption By (m <sup>3</sup> )	Annual Fuel Cost My (TL)
374294372	35882	208115

**Table 7.** Annual fuel consumption and annual fuel cost according to the annual heating energy requirement per apartment in the individual system

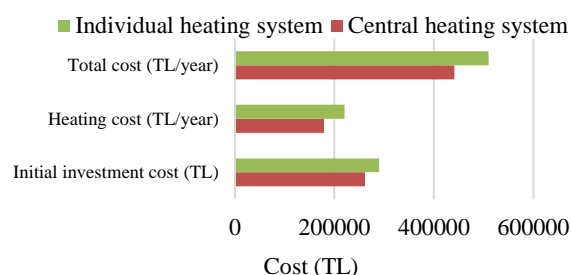
Floor	Home No	Annual Heating Max. Need (W)	Annual Fuel Consumption By (m <sup>3</sup> )	Annual Fuel Cost My (TL)
Ground floor	Home 1	36630480	4184	20920
	Home 2	35969280	4109	20543
1st floor	Home 3	45887280	5241	26207
	Home 4	46548480	5317	26585
2nd floor	Home 5	46217880	5279	26396
	Home 6	46548480	5317	26585
3th floor	Home 7	46548480	5317	26585
	Home 8	45556680	5204	26018
Loft	Home 9	13819080	1578	7892
	Home 10	21753480	2485	12424

Central and individual heating systems were compared in terms of initial investment cost. For this, the equipment to be used in both systems and their costs are taken into account. Table 4 shows the materials used for the central system and their quantities, and Table 5 shows the materials used for the individual system and their quantities. A comparison of the costs of central heating and individual heating systems is given in Table 8. After determining the annual fuel consumption calculated with Equation 5, the annual fuel consumption cost was found by using Equation 6.

**Table 8.** Costs of central heating and individual heating systems

Heating type	Initial investment cost (TL)	Natural gas consumption (m <sup>3</sup> /year)	Heating cost (TL/year)	Total cost (TL/year)
Central heating system	261687	35882	179409	441096
Individual heating system	289670	44031	220155	509825

As can be seen from the natural gas consumption and a cost table for the total heating of the building in Table 4 and the comparison in Figure 6, individual heating systems have higher costs than central heating systems in terms of both initial investment and heating cost. In this case, central heating systems are more advantageous in terms of the total cost.

**Figure 6.** Cost comparison of central heating system and individual heating systems

In terms of the number of pieces of equipment that makes up the system, central heating systems contain more elements than individual heating systems. Despite this, the high total costs of individual heating systems are due to the heating devices (combi) in individual heating systems.

In terms of labor time and labor cost, individual heating systems are shorter and less costly than central heating systems.

### 3. CONCLUSION

While residences constitute a large share of energy consumption, a significant portion of this energy need is obtained from fossil-based energy sources. Considering the price imbalance in fossil-based energy types and the damage of fuels to the environment, it becomes clear that energy savings and efficient devices should be used. For this reason, in this study, central and individual heating systems used in the heating of houses, which have a large share in energy consumption, are examined.

In this study, central and individual heating systems for heating a reinforced concrete building consisting of 5 floors and 10 flats in the center of Kars, which are located in the 4th Region according to TS825, are compared. In order to determine the heating energy need of the building, thermal insulation, and heat loss were calculated. TS825 method and limit values were taken into account in the calculation of thermal insulation and heat loss. When calculating the heat losses, the heat loss of each room is taken into account, and the total heat loss for the apartments and the building has been determined as 131,331 W. According to the energy needs of the building, the annual fuel consumption amount has been calculated as 35,882 m<sup>3</sup> for the central system, and 44,031 m<sup>3</sup> for the individual heating system, and the annual fuel consumption costs are calculated as 179,409 TL and 220,155 TL, respectively.

All devices and materials to be used for both systems are taken into account while calculating the cost. The initial investment costs for the central heating system and individual heating systems have been found to be 261,687 TL and 289,670 TL, respectively. While the total cost was found 441,096 TL for the central heating system, it has been found 508,825 TL for the individual heating system.

According to the values obtained as a result of the study;

- It has been observed that individual heating systems have higher costs than central heating systems in terms of both initial investment and heating cost.
- It has been determined that central heating systems are more advantageous in terms of initial investment cost, fuel consumption, and total cost.

Although the initial investment cost of individual heating systems is higher, it has been determined that central heating systems are generally preferred due to operational problems and independent operation, optional temperature control, and fuel cost concerns in individual heating systems.

## NOMENCLATURE

$A$	Area of the structure component [ $m^2$ ]
$a$	Unit gap leakage [ $m^3/m$ h]
$B_y$	Annual fuel consumption amount ( $m^3$ )
$c_p$	Specific heat of water [ $J/kg$ °C]
$C_{yak}$	Fuel unit price (TL/ $m^3$ )
$H$	Layout state of the building, adjacent and split [ $Wh/m^3$ °C]
$H_k$	Boiler efficiency (%)
$H_u$	Lower heating value of the fuel ( $kcal$ $m^{-3}$ )
$k$	Heat transfer coefficient of the building component [ $W/m^2$ °C]
$l$	Leakage gap perimeter [ $m$ ]
$Q$	Total heat loss of the room [ $W$ ]
$q_i$	Incremental heat loss [ $W$ ]
$q_s$	Air leak heat loss [ $W$ ]
$q_o$	Non-increasing heat loss [ $W$ ]
$Q_y$	Annual heating energy requirement ( $kcal$ )
$M_y$	Annual fuel cost (TL)
$R$	Room feature [0.9]
$Z_D$	Combined increment coefficient [%]
$Z_c$	Corner increment coefficient [1]
$Z_H$	Direction increment coefficient [%]
$\Delta T$	Indoor and outdoor temperature difference [°C]

## REFERENCES

- [1] Othan O, Omar MA. Bir hastane için iki farklı birleşik ısı ve güç sisteminin termo-ekonomik incelemesi. Gazi Üniversitesi Mühendislik Mimarlık Fakültesi Dergisi. 2023;38(3):1467-80.
- [2] Sinem I, Yavuz S. Investigation of biogas production potential from Livestock Manure by anaerobic digestion in Bingöl Province. Türk Doğa ve Fen Dergisi.11(1):116-22.
- [3] Öztürk D, Dener A. Power generation variation analysis of solar panels coated with TiO<sub>2</sub>. Türk Doğa ve Fen Dergisi.11(1):108-15.
- [4] Tırnık S. Hayvansal atıkların biyogaz üretim potansiyelinin hesaplanması: iğdır ili örneği. Journal of the Institute of Science and Technology. 2022;12(1):152-63.
- [5] Omar MA. Investigation of burners used in wall-hung combi-boilers: a comparative and cfd study. Environmental Engineering & Management Journal (EEMJ). 2022;21(12).
- [6] Omar MA, Altınışik K. Simulation of hydrogen production system with hybrid solar collector. International Journal of Hydrogen Energy. 2016;41(30):12836-41.
- [7] Terhan M, Özağdaş E, Omar MA. Ekonomizer, yoğunlaşmalı ekonomizer ve hava ön ısıtıcı tasarımları ile atık ısı geri kazanımının enerji ve ekonomik değerlendirilmesi. Gazi Üniversitesi Mühendislik Mimarlık Fakültesi Dergisi. 2023;38(4):2521-36.
- [8] Comaklı K, Terhan M. Energy and economic analysis of heat recovery from boiler exhaust flue gas. International Journal of Energy and Power Engineering. 2016;10(4):450-8.
- [9] Cockroft J, Cowie A, Samuel A, Strachan P. Potential energy savings achievable by zoned control of individual rooms in UK housing compared to standard central heating controls. Energy and Buildings. 2017;136:1-11.
- [10] Meng Z, Junqi Y, Anjun Z. Distributed model predictive control for central heating of high-rise residential buildings. Journal of Asian Architecture and Building Engineering. 2022:1-13.
- [11] Yürük M, Varyenli H, Martin K, Khanları A. Bireysel ısıtma sistemlerinde tesisat temizliğinin enerji verimliliği açısından deneysel olarak değerlendirilmesi. Politeknik Dergisi.1.
- [12] Omar MA, Altınışik K, Reşitoğlu İA. Kombiler için yarı küresel gözenekli metal matris yakıcının geliştirilmesi. Isı Bilimi ve Tekniği Dergisi. 2015;35(2):137-43.
- [13] Tahir MF, Haoyong C, Guangze H. Evaluating individual heating alternatives in integrated energy system by employing energy and exergy analysis. Energy. 2022;249:123753.
- [14] Pavlović B, Ivezić D, Živković M. State and perspective of individual household heating in Serbia: A survey-based study. Energy and Buildings. 2021;247:111128.
- [15] Zhang F. An individual household-based heating metering and charging management system for central heating in community residential buildings. International Journal of Heat and Technology. 2021;39(3):787-96.
- [16] Cho H-I, Cabrera D, Patel MK. Estimation of energy savings potential through hydraulic balancing of heating systems in buildings. Journal of Building Engineering. 2020;28:101030.
- [17] Saba F, Fericola V, Masoero MC, Abramo S. Experimental analysis of a heat cost allocation method for apartment buildings. Buildings. 2017;7(1):20.
- [18] Terhan M, Abak SS. Energy, exergy analysis and optimization of insulation thickness on buildings in a low-temperature district heating system. Journal of Thermal Engineering. 2023; 9 (1):161-178.
- [19] Isı Pay Ölçerler. EGE Danışmanlık Enerji Çözümleri. <http://www.egedanismanlik.com.tr/Enerji.html>. (Accessed:21.12.2022).
- [20] Şimşek E. Tesisat Teknolojisi. MEB-YÖK Program geliştirme projesi. [http://deneysan.com/Content/images/documents/ya-pi-tesisati\\_22028043.pdf](http://deneysan.com/Content/images/documents/ya-pi-tesisati_22028043.pdf). (Accessed:20.12.2022).
- [21] Küçükyalı R. Merkezi ve bireysel sistemlerde enerji tüketimi. Tesisat Mühendisliği Dergisi. 2007; 99:5-25.
- [22] Şık E. Doğal gaz yakıtlı ısıtma tesisatlarında emniyet ve yakıt tasarrufu sağlayacak otomatik kontrol düzeneğinin geliştirilmesi üzerine teorik ve deneysel araştırma: Trakya Üniversitesi Fen Bilimleri Enstitüsü; 2009.
- [23] T.C. Milli Eğitim Bakanlığı. Tesisat teknolojisi ve iklimlendirme. Kullanım sıcak su tesisatı. 2007 Ankara.

- [24] Omar MA, Altınışık K, Sertkaya AA, Adıgüzel N. Economic analysis of required heat energy for a residence by using condensing and conventional combi boiler. *Muğla Journal of Science and Technology*. 2016;2(1):38-42.
- [25] İzoder Derneği, Isı Yalıtımı. İzoder Yayınları. <http://www.izoder.org.tr>. (Accessed:11.12.2022).
- [26] Genceli, O. F., Parmaksızoğlu, İ. C., Kalorifer Tesisatı (7. Baskı), Makine Mühendisleri Odası, İstanbul, 2012
- [27] MMO. Kalorifer Tesisatı Proje Hazırlama Teknik Esasları. Yayın MMO/2001/259.
- [28] Yasemin O, Kırmacı V. Bartın ilinde kullanılan ısıtma sistemlerinin ekonomik ve çevresel etkilerinin incelenmesi. *Mühendislik ve Teknoloji Bilimleri Dergisi*. 2015;3(1):4-10.
- [29] Omar MA,. Konutların Isıtılmasında Merkezi ve Bireysel Isıtma Sistemlerinin Karşılaştırılması. 4. Uluslararası Mühendislik Ve Fen Bilimleri Kongreleri (ISPEC). 18-20 Ekim 2019 Ankara.

## Investigation Of Relative Story Shifts In Buildings With Projection Irregularities At Different Ratios

M. Zeki ÖZYURT<sup>1\*</sup> , Emir DEMİR<sup>2</sup> 

<sup>1</sup> Sakarya University, Engineering Faculty, Civil Engineering Department, Sakarya, Türkiye

<sup>2</sup> Sakarya University, Engineering Faculty, Civil Engineering Department, Sakarya, Türkiye

M. Zeki ÖZYURT ORCID No: 0000-0002-1593-4581

Emir DEMİR ORCID No: 0000-0002-9252-9651

\*Corresponding author: [ozyurt@sakarya.edu.tr](mailto:ozyurt@sakarya.edu.tr)

(Received: 25.01.2023, Accepted: 24.04.2023, Online Publication: 22.06.2023)

### Keywords

Types of  
Irregularity,  
Mode Superposition,  
Interstory Drift

**Abstract:** There are 3 major fault lines in our country, which are exposed to thousands of earthquakes every year, namely the North Anatolian Fault Zone and the East Anatolian Fault Zone. Therefore, earthquake effects are more important in terms of the structural behavior of the buildings built in our country. It is very important for building safety to design buildings as regularly as possible during the design phase. However, sometimes this is not possible for reasons such as architectural designs. In the study, 6 different models with the irregularity type of A3-Existence of Projections in the Plane and the symmetric reference model were analyzed according to Mode Superposition Method. The models analyzed in the study were modeled with the SAP2000 program. As a result of the analysis, the interstory drift performances of the models under the effect of earthquakes were examined. Comparisons were made in line with the results obtained from the analyzes and comments were made on the effect of structures with A3 irregularity type on the interstory drifts.

## Farklı Oranlarda Planda Çıkıntı Düzensizliğine Sahip Yapılarda Görelî Kat Ötelemelerinin İncelenmesi

### Anahtar Kelimeler

Düzensizlik Türleri,  
Mod Birleştirme  
Yöntemi,  
Görelî Kat  
Ötelemeleri

**Öz:** Her yıl binlerce deprem etkisine maruz kalan ülkemizde Kuzey Anadolu Fay Zonu ve Doğu Anadolu Fay Zonu olmak üzere 2 büyük fay zonu bulunmaktadır. Dolayısıyla ülkemizde yapılan yapıların yapısal davranışı açısından deprem etkilerinin önemi daha fazladır. Yapıların tasarım aşamasında olabildiğince düzenli olarak tasarlanması yapı güvenliği açısından çok önemlidir. Fakat bazen mimari tasarımlar gibi sebeplerle bu mümkün olmamaktadır. Çalışmada 2018 Türkiye Bina Deprem Yönetmeliğince açıklanan A3-Planda Çıkıntılar Bulunması düzensizlik türüne sahip 6 farklı modeli ve simetrik referans modeli mod birleştirme yöntemi ile analizi yapılmıştır. Çalışmada analizi yapılan modeller SAP2000 programından üç boyutlu olarak modellenmiştir. Analizler sonucu modellerin deprem etkisi altında yapılan görelî kat ötelemeleri performansları incelenmiştir. Analizlerden elde edilen sonuçlar doğrultusunda karşılaştırmalar yapıp A3 düzensizlik türüne sahip yapıların görelî kat ötelemeleri üzerindeki etkisi hakkında yorum yapılmıştır.

### 1. INTRODUCTION

Due to the location of Turkey, the damage to the buildings are mainly due to earthquakes. The effect of earthquake forces varies according to the characteristics of the structure. Therefore, while the structures are being designed, the regularity of the structural carrier system is of great importance in terms of any load transfer. For

this reason, the issue of irregularities is discussed in the relevant section of TBDY-2018 (Turkish Building Earthquake Code). These irregularities are examined under two headings as plan and vertical irregularities. In the models examined in the study, the presence of protrusions in the A3 plan, which is explained under the title of irregularity type in the plan, the effect of the irregularity type on the structure was examined.



In the study, 7 different models were designed as R (reference), A, B, C, D, E and F type. The reference model, the R-type model, has a symmetrical form, and the other 6 models have projections in the plan. In all models, ground story height is 5 m and normal story height is 3 m. The local soil class is taken from ZC.

In order to increase the building safety in earthquake resistant building design, some limitations were introduced in TBDY-2018 (2018 Turkish Building Earthquake Code). If there is no flexible joint or any connection between the column and the wall, the relative storey drift value cannot be greater than  $0.008\kappa$ . If the column and wall are independent of the frame, this value cannot be greater than  $0.016\kappa$ . Since the structural system examined in the study is reinforced concrete, the value of  $\kappa$  is taken as 1. [1]

## 2. PROJECTIONS IN THE PLAN

The structures in which the horizontal and vertical load effects on the structure are not transferred to the foundation through the carrier system in a regular manner are called irregular structures. As a result of the studies, it has been seen that regular structures are more effective than irregular structures under the effect of earthquakes. For this reason, some restrictions have been introduced for irregular structures in the regulation. These limitations were first defined in DBYBHY-2007 (Regulation on Buildings to be Constructed in Earthquake Zones) and entered into force. In TBDY-2018 (Turkish Building Earthquake Code), the regulation updated in 2018, no changes were made regarding irregularities. It is defined under the title of Irregular Buildings Under the Effect of Earthquake in Section 3.6 of TBDY-2018 (Turkish Building Earthquake Code). It has been examined under two sub-headings as irregularities in the plan and irregularities in the vertical. Within the scope of this study, A1 and A3, which are irregularities in the plan, only B2 irregularities among vertical irregularities will be examined. [2] [3][4]

### 2.1. Irregularities In The Plan

According to TBDY-2018 (2018 Turkish Building Earthquake Code), plan irregularities consist of 3 types: A1 torsional irregularity, A2 slab discontinuities, and A3 projections.

#### 2.1.1. A1 Torsional Irregularity

If the load-bearing system of the buildings is not made symmetrical, it will cause the rigidity center of the structure and the center of gravity not to coincide. Therefore, while the horizontal earthquake forces act on the rhythm center of the structure, torsion occurs around the vertical axis passing through the center of gravity of the structure. Torsion condition causes serious damage to structures under the effect of earthquake. The regulation brought limitations in these cases and enabled the buildings to be designed more safely. [3][5]

In the 2018 Turkish Building Earthquake Code, it is defined as "The case where the Torsional Irregularity Coefficient  $\eta_{bi}$ , which expresses the ratio of the maximum relative story drift at any story to the average relative drift in the same direction at that story, is greater than 1.2 for any of the two perpendicular earthquake directions".[1]

$$\eta_{bi} = (\Delta i^{(X)})_{max} / (\Delta i^{(X)})_{avr} > 1.2 \quad (1)$$

At the same time, it was emphasized that the calculation of the relative storey drifts,  $\pm 5\%$  additional eccentricity effects should be taken into account in the regulation. [3] In Figure 1, "The torsional irregularity situation" in TBDY 2018 is expressed.

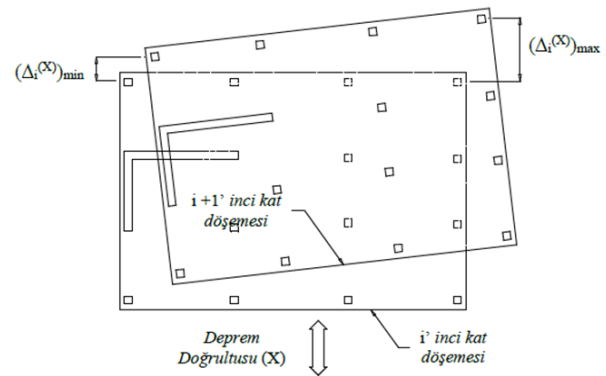


Figure 1. Torsional irregularity condition

$$(\Delta i^{(X)})_{avr} = 1/2[(\Delta i^{(X)})_{max} + (\Delta i^{(X)})_{min}] \quad (2)$$

$$\eta_{bi} = (\Delta i^{(X)})_{max} / (\Delta i^{(X)})_{avr} \quad (3)$$

$$\eta_{bi} > 1.2 \quad (4)$$

#### 2.1.2 A3 Irregularities In The Plan

In TBDY-2018 (Turkish Building Earthquake Code), it is defined as "the situation where both the dimensions of the protruding parts in the two perpendicular directions in the building story plans are greater than 20% of the total plan dimensions of the building in the same directions". [1] In Figure 2, "The case of protrusions in the A3 plan" in TBDY 2018 is shown.

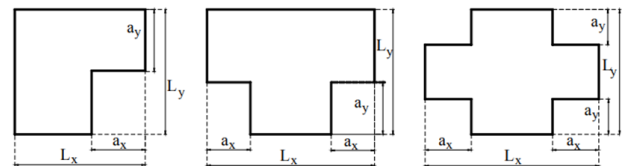


Figure 2. A3 case of protrusions in the plan

There may sometimes be protrusions in the building story plans due to the land form on which the buildings sit or due to the architectural design. These protrusions cause irregularities in the structure. In order to prevent such irregularities, the building form can be made more suitable by arranging the joints appropriately. [6] [7] [8]

## 2.2 Vertical Irregularities

According to TBDY-2018 (Turkish Building Earthquake Code), vertical irregularities consist of 3 types: B1 strength irregularity between adjacent stories, B2 stiffness irregularity between adjacent stories and B3 discontinuity of vertical elements of the carrier system.

### 2.2.1 B2 Stiffness Irregularity Between Adjacent Stories (Soft Story)

In TBDY-2018 (Turkish Building Earthquake Code), "For either of two perpendicular earthquake directions, excluding basement stories, the mean relative story drift ratio at any  $i$ th story is divided by the average relative story drift ratio at an upper or a lower storey, the Stiffness Irregularity Coefficient  $\eta_{ki}$ ". It is defined as "the condition of more than 2.0". [1]

$$\eta_{ki} = (\Delta i^{(x)} / h_i)_{avr} / (\Delta i + 1^{(x)} / h_{i+1})_{avr} > 2.0 \quad (5)$$

or

$$\eta_{ki} = (\Delta i^{(x)} / h_i)_{avr} / (\Delta i - 1^{(x)} / h_{i-1})_{avr} > 2.0$$

For this type of irregularity, the maximum height of the structure in the regulation. 28 m is allowed. In cases where this limit value is exceeded, it is not allowed to use the equivalent earthquake load method as the calculation method. [2]

## 3. MATERIALS AND METHOD

### 3.1 Mod Superposition Method

According to TBDY-2018 (Turkish Building Earthquake Code), the maximum values of the response magnitudes in each vibration mode taken into consideration are calculated by the modal calculation method by using the earthquake design spectrum for a given earthquake direction in the mode coupling method. The largest modal behavior magnitudes calculated for enough vibration modes but not simultaneous are then statistically combined to obtain approximate values of the largest behavior sizes. There are two types of mod merge rules. These are Perfect Quadratic Combination (TKB – CQC) and Square Root of Sum of Squares (KTKK – SRSS).

The sum of the base shear force modal effective masses calculated for all modes in both earthquake directions shall not be less than 95% of the total mass of the building. Mods that contribute less than 3% to the build will not be considered. In the three-dimensional calculation, the direction with a sufficient number of vibration modes will be taken into account. [1]

### 3.2 Displacement and Interstorey Drift

The movement of vertical carrier systems in the x or y direction is called displacement. The displacement of a vertical carrier system element at any Story relative to the vertical carrier system element at an upper or a lower

story is called the relative storey drift. In this study, the relative storey drifts of the structures in the x and y directions will be examined separately. In Figure 3, the interstorey drifts occurring at each storey are expressed visually.

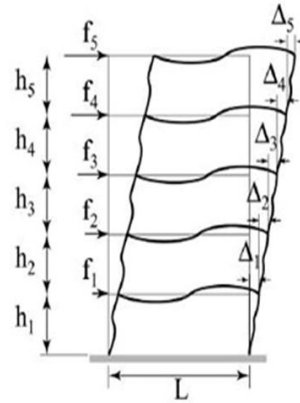


Figure 3. Relative story drift on each story

Earthquake resistant building design is of serious importance for countries like our country, which are affected by thousands of earthquakes every year. Limitations are defined in the 2018 Turkish Building Earthquake Code, which is used in our country, for the relative story offsets. These limitations are of vital importance in terms of protecting the safety of the building. [9]

It is limited to  $\Delta \leq 0.02$  in TDY-2007 (Turkish Earthquake Code). However, changes were made in the regulation that entered into force in 2018. In TBDY-2018 (Turkish Building Earthquake Code), these limitations were examined for two different situations, depending on whether the wall is adjacent to the column and whether it is separate. If the walls are adjacent to the column, the limit value has been reduced since it will prevent the vertical carrier systems from making any drifts. The ratio of the structural system behavior coefficient to the building importance factor multiplied by the relative storey drift is called the effective relative storey drift ( $\delta$ ).

$$\delta = (R/I) \times \Delta \quad (6)$$

$$\lambda = DD3 / DD2 \quad (7)$$

Flexible joint between the column and wall;

$$\lambda \times \delta_i / h_i \leq 0,016 \kappa \quad (8)$$

Lack of flexible joint between the column and wall;

$$\lambda \times \delta_i / h_i \leq 0,008 \kappa \quad (9)$$

$\kappa$  value is taken as 1 for reinforced concrete structures and 0,5 for steel structures [1] [4] [10]. In Figure 4, the flexible joint application between the vertical carrier systems and the wall is expressed visually.

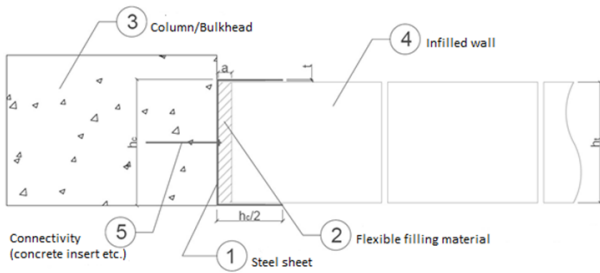


**Figure 4.** Flexible joint application between vertical carrier systems and the wall [10]

#### 4. NUMERICAL STUDY

The structure examined in the study consists of a reinforced concrete frame system with a total of 5 stories consisting of ground floor and 4 normal stories. The purpose of use of the building is office and residence, and the number of stories has been chosen as 5, since such structures are built with a maximum of 5 stories in Turkey. In the study, a total of 7 different models, namely R type (reference), A type, B type, C type, D type, E type and F type, were examined. At the same time, since it is the most common situation in workplace and residential type buildings, the ground story height of the examined buildings was chosen as 5 m and the other story heights as 3 m. In the study, analyzes were made by choosing the most common ZC soil class in our country. The distances between the axles are 5 m and the width and length of the structure is 30 m. The story system is beamed story running in two directions. Beams are designed as 300mm x 500mm columns 600mm x 60mm. Story thickness is 120mm. C30/37 concrete class was used as concrete material. The structure is in the Izmit region, at latitude  $40,760019^\circ$  and longitude  $29,934446^\circ$ . In this study, the projection ratio in the X-direction plane is shown as  $O_x$ , and the projection ratio in the Y-direction plane is shown as  $O_y$ . The earthquake level of the building was taken as DD-2. Modeling and analyzes in the study were made with the help of the SAP2000 program. [11] [12] The xy plane view of the analyzed models are given in Figure 5a-5g.

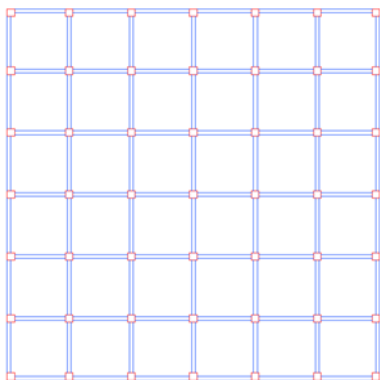


**Figure 5a.** Type R (Reference) Story Plan  
 $O_x = 0 / O_y = 0$

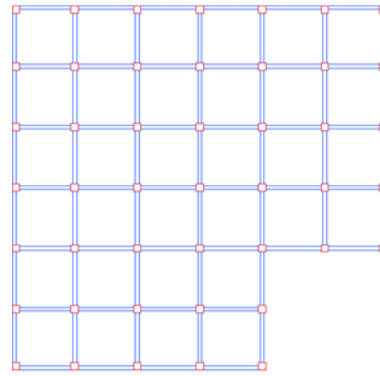


**Figure 5b.** Type A Story Plan  
 $O_x = 0,33 / O_y = 0,33$

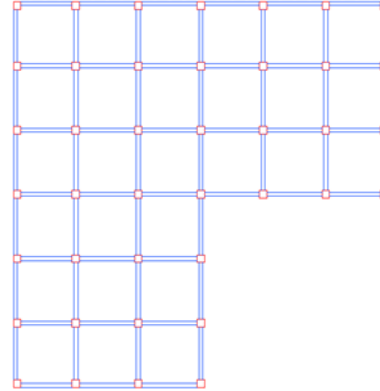


**Figure 5c.** Type B Story Plan  
 $O_x = 0,50 / O_y = 0,50$

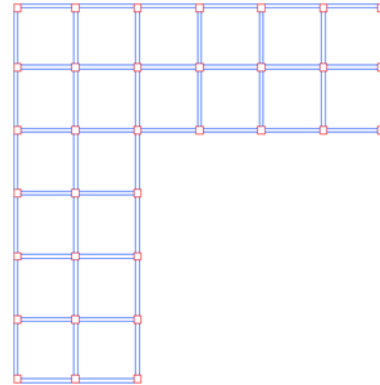


**Figure 5d.** Type C Story Plan  
 $O_x = 0,67 / O_y = 0,67$

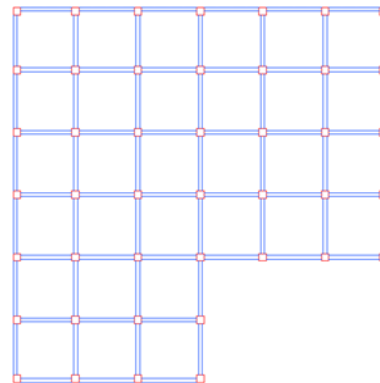


**Figure 5e.** Type D Story Plan  
 $O_x = 0,50 / O_y = 0,33$

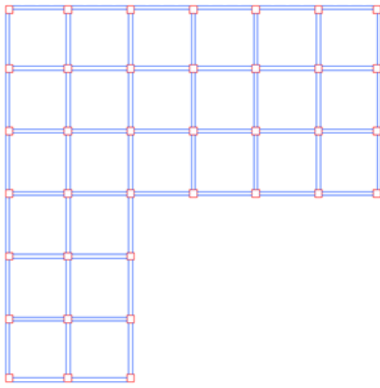


**Figure 5f.** Type E Story Plan  
Ox = 0,67 / Oy = 0,50

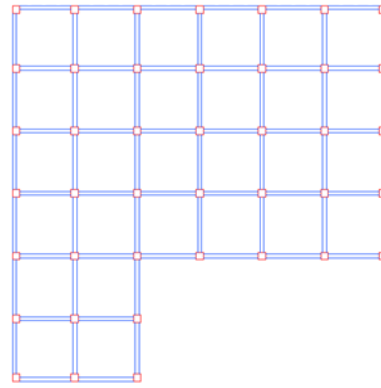


**Figure 5g.** Type F Story Plan  
Ox = 0,67 / Oy = 0,33

### 5. RESULTS

In Table 1, the drifts made at each story for the 1st and the 2nd mode in the x and y directions of the 7 models analyzed are shown. Ux represents the displacements in the x direction, Uy represents the displacements in the y direction. Units are taken in mm.[13] [14] [15]

**Table 1.** Displacement of the buildings on each story

		Type R	Type R	Type A	Type A	Type B	Type B	Type C	Type C	Type D	Type D	Type E	Type E	Type F	Type F
	Stories	Ux	Uy	Ux	Uy	Ux	Uy	Ux	Uy	Ux	Uy	Ux	Uy	Ux	Uy
RX	5	45,61	18,0	44,57	17,35	43,21	16,73	40,16	16,02	44,24	17,10	42,43	16,12	43,95	16,81
RX	4	40,61	16,0	39,67	15,46	38,43	14,90	35,67	14,23	39,37	15,24	37,73	14,34	39,11	14,97
RX	3	33,50	13,2	32,70	12,77	31,66	12,30	29,33	11,71	32,45	12,58	31,07	11,82	32,23	12,36
RX	2	24,31	9,67	23,71	9,29	22,94	8,93	21,2	8,46	23,53	9,15	22,51	8,57	23,37	8,98
RX	1	13,67	5,46	13,31	5,23	12,86	5,01	11,85	4,72	13,21	5,14	12,61	4,8	13,12	5,04
RX	0	0,00	0,00	0,00	0,00	0,00	0,00	0,00	0,00	0,00	0,00	0,00	0,00	0,00	0,00
RY	5	18,0	45,6	17,35	44,57	16,73	43,21	16,02	40,16	17,14	43,89	16,58	41,35	17,05	42,87
RY	4	16,06	40,6	15,46	39,67	14,9	38,43	14,23	35,67	15,27	39,05	14,76	36,76	15,19	38,12
RY	3	13,28	33,5	12,7	32,7	12,3	31,66	11,71	29,33	12,61	32,18	12,17	30,25	12,55	31,4
RY	2	9,67	24,3	9,29	23,7	8,93	22,94	8,46	21,2	9,17	23,33	8,83	21,89	9,11	22,74
RY	1	5,46	13,6	5,23	13,31	5,01	12,86	4,72	11,85	5,16	13,09	4,94	12,25	5,12	12,74
RY	0	0,00	0,00	0,00	0,00	0,00	0,00	0,00	0,00	0,00	0,00	0,00	0,00	0,00	0,00

In Figure 6-7, the story drifts of the analyzed models are shown graphically.

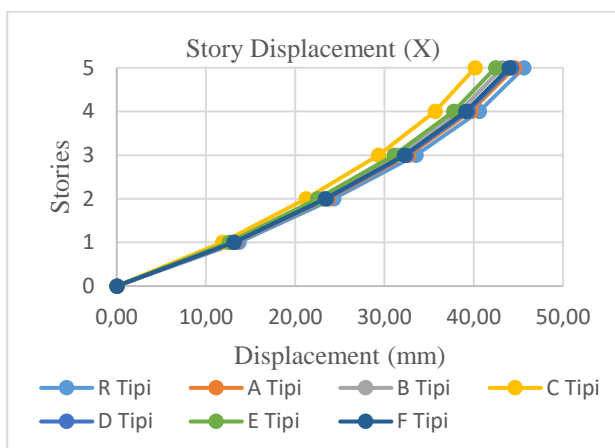


**Figure 6.** Story drifts of the analyzed seven models (X)

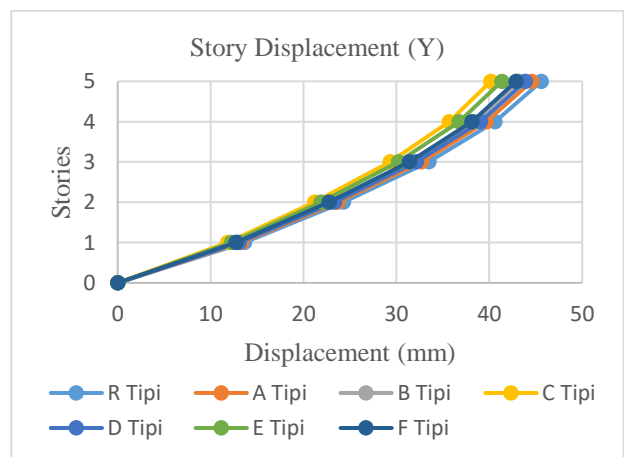


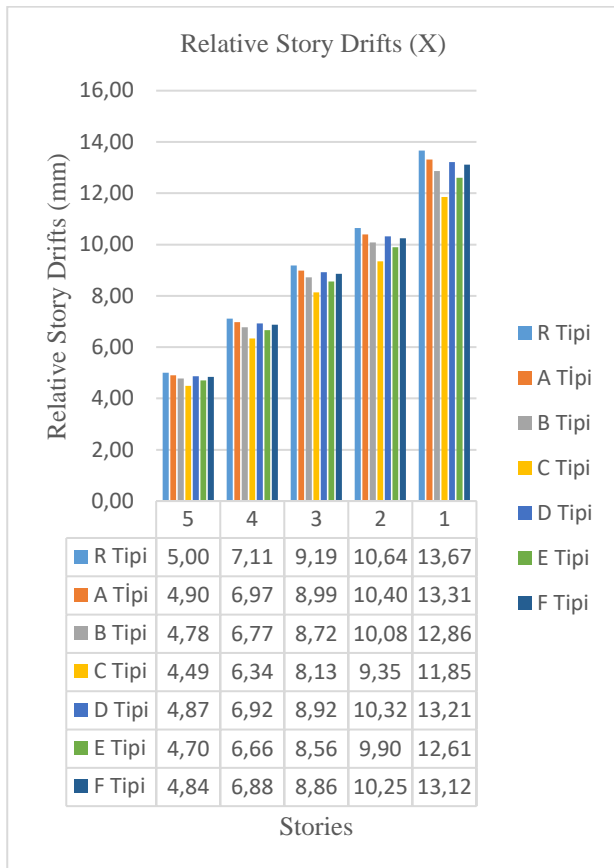
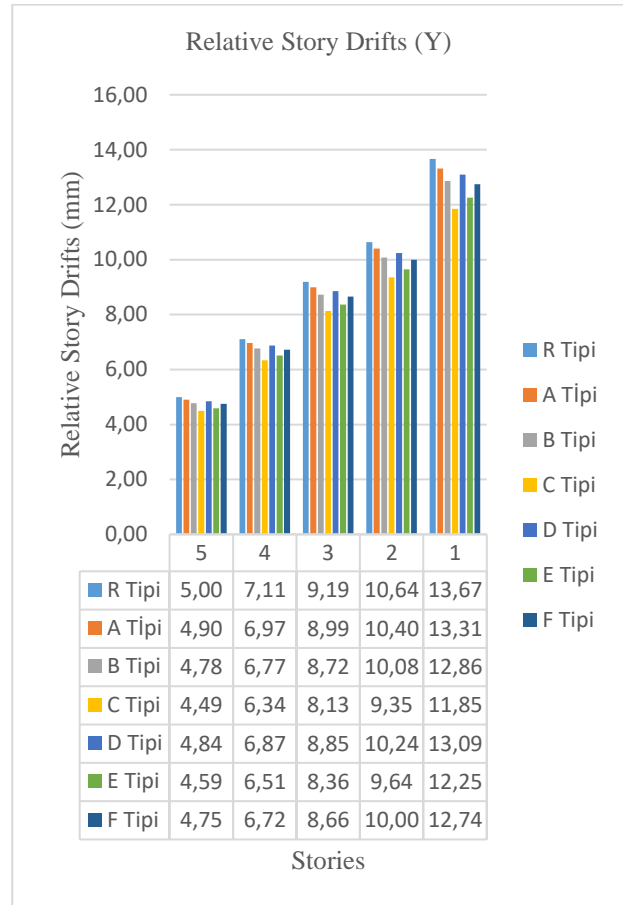
**Figure 7.** Story drifts of the seven models (Y)

The results of the relative story drifts obtained as a result of the analyzes made with the Mode Combination Method are shown in Table 2. [15] [16]

**Table 2.** Relative story drifts of the analyzed seven models

		Type R	Type R	Type A	Type A	Type B	Type B	Type C	Type C	Type D	Type D	Type E	Type E	Type F	Type F
	Stories	Ux	Uy	Ux	Uy	Ux	Uy	Ux	Uy	Ux	Uy	Ux	Uy	Ux	Uy
RX	5	5,00	1,94	4,9	1,89	4,78	1,83	4,49	1,79	4,87	1,86	4,70	1,78	4,84	1,84
RX	4	7,11	2,78	6,97	2,69	6,77	2,60	6,34	2,52	6,92	2,66	6,66	2,52	6,88	2,61
RX	3	9,19	3,61	8,99	3,48	8,72	3,37	8,13	3,25	8,92	3,43	8,56	3,25	8,86	3,38
RX	2	10,64	4,21	10,4	4,06	10,08	3,92	9,35	3,74	10,32	4,01	9,90	3,77	10,25	3,94
RX	1	13,67	5,46	13,31	5,23	12,86	5,01	11,85	4,72	13,21	5,14	12,61	4,80	13,12	5,04
RX	0	0,00	0,00	0,00	0,00	0,00	0,00	0,00	0,00	0,00	0,00	0,00	0,00	0,00	0,00
RY	5	1,94	5,00	1,89	4,9	1,83	4,78	1,79	4,49	1,87	4,84	1,82	4,59	1,86	4,75
RY	4	2,78	7,11	2,69	6,97	2,60	6,77	2,52	6,34	2,66	6,87	2,59	6,51	2,64	6,72
RY	3	3,61	9,19	3,48	8,99	3,37	8,72	3,25	8,13	3,44	8,85	3,34	8,36	3,44	8,66
RY	2	4,21	10,64	4,06	10,4	3,92	10,08	3,74	9,35	4,01	10,24	3,89	9,64	3,99	10,00
RY	1	5,46	13,67	5,23	13,31	5,01	12,86	4,72	11,85	5,16	13,09	4,94	12,25	5,12	12,74
RY	0	0,00	0,00	0,00	0,00	0,00	0,00	0,00	0,00	0,00	0,00	0,00	0,00	0,00	0,00

In Figure 8-9, the interstorey drifts of the seven models analyzed according to the storeys are given in a table.

**Figure 8.** Interstorey drifts of the seven models (X)**Figure 9.** Interstorey drifts of the seven models (Y)

#### 4. CONCLUSION

Since the R, A, B and C type models are symmetrical in plan in x and y directions in terms of projection ratio, it is observed that the storey drifts occurring in the x and y directions are the same.

In the R, A, B and C type models, it was observed that the peak displacement decreases due to the decrease in the structure weight as the A3 irregularity type coefficients  $O_x$  ( $a_x/L_x$ ) and  $O_y$  ( $a_y/L_y$ ) increase. It is seen that the coefficient of irregularity increased by 50 % between the type A model and the type B model, while the story drift decreased by 3.14 %. Similarly, between the A type and C type models, although the irregularity coefficient increased by 100 %, the story drift decreased by 9.9 %.

When the E and F type models are compared, the coefficient of A3 irregularity type in the x direction is the same, and the A3 irregularity type coefficient in the y direction  $O_y$  Considering that it is 0.50 in the E type and 0,33 in the F type, it is seen that the peak displacement in the F type model is higher than the peak displacement in the E type model has been observed. It is seen that while the irregularity coefficient decreased by 34% between the type E model and the type F model, the story drift decreased by 2.45%.

When the D and F type models are compared, the coefficient of irregularity type  $O_y$  in the y direction is the same for both models, and the coefficient of irregularity type  $O_x$  in the x direction is  $O_x$ , 0.50 in the D type model and 0.67 in the F type model, the displacement value at the apex is in the F type observed to be less. It is seen that the coefficient of irregularity between the type D model and the type F model increased by 34%, while the story drift decreased by 2.32%.

When the results obtained in the study are examined, it is observed that the structure period decreases as the A3 type irregularity coefficient increases. It is seen that the period value decreased by 1.05% despite the 50% increase in the irregularity coefficient between the type A model and the type B model. Moreover; It is seen that the period value decreased by 2.84%, despite the 100% increase in the irregularity coefficient between the type A and type C models.

On the other hand; As the structure weight decreases, the result is that the structure period decreases. For example, between the type R model and the type A model, although the structure weight decreases by 11.11%, the period value decreases by 0.73%. Similarly; Between type R and type A models, the structure weight decreases by 16.67%, whereas the period value decreases by 1.05%.

Regardless of whether the structure is symmetrical or asymmetrical in terms of projection ratio in plan, it is understood that the apex displacement of the structure decreases due to the increase in the A3 type irregularity coefficient ( $O_x$  and  $O_y$ ) and accordingly the decrease in the weight of the structure. In this respect, it was seen that the decrease in the weight of the structures over the displacements of the structures was more decisive than the increase in the A3 type irregularity coefficient ( $O_x$  and  $O_y$ ). It has been observed that the increase in the A3 type irregularity coefficient and the decrease in the structure weight are serious factors in the decrease in the structure period.

## REFERENCES

- [1] Türkiye Bina Deprem Yönetmeliği (TBDY-2018). 2018. T.C. Resmi Gazete; 30364.
- [2] Şimşek F. 2020. A3 Türü Düzensizliğw Sahip Betonarme Bir Yapının DBYBHY-2007 ve TBDY-2018 Esaslarına Göre İncelenmesi, İstanbul Teknik Üniversitesi, İstanbul.
- [3] <https://volkanatabey.com.tr/yapida-duzensizlik-durumlari-tbdy-2018/>
- [4] Deprem Bölgelerinde Yapılacak Binalar Hakkında Yönetmelik (DBYBHY-2007), Bayındırlık ve İskân Bakanlığı, Ankara.
- [5] <https://opustasarim.com/blog-bilgilendirme/f/yap%C4%B1-d%C3%BCzensizlikleri>
- [6] Ercömert M. 2007. A2 VE A3 Yapısal Düzensizliklerinin Çok Katlı Yapıların Deprem Davranışına Etkisi, Fırat Üniversitesi, Fen Bilimleri Enstitüsü, Elazığ.
- [7] <https://insapedia.com/turkiye-bina-deprem-yonetmeligi-a3-planda-cikintilar-bulunmasi>
- [8] Ulucan Z. Ç. Alyamaç K. E. 2008. A3 Düzensizliğine Sahip Yapıların Doğrusal Olmayan Kat Kesme Kuvvetlerinin İncelenmesi, Fırat Üniversitesi, Mühendislik Fakültesi, Elazığ.
- [9] Zhou, J., Bu, G.B., Li., K.N., 2012. Calculation Methods for Inter-Story Drifts of Building Structures, 15th World Conf. Earthq. Eng., no. 3, p. 7.
- [10] <https://help.idecad.com.tr/ideCAD/goereli-kat-oetelemelerin-sinirlendirilmesi>
- [11] CSI SAP2000 v22.0.0, "Integrated Finite Element Analysis and Design of Structures", Computers & Structures, Inc, Berkeley, California.
- [12] <https://tdth.afad.gov.tr>, Türkiye Deprem Tehlikesi Haritaları, Afad.
- [13] Çamyar H. 2009. Çerçevesiz Taşıyıcı Sistemlerde Düşeydeki Düzensizliklerin İncelenmesi, Sakarya Üniversitesi, Fen Bilimleri Enstitüsü, Sakarya.
- [14] Gürçay G. Manafidzaji K. 2021. Aegean 2nd International Applied Sciences Congress, İzmir, Turkey.
- [15] Arslan S. 2007. Betonarme Bim-nalarda Döşeme Boşluklarının Taşıyıcı Sistem Davranışlarına Etkileri, İstanbul Teknik Üniversitesi, Fen Bilimleri Enstitüsü, İstanbul.
- [16] Uysal Y. Aksoylu C. Arslan M. H. 2022. Betonarme Çerçevesiz Binaların Tasarımında Kullanılan Sonlu Eleman Programlarının TBDY-2019'da Yer Alan Periyot Taban Kesme Kuvveti ve Göreli Kat Ötelemesi Bağlamında Değerlendirilmesi, Kırıkkale Üniversitesi, Mühendislik Fakültesi, Kırıkkale.
- [17] Nowbahari F. A. 2021. Burulma Düzensizliği Bulunan Çok Katlı Çelik Çelik Yapıların 2018 Deprem Yönetmeliğine Göre Analiz ve Tasarımı, Sakarya Üniversitesi, Fen Bilimleri Enstitüsü, Sakarya.

## Investigation of Some Biological Properties of Propolis in Hawthorn Vinegar Extract

Büşra BILDIR<sup>1</sup> , Zeynep DEMİRKAN<sup>2</sup> , Bülent KAYA<sup>3\*</sup> , Fatma CAF<sup>4</sup> 

<sup>1</sup>Department of Nutrition and Dietetics, Faculty of Health Sciences, Bingöl University, Bingöl, Türkiye

<sup>2</sup>Department of Bee and Bee Products, Institute of Sciences, Bingöl University, Bingöl, Türkiye

<sup>3</sup>Department of Molecular Biology and Genetics, Faculty of Sciences and Arts, Bingöl University, Bingöl, Türkiye

<sup>4</sup>Department of Veterinary, Vocational School of Food, Agriculture and Livestock, Bingöl University, Bingöl, Türkiye

Büşra BILDIR ORCID No: 0000-0002-5631-1946

Zeynep DEMİRKAN ORCID No: 0000-0002-8101-8194

Bülent KAYA ORCID No: 0000-0002-1216-6441

Fatma CAF ORCID No: 0000-0002-0363-4848

\*Corresponding author: [bkaya@bingol.edu.tr](mailto:bkaya@bingol.edu.tr)

(Received: 8.12.2022, Accepted: 25.04.2023, Online Publication: 22.06.2023)

### Keywords

Propolis,  
Hawthorn  
Vinegar,  
Antioxidant,  
Phenolic,  
Flavonoid

**Abstract:** With the determination of the biological activity of different components in the chemistry of propolis, its importance has increased day by day and its use in the field of integrative medicine has become widespread. Propolis is not used in its crude form due to its physical properties, it has to be extracted. The type of solvent used in the extraction process is quite important for the efficiency of the biological activity of propolis. Solvents commonly used in propolis extraction; are water, ethanol, and methanol. Besides being quite easy to extract propolis components using ethanol; extraction of propolis with ethanol creates a usage limit for children, pregnant women, and Muslim people that don't use alcohol. The limited use of ethanol and the fact that it has some harm to health have led researchers to search for different types of solvents. As a result of this research, vegetable oils, and various kinds of vinegar have started to be in the literature as alternative solvents. In our study, the vinegar of hawthorn fruit, which is rich in flavonoids and has been used in traditional medicine for many years, was used in the extraction of propolis. The solubility of propolis in hawthorn vinegar was investigated in terms of its physicochemical properties (pH, titratable acidity, brix, and color) and bioactive properties (phenolic, flavonoid contents, and antioxidant activity). As a result of the investigation, it was observed that the addition of propolis to hawthorn vinegar caused changes in the physicochemical properties of vinegar at an acceptable level for the consumer and increased its bioactive properties. It is thought that propolis-added hawthorn vinegar will provide functionality in dishes where vinegar is used today, in salads, and even in foodstuffs such as brine and pickles.

## Propolisin Alıç Sirkesi Ekstraktında Bazı Biyolojik Özelliklerinin İncelenmesi

### Anahtar

### Kelimeler

Propolis,  
Alıç Sirkesi,  
Antioksidan,  
Fenolik,  
Flavonoid

**Öz:** Propolisin yapısındaki farklı bileşenlerin biyolojik aktivitesinin belirlenmesiyle, önemi gün geçtikçe artmış ve tamamlayıcı tıp alanında kullanımı yaygınlaşmıştır. Propolis fiziksel özelliklerinden dolayı ham halde kullanılamamakta, ekstraksiyon işleminden geçirilmesi gerekmektedir. Ekstraksiyon işleminde kullanılan çözücü tipi, propolisin biyolojik aktivitesinin etkinliği açısından oldukça önemlidir. Propolis ekstraksiyonunda yaygın olarak kullanılan çözücüler; su, etanol ve metanol olarak gösterilebilir. Etanol kullanarak propolis bileşenlerinin ekstraksiyonu oldukça kolay olmasının yanı sıra; propolisin etanol ile ekstraksiyonu çocuklar, hamileler ve alkol kullanmayan müslümanlar için kullanım sınırı oluşturmaktadır. Etanolün sınırlı dozda kullanımı ve sağlığa bazı zararlarının olması, araştırmacıları farklı çözücü tipleri aramaya yöneltmiştir. Bu araştırmalar sonucunda alternatif çözücüler olarak, bitkisel yağlar ve çeşitli sirkeler literatürde yer almaya başlamıştır. Çalışmamızda propolisin ekstraksiyonunda, flavonoidler bakımından zengin ve özellikle geleneksel tıp alanında uzun yıllardır kullanılan bir meyve olan alıç meyvesinin sirkesi kullanılmıştır. Alıç sirkesinde propolisin çözünürlüğü, fizikokimyasal özellikler

(pH, titrasyon asitliği, %briks ve renk) ve biyoaktif özellikler (fenolik ve flavonoid içerikleri ile antioksidan aktivite) açısından araştırılmıştır. Araştırma sonucunda alç sirkesine propolis ilavesinin sirkenin fizikokimyasal özelliklerinde tüketici için kabul edilebilir düzeyde değişikliğe neden olduğu ve biyoaktif özelliklerini arttırdığı gözlemlendi. Propolis katkılı alç sirkесinin; günümüzde sirkenin kullanıldığı yemeklerde, salata ve hatta salamura, turşu gibi gıda maddelerinin yapımında fonksiyonellik sağlayacağı düşünülmektedir.

## 1. INTRODUCTION

Propolis is a bee product in colors ranging from light yellow to dark brown, formed by the honey bee (*Apis mellifera*) combining resinous substances collected from different trees and plants with pollen, wax and its own sap [1]. Bees use propolis as an antiseptic against microbial infections and intruders that may occur in the hive. The chemical composition of propolis varies according to the collected flora, season and geographical region [2]. Crude propolis contains more than 300 components, and more than 180 compounds, most of which are polyphenols, have been identified as components of propolis. The main polyphenols in the content of propolis are phenolic acid and its esters, flavonoids, phenolic aldehydes, and ketone groups [3, 4]. It is not possible to use crude propolis directly due to the high amount of waxy substances it contains, the low proportion of the bioactive composition, and the pollution it contains [5]. Therefore propolis has to be extracted before consumption. With the extraction process, the phenolic components of propolis appear, and increases in antioxidant and antimicrobial activities occur. The most preferred solvent in the extraction process is ethanol, as it contains a large dipole moment in propolis content [6]. Apart from ethanol, other solvents such as water, chloroform [7], dimethylsulfoxide, methanol, ether, acetone [2], dichloromethane [8], ethyl acetate [9], and propylene glycol [10] can also be used in propolis extraction. Although the use of ethanol in propolis extraction is a simple and effective method, the intensity of the smell of alcohol combined with the smell of propolis limits its use in the cosmetics and pharmaceutical industries, as well as its use in pregnant women and children. For consumers with halal-haram sensitivity, the use of ethanol as a solvent in the extraction of propolis poses a problem [6]. Therefore, there is a need for a non-alcohol-based an effective extraction technique.

Vinegar is a special fermentation product produced by yeasts and acetic acid bacteria, which can be obtained from different raw materials that have fermentable carbon sources [11,12]. Due to the many phenolic compounds, amino acids, vitamins, organic acids, and melanoidin, it contains vinegar has positive effects on human health with its antioxidant, antimicrobial, anticarcinogenic, and antidiabetic properties [13]. Vinegar, which is among the fermented products, according to the raw materials used in its production; wine vinegar, fruit vinegar, fruit wine vinegar, cider vinegar, alcohol vinegar, grain vinegar, malt vinegar, flavored vinegar, and other vinegar are listed as [14]. Our country is very rich in terms of wild fruit species diversity, and one of these wild fruit varieties is

hawthorn (*Crataegus* spp. L.). The Hawthorn genus is distributed in the northern hemisphere with 200 species, and in Turkey with 17 different species and many taxa that grow naturally [15,16]. The main components of hawthorn fruit, which is generally consumed fresh, are flavonoids, triterpene acids, proanthocyanidins, organic acids, and some amines [17,18]. In addition to these, hawthorn fruit is also very rich in phenolic substances such as apigenin, quercetin, chlorogenic acid, gallic acid, vitexin, coumaric acid, caffeic acid, naringenin and cratenacin [19]. As for hawthorn vinegar, it is a local product obtained from the fruits collected from the hawthorn tree and is among the lesser-known vinegar in Turkey because it is produced on a local scale.

The number of propolis extracts that don't contain ethyl alcohol is increasing rapidly in the market. These are aqueous extract, herbal oil extracts (especially olive oil), essential oil extracts, extracts of multiple alcohols (glycerol, glycol, etc.) and less frequently are used, soaking in beverages, solving in products such as vinegar, brewing in different liquid mixtures and combinations of all these [5].

In our study, hawthorn vinegar obtained from hawthorn that a fruit frequently consumed in the Bingol region was used in propolis extraction. It is thought that the use of propolis in vinegar extraction will increase its use in future studies, by obtaining a product with increased nutritional value.

## 2. MATERIAL AND METHOD

### 2.1. Materials

Propolis (Bingöl Provincial Beekeepers' Association), hawthorn vinegar (Tijda Gıda Ltd. Şti), acetic acid (C<sub>2</sub>H<sub>4</sub>O<sub>2</sub>), phenolphthalein (C<sub>20</sub>H<sub>14</sub>O<sub>4</sub>), sodium hydroxide (NaOH), folin & ciocalteu's phenol reagent, sodium carbonate (Na<sub>2</sub>CO<sub>3</sub>), gallic acid (C<sub>6</sub>H<sub>2</sub>(OH)<sub>3</sub>CO<sub>2</sub>H), sodium nitrite (NaNO<sub>2</sub>), aluminium chloride (AlCl<sub>3</sub>), quercetin (C<sub>15</sub>H<sub>10</sub>O<sub>7</sub>), DPPH (2,2-diphenyl-1-picrylhydrazil), BHT (Butylated Hydroxytoluene), methyl alcohol (CH<sub>3</sub>OH). The propolis sample used in this study was collected from the Bingöl region, and hawthorn vinegar was purchased from a local market in Bingöl, Türkiye. All chemicals were used in analytical purity.



## 2.2. Methods

### 2.2.1. Extraction method

The samples to be used in the study were stored at +4 °C throughout the analysis period. 2 g of powdered propolis was added to 40 mL of hawthorn vinegar (HV) and the mixture was homogenized for 1 minute with the help of a homogenizer. The homogeneous mixture was stirred for 24 hours with the help of a magnetic fish in a stirrer at 150 rpm at 60 °C. At the end of the waiting period, the mixture was centrifuged at 3000 rpm for 10 minutes and the supernatant part was filtered with roughing filter paper thus propolis added hawthorn vinegar (PHV) was made ready for use.

### 2.2.2. Physicochemical analysis

To determine the physicochemical properties of hawthorn vinegar (HV) and propolis added hawthorn vinegar (PHV); pH, titratable acidity, brix, conductivity, and color measurement analyses were performed.

#### 2.2.2.1. pH and titratable acidity

pH values of HV and PHV samples were measured using a Thermo Scientific pH meter. The titratable acidity of the HV and PHV samples was calculated as acetic acid equivalents. Phenolphthalein was added to a 5 mL sample as an indicator and titrated with 0.1 N NaOH. By noting the volume of NaOH used in the titration, the percent titratable acidity was calculated in Equation (1) [20].

$$\text{Titratable acidity (\%)} = (V \times E \times 100) / M \quad (1)$$

V: volume of NaOH used, mL

E: 0.006005 (acid equivalent to 1 mL 0.1 N NaOH, g)

M: volume of sample, mL

#### 2.2.2.2. Brix

The amount of water-soluble solids (Brix) was analyzed for HV and PHV using an ISO-LAB handheld refractometer. The results were given in brix.

#### 2.2.2.3. Conductivity

Conductivity measurement was measured using Mettler Toledo brand portable conductivity meter for HV and PHV samples. Results were given in  $\mu\text{S}/\text{cm}$ .

#### 2.2.2.4. Color measurement

Color measurement was analyzed for HV and PHV samples using the Konica Minolta CM-5 colorimeter. Results were given as L\* (0: darkness, 100: lightness), a\* (-: greenness, +: redness), and b\* (-: blueness, +: yellowness).

### 2.2.3 Bioactive analysis

To determine the bioactive properties of hawthorn vinegar (HV) and propolis added hawthorn vinegar

(PHV) samples; total phenolic content, total flavonoid content and antioxidant activity (%DPPH) analyzes were performed in 3 repetitive.

#### 2.2.3.1. Total phenolic content and total flavonoid content

According to the method of Hajji et al., [21] total phenolic content analyzes were performed for HV and PHV samples. 500  $\mu\text{L}$  HV and 500  $\mu\text{L}$  PHV samples were taken into test tubes and 500  $\mu\text{L}$  of Folin reagent was added to them. Then, each test tube was vortexed by adding 500  $\mu\text{L}$  of  $\text{Na}_2\text{CO}_3$  and 3500  $\mu\text{L}$  of distilled water. The test tubes were kept in a dark laboratory environment for 90 minutes. At the end of the waiting period, 300  $\mu\text{L}$  of samples were pipetted into 96 well plates and measured at 760 nm in a microplate reader (Spectramax Plus 384 ELISA). Results were given as gallic acid equivalents.

According to the method of Zhishen et al., [22] Total flavonoid content analyses were performed for HV and PHV samples. 250  $\mu\text{L}$  of HV and 250  $\mu\text{L}$  of PHV were taken into test tubes. 150  $\mu\text{L}$  of  $\text{NaNO}_2$  was added to them and after waiting for 6 minutes, 75  $\mu\text{L}$  of  $\text{AlCl}_3$  was added. Test tubes were kept for 5 minutes in a laboratory environment, and 1000  $\mu\text{L}$  of NaOH and 2500  $\mu\text{L}$  of distilled water were added. After each addition, the samples were vortexed. Then, 300  $\mu\text{L}$  of samples were pipetted into 96 well plates and measured at 510 nm in a microplate reader (Spectramax Plus 384 ELISA). Results were given as quercetin equivalents [23].

#### 2.2.3.2. DPPH radical scavenging activity

According to the method of Hatano et al., [24] on top of 0.3 mL of HV and PHV samples, 2.7 mL of freshly prepared DPPH solution was added to the test tubes and the samples were vortexed, kept in the dark laboratory environment for 60 minutes. At the end of the waiting period, measurements were taken in a UV-Vis spectrophotometer (Shimadzu) at an absorbance of 517 nm. As a control, distilled water was used instead of the sample. Results were given as % inhibition.

## 3. RESULTS

### 3.1. Physicochemical Properties

#### 3.1.1. pH and titratable acidity

The pH values of the HV sample and the PHV sample were determined respectively as 2.96 and 2.98. In studies in the literature, pH values of hawthorn vinegar samples are 3.28 [25], 3.76 [26], 3.3 [20], 2.69 [27], 2.76 [28], 3.63 [29], 3.67 (red) and 3.25 (black) [30]. The results obtained in our study are similar to the literature findings.

The titratable acidity values as the acetic acid equivalent of the HV sample and the PHV sample were determined respectively as 2.58% and 2.22%. In similar studies, titratable acidity values of hawthorn vinegar samples

were as acetic acid equivalent; it has been reported as 2.2% [20], 0.82% [26], 2.29% [28], and 4.13% [29]. The titratable acidity results obtained in our study were similar to other studies. It has been stated that this parameter differs according to the production method and the raw material used [30].

### 3.1.2. Brix

The amount of water-soluble solids in HV and PHV samples was determined as approximately 4 brix. In similar studies, the amount of water-soluble solids in hawthorn vinegar samples; was 5.33 [25], 1.26 [26], 2.24 [27], 3.17 [28], 5.45 [29], 9.3 (red), and 15.6 (black) [30] as brix was represented by high variability. The brix values obtained in our study were in the range of brix values of hawthorn vinegar in the literature (1.26-15.6).

### 3.1.3. Conductivity

The conductivity values for HV and PHV samples were found respectively as 2.27 and 3.20  $\mu\text{S}/\text{cm}$ . In studies in the literature, the conductivity value of hawthorn vinegar was found to be 3.86 [25], and 1.36 [27]  $\mu\text{S}/\text{cm}$ . The conductivity values of both the HV sample and the PHV sample in our study are similar to other studies.

### 3.1.4. Color measurement

The color properties of vinegar are very important in terms of consumer perception, so color measurement was performed in the samples. The color ( $L^*$ ,  $a^*$ ,  $b^*$ ) values of the samples used in our study are given in Table 1.

**Table 1.** Color measurement results of hawthorn vinegar (HV) and propolis added hawthorn vinegar (PHV)

	$L^*$	$a^*$	$b^*$
HV	88.66	0.81	6.68
PHV	52.73	7.10	43.59

The “L” value ranges from 0-100 and indicates the brightness of a foodstuff. According to the results, hawthorn vinegar has a brighter appearance than propolis-added hawthorn vinegar. If the “a” value is “+”, it means redness, and according to the results, the redness of propolis added to hawthorn vinegar is higher than hawthorn vinegar. If the “b” value is “+”, it means yellowness, and according to the results, the yellowness of propolis added hawthorn vinegar is much higher than that of hawthorn vinegar. As a result, while the  $L^*$  value of the vinegar sample decreased with the addition of propolis, the  $a^*$  and  $b^*$  values increased. In similar studies in the literature, the color values ( $L^*$ ,  $a^*$ , and  $b^*$ ) of hawthorn vinegar samples were examined and the results are given in Table 2.

**Table 2.** Color measurement results of hawthorn vinegar samples

References	$L^*$	$a^*$	$b^*$
[25]	31.40	20.48	40.08
[26]	18.10	1.96	10.67
[27]	27.80	1.33	-0.30
[28]	61.3	4.47	33.1

When Table 2 is examined, it has been observed that the color values of the studies made with hawthorn vinegar

are in very different ranges. The  $L^*$  value of the HV sample used in the study is much higher than the results obtained in similar studies. It can be said that the  $L^*$  value of the PHV sample has a lower value, so its brightness has decreased. The  $a^*$  value of the HV sample used in the study is lower than the results obtained in similar studies. It can be said that the  $a^*$  value of the PHV sample has a higher value and is near to the studies in the literature. The  $b^*$  value of the HV sample used in the study is similar to the studies in the literature. It can be said that the  $b^*$  value of the PHV sample has a high value and its yellowness is more than the studies in the literature. It can be stated that the reason for this difference in the studies is due to the color of the shell of the hawthorn species [27]. In addition, it is thought that the heat treatment used in the extraction process affects the color properties of the samples.

## 3.2. Bioactive Properties

### 3.2.1. Total phenolic content and total flavonoid content

The total phenolic content (TPC) and total flavonoid content (TFC) of hawthorn vinegar (HV) and propolis added hawthorn vinegar (PHV) calculated as a result of the analyzes made in the study are given in Table 3.

**Table 3.** Total phenolic and total flavonoid content of hawthorn vinegar (HV) and propolis added hawthorn vinegar (PHV)

Analyzed Sample	TPC (mg GAE / L)	TFC (mg QE / L)
HV	56.76 $\pm$ 2.57	290.44 $\pm$ 4.19
PHV	73.55 $\pm$ 2.08	1364.89 $\pm$ 3.85

GAE: Gallic acid equivalence, QE: Quercetin equivalence

In a study by Kadaş et al., [25], the total phenolic content of the hawthorn vinegar sample was determined as 50.2  $\pm$  0.23 mg GAE/L, similar to our study. It was determined that the addition of propolis to the vinegar sample increased the total phenolic content (Figure 1). When other studies in the literature are examined, the total phenolic content values of hawthorn vinegar samples are 280  $\pm$  1 mg GAE/L [20], 306.80  $\pm$  5.07 mg GAE/L [26], 751.11  $\pm$  15.71 mg GAE/L [27], 647  $\pm$  0.115 mg GAE/L [28], and 24207  $\pm$  0.02 mg GAE/L [29]. The reason for this difference is thought to be related to the geographical region, location, climatic conditions, and soil structure where the hawthorn plant is grown [31].



**Figure 1.** Total phenolic content (TPC) of hawthorn vinegar (HV) and propolis added hawthorn vinegar (PHV)

In a study assessing propolis treated by different extraction methods the propolis/solvent ratio for extraction processes was determined as 1/20 (w/v), similar to our study [32]. In the study, maceration was carried out at room temperature using ethanol (70%) and water as solvent. At the end of the first day, the total phenolic content of propolis was 856 mg GAE/L in an ethanol, and 124 mg GAE/L in water solvent. The total phenolic content of the propolis-vinegar solution in our study was approximately 40% less than the total phenolic content of the water-propolis solution used in the study. It is difficult to compare the results obtained in different solvents. However, it is thought that the use of vinegar as a solvent in propolis extraction has the potential to increase the total phenolic content of propolis with different combinations of temperature and time. This potential may become kinetic in future studies to be.

It was determined that the total flavonoid substance content of the HV sample used in our study ( $290.44 \pm 4.19$  mg QE/L) increased approximately 5 times with the addition of propolis ( $1364.89 \pm 3.85$  mg QE/L) (Figure 2). The flavonoid content analyses made with hawthorn vinegar in the literature are  $50 \pm 2$  mg CE/L [20],  $136.16 \pm 0.97$  mg CE/L [26], and  $261 \pm 1.45$  mg CE/L [28] as catechin equivalence. Comparing the total flavonoid content, calculated as quercetin equivalent, with results calculated with different standards, such as catechin, is quite complex. In the literature, the total flavonoid content of propolis tinctures of Ukrainian origin was evaluated and the results were given as mg QE/L, similar to our study. All propolis tinctures were prepared 1/10 (w/v) ratio and with 70% ethanol. The solutions were first kept in closed containers at 40-50°C for about 3 hours and then extracted at room temperature for 21 hours. The total flavonoid content of propolis tinctures was found to range from  $4784.31$  mg QE/L  $\pm 8.80\%$  to  $6796.51$  mg QE/L  $\pm 0.52\%$  [33]. The total flavonoid content of the ethanol-propolis solution used in the study is approximately 3.5 times the total flavonoid content of the propolis-vinegar solution in our study. It is thought that increasing the solution concentration and changing the maceration method parameters in the future experiments to be carried out will change the flavonoid substance content obtained from propolis.

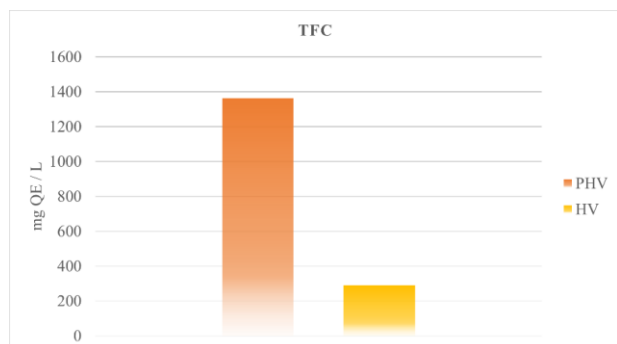


**Figure 2.** Total flavonoid content (TFC) of hawthorn vinegar (HV) and propolis added hawthorn vinegar (PHV)

More than 60 flavonoid substances, including reduced flavonoid types, namely catechin derivatives, as well as

oxidized flavonoid types such as quercetin, rutin, and chrysin, have been isolated from hawthorn fruit [34]. However, it is known that heat treatment applications reduce the total organic acids and total flavonoid content in the samples [35]. For example, Guo et al., [36] in their study with hawthorn fruit, determined that some contents, such as catechin, decreased after 10 minutes of heating. In addition, in the same study, it was determined that heat treatment caused an increase in two main compounds, quercetin, and apigenin. In our study, it is thought that the use of heat treatment in the extraction of the samples contributes to the increase in the total flavonoid substance content, and it is thought that this contribution is largely made by the compound called quercetin. Among the active ingredients for hawthorn, especially the quercetin content increases rapidly during heat treatment and the quercetin content is approximately ten times higher in processed hawthorn than in raw hawthorn [36]; shows that this compound can be used as a chemical quality indicator in the production of propolis-added vinegar. In addition, the quercetin compound plays a role in the prevention of Alzheimer's disease, which is increasing today [37]. For this reason, the necessity of producing innovative and healthy products such as propolis-added vinegar is increasing.

### 3.2.2. DPPH radical scavenging activity

DPPH radical scavenging activity method was used to determine the antioxidant capacity of the samples. DPPH radical scavenging activities of HV and PHV samples were found to be respectively  $53.38\% \pm 0.6\%$  and  $68.33\% \pm 0.4\%$ . Propolis samples collected from different regions by Akbar et al., [38] were extracted with ethanol at a ratio of 1/10 (w/v) for 24 hours. After the extracts were concentrated with the help of a rotary evaporator, freeze-dried powder extract was obtained. When the DPPH free radical scavenging activities of 8 propolis samples were examined, it was observed that the values varied between  $52.79\% \pm 1.09\%$  and  $68.39\% \pm 1.02\%$ . These results show that the HV and PHV samples used in our study are the same as the DPPH radical scavenging activities. Yıldırım [32] used ethanol (70%) and water as a solvent in the extraction of propolis at room temperature by maceration. At the end of the first day, the antioxidant activity of propolis was determined as 65% in ethanol and 52% in a water solvent. The results are almost the same as the antioxidant activity results obtained with the use of vinegar as a solvent in our study. This suggests that the substitution of vinegar instead of ethanol in propolis extraction will increase day by day.



**Figure 3.** DPPH radical scavenging activities (%) of hawthorn vinegar (HV), propolis added hawthorn vinegar (PHV), and BHT

Only in studies with hawthorn vinegar, DPPH radical scavenging activities were  $41\% \pm 1\%$  [20],  $55.59\% \pm 3.86\%$  [26], and  $54.9\% \pm 0.399\%$  [28] which is quite similar to our study. With the addition of propolis to hawthorn vinegar, it is clearly seen in Figure 3 that the DPPH radical scavenging activities of the samples increased and they took a value close to the synthetic antioxidant substance BHT. When Figure 3 is examined, the DPPH radical scavenging activities of the samples with a concentration of 1mg/mL and a synthetic antioxidant with the same concentration, BHT, are given as  $BHT > PAS > AS$ . The presence of some side effects of BHT, which is one of the synthetic antioxidants, has led studies to focus on antioxidants of plant origin [39]. In our study, it was determined that the PHV sample scavenged less but close amounts of DPPH radicals compared to BHT. It is thought that this situation will lead to plant-based antioxidant research.

#### 4. DISCUSSION AND CONCLUSION

Propolis collected from trees and plants by honey bees has a very complex content and can't be used crudely. Flavonoids and phenolic compounds in the content of propolis are related to the biological activity of propolis. Since the solvents used in propolis extraction extract different components, the extraction method and solvent selection are very important. It has been concluded that it would be more beneficial to conduct research in living systems with organic solvents. For this reason, the search for different solvents continues in addition to the organic solvents that are frequently used for propolis extraction. In a study conducted for this purpose, the solubility of propolis in vegetable oils was investigated. As a result of the study, the total polyphenol content, flavonoid content, and iron-reducing power of the olive oil extract of propolis; it has been determined that propolis is richer than corn, hazelnut, and sunflower oil extracts [40]. Another type of solvent used in propolis extract besides vegetable oils is vinegar. For this purpose, another study was conducted and the solubility of propolis in various kinds of vinegar was investigated. As a result of the examination, the total polyphenol, flavonoid content, and iron-reducing power of propolis in grape vinegar extract were found to be higher than organic (pomegranate, apple), commercial (pomegranate, apple, grape) and white vinegar extracts of propolis [41].

Vinegar, which has been widely used among people for centuries; is a healthy solution formed by the oxidation of sugar-containing fruits first to ethyl alcohol and then ethyl alcohol to acetic acid. In our study, vinegar was used as a propolis solvent, and hawthorn vinegar was chosen as a vinegar type. The fact that hawthorn fruit is rich in flavonoids and has been used for many years, especially in the field of alternative medicine, played an important role in this selection. In our study, the physicochemical and bioactive properties of hawthorn vinegar (HV) and propolis-added hawthorn vinegar samples (PHV) were examined separately. The data obtained show that propolis changes the physicochemical properties of vinegar. It is also among the results of our study that the bioactive properties of the propolis-added hawthorn vinegar sample increased compared to the hawthorn vinegar sample. It is thought that the heat treatment used especially during propolis extract significantly increases the quercetin content of vinegar. It is also thought that the alcohol formed in the first step of vinegar production and the resulting acetic acid contribute to the solubility of propolis. It is inevitable that vinegar, which has important effects on human health, should be included in the daily diet with the addition of propolis. Modifying the method applied in this study and applying it to different vinegar varieties will shed light on future studies. With the increase in the use of propolis-added vinegar in salads and sauces, a functional food supplement can be used in nutrition.

#### Acknowledgement

This study was carried out within the scope of the 100/2000 YÖK doctoral scholarship.

#### REFERENCES

- [1] Mot A, Soponar F, Sar C. Multivariate analysis of reflectance spectra from propolis: Geographical variation in romanian samples. *Talanta*. 2010; 81 (3): 1010-1015.
- [2] Anjum SI, Ullah A, Khan KA, Attaullah M, Khan H, Ali H et al. Composition and functional properties of propolis (bee glue): A review. *Saudi J Biol Sci*. 2019; 26 (1): 1695-1703.
- [3] Castaldo S, Capass F. Propolis, an old remedy used in modern medicine. *Fitoterapia*. 2002; 73 (1): 1-6.
- [4] Graikou K, Popova M, Gortzi O, Bankova V, Chinou I. Characterization and biological evaluation of selected mediterranean propolis samples. Is it a new type?. *LWT-Food Sci Technol*. 2016; 65: 261-267.
- [5] Yıldız O. Tüketilebilir propolis ekstralarında kullanılan çözücülerin (menstrualların) değerlendirilmesi (Evaluation of solvents (menstruums) used in consumable propolis extracts). *U Arı D.-U Bee J*. 2020; 20 (1): 24-37, DOI: 10.31467/uluaricilik.659556.
- [6] Bakkaloğlu Z, Arıcı M. Farklı çözücülerle propolis ekstraksiyonunun toplam fenolik içeriği, antioksidan kapasite ve antimikrobiyal aktivite üzerine etkileri. *Akademik Gıda*. 2019; 17 (4): 538-545.

- [7] Vera N, Solorzano E, Ordonez R, Maldonado L, Bedascarrasbure E, Isla M.I. Chemical composition of argentinean propolis collected in extreme regions and its relation with antimicrobial and antioxidant activities. *Nat Prod Commun.* 2011; 6 (6): 823-827.
- [8] Cauich-Kumul R, Segura-Campos MR. Bee propolis: Properties, chemical composition, applications, and potential health effects. In: Segura-Campos MR, editors. *Bioactive Compounds.* Cambridge, UK: Woodhead publishing; 2019. p. 227-243.
- [9] Correa YX, Valenzuela AL, Ardila AM, Rojas M, Mora CT. Colombian propolis as starting material for the preparation of nanostructured lipid carriers. *Brazilian Journal of Pharmacognosy.* 2019; 29 (3): 381-388.
- [10] Meto A, Colombari B, Meto A, Boaretto G, Pinetti D, Marchetti L. Propolis affects *Pseudomonas aeruginosa* growth, biofilm formation, eDNA release and phenazine production: Potential involvement of polyphenols. *Microorganisms.* 2020; 8 (2): 243.
- [11] Öztürk A, Özdemir Y, Göksel Z. Elma sirkesi ve teröpatik etkileri. *Tarım Bilimleri Araştırma Dergisi.* 2009; 2 (1): 155-158.
- [12] Şengün İY, Kılıç G. Farklı sirke çeşitlerinin mikroflorası, biyoaktif bileşenleri ve sağlık üzerine etkileri. *Akademik Gıda.* 2019; 17 (1): 89-101.
- [13] Şengün İY, Kılıç G. Dut sirkesinin mikrobiyolojik, fiziksel, kimyasal, antiradikal ve antimikrobiyal özellikleri. *Akademik Gıda.* 2018; 16 (2): 168-175.
- [14] Anonim. TSE-Sirke-Tarım kökenli sıvılardan elde edilen ürün-tarifler, özellikler ve işaretleme, TS 1880 EN 13188. Ankara: Türk Standartları Enstitüsü; 2013.
- [15] Seçmen Ö, Gemici Y, Görk G, Bekat L, Leblebici E. Tohumlu bitkiler sistematiği. İzmir: Ege Üniversitesi Ziraat Fakültesi Yayınları; 2000. s. 196.
- [16] Gültekin HC. Yabancıl meyveli ağaç türlerimiz ve fidan üretim teknikleri. Çevre ve Orman Bakanlığı, Ankara: Fidanlık ve Tohum İşleri Daire Başkanlığı; 2007.
- [17] Chang Q, Zuo Z, Harrison F, Chow MSS. Hawthorn. *The Journal of Clinical Pharmacology.* 2002; 42 (6): 605-612.
- [18] Arslan R, Bor Z, Bektas N, Meriçli AH, Ozturk Y. Antithrombotic effects of ethanol extract of *Crataegus orientalis* in the carrageenan-induced mice tail thrombosis model. *Thrombosis Research.* 2011; 127 (3): 210-213.
- [19] Çoklar H, Akbulut M, Kılınç S, Yıldırım A, Alhassan I. Effect of freeze, oven and microwave pretreated oven drying on color, browning index, phenolic compounds and antioxidant activity of hawthorn (*Crataegus orientalis*) fruit. *Not Bot Horti Agrobi.* 2018; 46 (2): 449-456.
- [20] Bakır S, Devcioglu D, Kayacan S, Toydemir G, Karbancioglu Guler F, Capanoglu E. Investigating the antioxidant and antimicrobial activities of different vinegars. *European Food Research and Technology.* 2017; 243 (12): 2083-2094.
- [21] Hajji M, Jarraya R, Lassoued I, Masmoudi O, Damak M, Nasri M. GC/MS and LC/MS analysis, and antioxidant and antimicrobial activities of various solvent extracts from *Mirabilis jalapa* tubers. *Process Biochemistry.* 2010; 45 (9): 1486-1493.
- [22] Zhishen J, Mengcheng T, Jianming W. The determination of flavonoid contents in mulberry and their scavenging effects on superoxide radicals. *Food Chem.* 1999; 64 (4): 555-559.
- [23] Chang C, Yang M, Wen H, Chern J. Estimation of total flavonoid content in propolis by two complementary colorimetric methods. *Journal of Food and Drug Analysis.* 2002; 10 (3): 178-182.
- [24] Hatano T, Kagawa H, Yasuhara T, Takuo O. Two new flavonoids and other constituents in licorice root: Their relative astringency and radical scavenging effects. *Chem Pharm Bull.* 1988; 36 (6): 2090-2097.
- [25] Kadaş Z, Evrendilek GA, Heper G. The metabolic effects of hawthorn vinegar in patients with high cardiovascular risk group. *J Food and Nutr Res.* 2014; 2 (9): 539-545.
- [26] Öztürk I, Caliskan O, Tornuk F, Ozcan N, Yalcin H, Baslar M, Sagdic O. Antioxidant, Antimicrobial, Mineral, Volatile, Physicochemical and Microbiological Characteristics of Traditional Home-Made Turkish Vinegars. *LWT-Food Sci Technol.* 2015; 63 (1): 144-151.
- [27] Tomar O, Çağlar A, Akarca G, Vatansever H. Physicochemical and sensory quality properties of yellow hawthorn fruit (*Crataegus tanacetifolia*) vinegar produced by traditional fermentation method. *European Journal of Science and Technology.* 2020; 19: 176-181.
- [28] Karadağ A, Bozkurt F, Bekiroglu H, Sagdic O. Use of principal component analysis and cluster analysis for differentiation of traditionally-manufactured vinegars based on phenolic and volatile profiles, and antioxidant activity. *Pol J Food Nutr Sci.* 2020; 70 (4): 347-360.
- [29] Özdemir GB, Özdemir N, Ertekin-Filiz B, Gökırmaklı Ç, Kök-Tas T, Budak NH. Volatile aroma compounds and bioactive compounds of hawthorn vinegar produced from hawthorn fruit (*Crataegus tanacetifolia* (lam.) pers.). *J Food Biochem.* 2021; 46 (3): e13676.
- [30] Cosmulescu S, Stoenescu AM, Trandafir I, Tutulescu F. Comparison of chemical properties between traditional and commercial vinegar. *Horticulturae.* 2022; 8 (3): 225.
- [31] Liu S, Chang X, Liu X, Shen Z. Effects of pretreatments on anthocyanin composition, phenolics contents and antioxidant capacities during fermentation of hawthorn (*Crataegus pinnatifida*) drink. *Food Chemistry.* 2016; 212 (1): 87-95.
- [32] Yıldırım HK. Assessment of propolis treated by different extraction methods. *Brazilian Archives of Biology and Technology.* 2022; 65 (2): 1-11.
- [33] Hudz N, Korytniuk O, Yezerska O, Motyka O, Turkina V, Korytniuk R, Wiczorek PP. Evaluation of the total flavonoid content and antimicrobial

- activity of the tinctures of propolis of Ukrainian origin. *Acta Pol Pharm Drug Res.* 2020; 77: 897-907.
- [34] Zhang J, Chai X, Zhao F, Hou G, Meng Q. Food applications and potential health benefits of hawthorn. *Foods.* 2022; 11 (18): 2861.
- [35] Wang ZX, Wan J, Li YR, Jang RW, X MQ, Zhou X. HPLC fingerprint of crude and processed hawthorn. *J Guangdong Pharm Univ.* 2020; 36 (5): 599-602.
- [36] Guo W, Bai J, Zhang Q, Duan K, Zhang P, Zhang J, Zhao J, Zhang W, Kong D. Influence of thermal processing on the quality of hawthorn: Quality markers of heat-processed hawthorn. *J Sep Sci.* 2022; 45 (19): 3774-3785.
- [37] Khan H, Ullah H, Aschner M, Cheang WS, Akkol EK. Neuroprotective effects of quercetin in alzheimer's disease. *Biomolecules.* 2019; 10 (1): 59.
- [38] Akbar A, Gul Z, Aziz S, Sadiq MB, Achakzai JK, Saeed S, Chein SH, Sher H. Bio-functional potential and biochemical properties of propolis collected from different regions of Balochistan Province of Pakistan. *Oxidative Medicine and Cellular Longevity.* 2022; 2022: 14.
- [39] Gülçin İ, Elias R, Gepdiremen A, Boyer L. Antioxidant activity of lignans from fringe tree (*Chionanthus virginicus* L.). *European Food Research and Technology.* 2006; 223 (6): 759-767.
- [40] Karakaş S. Türk propolisinin ticari bitkisel yağlarda çözünürlüğünün incelenmesi. [Yüksek lisans tezi]. Trabzon: Karadeniz Teknik Üniversitesi; 2012.
- [41] Kartal B. Türk propolisinin çeşitli sirkelerde çözünürlüğünün incelenmesi. [Yüksek lisans tezi]. Trabzon: Karadeniz Teknik Üniversitesi; 2019.

## Classifying RNA Strands with A Novel Graph Representation Based on the Sequence Free Energy

Enes ALGÜL<sup>1\*</sup> 

<sup>1</sup> Bingöl University, Engineering and Architecture Faculty, Department of Computer Engineering, Bingöl, Türkiye  
Enes ALGÜL ORCID No: 0000-0001-6597-4242

\*Corresponding author: [ealgul@bingol.edu.tr](mailto:ealgul@bingol.edu.tr)

(Received: 20.01.2023, Accepted: 05.05.2023, Online Publication: 22.06.2023)

### Keywords

Graph representations, RNA, Graph Kernel, Machine Learning

**Abstract:** Ribonucleic acids (RNA) are macromolecules found in all living cells and act as mediators between DNA and protein. Structurally, RNAs are more similar to the DNA. In this paper, we introduce a compact graph representation utilizes the Minimum Free Energy (MFE) of RNA molecules' secondary structure. This representation represents structural components of secondary RNAs as edges of the graphs, and MFE of these components represents their edge weights. The labeling process is used to determine these weights by considering both the MFE of the 2D RNA structures, and the specific settings in the RNA structures. This encoding makes the representation more compact by providing a unique graph representation for the secondary structural elements in the graph. Armed with the representation, we apply graph-based algorithms to categorize RNA molecules. We also present the result of the cutting-edge graph-based methods (All Paths Cycle Embeddings (APC), Shortest Paths Kernel/Embedding (SP), and Weisfeiler - Lehman and Optimal Assignment Kernel (WLOA)) on our dataset [1] using this new graph representation. Finally, we compare the results of the graph-based algorithms to a standard bioinformatics algorithm (Needleman-Wunsch) used for DNA and RNA comparison.

32

## Serbest Enerji Serisine Dayalı Yeni Bir Graf Temsili ile RNA Zincirlerini Sınıflandırma

### Anahtar Kelimeler

Graf gösterimleri, RNA, Graf çekirdek yöntemleri, Makine öğrenmesi

**Öz:** Ribonükleik asitler (RNA), tüm canlı hücrelerde bulunan makromoleküllerdir ve DNA ile protein arasında aracı görevi görürler. Yapısal olarak daha çok DNA'ya benzerler. Bu makalede, RNA moleküllerinin ikincil yapısının Minimum Serbest Enerjisini (MSE) kullanan kompakt bir grafik gösterimi sunuyoruz. Bu temsilde, RNA moleküllerinin yapısal bileşenleri grafların kenarlarını ve bu bileşenlerin MSE'si, kenar ağırlıklarını temsil eder. Etiketleme işlemi, hem iki boyutlu RNA yapılarının MSE'sini hem de RNA yapılarındaki belirli ayarları dikkate alarak kenar ağırlıkları belirlenir. Bu kodlama, graftaki ikincil yapı elemanlarına benzersiz bir graf temsili vererek gösterimi daha kompakt hale getirmek için kullanılır. Temsil ile donanmış olarak, RNA moleküllerini kategorilere ayırmak için graf tabanlı algoritmalar uyguluyoruz. Ayrıca, veri kümemizde [1] bu yeni graf temsili kullanarak en son graf tabanlı yöntemlerinin (All Paths Cycle Embeddings (APC), Shortest Paths Kernel/Embedding (SP) ve Weisfeiler - Lehman and Optimal Assignment Kernel (WLOA)) sonuçlarını sunuyoruz. Son olarak, graf tabanlı algoritmaların sonuçlarını DNA ve RNA karşılaştırması için kullanılan standart bir biyoinformatik algoritma (Needleman-Wunsch) ile karşılaştırıyoruz.

### 1. INTRODUCTION

DNA is a double-stranded nucleic acid that holds the blueprint for the development and function of all living beings, in the form of genetic code [29]. The code is a sequence of three base letters ('AAA', 'ATC', 'GTT',

'GTA', ...). RNA is a DNA-like single-stranded polymer of nucleotides made up of various kinds of nucleobase building blocks. One of the functions of RNA is to copy the blueprints of the DNA and translate them to the protein via ribosomes in the cell. Therefore, a new RNA is a complementary part of the DNA chain. Both molecules include bases (nucleotides).

The RNA's primary structure refers to the order of its nucleobases. The nucleotide sequences then fold upon themselves to build topological structures, known as 2D RNA structures. These 2D RNA structures composed of loops (hairpin loop, bulge, junction, and interior loop) and base pairs (stem/helix) [30]. The 2D RNA structure, which is more complex than the primary structure, holds more information than just the order of its nucleobases. Representing the primary RNA structures in graph data is relatively straightforward by using vertices for each nucleobase and edges for connections between adjacent nucleobases. However, representing complex secondary RNAs in graph data is a more challenging task. These structures can also fold onto themselves to build 3D complex shapes, which are more similar to protein shapes, but are chemically more similar to DNA. Therefore, RNA contains sequence, structural, and shape information.

RNA's biological functions are closely linked to its structure [2]. The 2D structures of RNA are predicted and may differ from their actual shapes. Therefore, it is essential to utilize a robust tool for efficiently generating secondary structures. The prediction of the biological functions of RNA is related to obtaining useful information contained in the structure of RNA. Currently, the research community primarily employs two methods for generating secondary RNA structures. One approach focuses on minimizing free energy, while the other approach involves determining the association of nucleotides through the distance between their atoms. The following challenges are encountered during the encoding of secondary RNA structures.

- How to transform secondary RNA structures into a graph data form, as well as extract valuable structural features of 2D structures?
- How reduce the size of 2D RNA graph data?
- How to make pairwise comparison of RNA strands using their 2D structures to predict their biological tasks?
- How to solve multi-class classification problem of 2D RNA representations?

This article presents novel and advanced techniques to tackle these problems by encoding RNA secondary structural motifs as edges and connections between them as vertices. Additionally, to gain more features for encoding 2D RNAs in the graph data form, the total MFE is encoded as edge weights.

## 2. RELATED WORK

A Graph  $G = (V, E)$  can be defined as set of nodes and edges ( $V, E \subseteq V \times V$ ), and their labels. An edge ( $E$ ) connects two nodes. A path is a sequence of vertices in a given graph.

RNA can be represented as a graph by encoding each RNA nucleobase as a node and placing edges between neighboring nodes. In this representation, X3DNA [3] is used to extract bound base pairs. In the graph representation of RNA, each node is labelled with its

associated base. This representation was first used in the 1970s by Waterman [4] and has been used in various studies since then.

In 2004, the RAG [5] introduced a graph representation using existing and hypothetical secondary structural components of RNAs. The RAG web resource enumerates the number of nodes in graphs of RNA motifs according to their 2D complexity and classifies them based on functional types. RAG introduces a tree graph representation for hypothetical RNA tree shapes and a dual graph representation for other RNA structures that include both trees and pseudoknots. RAG uses labelled vertices and directed edges in graphs, and in the RAG representation, it assigns stems as edges and loops as nodes.

In 2012, Knisley et al [6] developed a dual graph RNA representation that can encode all structural types of 2D RNAs. They employed a multi-graph secondary RNA representation by using existing graph-theoretic descriptors to categorize all likely secondary RNA topologies with stems encoded as nodes and other structural motifs encoded as edges.

In 2016, a novel method was introduced by Huang et al [7], where RNA molecules were encoded by transforming graphs into topological spectrums. The subgraphs of the RNA strands are defined as their topological fingerprints and are classified the RNA strands by comparing the fingerprints.

In 2018, a variety of RNA graph-based representations were introduced, including 1D/2D/3D RNA structures [8]. In the 1D RNA graph representation, nucleotides were encoded as nodes; in the 2D RNA graph representation, X3DNA was used to generate structures. In this representation, matched base-pair is indicated by adding cross-link edges. The  $(x, y, z)$  coordinate information of the C3 atom is used to provide 3D RNA graph representation.

## 3. A NEW GRAPH REPRESENTATION

All 2D RNA structures are predicted structures and closely related to their structural components [2, 8, 10-14]. 2D RNA structural components can be predicted by free energy minimization. Many techniques have been developed to predict 2D RNA structures. First, a dynamic algorithm [15] was developed by Zuker and Stiegler in the 1980s for generating secondary RNA structures utilizing MFE in loops. Subsequently, widely used methods like the Mfold Web Server, Vienna RNA Software, and many other studies [8, 10, 11, 13, 16, 18] have used the MFE approach to predict secondary RNA structures.

X3DNA [3] can generate and visualize 2D/3D RNA structures from PDB files using the distance between atoms of base pairs. X3DNA considers the orientation and relative position of atoms (C3, O2) of two bases to predict 2D RNA structures [17].



### 3.1. Sequence Free Energy

In this work, our approach is to receive all MFEs of 2D RNA structural components and transform them into a graph-structured data form.

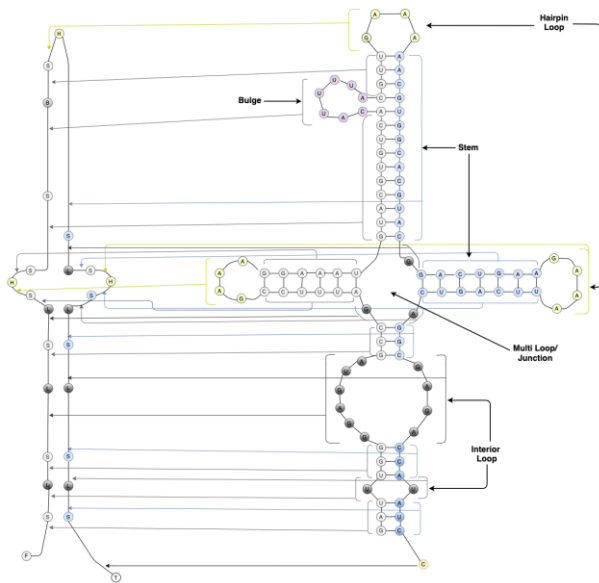


**Figure 1.** The structure of the Escherichia coli Riboswitch is represented in 2D using the MFE information obtained from the 4Y1M.pdb file.

Our secondary RNA graph representation is divided into three categories: stems/helices, loops, and unpaired parts of the chain. We construct a graph using the MFE for the stems/helices shown in Table 1 produced by Vendex et al [19, 20] and loops shown in Figure 2 produced by Tinoco et al. [21], and a regular tetrahedral approach for unpaired part of the RNA chain as follows.

**Table 1.** MFE between base pairs received from [19].

Base pair	kcal/mol
<i>U - G</i>	- 4.45
<i>U - U</i>	- 5.82
<i>C - G</i>	- 5.53
<i>U - A</i>	- 4.42
<i>U - C</i>	- 0.37
<i>U - A</i>	- 4.42

The paired parts of RNAs are called stems or helices. The highest negative energy arises among the most sturdy RNA base pairs. X3DNA [3] is utilised to generate base pair information.

The edge weight of loops in RNA molecules is determined by using the MFE on hairpin, interior, and bulge loops as seen in Figure 2 [21]. This method, although being one of the oldest techniques, is still used today for computing MFE [22]. However, we have no information of MFE on junctions available, and they are utilised similarly to the interior loops when calculating edge weights.

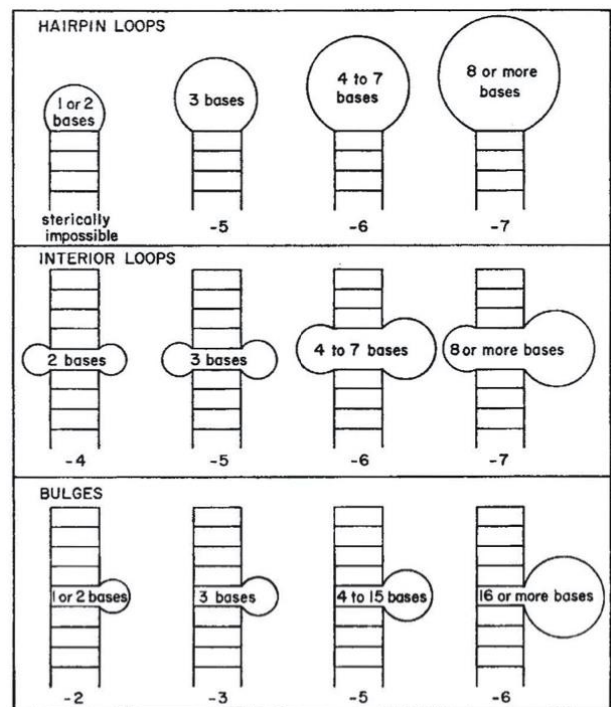


**Figure 2.** This figure is received from [21]. The MFE information on loops.

Pretty much, 24 percent of RNA molecules in the York RNA Dataset [1] lack 2D structural components and are unpaired. This affects correctly categorizing RNA molecules using learning methods. To solve this problem, we developed an advanced approach for encoding these unpaired RNA strands based solely on their base sequences. We used 3-base codes as edge weights to make the graph smaller (see Figure 3). Each of 3-base codes  $A(1,1,1)$ ,  $G(-1,-1,1)$ ,  $U(1,-1,-1)$ , and  $C(1,-1,-1)$  is encoded as a regular tetrahedron with equal distance between any paired bases ( $2\sqrt{2}$ ) (see Figure 4). We used K-medoids to reduce the group of possible 64 sequences to 4 for generating the code-book's code-words. Then, Learning Vector Quantization (LVQ) utilized these code-words to cluster edge weights into four classes. We made this improvement because some graph kernels solely apply to a finite number of discrete node labels.

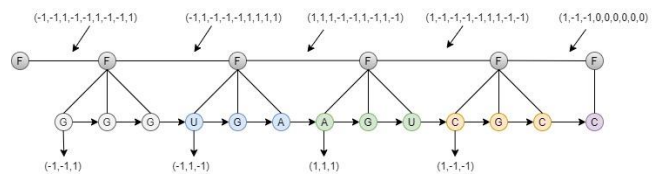


**Figure 3.** Unpaired part of the strands represented into weighted graph structured data using base sequences obtained from 1a3m.pdb (chain B) file.

RNA strands with 2D structures also have unpaired sequences, known as tails and queues, from the 5' to 3' of RNA strands. The same method discussed previously is applied to these tails and queues.

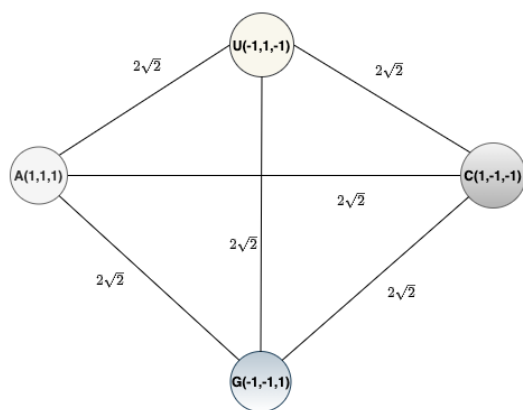


**Figure 4.** A regular tetrahedron represents base position.

Some graph kernels, such as the WL kernel, operate on discrete labels. Therefore, edge weights are refined as follows: the edge labels of 3-base codes are integers ranging from (-1 to 4). For other edge weights, we divided them by 10 if their absolute value was greater than 5, and rounded all numbers to tenths to reduce the number of decimal places to one.

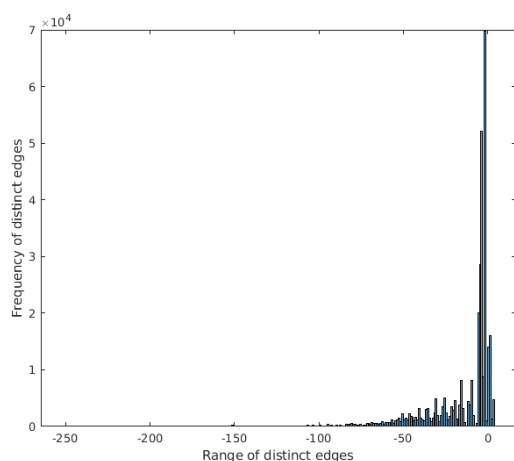


**Figure 5.** The histogram illustrates the range of edge labels prior to edge modifications [-252.0 to 4.0]

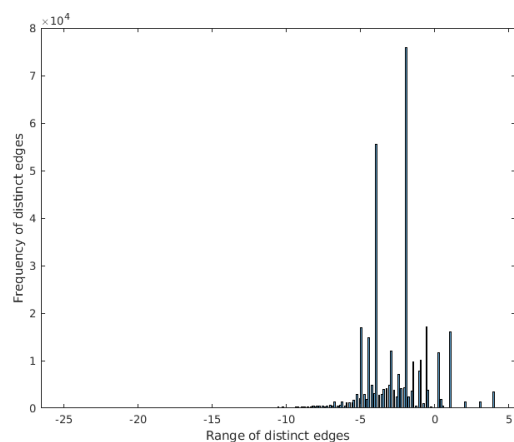


**Figure 6.** The histogram illustrates the range of edge labels after modifications [-26.0 to 4.0].

As illustrated in Figure 5 and Figure 6, the range of edge weights significantly reduced. This representation allows

for relevant information to be retained while decreasing the number of vertices and edges by 75.4%.

## 5. DATA

The RNA Graph Classification Dataset used in this work was compiled by the University of York [1]. The dataset was labelled by using the biological function of the RNA molecules and includes 3178 RNA chains in the PDB files. The sequence and  $(x, y, z)$  coordinates information of the nucleobases were extracted from the pdb files.

This dataset is the largest dataset based on the categorization of RNA molecules according to their biological functions. The RNA classes are RIBONUCLEASE (14), RIBOSWITCH (227), MRNA (179), RIBOZYME (259), RRNA (1135), SRP (57), TRNA (581), and OTHER (726). The amount of each class of RNA is represented in parentheses. Detailed information about the dataset is available in [1], and the dataset is available for download at the <https://www.cs.york.ac.uk/cvpr/RNA.html> web site.

## 5. CLASSIFICATION METHODS

We apply pairwise graph comparison methods to categorize RNA structures according to their 8 types of biological function. In particular, we use graph kernels previously used on the other RNA datasets.

### 5.1. Weisfeiler-Lehman Optimal Assignment Kernel (WLOA)

The Weisfeiler-Lehman (WL) is a graph kernel function that compares the structural similarity of labelled graph pairs [31]. This cutting-edge kernel method treats each graph as a sequence of its labels. The WL method recursively relabels the nodes of graphs according to their neighbourhood node labels and makes a comparison of the resulting node and edge labels at each iteration [23]. For a fixed number of iterations, the edge refinement process is repeated. At each iteration, the WL kernel sorts the edge and node labels, uses a global hash function for compression, and counts common labels [25].

Optimal Assignment (OA) [24] is a kernel function based on the optimal assignment problems between the nodes of graph pairs [32]. OA counts the similarity score of the perfect match between the node labels of graph pairs for classification problems. WLOA receives an OA kernel where the labels are obtained by the WL method [25], with the starting label corresponding to the encoded RNA graph's vertex labels [1]. This method provides the highest classification accuracy in applying classifier methods to our dataset.

### 5.2. Shortest Path Kernel/ Embedding (SPK)

A walk kernel calculates the similarity of two graphs by determining the number of shared walks of a specific type in both graphs. The Shortest path kernel (SPK) [26] is a type of walk-based kernel that computes the

shortest walks between graph pairs to measure the similarities between two vertices within a graph.

$$K_{SP}(G, H) = \sum_{p_i \in SP(G)} \sum_{p_j \in SP(H)} K_B(p_i, p_j) \quad (1)$$

Here,  $SP(\cdot)$  represents the set of shortest paths, and  $K_B$  is a delta kernel that compares all shortest distances in the graph. Each path is represented by a label sequence, and in our application, we compute the SP length for each RNA strand and represent it as a histogram of these paths in a feature space. The edge lengths are determined by the RNA edge weights, and the paths are labelled by their start and end vertex labels.

### 5.3. All Paths and Cycles Kernel /Embedding (APC)

The APC is a kernel function [27] based on counting all possible paths, including cycles, within a graph, unlike SP kernel which only computes the shortest path.

$$K_{APC}(G_1, G_2) = \sum_{p_i \in PC(G_1)} \sum_{p_j \in PC(G_2)} K_B(p_i, p_j) \quad (2)$$

Here,  $K_B(\cdot)$  is a base kernel, and  $PC(\cdot)$  represents a group of all possible paths, including cycles, on  $G$ . The maximum length of the path must be limited, and the amount of the discrete node/edge labels must be less than 4. To apply this method to the primary and secondary RNA structure, we label the bases of RNA strands with three labels  $A/U$ ,  $G/C$ , and *other*. Similarly, we label the nodes with three labels  $F$ ,  $N/Q/H$ , and  $B/L$ /other to apply this method to our introduced representation. With these limitations, this kernel is computationally very efficient. This kernel has the same explicit embedding as the SP, such as the histogram of discrete labelled paths [1].

### 5.4. Needleman - Wunsch Algorithm

The Needleman-Wunsch algorithm [28] is a popular sequence-based method in application of DNA and protein for comparison. Since RNA nucleobase sequences are similar to that of DNA, Needleman-Wunsch algorithm can also be operated on RNA sequences for comparison. The RNA nucleotides are

denoted as a sequence of 4 letters (A, C, U, G) and the Needleman-Wunsch algorithm [28] used to align these

strings. The Jukes-Cantor method is employed to count the distances between RNA sequences.

$$d = -\frac{3}{4} \log \left( 1 - \frac{4}{3} p \right) \quad (3)$$

Where, the distances between RNA sequences denotes  $p$  with the range of,  $0 \leq p \leq 1$ , for the portion of sets that are distinct. A distance matrix,  $D$ , is then populated with these distances, and multidimensional scaling is applied to map these distances into a feature space.

## 3. RESULTS

We presented the results from the introduced graph representations of secondary RNAs, utilizing the cutting-edge graph kernels algorithms to categorise RNA strands from the York RNA Graph dataset.

This analysis aims to determine if the introduced representation is effective in classifying RNA strands by reducing complexity and increasing accuracy. Various structural information from RNA, including topology, sequence, and the introduced representations, were also evaluated to classify RNA molecules. The RNA sequence representation from [1] consists of base labels and edges located between adjacent bases, while the 2D RNA representation from [1] includes edges of the graph but no labels of bases. The NR-W representation is a weighted secondary graph representation of RNA introduced in the Section 3.1. On the other hand, the NR-UW is an unweighted representation of the same graph, in which the edge weights have been eliminated.

**Table 2.** The prediction accuracy of various methods and representations, such as APC, WLOA, SP, and SA on the York RNA Graph Dataset. \*These classification results are taken from our previous study [1].

	Seq*	Top*	Seq+Top*	NR-W	NR-UW
WLOA	92.0	73.1	<b>92.4</b>	86.6	77.5
SP	<b>91.3</b>	79.5	91.1	79.6	75.4
APC	<b>90.3</b>	85.4	89.9	80.8	79.4
SA	89.2				

**Table 3:** The classification time for the York RNA Dataset utilising various methods and representations, such as APC, WLOA, SP, and SA, expressed in units of seconds (s), minutes (m), and hours (h).

	Seq		Top		Seq + Top		NR-W		NR-UW	
	Acc.	speeds	Acc.	speeds	Acc.	speeds	Acc.	speeds	Acc.	speeds
WLOA	<b>92.0</b>	16m 32s	73.1	5m 32s	<b>92.4</b>	3m 13s	86.9	2h 59m 44s	77.5	19s
SP	91.3	10h 36m 14s	79.5	10h 40m 10s	91.1	10h 43m 15s	80.9	13m 1s	75.4	10m 19s
APC	90.3	17m 57s	<b>85.4</b>	16m 33s	89.9	24m 20s	79.5	1m 46s	79.4	1m 9s

Then, we used graph kernel methods and machine learning classification algorithms to evaluate the outcome of various techniques on various sources of RNA information. Bagged Trees performed the best with the SPK method utilising NR-UW, while Quadratic SVM and Cubic SVM produced the most advanced results with WLOA on the same representation when

PCA was applied. Furthermore, Subspace KNN achieved the most favourable outcomes with the APC method when utilising all representations, as well as with the SPK using NR-W, Top, Seq, and with WLOA using NR-W.

Moreover, we analyzed the outcome of classifications using ROC curves and found that Subspace KNN had a TPR of 94% and an AUC of 98%. Our experiments revealed that using reduced graph representations resulted in lower performance but faster execution time.

The highest performance was achieved when applying WLOA to the Seq + Top representation of RNA, with an outcome of 92.4% accuracy. The introduced NR-W representation had an accuracy of 86.6% and performed better than the topology graph representation of 2D RNA. The 2D RNA graph representation revealed the highest accuracy (85.4%) when using the APC method. Our introduced NR-W representation had a higher accuracy of 86.6% when using the WLOA kernel, as it includes both sequence and edge labels of reduced graph representation, whereas the topology representation solely consists of edge information of the exact graph representation. As shown in Table 2 and Table 3, incorporating Minimum Free Energy as edge weights on structural components produced better outcomes. However, combining the topology with the sequence (Seq + Top) provided superior performance than NR-W.

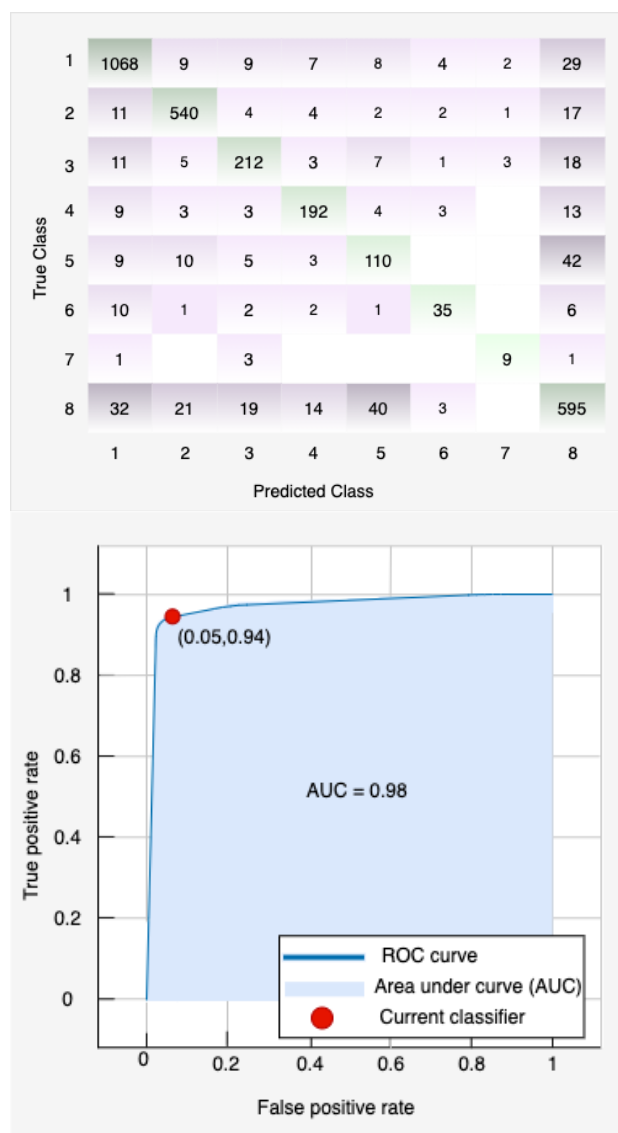


**Figure 7.** Evaluation of the NR-W using the ROC Curve and Confusion Matrix using WL-OA kernel.

Eliminating the weights from the edge of the full graphs decreased the accuracy (79.4%) when applying APC. The outcomes indicate that using weighted RNA graph representations improves performance compared to unweighted RNA graph representations when using WLOA, SP, and APC kernel methods.

Overall, our introduced representation effectively reduced the exact graph size and improved classification accuracy for 2D RNA structures. Despite this, the primary RNA representation performed better than all 2D RNA representations. For achieving greater classification accuracy, more advanced graph representations are needed for encoding 2D RNA structures.

## 7. CONCLUSION

In this research article, we addressed the problem of representing 2D RNA structures. We investigated existing representations and introduced a novel RNA graph representation using various methods, including investigating the impact of minimum free energy (MFE) on predicting RNA function. We also considered infrequent parts of the RNA structure and applied alternative approaches to encoding them, ultimately building a compact graph representation.

We successfully transformed MFE into a graph-based representation and demonstrated that representing MFE as weights of graph edges, along with refinements on infrequent parts of the RNA graph representation, improves classification accuracy.

We applied a standard sequence-alignment method and the most advanced graph kernel methods to the graph representations for producing a Gramian matrix. Then, we utilised machine learning classification algorithms to this matrix to categorise it into high-level classes. The highest result from [1] using WLOA on the Seq had an accuracy of 92.0%. However, our representation, using the WLOA method on the 2D RNA structure and with 75% fewer vertices, achieved the best result with an accuracy of 86.6% and performed better than the highest results from [1] using the same graph kernels. The unweighted graph representation of the 2D RNA can also classify RNA molecules but with a trade-off of increased speed but lower accuracy.

Despite this success, the results from all 2D RNA graph representations did not perform as well as the primary RNA graph representation due to the loss of information and unpredictability of actual 2D RNA shapes.

## REFERENCES

- [1] E. Algul and R. C. Wilson, "A database and evaluation for classification of RNA molecules using graph methods," in *Graph-Based Representations in Pattern Recognition*, D. Conte, J.-Y. Ramel, and P. Foggia, Eds. Cham: Springer International Publishing, 2019, pp. 78–87.

- [2] D. Bechhofer and M. Deutscher, "Bacterial ribonucleases and their roles in rna metabolism," *Critical Reviews in Biochemistry and Molecular Biology*, vol. 54, pp. 242–300, 05 2019.
- [3] "3dna: a suite of software programs for the analysis, rebuilding and visualization of 3-dimensional nucleic acid structures," x3dna.org. [Online]. Available: <http://x3dna.org/>
- [4] M. S. WATERMAN, "Secondary structure of singlestranded nucleic acids," *Studies in Foundations and Combinatorics Advances in Mathematics Supplementary Studies*, vol. 1, pp. 167–212, 1978. [Online]. Available: <http://citeseerx.ist.psu.edu/viewdoc/download?doi=10.1.1.15.4425rep=rep1type=pdf>
- [5] D. Fera, N. Kim, N. Shiffeldrim, J. Zorn, U. Laserson, H. H. Gan, and T. Schlick, "Rag: Rna-as-graphs web resource," *BMC Bioinformatic*, vol. 5, 07 2004. [Online]. Available: <https://bmcbioinformatics.biomedcentral.com/articles/10.1186/1471-2105-5-88>
- [6] D. Knisley, J. Knisley, C. Ross, and A. Rockney, "Classifying multigraph models of secondary rna structure using graph-theoretic descriptors," *ISRN Bioinformatics, International Scholarly Research Network*, 11 2012. [Online]. Available: <https://doi.org/10.5402/2012/157135>
- [7] J. Huang, K. Li, and M. Gribskov, "Accurate classification of rna structures using topological fingerprints," *PLOS ONE*, vol. 11, no. 10, pp. 1–19, 10 2016. [Online]. Available: <https://doi.org/10.1371/journal.pone.0164726>
- [8] R. C. Wilson and E. Algul, "Categorization of rna molecules using graph methods," in *Structural, Syntactic, and Statistical Pattern Recognition*, X. Bai, E. R. Hancock, T. K. Ho, R. C. Wilson, B. Biggio, and A. Robles-Kelly, Eds. Cham: Springer International Publishing, 2018, pp. 439–448.
- [9] S. V. N. Vishwanathan, N. N. Schraudolph, R. Kondor, and K. M. Borgwardt, "Graph kernels," *Journal of Machine Learning Research*, vol. 11, pp. 1201–1242, 2010.
- [10] G. M. Blackburn, M. J. Gait, D. Loakes, D. M. Williams, J. A. Grasby, M. Egli, A. Flavell, S. Allen, J. Fisher, A. M. Pyle, *et al.*, *Nucleic acids in chemistry and biology*. Royal Society of Chemistry, 2006.
- [11] M. Zuker, "Mfold web server for nucleic acid folding and hybridization prediction," *Nucleic Acids Research*, vol. 31, no. 13, pp. 3406–3415, 07 2003. [Online]. Available: <https://doi.org/10.1093/nar/gkg595>
- [12] H. Jabbari, I. Wark, and C. Montemagno, "Rna secondary structure prediction with pseudoknots: Contribution of algorithm versus energy model," *PLOS ONE*, vol. 13, pp. 1–21, 04 2018.
- [13] Y. Wu, B. Shi, X. Ding, T. Liu, X. Hu, K. Y. Yip, Z. R. Yang, D. H. Mathews, and Z. J. Lu, "Improved prediction of RNA secondary structure by integrating the free energy model with restraints derived from experimental probing data," *Nucleic Acids Research*, vol. 43, pp. 7247–7259, 07 2015.
- [14] K. Doshi, J. Cannone, C. Cobaugh, and R. Gutell, "Evaluation of the suitability of free-energy minimization using nearest-neighbor energy parameters for rna secondary structure prediction," *BMC bioinformatics*, vol. 5, p. 105, 09 2004.
- [15] M. Zuker and P. Stiegler, "Optimal computer folding of large RNA sequences using thermodynamics and auxiliary information," *Nucleic Acids Research*, vol. 9, no. 1, pp. 133–148, 01 1981. [Online]. Available: <https://doi.org/10.1093/nar/9.1.133>
- [16] I. L. Hofacker, "Vienna RNA secondary structure server," *Nucleic Acids Research*, vol. 31, no. 13, pp. 3429–3431, 07 2003. [Online]. Available: <https://doi.org/10.1093/nar/gkg599>
- [17] L. Wang, Y. Liu, X. Zhong, H. Liu, C. Lu, C. Li, and H. Zhang, "Dmfold: A novel method to predict rna secondary structure with pseudoknots based on deep learning and improved base pair maximization principle," *Frontiers in Genetics*, vol. 10, p. 143, 2019.
- [18] P. S. Klosterman, M. Tamura, S. R. Holbrook, and S. E. Brenner, "SCOR: a Structural Classification of RNA database," *Nucleic Acids Research*, vol. 30, pp. 392–394, 01 2002.
- [19] X. Lu and W. K. Olson, "3DNA: a software package for the analysis, rebuilding and visualization of three-dimensional nucleic acid structures," *Nucleic Acids Research*, vol. 31, pp. 5108–5121, 09 2003.
- [20] F. Vendeix, A. Munoz, and P. Agris, "Free energy calculation of modified base-pair formation in explicit solvent: A predictive model," *RNA (New York, N.Y.)*, vol. 15, pp. 2278–87, 10 2009.
- [21] I. TINOCO, O. C. UHLENBECK, and M. D. LEVINE, "Estimation of Secondary Structure in Ribonucleic Acids," *Nature*, vol. 230, pp. 362–367, 04 1971. [Online]. Available: <https://doi.org/10.1038/230362a0>
- [22] N. Nicolo, "Learning with kernels on graphs: Dag-based kernels, data streams and rna function prediction," *Alma Mater Studiorum-Universita di Bologna*, 2014. [Online]. Available: <https://pdfs.semanticscholar.org/313b/7d182e81e021faed1cf650f480fdeaeeb3d6.pdf>
- [23] G. K. D. de Vries, "A fast approximation of the weisfeiler-lehman graph kernel for rdf data," in *Machine Learning and Knowledge Discovery in Databases*, H. Blockeel, K. Kersting, S. Nijssen, and F. Zelezný, Eds. Berlin, Heidelberg: Springer Berlin Heidelberg, 2013, pp. 606–621.
- [24] N. M. Kriege, P.-L. Giscard, and R. C. Wilson, "On valid optimal assignment kernels and applications to graph classification," in *Advances in Neural Information Processing Systems*, 2016, pp. 1615–1623.
- [25] N. Shervashidze, P. Schweitzer, E. J. van Leeuwen, K. Mehlhorn, and K. M. Borgwardt, "Weisfeiler-lehman graph kernels," *Journal of Machine Learning Research*, vol. 12, pp. 2539–2561, 2011. [Online]. Available: <http://dl.acm.org/citation.cfm?id=2078187>

- [26] K. M. Borgwardt and H. Kriegel, "Shortest-path kernels on graphs," in Proceedings of the 5th IEEE International Conference on Data Mining (ICDM 2005), 27-30 November 2005, Houston, Texas, USA, 2005, pp. 74–81. [Online]. Available: <http://dx.doi.org/10.1109/ICDM.2005.132>
- [27] P.-L. Giscard and R. C. Wilson, "The all-paths and cycles graph kernel," arXiv preprint arXiv:1708.01410, 2017.
- [28] S. B. Needleman and C. D. Wunsch, "A general method applicable to the search for similarities in the amino acid sequence of two proteins," *Journal of Molecular Biology*, vol. 43, no. 3, pp. 443–453, 1970.
- [29] Schmidt, Marco F. "DNA: Blueprint of the Proteins." *Chemical Biology: and Drug Discovery*. Berlin, Heidelberg: Springer Berlin Heidelberg, 2022. 33-47.
- [30] Ou, Xiujuan, et al. "Advances in RNA 3D Structure Prediction." *Journal of Chemical Information and Modeling* 62.23 (2022): 5862-5874.
- [31] Schulz, Till Hendrik, et al. "A generalized weisfeiler-lehman graph kernel." *Machine Learning* 111.7 (2022): 2601-2629.
- [32] Salim, Asif, S. S. Shiju, and S. Sumitra. "Graph kernels based on optimal node assignment." *Knowledge-Based Systems* 244 (2022): 108519.

## Epidemic Spread Analysis in Social Communication Networks With Sir Model

Yiğit Alisan<sup>1\*</sup> , Nagehan İlhan<sup>2</sup> 

<sup>1</sup> Adana Alparslan Türkeş Science and Technology University, Department of Information Technology Adana, Türkiye

<sup>2</sup> Harran University, Engineering Faculty, Computer Engineering Department, Şanlıurfa, Türkiye

Yiğit Alisan ORCID No: 0000-0003-2943-7743  
Nagehan İlhan ORCID No: 0000-0002-1367-9230

\*Corresponding author: [yalisan@atu.edu.tr](mailto:yalisan@atu.edu.tr)

(Received: 20.01.2023, Accepted: 16.05.2023, Online Publication: 22.06.2023)

### Keywords

Centrality measures, Social network analysis, Community detection, SIR model

**Abstract:** Compartmental mathematical models are frequently used in epidemiology. These models are based on certain assumptions to mathematically model real-life events. However, these assumptions have some limitations. One of these limitations is that they assume that the community is homogeneous, although communities are often heterogeneous. For example, a community may have people or super-spreaders who are not in contact with anyone infected with the virus. In case of limited opportunities, the rate of disease spread can be reduced by vaccinating super-spreaders instead of normal individuals. In the study, centrality values of each individual in the community are determined using a real data set. Vaccinated (immune) and infected individuals are then selected according to certain criteria, and disease spread is simulated. Finally, results are produced using the SIR model, which is the basis of compartmental models. According to the results obtained, the minimum amount of vaccine required to prevent disease spread is calculated. As a result, it was concluded that using the recommended method instead of traditional methods to prevent the spread of disease in the community will result in a 14.39% reduction in vaccine usage.

## Sır Modeli ile Sosyal İletişim Ağlarında Salgın Yayılım Analizi

### Anahtar

Kelimeler  
Merkezlilik ölçüleri, Sosyal ağ analizi, Topluluk tespiti, SIR modeli

**Öz:** Bölmeli matematiksel modeller epidemiyolojide sıklıkla kullanılmaktadır. Bu modeller, gerçek hayattaki olayları matematiksel olarak modellemek için belirli varsayımlar üzerine kuruludur. Ancak, bu varsayımların bazı sınırlamaları vardır. Bu sınırlamalardan biri, gerçekte toplulukların genellikle heterojen olmasına karşın, topluluğun homojen olduğunu varsaymalarıdır. Örneğin, bir toplulukta virüs bulaşmış herhangi bir kişiyle temas halinde olmayan kişiler veya süper yayıcılar bulunabilmektedir. Kısıtlı imkanların olması durumunda normal bireyler yerine öncelikle süper yayıcıların aşılınmasıyla hastalık yayılım hızı azaltılabilmektedir. Yapılan çalışmada gerçek bir veri seti kullanarak topluluktaki her bireyin merkezilik değerlerini belirlenmektedir. Daha sonra aşılınmış (bağışıklıklı) ve enfekte olmuş bireyler belirli kriterlere göre seçilmekte ve hastalık yayılımı simüle edilmektedir. Son olarak kompartıman modellerinin temeli olan SIR modelini kullanarak sonuçlar üretilmektedir. Elde edilen sonuçlara göre hastalık yayılımının önlenmesi için kullanılması gereken asgari aşı miktarı elde edilmektedir. Sonuç olarak, toplumda hastalık yayılımını önlemek için geleneksel yöntemler yerine önerilen yöntemin kullanılmasıyla aşı kullanımında % 14,39'luk bir azalma sağlayacağı sonucuna varılmıştır.

## 1. INTRODUCTION

Mathematical models used in the field of epidemiology can produce useful outputs to make predictions about the possibility of emerging diseases turning into epidemics,

mortality rate, effectiveness of the measures taken, etc. and to prepare for possible scenarios. The studies that began in 1766 with Daniel Bernoulli's mathematical model of smallpox [1] were first developed by Hamer in 1906, considering the assumption that the number of new

cases depends on the number of infected individuals and the number of individuals susceptible to the disease [2]. In 1911, Ross developed a differential model of the number of cases and epidemic control [4]. The model called SIR (Susceptible – Infectious – Removed / Recovered), created by Kermack – McKendrick in 1927, constitutes the basic logic of compartment models of the spread of infectious diseases in communities by assuming that there is no new individual entry [3]. The SIR model is based on some assumptions such as that community is closed, the population is fixed, individuals are homogeneous, there are no birth or death (except infectious diseases), and the disease is only contagious from person to person. In the studies on the constraints in the SIR model, new models such as SIS, SEIS, SIRS, SEIRS, SEIR, MSIR, MSEIR, and MSEIRS were created. In the Kermack–McKendrick basic epidemic model, it is assumed that each individual is in equal contact. However, in epidemics, it is often observed that there are few "super spreaders" that cause the disease to spread in the community. At the same time, most of the sick individuals do not transmit the disease at all or infect a minimal number of individuals [6]. In the Netherlands, 96% of the population was vaccinated against measles, but in 1999 a 5-person case of measles in a small school turned into an epidemic of 3000 people [7]. In 2003, one of two SARS individuals who traveled to Canada infected five more people in Toronto, causing an outbreak of 200 people in total [8]. The difference in the contact rates of individuals may vary according to their social environment, age, gender, environment, and behavior. This type of heterogeneity can be seen at any scale and in every epidemic. These conditions may cause differences in variables such as contagiousness and susceptibility to the disease [9]. Thanks to such advances, there are studies in epidemiology that focus on individual-based approaches and network modeling to avoid assumptions that are incompatible with real life in order to simplify mathematical equations in compartment models [10, 27]. However, there may be some difficulties in the addition of a dynamic network structure in compartment models [28]. In this study, instead of the assumption that the population structure is homogeneous, a heterogeneous population structure that is more representative of the actual community was used. Basically, in order to prevent the spread of the disease to the maximum extent with the minimum amount of vaccine, the prevention of the spread of the disease was simulated by immunizing the individuals who make up the community according to their degree of centrality in the network.

The study consists of the following sections. In the introduction, basic information about the pandemic, compartment models, constraints, and social networks is given. In the literature review section, studies on the use of compartment models and social networks in the field of epidemiology are included. In the Materials and Method section, the basic SIR model, basic degrees of centrality and calculation methods used in the feature inference of the nodes that make up the networks, and basic information about the data set used in the application are presented. In the findings section, the effects of a total of 7 different infected and immune individual

communities on disease spread in networks are presented numerically and visually on the sample data set. In the conclusion section, the contribution of the study to the literature and some limitations are emphasized.

## 2. MATERIAL AND METHOD

New models such as SIR [5], SEIR ([12] [13][14]), SIRS ([15] [16] [17] [18]), SEIRS ([19][20][21]), MSIR ([22][23][24]), MSEIR [25], etc., which are shown as the basis of compartment models, were created by adding new compartments according to the need. Additionally, efforts have been made to address some of the drawbacks of compartment models. Saeedian et al. [31] believed that individual experiences had a direct bearing on how the epidemic evolved and introduced memory to the SIR basic model to account for these impacts. A fractional SIR model with birth and death rates in heterogeneous complex networks was developed in the paper of Huo and Zao [26]. Studies on the presumption that the population in the models is homogeneous are also available [27]. It was underlined that statically built networks gave inaccurate data concerning infection spread paths compared to dynamic networks in the study by Isella et al. [29] to explore the spreading behavior of diseases in networks. The impact of population structure on infectious diseases has also been the subject of numerous studies [30]. Bansal et al. used heterogeneous network models rather than homogeneous network models in compartment models used in the field of epidemiology to conduct investigations on disease spread variability [27]. There has been researching on how disease knowledge affects the spread of diseases in static networks [32]. Additionally, employing random regular networks on the SIR and SIS models, which serve as the foundation for compartment models, the impacts of network parameters on epidemic propagation were investigated [33]. Olinky and Stone [34] reached the conclusion that the traditional compartment-type models' assumption that the disease will end when the transmission rate falls below a particular threshold is invalid in heterogeneous networks and that the spread of epidemics is correlated with the properties of the networks. A thorough investigation into the dynamic behavior of epidemics in large and diverse networks was carried out by Barthélemy et al. [35].

In addition to the number of nodes and edges, networks can also show different characteristics according to the relationships between nodes. Different studies have been conducted to determine the value of nodes according to their location in networks [36][37][49][50]. Wang et al. proposed a new measure of centrality called efficiency centrality (EffC) [38]. The results obtained by simulating the spread of the epidemic in 4 real networks with the SIR model showed that the proposed method was effective and feasible. In the SIR model, it was noted that heterogeneous contact patterns compared to homogeneous scenarios caused earlier and larger outbreaks for a wide range of parameter values, with smaller outbreaks occurring in some parameter combinations [40].



## 2.1. Material and Method Subheading

### 2.1.1. Data Set

Data from the 2009 exhibit "Infectious: Stay Away" at the Science Gallery in Dublin were used to create the data set that serves as a representation of the sample population [41]. Visitors to the exhibition were knotted together, and an edge was created to represent the face-to-face contact between these visitors that lasted at least 20 seconds. Many edges between two nodes could signify multiple points of contact between the nodes. Data from the day with the most interactions is present in the network. The data were obtained between the hours of 10.00-14.00, when the interaction was high. Table 1 displays the dataset's basic numerical data.

**Table 1.** Basic information of the dataset

Property	Value
Node number	410
Number of links	17,298
Median distance	4
p-value	0.8790
Number of unique edges	2,765
Average edge multiplicity	6.2560
Maximum spoke size	410
Average distance	3.5679
Diameter	9

### 2.1.2. SIR Model

The model, which Kermack and McKendrick introduced to the literature in 1927, includes a total of 3 compartments (Figure 1) [3]. It is presumed that people in the first compartment, S (Susceptible – Sensitive), do not already have the disease but are susceptible to it. People who have the disease, which is present in the S compartment as well and spreads at a consistent rate, go on to the I (Infectious) compartment. The final compartment of the model, R (Removed / Recovered - Death / Immunity), contains individuals from compartment I who have endured the sickness at a constant rate, developed immunity, or perished as a result of the disease.



**Figure 1.** SIR Model [3]

When developing the SIR model, some presumptions were made. The population is fixed, there is no other cause of death besides birth or disease, those who have developed an immunity to the disease do not relapse, each person spreads the disease equally, and the disease only spreads between people in these situations where society is homogeneous (in terms of age, social position, geography, etc.) and closed to outside influences.

$$\frac{dS(t)}{dt} = -\beta S(t)I(t) \quad (1)$$

$$\frac{dI(t)}{dt} = \beta S(t)I(t) - \gamma I(t) \quad (2)$$

$$\frac{dR(t)}{dt} = \gamma I(t) \quad (3)$$

If the  $\beta$  and  $\gamma$  used in the equations of the SIR model (Equations 1-3) are patient and recovery constant values  $t$ , respectively, indicate time [31]. The sum of the values  $S(t)$ ,  $I(t)$ , and  $R(t)$  at any given stage is equal to the population size ( $N$ ). An important parameter in epidemiology is the parameter  $R_0$ , which is the basic coefficient of reproduction. It is defined as the average number of secondary cases transmitted by a single infected individual placed in a fully favorable population. In other words,  $R_0$  shows us the initial rate of spread of the disease. Therefore, if  $R_0$  is  $> 1$ , there will be an outbreak, and if  $R_0$  is  $< 1$ , infected persons will recover (or die) before they can replace them with newly infected people. For the SIR model, the value  $R_0$  is calculated as in Equation 4:

$$R_0 = \frac{\beta}{\gamma} \quad (4)$$

### 2.1.3. Graph Analysis

A graph is a type of structure where different objects are represented as nodes and their connections as edges. In the literature, the letter "G" is typically used to symbolize the graph, the letter "V" for the nodes that make up the graph, and the letter "E" for the edges ([42][43]). There are numerous ways to think about the network structure that emerges from a graph illustrating the connections between nodes and edges. He describes the edges that depict the relationship between these nodes as the connection between social beings, in accordance with Wasserman and Faust [44]. In addition, according to Katz et al., the relationship between individuals can represent different structures such as work, friendship, kinship [45]. Centrality criteria is a criterion that is used to specify the degree of importance relative to the interrelationships of the nodes that make up the network structure. Freeman noted that degree centrality could be used to measure information transfer and communication, centrality between to measure mediation status or control of interest, and proximity centrality could be used to estimate the level of efficiency and appropriateness [47][50]. Studies on these centrality measures were based on Freeman ([46], [47], [48]) in the 1970s [49]. The measure of centrality of intervalence [48] and the measure of the centrality of proximity [53] can produce better results with their low calculation cost. Degree Centrality is calculated according to the sum of the relationships of the nodes that make up the network structure directly with each other [50], [51]. It is formulated using the neighborhood matrix ( $A = (a_{ij})$ ) as shown in Equation 5.  $\sigma_D$  degree centrality,  $j$  degree centrality is the desired node,  $n$  is the total number of nodes in the network, and  $a_{ij}$  refers to the distance between  $i$  and  $j$  nodes in the neighborhood matrix.

$$\sigma_D(j) = \sum_{i=1}^n a_{ij} \quad (5)$$

Closeness Centrality is used to specify the total distances of one node to other nodes. The smaller the distance

between one node in the network and the other nodes, the higher the proximity center [44], [52]. The proximity used in the centralization calculation is shown in Equation 6,  $\sigma_C$  closeness centrality,  $j$  closeness centrality value is the node to be calculated,  $n$  is the total number of nodes in the network, and  $d_G(j, i)$  denotes the shortest distance between  $i$  and  $j$  nodes.

$$\sigma_C(j) = \frac{1}{\sum_{i=1}^n d_G(j, i)} \quad (6)$$

**Betweenness Centrality** In a network, a node's ability to serve as an intermediary and make connections between other nodes who do not already have them is known as centrality. A node must be significant and probably have a high Betweenness Centrality if it discovers the only path via which other nodes such as communication, connectivity, transportation, or transaction must travel [46]. The Betweenness Centrality is used to calculate the centrality shown in Equation 7  $\sigma_B$  the Betweenness Centrality,  $j$  is the node whose Betweenness Centrality value is to be calculated,  $n$  is the total number of nodes in the network,  $g_{ix}$  is the shortest distance between nodes  $i$  and  $x$ , and the  $g_{ix}(j)$  denotes the shortest distance between nodes  $i$  and  $x$  that passes through node  $j$ .

$$\sigma_B(j) = \sum_{i=1, i \neq j}^n \sum_{x=1, x < i, x \neq j}^n \frac{g_{ix}(j)}{g_{ix}} \quad (7)$$

### 3. RESULTS

Using the community network obtained using the sample dataset shown in Figure 2 to demonstrate the importance of the degree of centrality of the nodes in the networks representing the community in the disease spread, the nodes with the characteristics of 41 nodes infected and 41 nodes with immune characteristics, which is 10% of the total population, are selected before determining the input parameters to the SIR model. Then, if the nodes selected as infected transmit the disease instantly, the total number of infected individuals is reached at the end of the exhibition. The 41 randomly infected nodes in State 1, State 2, and State 3 are the same. The 41 randomly selected nodes in State 1, State 4, and State 5 are the same.



Figure 2. Network structure formed between 10.00-14.00.

The numerical values of the infected individuals obtained as a result of the simulation of the sample cases are shown in Figure 3.

Table 2. Selection patterns of nodes used in the sample cases

Cases	Infected node selection method	Recovered node selection method
Case 1	Random	Random
Case 2	Random	Closeness Centrality
Case 3	Random	Betweenness Centrality
Case 4	Closeness Centrality	Random
Case 5	Betweenness Centrality	Random
Case 6	Closeness Centrality	Betweenness Centrality
Case 7	Betweenness Centrality	Closeness Centrality

In Case 1, infected and recover nodes are randomly selected in the network. Then, as a result of the spread of the disease to the nodes that are infected throughout the exhibition and the nodes that do not have immune characteristics and then infects the other nodes with which the nodes that are infected with the disease interact, the number of 41 infected individuals, which initially corresponds to 10% of the total population, reached 294 at the end of the exhibition, infecting approximately 72% of the population. In Case 2, infected individuals were randomly selected. The top 41 individuals with the highest proximity centrality value were selected as immune. In this case, the number of infected individuals reached 291 at the end of the exhibition, infecting about 71% of the population. In Case 3, infected individuals were randomly selected. The first 41 individuals with the highest centrality values among them were selected as immune. In this case, the number of infected individuals reached 280 at the end of the exhibition, infecting about 68% of the population.

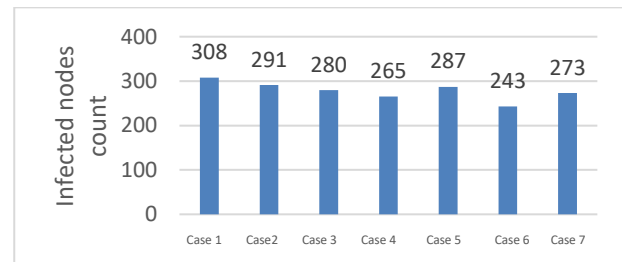


Figure 3. Infected individual values from cases

In Case 4, infected individuals consisted of the top 41 individuals with the highest closeness centrality value. Immune individuals were randomly selected. In this case, the number of infected individuals reached 265 at the end of the exhibition, infecting about 64% of the population. In Case 5, the top 41 individuals with the highest betweenness centrality value among infected individuals were selected. Immune individuals were randomly selected. In this case, the number of infected individuals reached 287 at the end of the exhibition, infecting 70% of the population. In Case 6, infected individuals consisted of the top 41 individuals with the highest closeness centrality value. The group of immune individuals consists of the top 41 individuals with the highest betweenness centrality value among them. In this case, the number of infected individuals reached 287 at the end of

the exhibition, infecting approximately 59% of the population. Finally, in Case 7, the top 41 individuals with the highest centrality value among infected individuals were selected. The group of immune individuals consists of the top 41 individuals with the highest value of closeness centrality. In this case, the number of infected individuals reached 273 at the end of the exhibition, infecting about 66% of the population.

**Table 3.** Percentage infected distribution rates

%	Case 1	Case 2	Case 3
10	71,71	70,98	68,29
20	61,95	60,24	56,83
30	50,98	48,05	46,34
40	43,17	36,83	33,66
50	35,37	29,51	20,98
60	27,80	20,00	14,15
70	21,22	14,15	8,78
80	13,66	7,80	4,39
90	9,27	2,93	1,95

In Table 3, when vaccination is carried out, the changes in the ratio of infected individuals to the total population as a result of the percentage of vaccinated are shown if the people to be vaccinated are randomly selected (Case 1) and if they are made by taking into account centrality criteria such as betweenness centrality values (Case 3) and closeness centrality values (Case 2) according to their location in the network. As can be seen in Table 3, in case 10% of the randomly selected individuals from the total population are immunized by administering vaccine, the randomly selected 10% infected individuals infect approximately 71% of the total population at the end of the exhibition.

**Table 4.** Differences between percentile results for situations

%	Case 1 - Case 2	Case 1 - Case 3	Case 2 - Case 3
10	0,73	3,41	2,68
20	1,71	5,12	3,41
30	2,93	4,63	1,71
40	6,34	9,51	3,17
50	5,85	14,39	8,54
60	7,80	13,66	5,85
70	7,07	12,44	5,37
80	5,85	9,27	3,41
90	6,34	7,32	0,98

In case 2, in the same conditions, it is seen that if the 41 individuals with the highest closeness centrality value corresponding to 10% in the total population are immunized by administering vaccine, the randomly selected 10% infected individual infects approximately 70.98% of the total population at the end of the exhibition. In case 3, if the 41 individuals with the highest betweenness centrality value of 10% of the total population are immunized by administering the vaccine under the same conditions, the randomly selected 10% infected individual infects approximately 70.98% of the total population at the end of the exhibition. In Table 4, the largest difference between the 3 cases is 14.39% of the 50% vaccination rate between Case 1 and Case 3. According to this result, if 205 individuals, corresponding to 50% of the total population, are randomly selected and immunized by being vaccinated, 41 infected individuals, of which 10% are randomly selected at the beginning, infect 35.37% of the total population at the end of the

exhibition. If 205 individuals, corresponding to 50% of the total population, are selected from among the individuals with the highest intervalence centrality value instead of randomly, 41 infected individuals of 10% randomly selected at the beginning infect 20.98% of the total population at the end of the exhibition. The largest proportional difference between the criteria of intervalence and closeness centrality is seen in the vaccination rate of 8.54% and 50%. It is seen that if the betweenness centrality values are used instead of the closeness centrality values as the selection criterion of individuals corresponding to 50% of the total population, the infection spread rate will be 8.54% less.

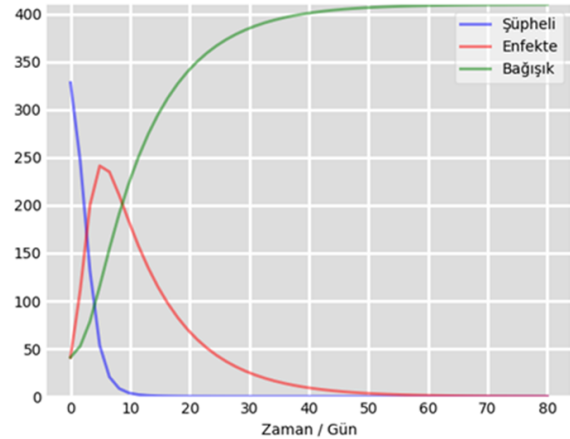


**Figure 4.** SIR model output

Covid-19 spread analysis was performed by applying the SIR model to the existing data set and the result graph is shown in Figure 4. Studies show that the R0 value varies between 2.2-2.6 ratio. The disease is transmitted from person to person through cough or sneeze droplets. The incubation period from the person's exposure to the virus lasts 2-14 days [55][56][57]. SIR is one of the model parameters (value is 1 / 14, (value is 1.2, S value is 410, I and R values are 41. When the result graph is examined, the number of infected patients reaches its peak with approximately 250 individuals infected in the first 10 days and then shows that the spread will decrease and end in an average of 50 days.

#### 4. DISCUSSION AND CONCLUSION

As a result of the studies carried out, compartment-type estimation models frequently used in the field of epidemiology have limitations [28] and one of the most important of these limitations is the assumption that all the individuals constituting the society have the same characteristics [27][41]. In real life, it is seen that the individuals who make up the society have different characteristics such as profession, age, education, social environment and these characteristics have a significant impact on the spread of the disease. Today, it is necessary to use the assets in the best way for the rapid solution against the infectious diseases that develop suddenly and spread to many parts of the world at a level that can be called a pandemic. A vaccine is used as the primary treatment method to prevent and control infectious diseases that have rapidly reached the level of a pandemic. In the absence of existing solutions in new pandemics,

vaccine development studies gain importance. For example, the time it took to find the first vaccine and control the disease was approximately one year during the most recent Covid-19 pandemic [39]. Two years after the first effective vaccine is available, access to the vaccine is still limited in some countries. In this case, it is also important that the vaccines obtained are used systematically and consciously in order to control the spread of the pandemic in countries with limited access to vaccines due to economic reasons. With this awareness, many countries have developed different strategies to use the available vaccines effectively and efficiently by identifying priority groups in vaccination. In the study, sample cases were simulated on the selection of individuals to be vaccinated. According to the results obtained, the rate of infected individuals is 14.39% less if the individuals to be vaccinated are selected according to their degree of centrality instead of being randomly selected. Considering the population of Turkey, it means that approximately 12 million vaccines are used less and financial savings in order to stop the spread of the epidemic.

### Acknowledgement

This paper was produced from the thesis study named "Dinamik Ağlarda Hastalık Yayılma Analizi".

### REFERENCES

- [1] D. Bernoulli, S. Blower, "An attempt at a new analysis of the mortality caused by smallpox and of the advantages of inoculation to prevent it", *Reviews in medical virology*, vol. 14, no. 5, p. 275, 2004.
- [2] W. H. Hamer, "Epidemic disease in England: the evidence of variability and of persistency of type", Bedford Press, 1906.
- [3] W. O. Kermack, A. G. McKendrick, G. T. Walker, "A contribution to the mathematical theory of epidemics", *Proceedings of the Royal Society of London. Series A, Containing Papers of a Mathematical and Physical Character*, vol. 115, no. 772, pp. 700-721, 1927.
- [4] R. Ross, "The prevention of malaria", John Murray, 1911.
- [5] W. O. Kermack, A. G. McKendrick, and G. T. Walker, "A contribution to the mathematical theory of epidemics", *Proceedings of the Royal Society of London. Series A, Containing Papers of a Mathematical and Physical Character*, vol. 115, no. 772, pp. 700-721, 1927.
- [6] "Transmission Dynamics of the Etiological Agent of SARS in Hong Kong: Impact of Public Health Interventions", *Science*, <https://science.sciencemag.org/content/300/5627/1961.abstract> (accessed May 29, 2021).
- [7] "Measles outbreak", Netherlands, April 1999-January 2000, <https://www.cabdirect.org/cabdirect/abstract/20002012656>
- [8] "Identification of Severe Acute Respiratory Syndrome in Canada- NEJM." <https://www.nejm.org/doi/full/10.1056/NEJMoa030634> (accessed May 29, 2021).
- [9] H. W. Hethcote and J. A. Yorke, "Gonorrhea Transmission Dynamics and Control", Springer, 2014.
- [10] M. E. J. Newman, "The structure and function of complex networks", *SIAM Review*, vol. 45, no. 2, pp. 167-256, 2003.
- [11] S. Jain, S. Kumar, "Dynamical analysis of SEIS model with nonlinear innate immunity and saturated treatment", *The European Physical Journal Plus*, 136(9), 952, 2021.
- [12] S. Annas, M. I. Pratama, M. Rifandi, W. Sanusi, S. Side, "Stability analysis and numerical simulation of SEIR model for pandemic COVID-19 spread in Indonesia", *Chaos, Solitons & Fractals*, 139, 110072, 2020.
- [13] S. He, Y. Peng, K. Sun, "SEIR modeling of the COVID-19 and its dynamics", *Nonlinear Dynamics*, vol. 3, no. 101, pp. 1667-1680, 2020.
- [14] P. E. Lekone, B. F. Finkenstädt, "Statistical inference in a stochastic epidemic SEIR model with control intervention: Ebola as a case study", *Biometrics*, vol. 4, no. 62, pp. 1170-1177, 2006.
- [15] M. B. Hooten, J. Anderson, & L. A. Waller, "Assessing North American influenza dynamics with a statistical SIRS model. Spatial and Spatio-Temporal", *Epidemiology*, vol. 1, no. 2-3, pp. 177-185, 2010.
- [16] A. Lahrouz, L. Omari, D. Kiouach, & A. Belmaâti, "Complete global stability for an SIRS epidemic model with generalized non-linear incidence and vaccination", *Applied Mathematics and Computation*, 218(11), pp. 6519-6525, 2012.
- [17] C.-H. Li, C.-C. Tsai, S.-Y. Yang, "Analysis of epidemic spreading of an SIRS model in complex heterogeneous network", *Communications in Nonlinear Science and Numerical Simulation*, 19(4), pp. 1042-1054, 2014.
- [18] C. Vargas-De-León, "On the global stability of SIS, SIR and SIRS epidemic models with standard incidence", *Chaos, Solitons & Fractals*, 44(12), pp. 1106-1110, 2011.
- [19] K. L. Cooke, P. Van Den Driessche, "Analysis of an SEIRS epidemic model with two delays", *Journal of Mathematical Biology*, 35(2), pp. 240-260, 1996.
- [20] B. K. Mishra, D. K. Saini, "SEIRS epidemic model with delay for transmission of malicious objects in computer network", *Applied Mathematics and Computation*, 188(2), pp. 1476-1482, 2007.
- [21] W. Wang, "Global behavior of an SEIRS epidemic model with time delays", *Applied Mathematics Letters*, 15(4), pp. 423-428, 2002.
- [22] D. Bichara, A. Iggidr, G. Sallet, "Global analysis of multi-strains SIS, SIR and MSIR epidemic models", *Journal of Applied Mathematics and Computing*, 44(1), pp. 273-292, 2014.
- [23] A. Menon, N. K. Rajendran, A. Chandrachud, & G. Setlur, "Modelling and simulation of COVID-19 propagation in a large population with specific reference to India", *MedRxiv*, 2020.
- [24] B. Rahman, E. Sadraddin, A. Porreca, "The basic reproduction number of SARS-CoV-2 in Wuhan is

- about to die out, how about the rest of the world? " *Reviews in Medical Virology*, 30(4), e2111, 2020.
- [25] X. Chen, A. Zhang, H. Wang, A. Gallaher, X. Zhu, "Compliance and containment in social distancing: Mathematical modeling of COVID-19 across townships", *International Journal of Geographical Information Science*, 35(3), pp. 446–465, 2021.
- [26] J. Huo, H. Zhao, "Dynamical analysis of a fractional SIR model with birth and death on heterogeneous complex networks", *Physica A: Statistical Mechanics and Its Applications*, 448, pp. 41–56, 2016.
- [27] S. Bansal, B. T. Grenfell, L. A. Meyers, "When individual behaviour matters: homogeneous and network models in epidemiology", *Journal of The Royal Society Interface*, vol. 4, pp. 879-891, 2007.
- [28] L. Pellis et al., "Eight challenges for network epidemic models", *Epidemics*, vol. 10, pp. 58-62, 2015.
- [29] L. Isella, J. Stehlé, A. Barrat, C. Cattuto, J.-F. Pinton, and W. V. den Broeck, "What's in a crowd? Analysis of face-to-face behavioral networks", *Journal of Theoretical Biology*, vol. 271, no. 1, pp. 166-180, 2011.
- [30] A. d'Onofrio, "A note on the global behaviour of the network-based SIS epidemic model", *Nonlinear Analysis: Real World Applications*, vol. 9, no. 4, pp. 1567–1572, 2008.
- [31] M. Saeedian, M. Khalighi, N. Azimi-Tafreshi, G. R. Jafari, and M. Ausloos, "Memory effects on epidemic evolution: The susceptible-infected-recovered epidemic model", *Phys. Rev. E*, vol. 95, no. 2-1, p. 022409, 2017.
- [32] A. Azizi, C. Montalvo, B. Espinoza, Y. Kang, and C. Castillo-Chavez, "Epidemics on networks: Reducing disease transmission using health emergency declarations and peer communication", *Infectious Disease Modelling*, vol. 5, pp. 12-22, 2020.
- [33] M. Nadini, A. Rizzo, M. Porri, "Epidemic Spreading in Temporal and Adaptive Networks with Static Backbone", *IEEE Transactions on Network Science and Engineering*, vol. 7, no. 1, pp. 549-561, 2020.
- [34] R. Olinky, L. Stone, "Unexpected epidemic thresholds in heterogeneous networks: The role of disease transmission", *Physical Review E*, 70(3), 030902, 2004.
- [35] M. Barthélemy, A. Barrat, R. Pastor-Satorras, & A. Vespignani, "Dynamical patterns of epidemic outbreaks in complex heterogeneous networks", *Journal of Theoretical Biology*, 235(2), 275–288, 2005.
- [36] S. P. Borgatti, M. G. Everett, "A Graph-theoretic perspective on centrality", *Social Networks*, 28(4), 466–484, 2006.
- [37] K. Faust, "Centrality in affiliation networks", *Social Networks*, 19(2), 157–191, 1997.
- [38] S. Wang, Y. Du, Y. Deng, "A new measure of identifying influential nodes: Efficiency centrality", *Communications in Nonlinear Science and Numerical Simulation*, 47, 151–163, 2007.
- [39] C. Zimmer, J. Corum, S.-L. Wee, "Coronavirus Vaccine Tracker", *The New York Times*, Jun. 10, 2020. Erişim tarihi: Sep. 21, 2021, Erişim linki: <https://www.nytimes.com/interactive/2020/science/coronavirus-vaccine-tracker.html>
- [40] L. E. C. Rocha, V. D. Blondel, "Bursts of Vertex Activation and Epidemics in Evolving Networks", *PLOS Computational Biology*, vol. 9, no.3, e1002974, 2013.
- [41] M. J., Keeling, K. T. D. Eames, "Networks and epidemic models", *Journal of The Royal Society Interface*, vol. 2, no. 4, pp. 295–307, 2005.
- [42] "Infectious" veri seti, <http://konect.cc/networks/sociopatterns-infectious>, (erişim tarihi: 05.06.2021).
- [43] M. C. Golombic, "Algorithmic graph theory and perfect graphs", Elsevier, 2004.
- [44] B. Bollobás, "Modern graph theory, vol. 184. Springer Science Business Media, 2013.
- [45] S. Wasserman, K. Faust, "Social network analysis: Methods and applications", 1994.
- [46] N. Katz, D. Lazer, H. Arrow, N. Contractor, "Network theory and small groups", *Small group research*, vol. 35, no. 3, pp. 307-332, 2004.
- [47] L. C. Freeman, "A Set of Measures of Centrality Based on Betweenness," *Sociometry*, vol. 40, no. 1, pp. 35-41, 1977.
- [48] L. C. Freeman, "Centrality in social networks conceptual clarification", *Social networks*, vol. 1, no. 3, pp. 215-239, 1978.
- [49] L. C. Freeman, D. Roeder, R. R. Mulholland, "Centrality in social networks: ii. experimental results", *Social Networks*, vol. 2, no. 2, pp. 119-141, 1979.
- [50] J. Zhang, Y. Luo, "Degree Centrality, Betweenness Centrality, and Closeness Centrality in Social Network," pp. 300-303, 2017.
- [51] J. M. Bolland, "Sorting out centrality: An analysis of the performance of four centrality models in real and simulated networks", *Social Networks*, vol. 10, no. 3, pp. 233-253, 1988.
- [52] M. E. Shaw, "Group Structure and the Behavior of Individuals in Small Groups", *The Journal of Psychology*, vol. 38, no. 1, pp. 139-149, 1954.
- [53] M. A. Beauchamp, "An improved index of centrality", *Behavioral Science*, vol. 10, no. 2, pp. 161-163, 1965.
- [54] G. Sabidussi, "The centrality index of a graph", *Psychometrika*, vol. 31, no. 4, pp. 581–603. Scopus, 1966.
- [55] N. Chen, M. Zhou, X. Dong, J. Qu, F. Gong, Y. Han, Y. Qiu, J. Wang, Y. Liu, Y. Wei, J. Xia, T. Yu, X. Zhang, L. Zhang, "Epidemiological and clinical characteristics of 99 cases of 2019 novel coronavirus pneumonia in Wuhan, China: a descriptive study", *Lancet (London, England)*, vol. 395, no. 10223, pp. 507–513, 2020.
- [56] E. Prompetchara, C. Ketloy, T. Palaga, "Immune responses in COVID-19 and potential vaccines: Lessons learned from SARS and MERS epidemic", *Asian Pacific Journal of Allergy and Immunology*, vol. 38, no. 1, pp. 1–9, 2020.

- [57] F. Wu, S. Zhao, B. Yu, Y. -M. Chen, W. Wang, Z.-G. Song, Y. Hu, Z.-W. Tao, J.-H. Tian, Y.-Y. Pei, "A new coronavirus associated with human respiratory disease in China", *Nature*, vol. 579, no.7798, pp. 265–269, 2020.

## Parameter Analysis of Convolutional Neural Network Operated on Embedded Platform for Estimation of Combustion Efficiency in Coal Burners

Veysel GÜNDÜZALP<sup>1\*</sup>, Gaffari ÇELİK<sup>2</sup>, Muhammed Fatih TALU<sup>3</sup>, Cem ONAT<sup>4</sup>

<sup>1,3</sup> Inonu University, Faculty of Engineering, Department of Computer Engineering, Malatya, Türkiye

<sup>2</sup> Agri Ibrahim Cecen University, Vocational School, Department of Computer Technology, Ağrı, Türkiye

<sup>4</sup> Adiyaman University, Faculty of Engineering, Department of Mechanical Engineering, Adiyaman, Türkiye

Veysel GÜNDÜZALP ORCID No: 0000-0002-9199-5749

Gaffari ÇELİK ORCID No: 0000-0001-5658-9529

Muhammed Fatih TALU ORCID No: 0000-0003-1166-8404

Cem ONAT ORCID No: 0000-0002-4295-4860

\*Corresponding author: [vgunduzalp@gmail.com](mailto:vgunduzalp@gmail.com)

(Received: 17.10.2022, Accepted: 16.05.2023, Online Publication: 22.06.2023)

### Keywords

Coal,  
Combustor,  
Combustion  
Efficiency,  
Image  
Processing,  
Convolutional  
Neural Networks

**Abstract:** Accurately and effectively calculating combustion efficiency in coal burners is crucial for industrial boiler manufacturers. Two main approaches can be used to calculate boiler efficiency: 1) Analyzing the gas emitted from the flue; 2) Visualizing the combustion chamber in the boiler. Flue gas analyzers, which are not user-friendly, come with high costs. Additionally, the physical distance between the flue and the combustion chamber causes the measurement to be delayed. Methods based on visualizing the combustion chamber do not have these disadvantages. This study proposes a system based on visualizing the combustion chamber and has two contributions to the literature: 1) for the first time, the modern Convolutional Neural Networks (CNN) approach is used to estimate combustion efficiency; 2) the CNN architecture with optimal parameters can work on an embedded platform. When classical classification techniques and a CPU-supported processor card are used, efficiency can be calculated from one flame image in 1.7 seconds, while this number increases to approximately 20 frames per second (34 times faster) when the proposed CNN architecture and GPU-supported processor card are used. The results obtained demonstrate the superiority of the proposed CNN architecture and hardware over classical approaches in estimating coal boiler combustion efficiency.

## Kömür Yakıcılarında Yanma Verimi Tahmini için Gömülü Platformda Çalışabilen Evrimsel Sinir Ağının Parametre Analizi

### Anahtar Kelimeler

Kömür,  
Yakıcı Sistem,  
Yanma Verimi,  
Görüntü İşleme,  
Evrimsel Sinir  
Ağları

**Öz:** Kömür yakıcılarında yanma veriminin doğru ve etkin bir şekilde hesaplanması endüstriyel kazan üreticileri için oldukça önemlidir. Kazan veriminin hesaplanabilmesi için iki temel yaklaşımın olduğu görülmektedir: 1) bacadan çıkan gazın analizi; 2) kazandaki yanma odasının görüntülenmesi. Kullanımı yeterince kolay olmayan baca gazı analizörleri yüksek maliyete sahiptir. Ayrıca baca ile yanma odası arasındaki fiziksel uzaklık yapılan ölçümün zaman gecikmeli olmasına neden olmaktadır. Yanma odasının görüntülenmesine dayalı yöntemler bahsedilen dezavantajları içermemektedir. Bu çalışmada önerilen ve yanma odasının görüntülenmesine dayanan sistemin literatüre iki katkısı bulunmaktadır: 1) yanma veriminin tahmininde ilk defa modern evrimsel sinir ağları (ESA) yaklaşımının kullanılması; 2) Optimum parametrelere sahip ESA mimarisinin gömülü bir platformda çalışabilmesi. Klasik sınıflandırma teknikleri ve CPU destekli bir işlemci kartı kullanıldığında, 1,7 saniyede 1 adet alev formu görüntüsünden verim hesaplanabilirken, önerilen ESA mimarisi ve GPU destekli bir işlemci kartı kullanıldığında bu sayı saniyede yaklaşık 20 adet seviyesine çıkmaktadır (34 kat hızlı). Elde edilen sonuçlar, kömür kazanı yanma verimi tahmininde önerilen ESA mimarisinin ve donanımının klasik yaklaşımlara olan üstünlüğünü açık bir şekilde ortaya koymaktadır.

## 1. INTRODUCTION

The increase in the combustion efficiency of the coal boiler is of great importance for human health, as it causes a decrease in carbon dioxide emissions [1]. In addition, the increase in efficiency provides economic benefits to the enterprises as it will cause the targeted heat energy to be met with less amount of coal.

Classical approaches use the outputs of flue gas analyzers to calculate boiler efficiency [2]. Designers have generally chosen to reduce the oxygen concentration in the flue gas for better efficiency. Many researchers aimed to reduce NO<sub>x</sub> emissions in coal boilers and tried different optimization techniques to achieve this. It is in the subcategory of flue gas inspection for low NO<sub>x</sub> emissions. Lee and Jou reduced the oxygen concentration of the gas in the chimney by 1% to increase the combustion efficiency by 0.6% [3]. Hao et al. used a genetic algorithm (GA) and artificial neural network (ANN) to optimize NO<sub>x</sub> emission in boilers using powdered coal as fuel [4]. In this study of Hao, genetic algorithms were used to determine the current state to optimize the ANN [5]. In addition, it is possible to see researchers that try to reduce the NO<sub>x</sub> level of accidents below the legal level in their countries with ant colonies and genetic algorithm methods [6]. Liu et al. made important studies on boilers using different fuels [7]. In the aforementioned study, wood sawdust was used as fuel. Liu et al. In these studies, an extra air inlet was added to the boiler, and the effect of this inlet on NO<sub>x</sub> and CO emissions was observed according to the altitude. Kauprianov et al. gave detailed information about the relationship between heat losses and the density of the gas in the chimney [8].

The studies mentioned above adopt the flue gas analysis approach to increase boiler efficiency. However, there are three disadvantages to using flue gas analyzers: 1) high cost; 2) difficulty of use; 3) time delay. For flue gas analyzers to be used in a coal burner system with a high market price, a hole must be drilled in the chimney and the measuring apparatus (metal rod) must be fixed in the drilled hole. This process creates significant difficulty for the user. In addition, the system's performance is adversely affected due to the time delay. In addition, these devices, which can measure once per second, require special-purpose licensed software.

Another preferred method to understand boiler efficiency is observing the flame form by the technical staff and manually making the necessary interventions. For this, the coal burner's existing combustion chamber inspection hole is used. This method, which is based on human observation, has disadvantages such as human error, forgetting, and failure to intervene promptly.

Observing the flame form using image processing techniques is a cost-effective, fast, easy-to-use, and error-prone method compared to manual or classical flue gas measurement methods. When the studies on the flame are examined, it seems that the first remarkable studies are related to the imaging of the combustion

chamber. With the flame images, the combustion status of the burner system can be monitored instantly. Yamaguchi et al. to understand the response of the system-to-air ratio differences, evaluated the intensity of the flame using sensors [9]. Lino et al. used image processing to determine the movements of the flame [10]. In the aforementioned study, the variation of flame brightness versus time was investigated. Huang et al. studied flame images in detail [11]. Onat [1] et al. carried out studies that could extract the attributes of the flame form and match the air excess coefficient ( $\lambda$ ) with artificial learning methods. However, these studies could not go beyond the use of classical feature extraction and classification techniques.

Contrary to classical studies, the use of Convolutional Neural Networks (CNN) is recommended in this article to calculate the yield from the image. Thanks to this approach, feature extraction and classification can be done together. In Fig. 1, the general working principle of the classical and proposed approaches is shown together.

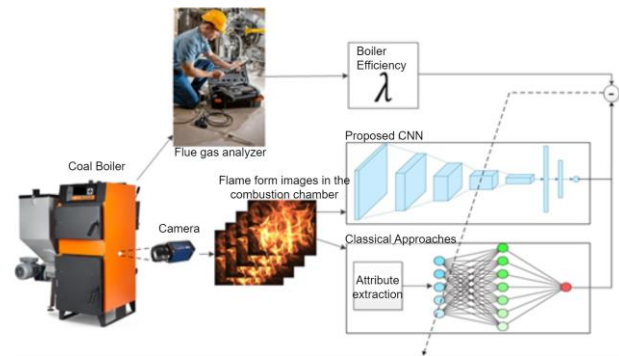


Figure 1. The general operation of the system

## 2. MATERIAL

The data obtained through a camera placed at the mouth of a boiler, which was positioned to visualize combustion inside the boiler, was used to estimate combustion efficiency from flame images in this study. The combustion section is visualized through the camera placed in the observation section of the boiler. The images are captured as instantaneous 2D images using a CCD camera connected to a computer. The camera has a resolution of 659x494 pixels. As a result, a dataset containing 9965 flame image samples was created. The sample data is presented in Fig. 2.

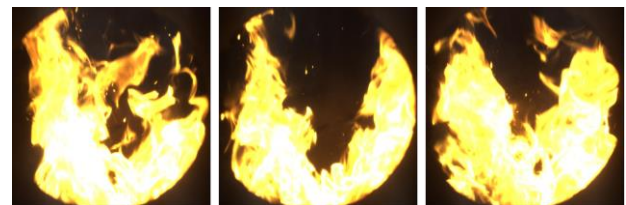


Figure 2. Sample flame images

## 3. METHODS

In this section, the classical methods used to extract features from flame form images obtained from the combustion chamber of the coal boiler are expressed. In addition, the proposed convolutional neural network



architecture for the estimation of combustion efficiency is mentioned.

### 3.1 Classical Feature Extraction Methods

Classical methods such as Hue-Hist, Gray co-occurrence matrix, Blue-Hist, PCA, RES, and Multivariate normal distribution were used to extract the features.

#### 3.1.1 Hue-Hist

Flame form image is obtained in RGB format. Therefore, first RGB→HSV color space conversion is performed and then the histogram of the H channel is obtained. Since the number of parts in the histogram was taken as 255, a 1x255 feature was obtained from each image [12,13].

#### 3.1.2. Gray co-occurrence matrix

The flame from the image in RGB format is converted to gray format and the co-occurrence matrix is calculated. This matrix contains the second-order statistical features of an image. As is known, first-order statistics do not contain any information about the positions of different intensity values in the image. Contains the number of patterns formed by pairs of pixels within a predetermined distance range. This 8x8 matrix contains a total of 1x64 attribute information [14,15].

#### 3.1.3. Blue-Hist

As a result of the studies on the channels of the RGB flame image, it has been seen that it is possible to observe the outer environment of the flame form by using the B channel. This provides important information about the size of the flame form. For this reason, the histogram data of channel B is calculated and a 1x255 feature is obtained [12].

#### 3.1.4. PCA

After the gray conversion of the RGB image is realized, its size is reduced by the PCA method. In the dimension reduction process, the two largest eigenvalues of the gray density matrix are used [16,17].

#### 3.1.5 Radial energy signal (RES)

Radiant energy signal is in the form of waves or particles, mainly in the form of electromagnetic radiation. Heat is an example of radiant energy. The average value of image color intensities is expressed as radiant energy [18,19].

#### 3.1.6. Multivariate normal distribution

The similarity of each pixel in the flame form image to a particular model is calculated. First, the mean and covariance of an image expressing optimal combustion are calculated. Then, the similarity of each pixel in the

newly obtained flame form image to the optimal form is calculated with the following formula [12].

$$Feature[t] = \frac{1}{\sqrt{|\Sigma_k|} (2\pi)^d} \exp\left(-\frac{1}{2} (k_{i,j} - \mu_k) \Sigma^{-1} (k_{i,j} - \mu_k)^T\right) \quad (1)$$

### 3.2. Proposed CNN Architecture

Since 2012, CNN architectures have dominated the field of machine learning, and most classical image processing and computer vision techniques have been redesigned with these architectures. The success of CNN has been experienced in various fields, particularly in image classification [20], object detection [21], scene classification [22], activity recognition from physical movements [23], Covid-19 detection from X-ray and CT images [24], brain MRI segmentation [25], brain tumor diagnosis [26], ECG arrhythmia classification [27], Covid-19 diagnosis from cough sound [28], Parkinson's disease detection from speech signals [29], etc., significantly improving the performance in these areas. The success of CNN has drawn the attention of many researchers in this direction.

In this study, the flame-efficiency matching accuracy of many different CNN architectures was examined and the parameters of the optimum architecture were determined. The optimum CNN architecture obtained is shown in Table 1. The total number of parameters in the architecture with a 23-layer structure is 219.891. Mean Squared Error (MSE) has been used to update the weights of the proposed architecture [30].

$$Loss_{MSE} = \frac{1}{C} \sum_{i=1}^C (\lambda_i - \lambda'_i)^2 \quad (2)$$

Here, C represents the number of samples,  $\lambda_i$  represents the  $\lambda$  value corresponding to the  $i$ th flame, and  $\lambda'_i$  represents the estimated  $\lambda$  value.

**Table 1.** Optimal CNN architecture

Layer	Size	Parameter
conv2d_1 (Conv2D)	(128, 128, 16)	448
conv2d_2 (Conv2D)	(128, 128, 16)	2320
activation_1 (Activation)	(128, 128, 16)	0
batch_normalization_1 (Batch Normalization)	(128, 128, 16)	64
max_pooling2d_1 (MaxPooling2D)	(64, 64, 16)	0
conv2d_3 (Conv2D)	(64, 64, 16)	2320
activation_2 (Activation)	(64, 64, 16)	0
batch_normalization_2 (Batch Normalization)	(64, 64, 16)	64
max_pooling2d_2 (MaxPooling2D)	(32, 32, 16)	0
conv2d_4 (Conv2D)	(32, 32, 16)	2320
activation_3 (Activation)	(32, 32, 16)	0
batch_normalization_3 (Batch Normalization)	(32, 32, 16)	64
max_pooling2d_3 (MaxPooling2D)	(16, 16, 16)	0
conv2d_5 (Conv2D)	(16, 16, 16)	2320
conv2d_6 (Conv2D)	(16, 16, 16)	2320
activation_4 (Activation)	(16, 16, 16)	0
flatten_1 (Flatten)	(4096)	0
dense_1 (Dense)	(50)	204850
activation_5 (Activation)	(50)	0
batch_normalization_4 (Batch Normalization)	(50)	200
dropout_1 (Dropout)	(50)	0
dense_2 (Dense)	(50)	2550
activation_6 (Activation)	(50)	0
dense_3 (Dense)	(1)	51

## 4. RESULTS AND DISCUSSION

In this study, a CNN-based architecture has been proposed for predicting combustion efficiency from flame images. 90% of the dataset used was reserved for training and the remaining 10% was used for testing. The proposed architecture was trained for 150 epochs using the Adam optimization algorithm (with  $lr=1e-2$ ). The performance of the architectures was evaluated using the R metric, which is defined as follows [12].

$$R = \left( \frac{\sum_{i=1}^C (\lambda_i - \bar{\lambda})(\lambda'_i - \bar{\lambda}')}{\sqrt{\sum_{i=1}^C (\lambda_i - \bar{\lambda})^2 \sum_{i=1}^C (\lambda'_i - \bar{\lambda}')^2}} \right) \times 100 \quad (3)$$

Here,  $C$  represents the number of samples,  $\lambda_i$  represents the  $\lambda$  value corresponding to the  $i$ th flame,  $\bar{\lambda}$  represents the average of  $\lambda_i$  values,  $\lambda'_i$  represents the estimated value, and  $\bar{\lambda}'$  represents the average of  $\lambda'_i$  values.

### 4.1. Classical Approaches

In this section, image- $\lambda$  matching accuracies of classical approaches are examined. Firstly, features were obtained from colored flame form images by using the feature extraction methods mentioned (see Table 2). Then, the feature vectors were mapped to the relevant  $\lambda$  coefficient with the ANN method. The obtained accuracy values are shown in Table 2. As can be seen from the results, the highest matching accuracy was obtained with the Multivariate normal distribution method.

**Table 2.** Classical feature extraction methods and their results

Method	Attribute	Working time	Success
	Count		
Hue-hist (0-255) [13]	255	1.366	77.00
Gray co-occurrence matrix [15]	64	0.901	85.50
Blue-hist (255) [15]	255	1.564	73.10
PCA [17]	2	1.693	70.40
RES [19]	4	1.971	64.20
Multivariate normal distribution	768	0.351	95.10

## 4.2. Proposed Approach

In this section, the parameters of the optimum CNN architecture that will best match the image- $\lambda$  are investigated. The answers to the questions listed below were sought to discover the optimal architecture:

- What should be the optimal value of the image resolution to be given as input to the CNN architecture?
- What should be the optimal value of "batch size" in the training process?
- What should be the optimal number of layers in the architecture?

### 4.2.1. Image resolution effect

In this experimental study, the effect of image size on image- $\lambda$  matching is analyzed. Accordingly, the input image dimensions of the flame form were converted to 128x128, 64x64, 48x48, and 32x32, and training and testing were carried out using a CNN with the same parameters (number of layers, number of iterations, etc.). The obtained accuracy and time results are given in Table 3. Contrary to the classification problem, the input image size is expected to have a large effect on the output value in the regression problem. When the results in Table 3 were examined, it was seen that the image size had a significant effect on the accuracy and time results. As the size increases, the matching accuracy and time spent by CNN increase. Accordingly, the highest matching accuracy was obtained with the image size of 128x128.

**Table 3.** Accuracy and time effect of image size

Resolution	Success		Time
	Train	Test	Train(sec)
32x32	93.87	94.45	1400
48x48	96.48	93.56	1800
64x64	93.98	94.67	2100
128x128	97.33	95.55	2400

### 4.2.2. Pack size effect

It is known that the pattern packet size has a large effect on the direction and speed of convergence. It is known that the patterns are trained one by one (stochastic), in small packages (mini-batch), or as a whole (full batch). In this experimental study, to determine the optimum packet size, the training process was carried out by choosing different packet sizes, provided that the total number of images remained constant. The results obtained are given in Table 4. When the results are examined, it is seen that the most suitable package size is 48. When a package size lower or higher than this value is selected, the accuracy values obtained for the training and test set decrease.

**Table 4.** The effect of packet size on accuracy and time

Package size	Success		Time
	Train	Test	
16	94.45	90.19	
25	95.14	93.76	
48	<b>97.33</b>	<b>94.67</b>	
100	93.87	82.38	
200	90.24	91.05	

### 4.2.3. Layer count effect

In this experimental study, the effect of CNN architectures with different layer numbers on image- $\lambda$  matching accuracy is examined. Accordingly, seven different architectures with different layer numbers were created and the accuracy values in the training/test sets were obtained (see Table 5). When the results were examined, it was seen that the highest accuracy values were achieved with the 23-layer CNN architecture. The detailed version of this architecture, where the total number of parameters is 219.891, is presented in Table 1.

**Table 5.** The effect of the number of layers

Number of Layers	Success	
	Train	Test
4	64.63	68.87
10	87.92	70.16
16	95.95	92.44
18	91.56	92.03
<b>23</b>	<b>97.33</b>	<b>96.34</b>
33	95.03	90.34
42	86.96	89.56

### 4.2.4. Google colaboratory

The learning accuracy of CNN is directly proportional to the data size in the training set. The larger the dataset, the higher the accuracy. However, the increase in data size complicates the training process. It is very difficult to train complex CNNs with a large number of parameters. Personal computers cannot provide a solution at this point, and the use of servers becomes mandatory. For this reason, Google Colaboratory service, which is offered free of charge by Google, was used in this study. Thanks to this service, the above-mentioned parameter effects studies were carried out using a server with many libraries installed and an NVIDIA Tesla T4 graphics card.

### 4.2.5. Embedded platform

In this experimental study, the online performance of image- $\lambda$  matching is investigated. Accordingly, the matching process was carried out in two different concepts: 1) the classical approach was used on a CPU-supported processor card; 2) the Optimum recommended CNN is used on a GPU-supported processor card. In the experimental study with the first concept, it was seen that each flame image can be mapped to the relevant  $\lambda$  value in 1.7 seconds. On the other hand, when the proposed operating concept is used, it is seen that an average of 20 flame images can be mapped to the  $\lambda$  value in 1 second (see Fig. 3).

```

-----START-----
1. Estimated lambda value of the image: 7.82, Elapsed time: 0.23s
2. Estimated lambda value of the image: 6.78, Elapsed time: 0.11s
3. Estimated lambda value of the image: 6.92, Elapsed time: 0.04s
4. Estimated lambda value of the image: 7.04, Elapsed time: 0.04s
5. Estimated lambda value of the image: 6.90, Elapsed time: 0.04s
6. Estimated lambda value of the image: 7.04, Elapsed time: 0.04s
7. Estimated lambda value of the image: 6.62, Elapsed time: 0.04s
8. Estimated lambda value of the image: 7.01, Elapsed time: 0.04s
9. Estimated lambda value of the image: 8.09, Elapsed time: 0.07s
10. Estimated lambda value of the image: 6.82, Elapsed time: 0.06s
11. Estimated lambda value of the image: 6.39, Elapsed time: 0.04s
12. Estimated lambda value of the image: 6.69, Elapsed time: 0.04s
13. Estimated lambda value of the image: 6.80, Elapsed time: 0.04s
14. Estimated lambda value of the image: 6.88, Elapsed time: 0.04s
15. Estimated lambda value of the image: 9.20, Elapsed time: 0.04s
16. Estimated lambda value of the image: 9.12, Elapsed time: 0.04s
17. Estimated lambda value of the image: 8.76, Elapsed time: 0.05s
18. Estimated lambda value of the image: 8.94, Elapsed time: 0.04s
19. Estimated lambda value of the image: 9.13, Elapsed time: 0.03s
20. Estimated lambda value of the image: 9.24, Elapsed time: 0.03s
21. Estimated lambda value of the image: 9.28, Elapsed time: 0.03s
22. Estimated lambda value of the image: 9.35, Elapsed time: 0.04s
23. Estimated lambda value of the image: 9.79, Elapsed time: 0.04s
24. Estimated lambda value of the image: 9.01, Elapsed time: 0.04s
25. Estimated lambda value of the image: 9.64, Elapsed time: 0.04s
26. Estimated lambda value of the image: 9.81, Elapsed time: 0.04s
27. Estimated lambda value of the image: 9.64, Elapsed time: 0.06s
28. Estimated lambda value of the image: 9.96, Elapsed time: 0.06s
29. Estimated lambda value of the image: 9.81, Elapsed time: 0.03s
30. Estimated lambda value of the image: 8.93, Elapsed time: 0.03s
31. Estimated lambda value of the image: 9.93, Elapsed time: 0.04s
32. Estimated lambda value of the image: 9.39, Elapsed time: 0.04s
33. Estimated lambda value of the image: 9.96, Elapsed time: 0.04s
34. Estimated lambda value of the image: 9.38, Elapsed time: 0.04s
35. Estimated lambda value of the image: 10.06, Elapsed time: 0.05s
36. Estimated lambda value of the image: 9.64, Elapsed time: 0.06s
37. Estimated lambda value of the image: 10.04, Elapsed time: 0.03s
38. Estimated lambda value of the image: 9.98, Elapsed time: 0.03s
39. Estimated lambda value of the image: 9.98, Elapsed time: 0.03s
40. Estimated lambda value of the image: 9.98, Elapsed time: 0.04s
-----END-----

```

**Figure 3.** Image- $\lambda$  matching time of the embedded platform (online)

### 4.3. Matching Results of Best Classical Approach and Optimum CNN Architecture

This section compares the best results of the classical and current approaches. As it will be remembered, the highest matching accuracy among classical approaches was obtained by classifying the multivariate normal distribution features with ANN. The image- $\lambda$  matching accuracy of the proposed CNN architecture (with optimum parameters) with this method is shown in Fig. 4. Accordingly, the red colored line shows the actual  $\lambda$  value, the green CNN result, and the blue ANN result. As can be seen, the proposed CNN architecture can predict  $\lambda$  with high accuracy. If you pay attention, the CNN architecture also performs the filtering of the result while estimating  $\lambda$ .

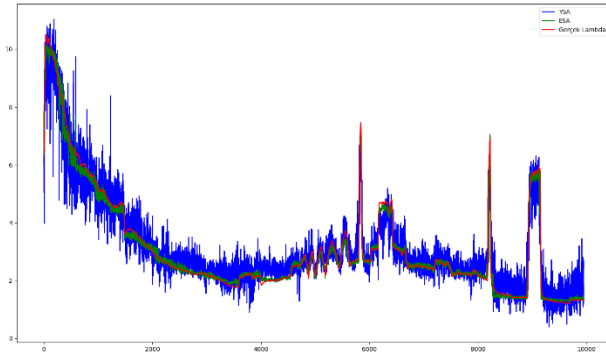


Figure 4. Image- $\lambda$  matching time of the embedded platform (online)

## 5. CONCLUSION

In this study, a new method is proposed to calculate the combustion efficiency of coal boilers. This method involves viewing the combustion chamber via a camera and mapping the relevant images to the efficiency coefficient  $\lambda$  taken from a flue gas analyzer. The proposed approach has two important differences from previous image- $\lambda$  matching studies: 1) CNN architecture is used; 2) Optimum CNN architecture is run on an embedded platform.

As a result of the experimental studies, it has been observed that the flame images can be mapped to the  $\lambda$  coefficients with the highest accuracy (97% for training, 94% for testing) when the following parametric values are used.

- The flame from the image resolution should be 128x128.
- Pack size 48 should be selected in the training process.
- CNN architecture should have 23 layers.

## REFERENCES

- [1] Onat C, Talu MF, Daskin M, Mercimek M. Otomatik Beslemeli Kömür Kazanlarında Alev Formu İle Yanma Verimi Arasındaki İlişkinin İncelenmesi. *Mühendis ve Makine* 2015; 669: 70–79, 2015.
- [2] Testo SE, KGaA Co. Baca gazı ölçüm cihazları. 2019 [cited 2019 October 30. Available from: <https://www.testo.com/tr-TR/ueruenler/gaz-oelcuem-cihazlatri>.
- [3] Lee CL, Jou CJG. Saving fuel consumption and reducing pollution emissions for industrial furnaces. *Fuel Process. Technol.* 2011; 92(12):2335–2340.
- [4] Hao Z, Kefa C, Jianbo M. Combining neural network and genetic algorithms to optimize low NOx pulverized coal combustion. *Fuel*: 2011; 80 (15): 2163–2169.
- [5] Hao Z, Qian X, Cen K, Jianren F. Optimizing pulverized coal combustion performance based on ANN and GA. *Fuel Process. Technol.* 2004; 85 (2–3):113–124.
- [6] Zheng Z, Yao M. Charge stratification to control HCCI: Experiments and CFD modeling with n-heptane as fuel. *Fuel*. 2009; 88(2): 354–365.
- [7] Liu D, Yan J, Wang F, Huang Q, Chi Y, Cen K. Experimental reconstructions of flame temperature distributions in laboratory-scale and large-scale pulverized-coal fired furnaces by inverse radiation analysis. *Fuel*. 2012; 93: 397–403.
- [8] Kuprianov V, Chullabodhi C, Jornjumrus W. Cost based optimization of excess air for fuel oil/gas-fired steam boilers. *RERIC Int. Energy J.*1999; 21(2): 83–91.
- [9] Yamaguchi T, Grattan KTV, Uchiyama H, Yamada T. A practical fiber optic air-ratio sensor operating by flame color detection. *Rev. Sci. Instrum.* 1997; 68(1): 197–202.
- [10] Lino N, Tsuchino F, Yano T. TIMEWISE VARIATION OF TURBULENT JET DIFFUSION FLAME SHAPE BY MEANS OF IMAGE PROCESSING. *J. Flow Vis. Image Process.*1998; 5(4): 275–281.
- [11] Huang Y, Yan Y, Lu G, Reed A. On-line flicker measurement of gaseous flames by image processing and spectral analysis. *Meas. Sci. Technol.* 1999; 10(8): 726–733.
- [12] Golgiyaz S, Talu MF, Daşkın M, Onat C. Estimation of excess air coefficient on coal combustion processes via gauss model and artificial neural network. *Alexandria Eng. J.*2022; 61(2): 1079–1089. doi: 10.1016/j.aej.2021.06.022.
- [13] Baek WB, Lee SJ, Baeg SY, Cho CH. Flame image processing & analysis for optimal coal firing of thermal power plant. *ISIE 2001 IEEE Int. Symp. Ind. Electron. proceedeing, Vols I-III.* 2001; 928-931.
- [14] Eleyan A, Dem H. Co-occurrence matrix and its statistical features as a new approach for face recognition. *Comp Sci.* 2011; 19(1).
- [15] TALU MF, ONAT C, DASKIN M. Prediction of Excess Air Factor in Automatic Feed Coal Burners by Processing of Flame Images. *Chinese J. Mech. Eng.* 2017; 30(3): 722–731.
- [16] Chen LC, Papandreou G, Schroff F, Adam H. Rethinking Atrous Convolution for Semantic Image Segmentation. 2017. arXiv:1706.05587
- [17] Chen J, Chan LLT, Cheng YC. Gaussian process regression based optimal design of combustion systems using flame images. *Appl. Energy.* 2013; 111: 153–160.
- [18] Huang B, Luo Z, Zhou H. Optimization of combustion based on introducing radiant energy signal in pulverized coal-fired boiler. *Fuel Process. Technol.* 2010; 91(6): 660–668. doi: 10.1016/j.fuproc.2010.01.015.
- [19] Huang B, Luo Z, Zhou H. Optimization of combustion based on introducing radiant energy signal in pulverized coal-fired boiler. *Fuel Process. Technol.* 2010; 91(6): 660–668.
- [20] Krizhevsky A, Sutskever I, Hinton GE. ImageNet Classification with Deep Convolutional Neural Networks. 2012; 25(2). doi:10.1145/3065386.
- [21] Girshick R, Donahue J, Darrell T, Malik J. Rich feature hierarchies for accurate object detection and semantic segmentation. Nov. 2013.

- [22] Farabet C, Couprie C, Najman L, LeCun Y. Learning Hierarchical Features for Scene Labeling. *IEEE Trans. Pattern Anal. Mach. Intell.* 2013; 35 (8): 1915–1929.
- [23] ÇALIŞAN M, TALU MF. Comparison of Methods for Determining Activity from Physical Movements. *J. Polytech.* 2020; 0900(1): 17–23.
- [24] Celik G. Detection of Covid-19 and other pneumonia cases from CT and X-ray chest images using deep learning based on feature reuse residual block and depthwise dilated convolutions neural network. *Appl. Soft Comput.* 2023; 133: 109906. doi: 10.1016/j.asoc.2022.109906.
- [25] Çelik G, Talu MF. A new 3D MRI segmentation method based on Generative Adversarial Network and Atrous Convolution,. *Biomed. Signal Process. Control.* 2022; 71: 103155. doi: 10.1016/j.bspc.2021.103155.
- [26] Başaran E. A new brain tumor diagnostic model: Selection of textural feature extraction algorithms and convolution neural network features with optimization algorithms. *Comput. Biol. Med.* 2022; 148: 105857. doi: 10.1016/j.compbiomed.2022.105857.
- [27] Rawal V, Prajapati P, Darji A. Hardware implementation of 1D-CNN architecture for ECG arrhythmia classification. *Biomed. Signal Process. Control.* 2023; 85: 104865. doi: 10.1016/j.bspc.2023.104865.
- [28] Hamdi S, Oussalah M, Moussaoui A, Saidi M. Attention-based hybrid CNN-LSTM and spectral data augmentation for COVID-19 diagnosis from cough sound. *J. Intell. Inf. Syst.* 2022; 59(2): 367–389. doi: 10.1007/s10844-022-00707-7.
- [29] Polat K, Nour M. Parkinson disease classification using one against all based data sampling with the acoustic features from the speech signals. *Med. Hypotheses.* 2020; 140:109678. doi: 10.1016/j.mehy.2020.109678.
- [30] Golgiyaz S, Talu MF, Onat C. Artificial neural network regression model to predict flue gas temperature and emissions with the spectral norm of flame image. *Fuel*, 2019; 255: 115827. doi: 10.1016/j.fuel.2019.115827.

## Evaluation of Machining Parameters Affecting Cutting Forces in Dry Turning of GGG50 Ductile Cast Iron

Rüstem BİNALİ<sup>1\*</sup> , Mustafa KUNTOĞLU<sup>1</sup> 

<sup>1</sup> Selcuk University, Technology Faculty, Mechanical Engineering Department, Konya, Türkiye

Rüstem BİNALİ ORCID No: 0000-0003-0775-3817

Mustafa KUNTOĞLU ORCID No: 0000-0002-7291-9468

\*Corresponding author: [rustem.binali@selcuk.edu.tr](mailto:rustem.binali@selcuk.edu.tr)

(Received: 25.11.2022, Accepted: 16.05.2023, Online Publication: 22.06.2023)

### Keywords

Cutting forces,  
Cast iron,  
Optimization,  
Turning

**Abstract:** Cutting forces in turning have dramatic impact on the cutting stability, tool wear index and surface quality. Machinability of cast iron is important as per this material is served as the main source in manufacturing specific parts of automotive industry. Also, this special material may require final operation to eliminate the manufacturing related defects and residuals. In this context, this study focuses on the optimization and analysis of cutting forces during dry turning of GGG50 material. Thus, Taguchi based experimental design was applied using three levels of cutting speed, feed rate and cutting depth and totally 9 experiments were performed. The discussions on the cutting forces were made based on statistical analysis, optimization approach and graphical presentations. Accordingly, feed rate is the most influential parameter on cutting forces with the contribution rate about 71.2 %. Cutting speed and cutting depth follows it with the contributions of 21.7 % and 1.5 %. To achieve the minimized cutting forces the parameter group should be; 0.16 mm, 0.2 mm/rev, 80 m/min. This study is expected to be an auxiliary resource for designers and manufacturers in the field to improve the machinability aspects of casted materials.

## GGG50 Sfero Döküm Demirin Kuru Tornalanmasında Kesme Kuvvetlerini Etkileyen İşleme Parametrelerinin Değerlendirilmesi

### Anahtar Kelimeler

Kesme kuvvetleri,  
Dökme demir,  
Optimizasyon,  
Tornalama

**Öz:** Tornalamadaki kesme kuvvetlerinin kesme stabilitesi, takım aşınma indeksi ve yüzey kalitesi üzerinde önemli etkisi vardır. Dökme demirin işlenebilirliği önemlidir, çünkü bu malzeme otomotiv endüstrisinin belirli parçalarının imalatında ana kaynak olarak hizmet eder. Ayrıca bu özel malzeme, imalattan kaynaklanan kusurları ve artıkları ortadan kaldırmak için son işlem gerektirebilir. Bu bağlamda, bu çalışma GGG50 malzemesinin kuru tornalanması sırasında kesme kuvvetlerinin optimizasyonu ve analizine odaklanmaktadır. Bu nedenle, kesme hızı, ilerleme hızı ve kesme derinliği olmak üzere üç seviye kullanılarak Taguchi tabanlı deney tasarımı uygulanmış ve toplam 9 deney gerçekleştirilmiştir. Kesme kuvvetleri ile ilgili tartışmalar, istatistiksel analiz, optimizasyon yaklaşımı ve grafiksel sunumlara dayalı olarak yapılmıştır. Buna göre ilerleme hızı, yaklaşık %71,2'lik katkı oranı ile kesme kuvvetleri üzerinde en etkili parametredir. Bunu %21,7 ve %1,5'lik katkılarla kesme hızı ve talaş derinliği takip etmektedir. En aza indirilmiş kesme kuvvetlerini elde etmek için parametre grubu şöyle olmalıdır; 0,16 mm, 0,2 mm/dev, 80 m/dak. Bu çalışmanın, döküm malzemelerin işlenebilirlik yönlerinin iyileştirilmesi konusunda tasarımcı ve üreticilere yardımcı bir kaynak olması beklenmektedir.

### 1. INTRODUCTION

Machinability studies are very important in the machining industry to determine the interactions between the workpiece and the cutting tool material before production. Although machinability studies are

widely carried out today, its popularity is maintained. The reason for this is developing technology and increasing material need. New materials and cutting tools are produced every day. The need for new types of tools and materials is to achieve maximum efficiency with lower costs. Among the machinability studies, various machining methods are used. The most widely

used method among them is turning with a single-edged cutting edge [1-5]. Among the machinability output parameters, although all parameters are important, the cutting force, which directly and indirectly affects other parameters, is very important. Changes in cutting force can cause oscillations on the part, resulting in poor machined surface quality, tool wear, temperature rise and vibration following wear, and an increase in the amount of energy consumed for machining with increased force [6-8]. Between the commonly used cast iron materials is the spheroidal graphite cast iron material. Although the mechanical properties of spheroidal graphite cast iron materials are closer to steels, they have high strength and ductility. Among the usage areas of this type of cast iron, there are materials such as gears, press machines, flywheels, tractor parts and cylinders [9-11]. The literature review of the machinability studies on cast irons is given below.

Mavi and Korkut investigated the change in surface roughness on the material surface after machining on vermicular graphite cast iron. They stated that the cast iron material gave the best surface roughness value in processing at the highest speed [12]. Binali, in his study, studied the temperature change in the machining of GGG50 spheroidal graphite cast iron material by turning. As a result of his study, he stated that the most effective parameter on the temperature was the cutting speed [13]. Karabulut and Güllü investigated the milling of vermicular graphite cast iron with cutting tools with different approach angles. In their study, they stated that it is the most important factor in the increase of cutting forces in the direction of feed, as the amount of feed increases with the decrease in the value of the approach angle [14]. Düzce and Samtaş investigated the face milling process of GG25 casting material. In their study, they evaluated the temperature formations during machining with cutting tools with three different coatings (TiAlN coated, TiN-TiCN-Al<sub>2</sub>O<sub>3</sub> coated and ALTiN coated). They determined that the most effective machining parameter affecting the temperature is the cutting tool with the most suitable coating type for the cutting depth and the minimum temperature, the cutting tool with TiN-TiCN-Al<sub>2</sub>O<sub>3</sub> coating [15]. Ucu et al. carried out machinability tests of austempered ductile cast iron material by turning tests. In their study, surface roughness, tool wear and cutting forces were evaluated. As a result of their studies, they stated that the surface roughness decreased with increasing cutting speed. They also stated that austempering at low temperatures had a positive effect on the workpiece surface [16].

As can be seen in the literature research, there are machinability studies of spheroid graphite casting materials, but GGG50 is not at a sufficient level for spheroid graphite casting materials. For this reason, in our study, the machinability of the GGG50 material on the conventional lathe was determined according to the cutting force values that occur during the process. In this context, the cutting force generated during chip removal was measured with the help of a dynamometer. The main purpose here is to obtain the minimum cutting force value and to ensure that other machinability output

parameters are obtained at an ideal level. Taguchi based S/N ratio, 3D graphical evaluation and ANOVA statistical analysis were used to determine the effects of machining parameters on cutting force values in order to obtain optimum values.

## 2. MATERIAL AND METHOD

The details of the cutting tool and material used in the experimental studies and the turning tests performed to determine the properties and cutting force values are given in this section. In addition, the details of the experimental design used are included.

### 2.1. Cutting Tool and Workpiece Material

In the machinability experiments, the cutting force values were compared for the optimization of the machining parameters of the GGG50 casting material. This material is brittle and short chips are formed during machining. Machinability is better than other cast iron materials. Tensile Strength is 500 N/mm<sup>2</sup> and hardness is approximately 170-220HB. The chemical composition of the elements in the GGG50 spheroidal graphite casting material used in the studies are given in Table 1 as a percentage. The material used in the experimental studies has a cylindrical geometry and its dimensions are 30 mm in diameter and 100 mm in length. A new cutting tool material was used for each experiment and the cutting tool has a TiC coating and CCMT 09T308-304 code. The cutting tool was selected according to the workpiece material in line with the recommendations received from the manufacturers. Cutting tool specifications are given in Table 2.

**Table 1.** Chemical composition of GGG50 cast iron [17]

Material	C	Mg	Mn	P	Si	S
GGG50	3.5-3.8	0.06-0.12	0.4	0.1	2-3	0.01

**Table 2.** The cutting tool used and its properties

Cutting tool code	Cutting tool quality	Cutting Edge Length	Thickness	Corner Radius
CCMT 09T308-304	P25	9.7 mm	3.97 mm	0.8 mm

### 2.2. Machine Tool Test Procedure

Experiments were made on De Lorenzo S547-8899 lathe. Machine specifications are given in Table 3. In the experimental studies, the processed materials were connected between the chuck and the tailstock, and the connection of the test bench and the workpiece and the tool holder-cutting tool connections are given in Figure 1.

**Table 3.** Machine tool properties

Technical Specifications	Value	Unit
Maximum workpiece diameter	460	mm
Distance between chuck and tailstock	1500	mm
Spindle speed range	25-1800	rev/min
Spindle speed number	12	piece
Feed range	0.04-2.46	mm
Number of feeds	122	piece
Maximum tool holder size	25x25	mm
Motor power	5.5	kW

**Figure 1.** The clamping system of the lathe, workpiece and cutting tool

### 2.3. Taguchi Based Experimental Design

When it is desired to get the highest efficiency from the work done in physical experiments, it is necessary to try the interaction of all values of the processing parameters with each other. However, these increases both processing time and cost [18-20]. For this reason, Taguchi-based experimental approaches are used to achieve the desired process outputs with minimum cost and time. Three different cutting speed, feed rate and cutting depth parameters were used in the study, and the Taguchi L9 orthogonal array of the parameters used are given in Table 4.

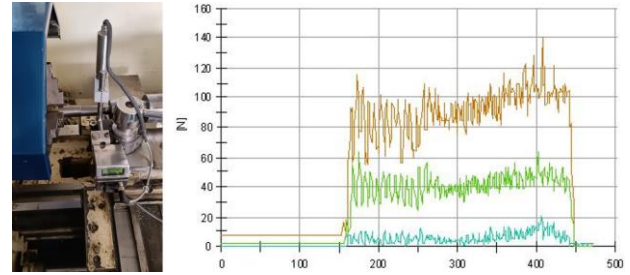
**Table 4.** Machining parameters and Taguchi-based orthogonal experimental design

Experimental No	Feed (f) (mm/rev)	Cutting depth (d) (mm)	Cutting Speed (Vc) (m/min)
1	0.2	0.12	60
2	0.2	0.16	80
3	0.2	0.2	130
4	0.4	0.12	80
5	0.4	0.16	130
6	0.4	0.2	60
7	0.6	0.12	130
8	0.6	0.16	60
9	0.6	0.2	80

### 2.4. Measurement of Cutting Forces

The dynamometer used for force measurement in the experimental study is a TelC DKM2000 turning dynamometer. The dynamometer can measure the forces occurring during the operation in the three axes direction and with the help of the strain gage. The dynamometer body is mounted with a clamp and successfully measures the shear forces occurring in the cutting zone. The device can be directly connected to the computer and data

tracking, processing and recording can be done with its own XKM2000 software. The body of the dynamometer and the appearance of the signal screen followed by the computer are given in Figure 2.

**Figure 2.** Connecting the dynamometer to the bench and the monitored signal display

## 3. RESULTS

### 3.1. Graphical Evaluation

Graphical representation is an effective technique to observe the impacts of input parameters not only with the certain values applied in the experiments but also for the intermediate values. This kind of approach provides to understand how two design parameters affect the output parameter simultaneously. The combined different levels of inputs give the final surface by merging the different overlap points as can be seen in Figure 3. First, increase in feed rate increases the cutting forces with no exception when looking at its combination between cutting speed and cutting depth. This can be explained with the influence of the elevated load comes to the cutting tool with higher feed values [21, 22]. Also, higher feed rate values make the cutting tool faster and material removal rate increases [3]. Increase in cutting depth has complex impact on the cutting forces as can be seen in two graphs. At high cutting speeds, high levels of cutting depth can be applied which can be explained by the elevated cutting speed make easier chip formation [23, 24]. A similar situation was stated in the study conducted by Karabulut and Güllü [14]. Also in other scenario, at low cutting speed, cutting the material become harder and with the increase of cutting depth, cutting forces become higher. Such studies and results are available in the literature [25, 26]. For short, it is true that feed rate has a determined effect on cutting forces, but the other two parameters have controversial influences. In practice, it would be better to apply the parameter levels which give the lowest cutting forces.



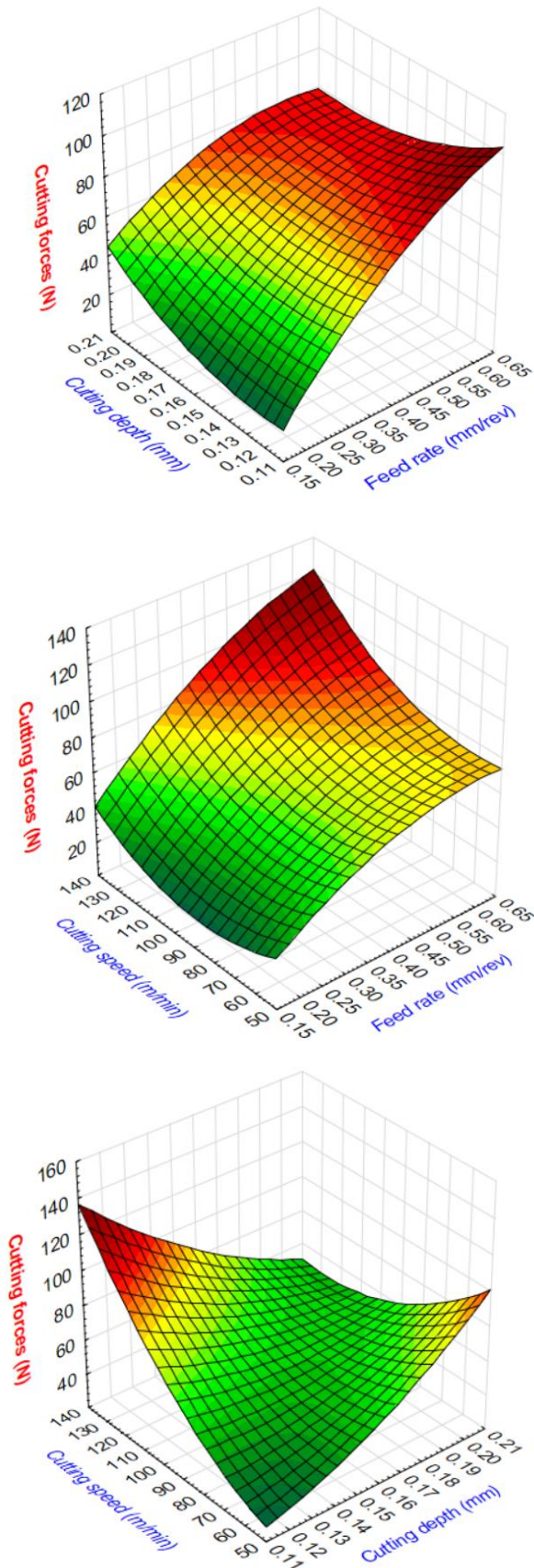


Figure 3. The combinations of turning parameters versus cutting forces

### 3.2. Optimization

Optimization is one of the important approaches in engineering world since it provides the best options for

obtaining the desired results after an experimental work [27, 28]. There are numerous optimization methods which already have been preferred to analyze the machining data such as cutting forces [29, 30]. Since there are many input parameters that belongs to machine tool, cutting tool and work material, achieving the best conditions in any type of operation is a difficult challenge. From this point of view, it is significant to obtain a series of optimum results in terms of basic machining parameters. With this motivation, this study focused on the optimization of turning parameters during machining of cast iron. Two different approaches can be used in this direction i.e. means plot or S/N ratios. Taguchi based plot for means were utilized to reach the optimum parameter combinations as can be seen in Figure 4. Also, Table 5 gives the calculated values of the means. Mean of means plots give the points that placed from minimum to maximum for each level of turning parameters. Accordingly, nominal rate of cutting depth and cutting speed namely 0.16 mm and 80 m/min are the best options for minimum cutting forces. This explains the varying impact of these two parameters in 3d graphs demonstrated before. On the other hand, feed rate seems as the most influential factor on the cutting forces according to the difference between highest and lowest values in the graph. Plus, optimum value of the feed rate is 0.2 mm/rev which is compatible with the graphical results. There are studies in the literature that the feed rate was the most effective parameter on the cutting force [31]. In this case, it can be stated that the study is compatible with the literature.

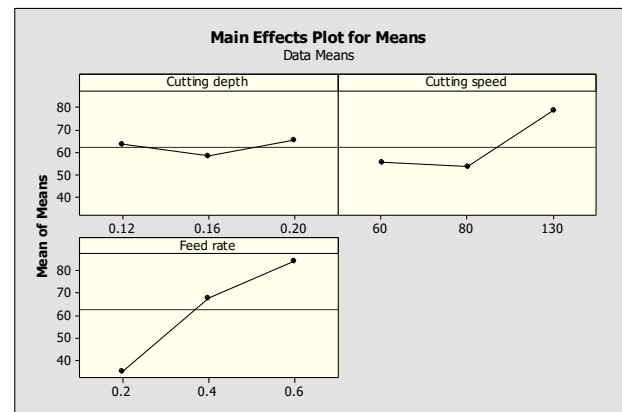


Figure 4. Optimized results of turning parameters for cutting forces

Table 5. Response table for means

Level	Cutting depth	Cutting speed	Feed rate
1	63.67	55.33	35.33
2	58.33	53.67	67.67
3	65.33	78.33	84.33
Delta	7	24.67	49.00
Rank	3	2	1

### 3.2. Statistical Analysis

Statistical analysis is an effective way to discover the effective parameters and ineffective parameters when looking at their influences on a response parameter [32, 33]. ANOVA is a way that broadly applied especially in machining area [31, 34-36]. That's why in here, it is aimed to use this approach to evaluate the parameter influences on cutting forces. Table 6 gives the results

including turning parameters and statistical indicators. Accordingly, feed rate was found as the most effective parameter with the contribution rate about 71.2 % and it was followed by the cutting speed and cutting depth respectively with the contributions about 21.7 % and 1.5 % respectively. Other statistics such as P and F values are compatible with the percent contribution results.

**Table 6.** Statistical analysis of the turning parameters for cutting forces

Source	DF	Seq SS	Adj MS	F-value	P-value	PC (%)
Cutting depth	2	80.22	40.11	0.27	0.788	1.5
Cutting speed	2	1140.22	570.11	3.83	0.207	21.7
Feed rate	2	3724.22	1862.11	12.52	0.074	71.2
Residual Error	2	297.56	148.78	-	-	5.6
Total	8	5242.22	-	-	-	100

#### 4. CONCLUSION

This study is aimed to make an analysis about the machinability characteristics of GGG50 cast iron considering the cutting forces as the response parameter. From the data analysis performed based on the statistical evaluation, graphical demonstration and optimization approaches, the following deductions can be done.

- According to the 3d graphs, feed rate has a determined effect on cutting forces, but the other two parameters have controversial influences. Increase in feed rate increases the cutting forces with no exception.
- To obtain the minimum cutting forces the parameter group should be as 0.16 mm for cutting depth, 0.2 mm/rev for feed rate, and 80 m/min for cutting speed respectively.
- In the literature, it has been stated that the most effective parameter in the study on temperature for this material is the cutting speed. In this study, feed rate was found as the most effective parameter with the contribution rate about 71.2 % and it was followed by the cutting speed and cutting depth respectively with the contributions about 21.7 % and 1.5 % respectively.
- Researchers who carry out such studies can perform operations such as milling and drilling for this type of material. They can also experiment with minimal quantity of lubrication and different types of cutting fluids, except for dry machining.

#### REFERENCES

[1] Kuntoğlu M, Acar O, Gupta MK, Sağlam H, Sarıkaya M, Giasin K, et al. Parametric optimization for cutting forces and material removal rate in the turning of AISI 5140. *Machines*. 2021;9(5):90.

[2] Usca ÜA, Uzun M, Kuntoğlu M, Sap E, Gupta MK. Investigations on tool wear, surface roughness, cutting temperature, and chip formation in machining of Cu-B-CrC composites. *The*

*International Journal of Advanced Manufacturing Technology*. 2021;116(9):3011-25.

[3] Salur E. Understandings the tribological mechanism of Inconel 718 alloy machined under different cooling/lubrication conditions. *Tribology International*. 2022;107677.

[4] Binali R, Patange AD, Kuntoğlu M, Mikolajczyk T, Salur E. Energy Saving by Parametric Optimization and Advanced Lubri-Cooling Techniques in the Machining of Composites and Superalloys: A Systematic Review. *Energies*. 2022;15(21):8313.

[5] Barış Ö, Akgün M, Demir H. AA 6061 Alaşımının tormalanmasında kesme parametrelerinin yüzey pürüzlülüğü üzerine etkisinin analizi ve optimizasyonu. *Gazi Mühendislik Bilimleri Dergisi*. 2019;5(2):151-8.

[6] Grzesik W. *Advanced machining processes of metallic materials: theory, modelling and applications*: Elsevier; 2008.

[7] Binali R, Coşkun M, Neşeli S. An Investigation of Power Consumption in Milling AISI P20 Plastic Mold Steel By Finite Elements Method. *Avrupa Bilim ve Teknoloji Dergisi*. 2022(34):513-8.

[8] Binali R, Yıldız S, Neşeli S. S960QL Yapı Çeliğinin İşlenebilirliğinin Sonlu Elemanlar Yöntemi ile İncelenmesi. *Avrupa Bilim ve Teknoloji Dergisi*. 2021(31):85-91.

[9] Karaman S. Küresel grafitli dökme demirlerin (GGG40, GGG50, GGG60, GGG70) üretim sürecinin ve mekanik özelliklerinin incelenmesi: Trakya Üniversitesi Fen Bilimleri Enstitüsü; 2011.

[10] Kaçal A, Gülesin M, Melek F. GGG 40 Küresel grafitli dökme demirlerin ince tormalama operasyonlarında kesme kuvvetlerinin ve yüzey pürüzlülüğünün değerlendirilmesi. *Politeknik Dergisi*. 2008;11(3):229-34.

[11] Şahinoğlu A, Güllü A, Dönertaş MA. GGG50 malzemenin torna tezgâhında işlenmesinde kesme parametrelerinin titreşim, ses şiddeti ve yüzey pürüzlülüğü üzerinde etkisinin araştırılması. *Sinop Üniversitesi Fen Bilimleri Dergisi*. 2017;2(1):67-79.

[12] Mavi A, Korkut I. The effects of austempering temperature and time on the machinability of vermicular graphite iron. *Materials Testing*. 2014;56(4):289-93.

[13] Binali R. Optimization of Parameters Affecting Cutting Temperatures During Turning of GGG50 Cast Iron. *2nd International Conference on Engineering and Applied Natural Sciences*2022. p. 652-6.

[14] Karabulut Ş, Güllü A. Farklı yavaşma açıları ile vermiküler grafitli dökme demirin frezelenmesinde kesme kuvvetlerinin araştırılması ve analitik modellenmesi. *Gazi Üniversitesi Mühendislik Mimarlık Fakültesi Dergisi*. 2013;28(1).

[15] Düzcü R, Samtaş G. GG25 Dökme Demirin Frezelenmesinde Kesme Parametrelerinin Kesme Sıcaklığı Üzerine Etkisi ve Optimizasyonu. *İmalat Teknolojileri ve Uygulamaları*.2(3):20-33.

[16] Uzun İ, Aslantaş K, Taşgetiren S, Gök K. Östempelenmiş küresel grafitli dökme demirin sinterlenmiş karbür kesici takım ile tormalama

- işleminde takım performansının incelenmesi. Gazi Üniversitesi Mühendislik Mimarlık Fakültesi Dergisi. 2007;22(4):739-44.
- [17] matmatch.com.  
<https://matmatch.com/materials/minfm32356-din-1693-1-grade-ggg-50-cast-condition;> 2022 [Available from: <https://matmatch.com/materials/minfm32356-din-1693-1-grade-ggg-50-cast-condition>].
- [18] Binali R, Yıldız S, Neşeli S. Parametric optimization for machinability parameters of S960QL structural steel during milling by finite elements. Selcuk University Journal of Engineering Sciences. 2022;21(1):26-31.
- [19] Binali R, Yıldız S, Neşeli S. Investigation of Power Consumption in the Machining of S960QL Steel by Finite Elements Method. European Journal of Technique (EJT). 2022;12(1):43-8.
- [20] Kıvak T. Optimization of surface roughness and flank wear using the Taguchi method in milling of Hadfield steel with PVD and CVD coated inserts. Measurement. 2014;50:19-28.
- [21] Kuntoğlu M. Prediction of progressive tool wear and cutting tool breakage using acoustic emission and cutting force signals in turning. Msater's Thesis, Institute of Science and Technology, Selcuk University, Konya, Turkey. 2016.
- [22] Kuntoğlu M, Sağlam H. On-line Tool Breakage Detection Using Acoustic Emission, Cutting Force and Temperature Signals in Turning.
- [23] Usca ÜA, Uzun M, Şap S, Kuntoğlu M, Giasin K, Pimenov DY, et al. Tool wear, surface roughness, cutting temperature and chips morphology evaluation of Al/TiN coated carbide cutting tools in milling of Cu-B-CrC based ceramic matrix composites. journal of materials research and technology. 2022;16:1243-59.
- [24] Habib N, Sharif A, Hussain A, Aamir M, Giasin K, Pimenov DY, et al. Analysis of hole quality and chips formation in the dry drilling process of Al7075-T6. Metals. 2021;11(6):891.
- [25] Binali R, Kuntoğlu M, Pimenov DY, Usca ÜA, Gupta MK, Korkmaz ME. Advance monitoring of hole machining operations via intelligent measurement systems: A critical review and future trends. Measurement. 2022;111757.
- [26] Gupta MK, Korkmaz ME, Sarıkaya M, Krolczyk GM, Günay M, Wojciechowski S. Cutting forces and temperature measurements in cryogenic assisted turning of AA2024-T351 alloy: An experimentally validated simulation approach. Measurement. 2022;188:110594.
- [27] Asiltürk I, Neşeli S. Multi response optimisation of CNC turning parameters via Taguchi method-based response surface analysis. Measurement. 2012;45(4):785-94.
- [28] Neşeli S, Yıldız S, Türkeş E. Optimization of tool geometry parameters for turning operations based on the response surface methodology. Measurement. 2011;44(3):580-7.
- [29] Salur E, Aslan A, Kuntoğlu M, Güneş A, Şahin Ö. Optimization of cutting forces during turning of composite materials. Acad Platf J Eng Sci. 2020;8:423-31.
- [30] Yurtkuran H, Korkmaz ME, Günay M. Modelling and optimization of the surface roughness in high speed hard turning with coated and uncoated CBN insert. Gazi University Journal of Science. 2016;29(4):987-95.
- [31] Aslan A. Optimization and analysis of process parameters for flank wear, cutting forces and vibration in turning of AISI 5140: A comprehensive study. Measurement. 2020;163:107959.
- [32] Gunay M, Yasar N, Korkmaz ME, editors. Optimization of drilling parameters for thrust force in drilling of AA7075 Alloy. Proceedings of the International Conference on Engineering and Natural Sciences, Sarajevo, Bosnia and Herzegovina; 2016.
- [33] Asiltürk I, Neşeli S, Ince MA. Optimisation of parameters affecting surface roughness of Co28Cr6Mo medical material during CNC lathe machining by using the Taguchi and RSM methods. Measurement. 2016;78:120-8.
- [34] Yaşar N, Günay M, Kılık E, Ünal H. Multiresponse optimization of drillability factors and mechanical properties of chitosan-reinforced polypropylene composite. Journal of Thermoplastic Composite Materials. 2022;35(10):1660-82.
- [35] Korkmaz ME, Günay M. Finite element modelling of cutting forces and power consumption in turning of AISI 420 martensitic stainless steel. Arabian Journal for Science and Engineering. 2018;43(9):4863-70.
- [36] Işık R, Özlü B, Demir H. St-37 Malzemesinin Lazer ile Kesme İşleminde Seçilen Parametrelerin Etkisinin Deneysel ve İstatiksel Olarak İncelenmesi. Firat University Journal of Engineering. 2021;33(1).

## Evaluation of benzaldehyde derivatives as being bovine kidney aldose reductase inhibitors

Bülent ŞENGÜL<sup>1\*</sup> 

<sup>1</sup> Department of Health Care Services, Vocational School of Health Services, Bayburt University, Bayburt, Türkiye

Bülent ŞENGÜL ORCID No: 0000-0002-9998-6564

\*Corresponding author: [bulentsengul@bayburt.edu.tr](mailto:bulentsengul@bayburt.edu.tr)

(Received: 14.11.2022, Accepted: 16.05.2023, Online Publication: 22.06.2023)

### Keywords

Inhibition,  
Molecular  
docking,  
Polyol  
pathway,  
Benzaldehydes

**Abstract:** Aldose reductase (AR) catalyzes the production of sorbitol from glucose in the polyol pathway, and it is a critical enzyme that causes an aberrant aggregation of sorbitol in insulin-independent tissues, create some problems including retinopathy, neuropathy, and nephropathy. AR inhibition has been shown to be a viable approach for reducing these side effects. The current study aimed to introduce new AR inhibitors to the literature. For this purpose, benzaldehydes were examined as being AR inhibitors. Firstly, the homogenate was prepared from the bovine kidney, then inhibition studies were carried out. It was found that all derivatives inhibited AR. The inhibitory potency of 4- Phenyl benzaldehyde (**3**) and 2- Bromobenzaldehyde (**6**), having IC<sub>50</sub> values as 0.23 and 1.37 µM, respectively, was determined higher than standard inhibitor sorbinil. After *in vitro* inhibition studies, estimated binding energies and binding modes of derivatives with enzyme were predicted by molecular docking. Compound **3** exhibited a maximum docking score of -8,61 kcal/mol. In conclusion, these compounds especially compound **3** may be guiding agents that can be used to synthesize new drug candidate molecules to treat or prevent diabetic complications.

61

## Benzaldehit türevlerinin sıgır böbrek aldoz redüktaz inhibitörleri olarak değerlendirilmesi

### Anahtar Kelimeler

İnhibisyon,  
Moleküler  
doking,  
Poliol yolu,  
Benzaldehit

**Öz:** Aldoz redüktaz (AR), poliöl yolunda glikozdan sorbitol üretimini katalize eder ve insülin bağımsız dokularda anormal sorbitol agregasyonuna neden olan, retinopati, nöropati ve nefropati gibi bazı problemler yaratan kritik bir enzimdir. AR inhibisyonunun bu yan etkileri azaltmak için uygun bir yaklaşım olduğu gösterilmiştir. Mevcut çalışma, literatüre yeni AR inhibitörlerini tanıtmayı amaçlamıştır. Bu amaçla AR inhibitörleri olarak benzaldehitler incelenmiştir. İlk olarak sıgır böbreğinden homojenat hazırlanmış, ardından inhibisyon çalışmaları yapılmıştır. Çalışılan bütün benzaldehit türevlerinin AR'yi inhibe ettiği bulundu. 0,23 ve 1,37 µM IC<sub>50</sub> değerlerine sahip olan 4- Phenyl benzaldehide (**3**) ve 2- Bromobenzaldehide (**6**)'in inhibitör aktivitesi, standart inhibitör sorbinilden daha yüksek olduğu tespit edildi. *In vitro* inhibisyon çalışmalarından sonra, tahmini bağlanma enerjileri ve türevlerin enzime bağlanma modları moleküler docking ile tahmin edildi. Bileşik **3**, -8,61 kcal/mol'lük bir maksimum yerleştirme puanı sergiledi. Sonuç olarak, bu bileşikler, özellikle bileşik **3**, diyabetik komplikasyonların tedavisinde veya önlenmesinde yeni ilaç aday moleküllerinin sentezi için yol gösterici moleküller olabilir.

### 1. INTRODUCTION

Diabetes is a chronic metabolic disease marked by high blood sugar levels that cause long-term damage to blood vessels, nerves, kidneys, heart, and eyes [1, 2] Type 2 diabetes, the most prevalent type, develops in adults when the body becomes insulin resistant or produces insufficient insulin [3]. According to the 2019 data of the

International Diabetes Federation (IDF), the incidence of diabetes in adults between the ages of 20-79 was 9.33%. The number of people with diabetes was reported as 463 million in 2019 and the IDF predicts that this number may increase to approximately 580 million in 2030 and 700 million in 2045 [4]. In Turkey, its prevalence increased to 21% in 2015 [5]. In the 2020 data on diabetes prevalence

it has been reported that nearly 15% of the total adult population in Turkey has diabetes [6].

Many pathways are regulated during the development and evolution of diabetes to deal with excess glucose in the body. One of these mechanisms is the polyol pathway (PP) [5,6]. Aldose reductase (AR, EC 1.1.1.21) is the first enzyme of PP and reduces glucose to sorbitol in the presence of cofactor NADPH [8]. And then, in the presence of  $\text{NAD}^+$ , sorbitol dehydrogenase (SOD, EC 1.1.1.14) transforms sorbitol to fructose [9].

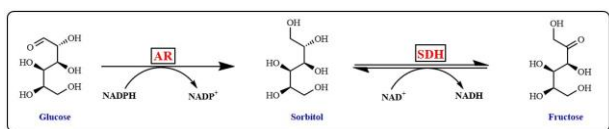


Figure 1. Polyol pathway

In a healthy body, only a small amount of glucose is converted to sorbitol so, blood glucose levels are within normal ranges [10,11]. Sorbitol is not able to penetrate through cell membranes and accumulate in the cell and produced an osmotic effect, causing tissue hydration [12]. Diabetic patients will have difficulties as a result of the problems that have occurred for their health quality. As sorbitol builds up in tissues, it sets in motion a cascade of events that leads to long-term diabetes consequences such as kidney damage, retinal disease, and cardiovascular disease [9-11]. Inhibition of AR activity of the AR for preventing glucose conversion to sorbitol could help avoid cell-level complications [16]. AR converts aldehydes derived from reactive oxygen species (ROS) into inert alcohols in the presence of the NADPH cofactor, in addition to converting glucose to sorbitol [17], [18]. The loss of NADPH induces an increase in GSH levels in cells with high AR activity, resulting in an increase in oxidative stress [15, 19, 20].

The function of aldose reductase in diabetes has been completely elucidated using AR inhibitors and knockout animals, and its inhibitors have been demonstrated to be able to ameliorate diabetes [21]. AR deletion or knockout investigations in mice have showed that AR deletion prevents the development of diabetes-induced retinal capillary degeneration, which is mediated by the creation of superoxide. AR knockout mice have also been shown to develop resistance to diabetic nephropathy [14,15]. Based on the above-mentioned explanations, the goal of this research was to study the *in vitro* inhibition effects of benzaldehyde derivatives (Figure 2) on AR to guide the synthesis of drugs that can be used in the treatment of diabetes. Besides, inhibitor-enzyme interactions were predicted by molecular docking study.

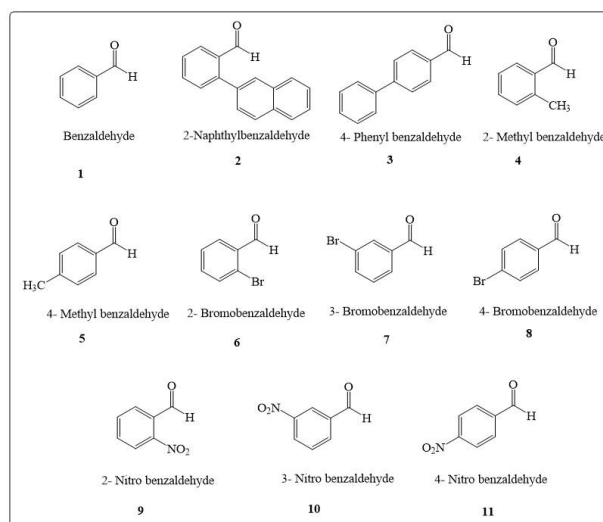


Figure 2. Benzaldehyde derivatives with investigated inhibition profile

## 2. MATERIAL AND METHOD

### 2.1. Materials

All chemicals that are used in activity determination and as inhibitors were procured from Sigma-Aldrich Co. and Merck (Darmstadt, Germany). The bovine kidney was obtained from a local butcher in Erzurum, Turkey.

### 2.2. Preparation of Kidney Homogenate

Kidney samples were washed with isotonic NaCl (0.9%) solution three times. About 10 g of the kidney tissue was chopped into small pieces, and then the cell membranes were ruptured by treatment with liquid nitrogen. The prepared sample was homogenized in 30 mL of 0.01 M phosphate buffer (pH 7.4) and was centrifuged at 13.500xg, at +4° for an hour by using refrigerated centrifuge. Then, the precipitated cell wastes were removed [24].

### 2.3. AR Activity Assay

The enzyme activity was measured using a modified method put by Cerelli et al.[25]. The depleted amount of NADPH at 340 nm was monitored spectrophotometrically for 3 minutes at 25°C. About 1mL total volume of the enzymatic reaction mix contained 0.8 M Naphosphate buffer (pH=5.5), 4.7 mM DL-glyceraldehyde, 0.11mM NADPH and enzyme solution.

### 2.4. Determination *In vitro* Inhibition Effects

For the determination of compounds' *in vitro* effects, the enzyme activities were assayed in the presence of at least five various compound concentrations. The control measurement having no compound was assumed as 100% and measurements in the presence of compounds were calculated as % activity [26]. Data were drawn as Activity%-[compound] graphs, and IC<sub>50</sub> values were calculated from the equations of these graphs [27].

## 2.5. Molecular Docking Studies

The three-dimensional (3D) structure of the aldose reductase (PDB ID: 2FZD, 1.08 Å) [28] was received from the PDB (Protein Data Bank). The structure of the receptor was arranged, minimized and optimized with the assistance of the Protein Preparation Wizard [29] module using the OPLS3e force field in the Maestro interface [30]. The LigPrep module was used to create two-dimensional drawings and three-dimensional conversions of the benzaldehyde derivative ligands. The OPLS3e force field was utilized to prepare and minimize protonation shows at pH 7.0 ± 2.0 and tautomers. The docking grid was created using the Receptor Grid Generation instrument and was placed on the center of the co-crystallized ligand, Tolrestat. The Glide extra precision (XP) method was used to molecularly attach all of the benzaldehyde derivatives to the target receptor AR [31]. In addition, Tolrestat was isolated from the crystal structure of the enzyme (AR) and docked again in order to validate the docking procedure. The best ligand pose was superpositioned with the co-crystallized ligand subsequent the re-docking method, and the RMSD (Root Mean Square Deviation) value was computed. Following the re-docking method, the top ligand posture was superpositioned with the co-crystal ligand, and the Root Mean Square Deviation (RMSD) value was calculated. The docking protocol's validation is shown by an RMSD value of less than 2 Å [32].

## 3. RESULTS

To examine the *in vitro* inhibition effects of benzaldehydes, bovine kidney homogenate was used as the source of AR enzyme. It was found that all benzaldehydes inhibited enzyme and 4- phenyl benzaldehyde (**3**) was the most effective inhibitor with IC<sub>50</sub> value of 0.23 μM which was lower than the IC<sub>50</sub> value of standard inhibitor determined by Rakowitz et al. [33] as 3.420 μM (**Table 1**).

**Table 1.** IC<sub>50</sub> values of benzaldehyde derivatives on bovine kidney AR

Compound No	Compound Name	IC <sub>50</sub> (μM)
<b>1</b>	Benzaldehyde	6300
<b>2</b>	2-Naphthylbenzaldehyde	34.65
<b>3</b>	4- Phenyl benzaldehyde	0.23
<b>4</b>	2- Methyl benzaldehyde	2650
<b>5</b>	4- Methyl benzaldehyde	2400
<b>6</b>	2- Bromobenzaldehyde	1.37
<b>7</b>	3- Bromobenzaldehyde	23.1
<b>8</b>	4- Bromobenzaldehyde	57.75
<b>9</b>	2- Nitro benzaldehyde	19.25
<b>10</b>	3- Nitro benzaldehyde	10.5
<b>11</b>	4- Nitro benzaldehyde	18.2
<b>SOR (Rakowitz et al. 2006)</b>	Sorbinyll	3.420

For the prediction of binding affinities and best poses, molecular docking studies were performed with AR receptor. Firstly, docking validation was performed with the co-crystallized ligand. The current study's docking results revealed that compound **3** had the highest effect, with a docking score of -8.31 kcal/mol, as shown in Table 2.

**Table 2.** XP docking scores and binding energies of benzaldehyde derivatives with AR receptor. Predicted docking scores and binding energy values were calculated as kcal/mol.

Compound Number	Docking Score	XP GScore	Glide emodel
<b>1</b>	-6,33	-6,33	-30,54
<b>2</b>	-8,01	-8,01	-39,57
<b>3</b>	-8,61	-8,61	-41,74
<b>4</b>	-6,84	-6,84	-30,15
<b>5</b>	-6,74	-6,74	-30,53
<b>6</b>	-6,57	-6,57	-27,34
<b>7</b>	-6,91	-6,91	-30,75
<b>8</b>	-6,81	-6,81	-31,7
<b>9</b>	-5,14	-5,14	-29,75
<b>10</b>	-6,05	-6,05	-34,18
<b>11</b>	-6,03	-6,03	-34,39
<b>Sorbinyll*</b>	-8,3	-8,35	-44,78

\* Sorbinyll was used as standard inhibitor for AR.

## 4. DISCUSSION AND CONCLUSION

Diabetes Mellitus (DM), a common disease, can cause health issues including blindness, neuron diseases, heart, and kidney failure [34]. In diabetic management, the level of PP becomes the most strategic aims to achieve [33, 34]. AR is the first enzyme of the PP. Various AR inhibitors have been studied extensively, with encouraging results in terms of preventing and reducing diabetes progression [37], [38]. In this paper, some benzaldehyde derivatives were examined being bovine kidney AR. Besides, molecular interactions of compounds and enzyme were estimated by the molecular docking method. As a result of *in vitro* inhibition studies, all derivatives were found to inhibit the enzyme and activity%-[derivative] graphs were drawn. The graphs of the two best inhibitors are given in **Figure 3**. Compound concentrations that halved the activity were calculated from the equations of these graphs (**Table 1**). The two most effective inhibitors were found as derivatives **3**, 4-phenylbenzaldehyde and **6**, 2-Bromobenzaldehyde, with IC<sub>50</sub> values of 0.23 and 1.37 μM correspondingly. These results determined that **3** and **6** are more effective than standard inhibitor, sorbinyll of which IC<sub>50</sub> value was found as 3.420 μM by Rakowitz et al. [33]. It was seen from **Table 1** that benzaldehyde had 6300 μM IC<sub>50</sub> value and methyl derivatives of benzaldehyde had less inhibitory potency than other derivatives.

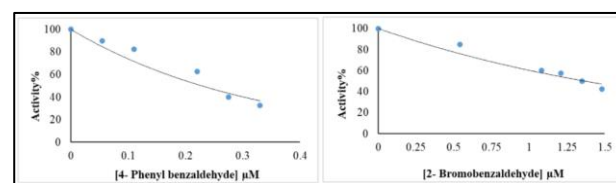


**Figure 3.** Activity%-[derivative] graphs of the two best inhibitors

The earlier study also found that a large number of synthesized derivatives such as thiazole-based compounds, 4H-1,2,4-triazole derivatives, N-benzyl(oxotriazinoindole), 2,4-thiazolidinediones, benzothiazolone-based carboxylic acid inhibited AR [25,26]. The study finds the inhibition potencies of **3** and **6** were higher than thiazole-based compounds, 4H-1,2,4-triazole derivatives and coumarin-thiosemicarbazone hybrids [11,37,39]. The effectiveness of inhibitory effects of benzaldehyde derivatives was determined less than N-

benzyl(oxotriazinoindole) and benzothiazolone-based carboxylic acid [35, 38, 40, 41, 42].

Molecular docking studies were also completed to theoretically support the experimental inhibition effects of benzaldehyde derivatives on the AR enzyme. Benzaldehyde derivatives and the positive control compound sorbinyl were docked to the ligand-binding site identified for the target protein using the extra precision (XP) docking methodology. The docking scores and estimated binding energies of benzaldehyde derivatives for the AR target enzyme are summarized in **Table 2**.

The re-docking approach was employed to verify the docking methodology in this research. Tolrestat was isolated from the crystal structure of the enzyme (AR) and docked again in order to validate the docking procedure. The best ligand pose was superpositioned with the co-crystallized ligand following on re-docking procedure, and the RMSD (Root Mean Square Deviation) value was computed. For the tolrestat ligand, the RMSD value was discovered to be 0,103 Å (**Figure 4**).

The earlier study also found that a large number of synthesized derivatives such as thiazole-based compounds, 4H-1,2,4-triazole derivatives, N-benzyl(oxotriazinoindole), 2,4-thiazolidinediones, benzothiazolone-based carboxylic acid inhibited AR [25,26]. The study finds the inhibition potencies of **3** and **6** were higher than thiazole-based compounds, 4H-1,2,4-triazole derivatives and coumarin-thiosemicarbazone hybrids [11,37,39]. The effectiveness of inhibitory effects of benzaldehyde derivatives was determined less than N-benzyl(oxotriazinoindole) and benzothiazolone-based carboxylic acid [35, 38, 40, 41, 42].

Molecular docking studies were also completed to theoretically support the experimental inhibition effects of benzaldehyde derivatives on the AR enzyme. Benzaldehyde derivatives and the positive control compound sorbinyl were docked to the ligand-binding site identified for the target protein using the extra precision (XP) docking methodology. The docking scores and estimated binding energies of benzaldehyde derivatives for the AR target enzyme are summarized in **Table 2**.

The re-docking approach was employed to verify the docking methodology in this research. Tolrestat was isolated from the crystal structure of the enzyme (AR) and docked again in order to validate the docking procedure. The best ligand pose was superpositioned with the co-crystallized ligand following on re-docking procedure, and the RMSD (Root Mean Square Deviation) value was computed. For the tolrestat ligand, the RMSD value was discovered to be 0,103 Å (**Figure 4**).

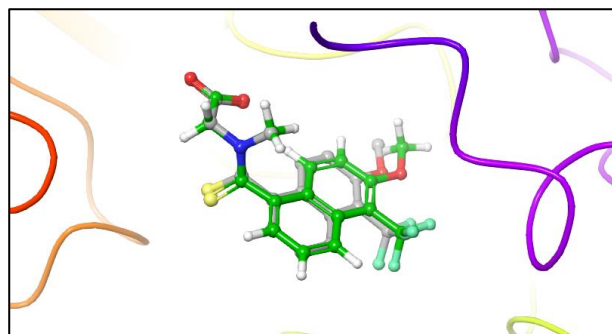


**Figure 4.** Docking validation of tolrestat adduct AR enzyme. AR receptor is depicted in the ribbon model. The co-crystallized ligand is represented in gray ball and stick modeling, while the re-docked ligand is shown in green ball and stick modeling.

As seen from **Table 2**, only the docking score of derivative **3** (-8,61 kcal/mol) was found to be higher than the standard inhibitor, sorbinyl, which had a docking score of -8,3 kcal/mol. Trp79, Trp20, Trp219, Trp111, Leu300, and Phe122 are among the residues in the highly hydrophobic active site pocket of AR [30,31]. When we examine the forms of interactions, we can see that; sorbinyl had an H bond with HIS110 residue and also showed pi-pi stacking interaction upon benzene moiety with indole moieties of Trp79 and Trp111 amino acids. And it displayed so many hydrophobic interactions with the active side pocket (**Figure 5**). Derivative **3**, which is the most effective inhibitor based on the results of *in vitro* inhibition experiments and molecular docking estimations, affected AR in a similar manner with standard inhibitor. As seen from **Figure 6**, compound **3**, had two hydrogen bonds with TYR48 and HIS110 residues. Benzene moiety of **3** also exhibited a pi-pi stacking interaction with the indole group of TRP111. Derivative **3** had so many polar and hydrophobic interactions through the same residues as sorbinyl. These interactions are consistent with a previous study, which was conducted by Salem et al. [47]. They reported in their study on the inhibition effects of novel meglitinides on AR that **15C** and **12B** had interaction with residues similar to those of our study.

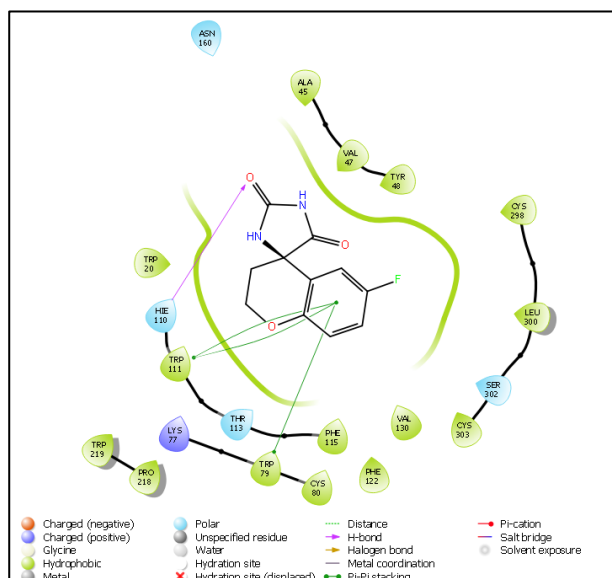


**Figure 5.** 2D ligand-receptor interaction diagram of standard AR inhibitor sorbinil

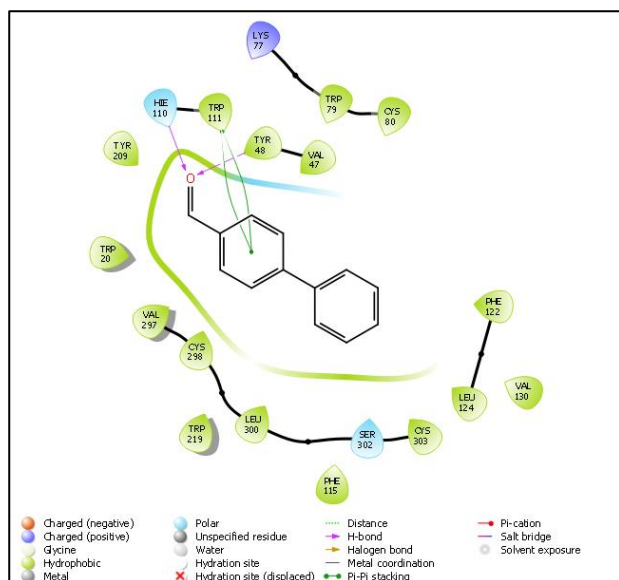


**Figure 6.** 2D ligand-receptor interaction diagram of best-scored compound derivative **3**.

In conclusion, the PP is activated when blood glucose levels are high and it is critical for preventing diabetes and diabetes-related complications. As a result, the AR inhibition strategy holds promise for the treatment of diabetes and related illnesses. In conclusion, all benzaldehyde derivatives inhibited AR in the micromolar range and compounds **3** and **6** had higher inhibitory potency than standard inhibitor with  $IC_{50}$  values of 0.23 and 1.37  $\mu$ M respectively. The docking score of **3** was also found to be higher than the standard inhibitor with the value of -8.61 kcal/mol. The results of the current study are hoped to be able to guide for further research on new drug candidates in the treatment of diabetes.

### Conflict of Interest

The author declares that there is no potential conflict of interest.

### Acknowledgments

Since enzyme inhibition studies were performed in the Biochemistry Research Laboratory of Atatürk University, Faculty of Science, Department of Chemistry, the author is thankful to Atatürk University, Faculty of Science, Department of Chemistry.

### Funding

The current research was supported by Bayburt University-Scientific Research Projects [Grant Number: 2018/01-69001-21].

### CRedit authorship contribution statement

Bülent Şengül: Conceptualization, Methodology, Data curation, Visualization, Investigation, Writing - review & editing.

### Data Availability Statement

The data that support the findings of this study are available from the corresponding author upon reasonable request.

## REFERENCES

- [1] Y. Demir, H. E. Duran, L. Durmaz, P. Taslimi, Ş. Beydemir, and İ. Gulçin, "The Influence of Some Nonsteroidal Anti-inflammatory Drugs on Metabolic Enzymes of Aldose Reductase, Sorbitol Dehydrogenase, and  $\alpha$ -Glycosidase: a Perspective for Metabolic Disorders," *Appl. Biochem. Biotechnol.*, vol. 190, no. 2, pp. 437–447, Feb. 2020, doi: 10.1007/s12010-019-03099-7.
- [2] F. Erdemir *et al.*, "Novel 2-aminopyridine liganded Pd(II) N-heterocyclic carbene complexes: Synthesis, characterization, crystal structure and bioactivity properties," *Bioorg. Chem.*, vol. 91, p. 103134, Oct. 2019, doi: 10.1016/j.bioorg.2019.103134.
- [3] L. Gilbert *et al.*, "A pilot study of pi-class glutathione S-transferase expression in breast cancer: correlation with estrogen receptor expression and prognosis in node-negative breast cancer," *J. Clin. Oncol.*, vol. 11, no. 1, pp. 49–58, Jan. 1993, doi: 10.1200/JCO.1993.11.1.49.
- [4] IDF diabetes atlas, "No Title," in *IDF diabetes atlas.* International Diabetes Federation (9th editio). Retrieved from <http://www.idf.org/about-diabetes/facts-figures>, 2019.
- [5] A. Oğuz, "The Prospective Urban Rural Epidemiology (PURE) study: PURE TURKEY," *Turk Kardiyol. Dern. Arsivi-Archives Turkish Soc. Cardiol.*, 2018, doi: 10.5543/tkda.2018.32967.
- [6] Anonim, "No Title," *Dünya Diyabet Günü*, 2020. <https://sggm.saglik.gov.tr/TR-76887/dunya-diyabet-gunu-2020.html>
- [7] W. H. Tang, S. Wu, T. M. Wong, S. K. Chung, and S. S. M. Chung, "Polyol pathway mediates iron-induced oxidative injury in ischemic-reperfused rat heart," *Free Radic. Biol. Med.*, vol. 45, no. 5, pp. 602–610, Sep. 2008, doi: 10.1016/j.freeradbiomed.2008.05.003.
- [8] S. S. M. Chung, E. C. M. Ho, K. S. L. Lam, and S. K. Chung, "Contribution of Polyol Pathway to Diabetes-Induced Oxidative Stress," *J. Am. Soc. Nephrol.*, vol. 14, no. suppl 3, pp. S233–S236, Aug. 2003, doi: 10.1097/01.ASN.0000077408.15865.06.
- [9] R. I. Lindstad, K. Teigen, and L. Skjeldal, "Inhibition of sorbitol dehydrogenase by nucleosides and nucleotides," *Biochem. Biophys. Res. Commun.*, vol. 435, no. 2, pp. 202–208, May 2013, doi: 10.1016/j.bbrc.2013.04.081.
- [10] Y. Demir, M. S. Özasan, H. E. Duran, Ö. İ. Küfrevioğlu, and Ş. Beydemir, "Inhibition effects of quinones on aldose reductase: Antidiabetic properties," *Environ. Toxicol. Pharmacol.*, vol. 70, p. 103195, Aug. 2019, doi: 10.1016/j.etap.2019.103195.
- [11] B. Sever, M. D. Altıntop, Y. Demir, G. Akalın Çiftçi, Ş. Beydemir, and A. Özdemir, "Design, synthesis, in vitro and in silico investigation of aldose reductase inhibitory effects of new thiazole-based compounds," *Bioorg. Chem.*, vol. 102, p. 104110, Sep. 2020, doi: 10.1016/j.bioorg.2020.104110.
- [12] T.-S. Kim *et al.*, "Overcoming NADPH product inhibition improves D-sorbitol conversion to L-



- sorbose,” *Sci. Rep.*, vol. 9, no. 1, p. 815, Dec. 2019, doi: 10.1038/s41598-018-37401-0.
- [13] T. Petrova *et al.*, “Factorizing selectivity determinants of inhibitor binding toward aldose and aldehyde reductases: structural and thermodynamic properties of the aldose reductase mutant Leu300Pro-fidarestat complex,” *J. Med. Chem.*, vol. 48, no. 18, pp. 5659–65, Sep. 2005, doi: 10.1021/jm050424+.
- [14] C. Yabe-Nishimura, “Aldose reductase in glucose toxicity: a potential target for the prevention of diabetic complications,” *Pharmacol. Rev.*, vol. 50, no. 1, pp. 21–33, Mar. 1998, [Online]. Available: <http://www.ncbi.nlm.nih.gov/pubmed/9549756>
- [15] M. Brownlee, “Biochemistry and molecular cell biology of diabetic complications,” *Nature*, vol. 414, no. 6865, pp. 813–820, Dec. 2001, doi: 10.1038/414813a.
- [16] Q. Huang, Q. Liu, and D. Ouyang, “Sorbinil, an Aldose Reductase Inhibitor, in Fighting Against Diabetic Complications,” *Med. Chem. (Los Angeles)*, vol. 15, no. 1, pp. 3–7, Jan. 2019, doi: 10.2174/1573406414666180524082445.
- [17] M. S. Özasan, R. Sağlamtaş, Y. Demir, Y. Genç, İ. Saraçoğlu, and İ. Gülçin, “Isolation of Some Phenolic Compounds from *Plantago subulata* L. and Determination of Their Antidiabetic, Anticholinesterase, Antiepileptic and Antioxidant Activity,” *Chem. Biodivers.*, vol. 19, no. 8, Aug. 2022, doi: 10.1002/cbdv.202200280.
- [18] C. Türkeş, Y. Demir, and Ş. Beydemir, “Anti-diabetic Properties of Calcium Channel Blockers: Inhibition Effects on Aldose Reductase Enzyme Activity,” *Appl. Biochem. Biotechnol.*, vol. 189, no. 1, pp. 318–329, Sep. 2019, doi: 10.1007/s12010-019-03009-x.
- [19] Y. Demir, M. Işık, İ. Gülçin, and Ş. Beydemir, “Phenolic compounds inhibit the aldose reductase enzyme from the sheep kidney,” *J. Biochem. Mol. Toxicol.*, vol. 31, no. 9, p. e21936, Sep. 2017, doi: 10.1002/jbt.21935.
- [20] F. S. Tokalı *et al.*, “Synthesis, biological evaluation, and in silico study of novel library sulfonates containing quinazolin-4(  $<sc>3 H</sc>$  )-one derivatives as potential aldose reductase inhibitors,” *Drug Dev. Res.*, Sep. 2021, doi: 10.1002/ddr.21887.
- [21] N. Trueblood and R. Ramasamy, “Aldose reductase inhibition improves altered glucose metabolism of isolated diabetic rat hearts,” *Am. J. Physiol. Circ. Physiol.*, vol. 275, no. 1, pp. H75–H83, Jul. 1998, doi: 10.1152/ajpheart.1998.275.1.H75.
- [22] H. Liu *et al.*, “Genetic deficiency of aldose reductase counteracts the development of diabetic nephropathy in C57BL/6 mice,” *Diabetologia*, vol. 54, no. 5, pp. 1242–1251, May 2011, doi: 10.1007/s00125-011-2045-4.
- [23] J. Tang, Y. Du, J. M. Petrush, N. Sheibani, and T. S. Kern, “Deletion of Aldose Reductase from Mice Inhibits Diabetes-Induced Retinal Capillary Degeneration and Superoxide Generation,” *PLoS One*, vol. 8, no. 4, p. e62081, Apr. 2013, doi: 10.1371/journal.pone.0062081.
- [24] B. Şengül and Ş. Beydemir, “The interactions of cephalosporins on polyol pathway enzymes from sheep kidney,” *Arch. Physiol. Biochem.*, vol. 124, no. 1, pp. 35–44, Jan. 2018, doi: 10.1080/13813455.2017.1358749.
- [25] M. J. Cerelli, D. L. Curtis, J. P. Dunn, P. H. Nelson, T. M. Peak, and L. D. Waterbury, “Antiinflammatory and aldose reductase inhibitory activity of some tricyclic arylacetic acids,” *J. Med. Chem.*, vol. 29, no. 11, pp. 2347–2351, Nov. 1986, doi: 10.1021/jm00161a033.
- [26] I. N. Korkmaz, “2-Amino thiazole derivatives as inhibitors of some metabolic enzymes: An in vitro and in silico study,” *Biotechnol. Appl. Biochem.*, Jul. 2022, doi: 10.1002/bab.2388.
- [27] I. N. KORKMAZ, “In Vitro Inhibition Effects of 2-Amino Thiazole Derivatives on Lactoperoxidase Enzyme Activity,” *Cumhuriyet Sci. J.*, vol. 43, no. 1, pp. 33–37, Mar. 2022, doi: 10.17776/cs.j.1017247.
- [28] H. Steuber, M. Zentgraf, C. Gerlach, C. A. Sottriffer, A. Heine, and G. Klebe, “Expect the Unexpected or Caveat for Drug Designers: Multiple Structure Determinations Using Aldose Reductase Crystals Treated under Varying Soaking and Cocrystallisation Conditions,” *J. Mol. Biol.*, vol. 363, no. 1, pp. 174–187, Oct. 2006, doi: 10.1016/j.jmb.2006.08.011.
- [29] G. Madhavi Sastry, M. Adzhigirey, T. Day, R. Annabhimoju, and W. Sherman, “Protein and ligand preparation: parameters, protocols, and influence on virtual screening enrichments,” *J. Comput. Aided. Mol. Des.*, vol. 27, no. 3, pp. 221–234, Mar. 2013, doi: 10.1007/s10822-013-9644-8.
- [30] Harder, E., Damm, W., Maple, J., Wu, C., Reboul, M., Xiang, J. Y., ... & Friesner, R. A. (2016). OPLS3: a force field providing broad coverage of drug-like small molecules and proteins. *Journal of chemical theory and computation*, 12(1), 281-296.
- [31] R. A. Friesner *et al.*, “Glide: A New Approach for Rapid, Accurate Docking and Scoring. 1. Method and Assessment of Docking Accuracy,” *J. Med. Chem.*, vol. 47, no. 7, pp. 1739–1749, Mar. 2004, doi: 10.1021/jm0306430.
- [32] E. Yuriev, M. Agostino, and P. A. Ramsland, “Challenges and advances in computational docking: 2009 in review,” *J. Mol. Recognit.*, vol. 24, no. 2, pp. 149–164, Mar. 2011, doi: 10.1002/jmr.1077.
- [33] D. Rakowitz, R. Maccari, R. Ottanà, and M. G. Vigorita, “In vitro aldose reductase inhibitory activity of 5-benzyl-2,4-thiazolidinediones,” *Bioorg. Med. Chem.*, vol. 14, no. 2, pp. 567–574, Jan. 2006, doi: 10.1016/j.bmc.2005.08.056.
- [34] B. F. Schrijvers, A. S. De Vriese, and A. Flyvbjerg, “From Hyperglycemia to Diabetic Kidney Disease: The Role of Metabolic, Hemodynamic, Intracellular Factors and Growth Factors/Cytokines,” *Endocr. Rev.*, vol. 25, no. 6, pp. 971–1010, Dec. 2004, doi: 10.1210/er.2003-0018.
- [35] C. Türkeş, M. Arslan, Y. Demir, L. Çoçaj, A. R. Nixha, and Ş. Beydemir, “ $N$ -substituted phthalazine sulfonamide derivatives as non-classical aldose reductase inhibitors,” *J. Mol.*

- Recognit.*, vol. 35, no. 12, Dec. 2022, doi: 10.1002/jmr.2991.
- [36] M. Akdağ, A. B. Özçelik, Y. Demir, and Ş. Beydemir, "Design, synthesis, and aldose reductase inhibitory effect of some novel carboxylic acid derivatives bearing 2-substituted-6-aryloxy-pyridazinone moiety," *J. Mol. Struct.*, vol. 1258, p. 132675, Jun. 2022, doi: 10.1016/j.molstruc.2022.132675.
- [37] Y. Demir *et al.*, "Determination of the inhibition profiles of pyrazolyl-thiazole derivatives against aldose reductase and  $\alpha$ -glycosidase and molecular docking studies," *Arch. Pharm. (Weinheim)*, vol. 353, no. 12, p. 2000118, Dec. 2020, doi: 10.1002/ardp.202000118.
- [38] Y. Demir and Z. Köksal, "Some sulfonamides as aldose reductase inhibitors: therapeutic approach in diabetes," *Arch. Physiol. Biochem.*, vol. 128, no. 4, pp. 979–984, Jul. 2022, doi: 10.1080/13813455.2020.1742166.
- [39] B. Sever *et al.*, "A new series of 2,4-thiazolidinediones endowed with potent aldose reductase inhibitory activity," *Open Chem.*, vol. 19, no. 1, pp. 347–357, Mar. 2021, doi: 10.1515/chem-2021-0032.
- [40] Y. Lei *et al.*, "Design of Benzothiazolone-Based Carboxylic Acid Aldose Reductase Inhibitors," *ChemistrySelect*, vol. 6, no. 20, pp. 4874–4880, May 2021, doi: 10.1002/slct.202101443.
- [41] A. Imran *et al.*, "Development of coumarin-thiosemicarbazone hybrids as aldose reductase inhibitors: Biological assays, molecular docking, simulation studies and ADME evaluation," *Bioorg. Chem.*, vol. 115, p. 105164, Oct. 2021, doi: 10.1016/j.bioorg.2021.105164.
- [42] M. Hlaváč *et al.*, "Novel substituted N-benzyl(oxotriazinoindole) inhibitors of aldose reductase exploiting ALR2 unoccupied interactive pocket," *Bioorg. Med. Chem.*, vol. 29, p. 115885, Jan. 2021, doi: 10.1016/j.bmc.2020.115885.
- [43] M. Ceylan *et al.*, "Synthesis, carbonic anhydrase I and II isoenzymes inhibition properties, and antibacterial activities of novel tetralone-based 1,4-benzothiazepine derivatives," *J. Biochem. Mol. Toxicol.*, vol. 31, no. 4, p. e21872, Apr. 2017, doi: 10.1002/jbt.21872.
- [44] Y. Temel and S. BAYINDIR, "The Synthesis of Thiosemicarbazone-Based Aza-Ylides as Inhibitors of Rat Erythrocyte Glucose 6-Phosphate Dehydrogenase Enzyme," *J. Inst. Sci. Technol.*, pp. 1503–1512, Sep. 2019, doi: 10.21597/jist.518012.
- [45] P. Alexiou, K. Pegklidou, M. Chatzopoulou, I. Nicolaou, and V. Demopoulos, "Aldose Reductase Enzyme and its Implication to Major Health Problems of the 21st Century," *Curr. Med. Chem.*, vol. 16, no. 6, pp. 734–752, Feb. 2009, doi: 10.2174/092986709787458362.
- [46] J. Sangshetti, R. Chouthe, N. Sakle, I. Gonjari, and D. Shinde, "Aldose Reductase: A Multi-disease Target," *Curr. Enzym. Inhib.*, vol. 10, no. 1, pp. 2–12, Oct. 2013, doi: 10.2174/15734080113096660007.
- [47] M. G. Salem, Y. M. Abdel Aziz, M. Elewa, M. S. Nafie, H. A. Elshihawy, and M. M. Said, "Synthesis, molecular modeling, selective aldose reductase inhibition and hypoglycemic activity of novel meglitinides," *Bioorg. Chem.*, vol. 111, p. 104909, Jun. 2021, doi: 10.1016/j.bioorg.2021.104909.



## Experimental Investigation of Photovoltaic Panel Performance in Bingöl Province for Different Parameters

Sinem KILIÇKAP IŞIK<sup>1\*</sup>, Perihan ÇULUN<sup>2</sup>

<sup>1,2</sup> Bingöl University, Faculty of Engineering and Architecture, Mechanical Engineering Department, Bingöl, Türkiye  
Sinem KILIÇKAP IŞIK ORCID No: 0000-0002-1044-5092

Perihan ÇULUN ORCID No: 0000-0002-1797-9695

\*Corresponding author: [sinemisik@bingol.edu.tr](mailto:sinemisik@bingol.edu.tr)

(Received: 24.02.2023, Accepted: 22.05.2023, Online Publication: 22.06.2023)

### Keywords

Bingöl,  
Renewable  
energy,  
Solar radiation,  
Photovoltaic  
panel,  
Inclination  
angle

**Abstract:** In the present study, an experimental research was conducted on the photovoltaic solar energy potential in Bingöl province. In the study, the electrical energy that the photovoltaic (PV) panel can produce hourly at an inclination angle of 39° and 45° and the panel surface temperature were investigated. The electrical energy that can be produced indoors and outdoors in winter conditions was calculated from the photovoltaic panel with 25 W power. It has been observed that the highest efficiency can be obtained at the 45° panel inclination angle. It has been concluded that while the average electric power produced at an angle of inclination of 45° is 9.68 W in outdoor conditions, it can be 1.22 W in indoor conditions. The data obtained will be an important reference in determining the panel size that will meet the consumption need and in the establishment of higher efficiency systems. It is stated that the payback period of grid-connected systems in provinces with high solar radiation such as Bingöl is 6 years on average. At the end of this period, it is clear that it will make significant contributions to both the landlords, the country's economy, and the environment in terms of reducing emissions.

## Bingöl İli Fotovoltaik Panel Performansının Farklı Parametreler İçin Deneysel Olarak İncelenmesi

### Anahtar Kelimeler

Bingöl,  
Yenilenebilir  
enerji,  
Güneş ışınımı,  
Fotovoltaik  
panel,  
Eğim açısı

**Öz:** Bu çalışmada Bingöl ilinde fotovoltaik güneş enerjisi potansiyeli üzerine deneysel bir araştırma yapılmıştır. Çalışmada, fotovoltaik (PV) panelin 39° ve 45° eğim açısında saatlik üretebileceği elektrik enerjisi ve panel yüzey sıcaklığı incelenmiştir. Kullanılan 25 W gücündeki panelden, kış şartlarında iç ve dış ortamda üretebilecek elektrik enerjisi hesaplanmıştır. En fazla verimin 45° panel eğim açısında elde edilebileceği görülmüştür. 45° eğim açısında ortalama üretilen elektrik gücünün dış ortam şartlarında 9.68 W iken iç ortam şartlarında ise 1.22 W olabileceği sonucuna varılmıştır. Elde edilen veriler tüketim ihtiyacını karşılayacak panel büyüklüğünün tespitinde ve daha yüksek verimli sistemlerin kurulmasında önemli bir referans olacaktır. Bingöl gibi yüksek güneş ışınımına sahip illerde şebeke bağlantılı sistemlerin geri ödeme süresinin ortalama 6 yıl olduğu belirtilmektedir. Bu sürenin bitiminde, hem maddi yönden ev sahiplerine hem ülke ekonomisine hem de emisyonların azaltılması hususunda çevreye önemli katkılar sağlayacağı açıktır.

### 1. INTRODUCTION

Energy will be one of the most important issues on which research will continue as long as human life continues. As a matter of fact, it is the most important parameter required to meet the basic needs of human beings. According to TEİAŞ 2022 data, 197536.2 GWh of the total 326014.8 GWh electricity produced was

produced from thermal power plants and 128478.6 GWh from renewable energy sources (hydraulic, geothermal, wind, solar) [1]. As can be seen, 61% of the annual electricity produced in Turkey is produced from thermal power plants, that is, fossil fuels, while the remaining 39% is produced from renewable energy sources. According to the same report, Turkey purchased 6414 GWh of electricity from foreign countries in 2022. On the other hand, 72536.1 GWh of energy, which is 36%

of the electrical energy produced from fossil fuels, was produced from natural gas [1]. Considering that the majority of natural gas is purchased from foreign countries, it is obvious that the importance to be given to renewable energy sources in our country should be increased. In addition, hard coal, lignite, liquid fuels and natural gas are used as fossil fuels in Turkey. Since the fossil fuels are about to run out and pollute the nature, use of them should be terminated and renewable energy resources should be expanded instead.

Renewable energy resources are more advantageous than fossil fuels in terms of being cleaner, cheaper, and unlimited resources, except for the initial cost [2]. The main renewable energy sources used in Turkey are hydraulic, geothermal, wind, solar and wave energy [3-8]. In addition, hydrogen energy, on which research has been intensified recently can be included in the class of clean and renewable energy sources, especially in terms of the fact that it can be obtained from both water and the sun, and only water is released as a result of combustion [9, 10]. One of these renewable energy sources, hydraulic energy sources known as hydraulic power plants (HES) cannot be said to be completely harmless for the environment. As a matter of fact, there are cases where many residential areas and forests are damaged in many HES regions. On the other hand, wind and wave energy is not the type of energy that can be obtained for every region of Turkey. In order to obtain

the necessary efficiency from wind energy, continuous winds must blow at a speed of at least 5 m/s for most of the year in the region where the power plant will be established. This condition is provided only in a few provinces. Similarly, wave power plants can be installed on sea coasts with high tides. However, solar energy is not like that. Turkey is one of the luckiest countries in terms of solar energy. As it can be understood from the "Turkey Solar Energy Potential Map" taken from the website of the Turkish Ministry of Energy and Natural Resources, there is solar radiation in the amount of 1400-1450 kWh/m<sup>2</sup>-year even in the region with the lowest solar radiation (Figure 1). In addition, the annual total sunshine duration in our country is 2741 hours, and the average annual radiation value is determined as 1527.46 kWh/m<sup>2</sup>. From Figure 1, the average annual radiation value of Bingöl is in the range of 1500-1700 kWh/m<sup>2</sup> and it is understood that it is one of the leading provinces in terms of solar radiation [11]. As can be seen from Table 1, the total installed solar power in Bingöl province is 1487.5 MW. 14 MW of this is under construction and 260 MW is in the planning stage [12]. The hybrid GES (solar power plant) installed in Bingöl has a power of 500 MW and constitutes only 33% of the total installed power [12]. In Figure 2 and Figure 3, examples of solar power plants installed in Bingöl province are given [13, 14].

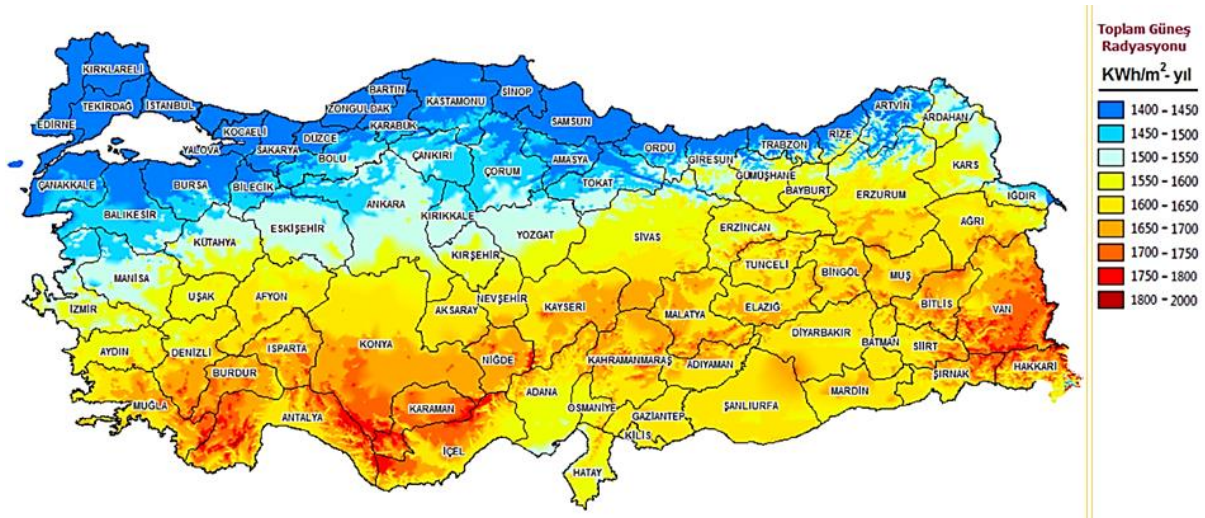


Figure 1. Turkey Solar Energy Potential Atlas [11].

Table 1. Installed capacity of existing renewable energy enterprises in Bingöl province [12].

Installed Energy	Capacities (MW)
Yukarı Kaleköy Dam and HES	627
Aşağı Kaleköy Dam and Hybrid GES	500
Özlüce Dam and HES	170
Kığı Dam and HES	138
Yedisu HES	23
Saf 1 HES	16
Doğu HES	10
Metaphor Wind Power Plant (RES)	3.50
<b>Grand Total</b>	<b>1487.5</b>

Although Turkey is a lucky country in terms of solar energy, it is understood that it does not benefit enough from this energy in practice. As a matter of fact, although the importance of solar collectors is obvious in most academic studies, solar collectors are not used in some buildings today with the excuses that they damage the building statics. The sacrifice of solar energy to such rent-seeking activities reveals the fact that the importance of renewable energy is not fully understood.



Figure 2. Aşağı Kaleköy hybrid solar power plant (Genç/Bingöl-500MW) [13].



Figure 3. Solhan GES (Solhan/Bingöl-4MW) [14].

Many studies are carried out by those who are aware of the importance of solar energy in our country. When the studies were examined, the importance of the effect of different panel angles on yields was clearly observed. As a matter of fact, ensuring that the sun's rays come as perpendicular to the panel as possible will ensure that the results are more efficient. In this respect, studies on testing different angles and determining the optimum angle in provinces with different latitudes and longitudes are important. In the study of Keskin et al. (2019), the performance analysis of the relevant province was carried out in the model established using the V6.78 version of the photovoltaic panel PVsyst program in the province of Niğde. There was a 1.72% difference between the data obtained from the model and the actual data. A total annual installed power of 1994.8 kWh was achieved. The values obtained in the case of the panel angle of  $33^\circ$  were higher than the values obtained in the case of  $10^\circ$ . It is understood that better results are obtained at an angle close to the  $37^\circ$  latitude of the relevant location [15]. Atlım et al. (2019) compared two solar energy systems placed differently in Balıkesir on the basis of daily and monthly data. According to the results obtained from monocrystalline and polycrystalline solar energy systems, it was stated that the panel angles significantly affect the efficiency. In the related study, it was determined that the results obtained for the solar energy system with  $27^\circ$  angle were higher than the system with  $9^\circ$  panel inclination, and the best result was  $29^\circ$  panel angle according to the simulation program. [16]. Güven (2022) investigated the panel performance and its relationship with panel surface temperature for one year data in his study in Denizli. In the study, it is mentioned that the panel performance decreases by 0.3% for every  $5^\circ\text{C}$  temperature increase on the panel surface [17]. Yıldırım and Aktacir (2021) investigated monthly average performance and panel surface temperature values for mono-Si, p-Si and CdTe type panels in Şanlıurfa. They explained that 345 kWh, 311 kWh and 234 kWh energy are produced in the unit area per year from Mono-Si, p-Si and CdTe type panels, respectively [18]. Kabul and Duran (2014), in their PV/T study in Isparta province, reduced the increased panel temperature by using cold water pipes, thus providing an efficiency increase of up to 7% and a power increase of 31% in the PV panel. In addition, they obtained hot water by using the heat from the hot panel surface. While the temperature of the uncooled panels was  $95^\circ\text{C}$

in July, the surface temperature of the water-cooled panel was measured as  $55^\circ\text{C}$  on average [19]. Kerem et al. (2020) investigated the effect of cooling the panel surface with water on the panel performance at Osmaniye Korkut Ata University Engineering Faculty. In the said study, an increase of 14% was achieved in the panel efficiency [20].

As it is understood from the studies carried out, it is necessary to determine the optimum working angles of each province with different latitudes in order to ensure the right angle to the panel surface. On the other hand, it is understood from the literature researches that such national studies were carried out for a limited number of provinces. Therefore, more studies are needed to form a general opinion in this area. In this study, the performance of photovoltaic panels at different angles has been investigated in the case of both indoor and outdoor use in Bingöl province. It is aimed to determine the best angle in Bingöl province by taking results for different angles.

## 2. MATERIAL AND METHOD

Bingöl province, with a surface area of 8125 km<sup>2</sup>, is located in the Upper Euphrates section of the Eastern Anatolia Region. It is located between  $38^\circ27'$  and  $40^\circ27'$  east longitudes and  $41^\circ20'$  and  $39^\circ54'$  north latitudes. The central district of Bingöl has an altitude of 1125 m. The province has a climate that is hot in summers and very cold in winters with its altitude and cool air mass coming from the north. The annual average temperature is  $12.1^\circ\text{C}$  and the annual average precipitation is 873.7 mm [21]. As stated in Turkey's solar map data, the annual sunshine duration of Bingöl province is 2719 hours and the annual radiation value is 1592 kWh/m<sup>2</sup> [22]. The annual solar radiation map by district is given in Figure 4.

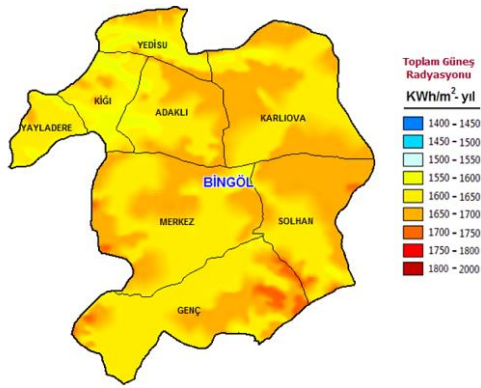


Figure 4. Solar radiation in Bingöl province [21].

The variation of daily radiation values according to months in the Central district of Bingöl province is given in Figure 5. According to Figure 5, while the months with the lowest solar radiation are December and January, the months with the highest solar radiation are June and July. The months with the highest and lowest sunshine duration are the same (Figure 6). In January, when the experiments were carried out, the daily average solar radiation was 1.83 kWh/m<sup>2</sup> (Figure 5) and the average daily sunshine duration was 4.14 hours (Figure 6).

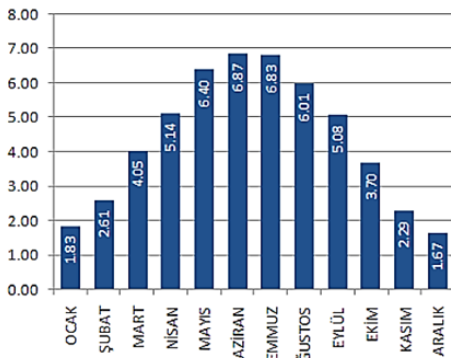


Figure 5. Global radiation values according to months (kWh/m<sup>2</sup>-day) in the central district of Bingöl province [23].

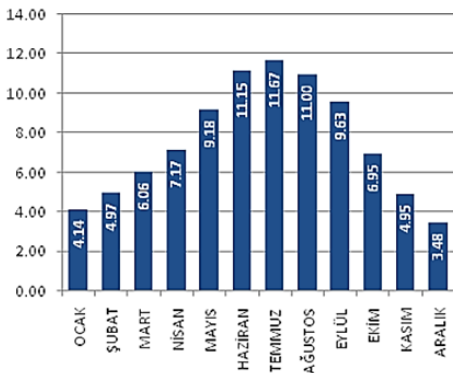


Figure 6. The daily sunshine duration (hours) according to the months in the Central District of Bingöl Province [23].

The electrical energy that can be produced varies according to the type and size of the solar panel used. As seen in Figure 7, the highest amount of energy is obtained from monocrystalline panels. Next come polycrystalline panels. Monocrystalline panels work much better in high-temperature environments and low-sunlight environments. In addition, monocrystalline solar panels have the highest efficiency of 15-20%. Compared to other panel types, they are more durable and have a longer lifespan of approximately 25 years. Monocrystalline solar panels consist of a single crystal, while polycrystalline panels consist of many crystals. While polycrystalline panels have lower efficiency (12-16%) than monocrystallines, their prices are cheaper. Polycrystalline solar panels perform much better in low temperature environments. Especially in cold countries, polycrystalline solar panels are preferred [24, 25]. For this reason, we preferred the monocrystalline solar panel, which has a longer life and high efficiency, in our study.

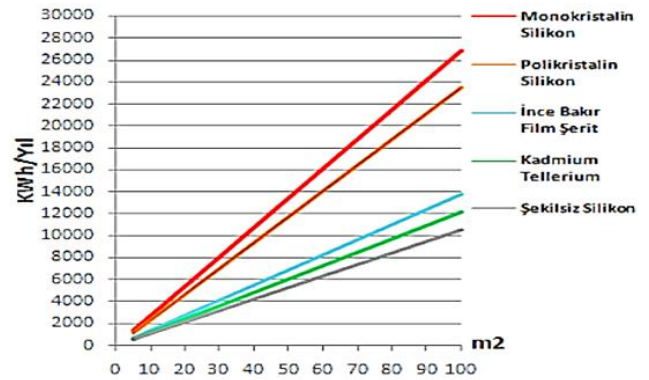
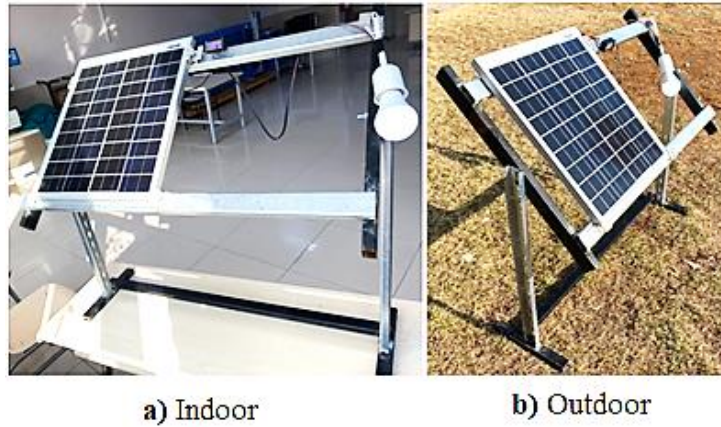


Figure 7. The annual amount of energy that can be produced (kWh-year) according to the type and area of the solar panel for the Central District of Bingöl province [23].

The experiments were carried out on sunny days in January. Hourly electrical power produced by photovoltaic panels in indoor and outdoor environments in Bingöl province was compared. The indoor environment experiment was carried out in the Fluid Mechanics Laboratory of the Mechanical Engineering Department of Bingöl University. The panel was placed in front of the sun-facing window in the laboratory as seen in Figure 8a. The outdoor experiment was carried out on an empty land in the city, away from the buildings, receiving direct sunlight (Figure 8b).



a) Indoor

b) Outdoor

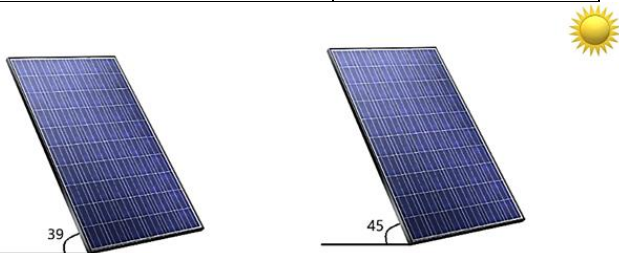
**Figure 8.** Experiment set set up for indoor (a) and outdoor (b) environments

Voltage and current values were read by connecting a voltmeter to the panel output. Panel surface temperature and ambient temperature measurements were made with a Cem brand 4-channel datalogger. In addition, a 9-Watt light bulb is connected to the panel output, and current output is provided. In the experiments, Lexron brand monocrystalline solar panel measuring 362 mm x 433 mm x 20 mm and a power of 25 W was used. The technical specifications of the solar panel used are given in Table 2. The solar panel has an area of 0.16 m<sup>2</sup> as calculated in Eq. 1. An angle-adjustable footrest is manufactured to place the panel. The photovoltaic panel is adjusted to 39° (Latitude angle of Bingöl province) and 45° angles in indoor and outdoor environments (Figure 9). One hour measurements were taken at different angles in the indoor and outdoor environments at noon when the sun comes vertically. Data were read at 2-minute time intervals.

$$\text{Area of Solar Panel (A)} = 0.362 \text{ m} \times 0.433 \text{ m} = 0.16 \text{ m}^2 \quad (1)$$

**Table 2.** Technical specifications of monocrystalline solar panel.

Power (W)	25
Number of Cells	36
Open Circuit Voltage (V)	24.84
Max. Voltage (V)	20.70
Short Circuit Current (A)	1.27
Max. Current (A)	1.21
Max. System Voltage (V)	1000
Module Dimensions (mm)	362*433*20
Weight (kg)	1.68

**Figure 9.** Photovoltaic panel inclination angles.

The average amount of power ( $P_{ave}$ , W) that can be obtained from a 25 Watt solar panel is equal to the

multiplication of the average current ( $I_{ave}$ , amper) and the average voltage ( $V_{ave}$ , volt) in the panel (Eq. 2) [26, 27].

$$P_{ave} = I_{ave} \times V_{ave} \text{ (W)} \quad (2)$$

The total amount of energy (YE, W) coming to the surface of the panel is equal to the multiplication of solar radiation (G, W/ m<sup>2</sup>) and the panel surface area (A, m<sup>2</sup>). The electrical efficiency ( $\eta$ ) of the photovoltaic panel is calculated by the ratio of the average electrical power ( $P_{ave}$ , W) to the total energy amount (YE, W) of the panel surface [26, 27]. It is given in Eq. 3 and Eq. 4.

$$YE = G \cdot A \text{ (W)} \quad (3)$$

$$\eta = P_{ave} \cdot YE^{-1} = P_{ave} \cdot (G \cdot A)^{-1} \quad (4)$$

### 3. RESULTS

Solar panels were placed in front of the window facing the sun in our laboratory for indoor conditions, and on an empty land in the city as an outdoor environment. The experiments were carried out at noon. The variation of panel surface temperatures according to the angle is given in Figure 10. According to Figure 10, indoor panel surface temperatures are maximum 30.6 °C and minimum 25.5 °C at a 45° panel inclination angle; At the 39° angle, it was observed that the maximum is 31.3 °C and the minimum is 29.6 °C. At the time of the experiments, the average indoor temperature was determined as 24.17 °C. At an inclination angle of 45° indoors, the maximum current on the panel is 0.13 A, and the voltage is 9.4 V; at an inclination angle of 39°, the current remained constant for one hour and was read as 0.10 A, and the maximum voltage as 9.4 V. The power change obtained according to these values is shown in Figure 11. In indoor winter conditions, a maximum of 1.22 W electrical power is obtained from a 25 W solar panel at an inclination angle of 45°, and a maximum of 0.94 W at an inclination angle of 39°. The hourly average power amounts calculated according to the data obtained from the experiments performed at different panel angles in indoor and outdoor conditions are given in Table 3.

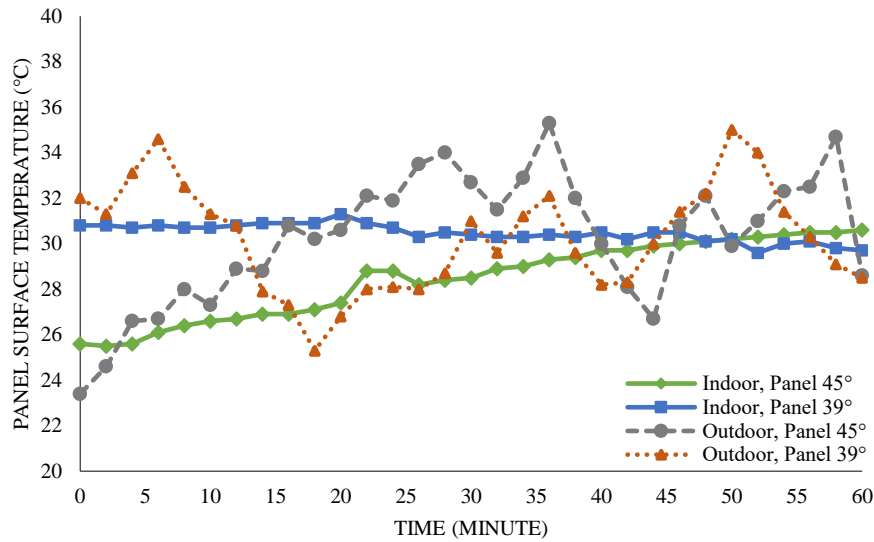


Figure 10. Variation of panel surface temperatures according to angle in indoor and outdoor conditions.

Table 3. Average hourly power amounts calculated at different panel angles in indoor and outdoor conditions [Ts: Panel surface temperature (°C), Tamb: Ambient temperature (°C)].

Panel Angles	Indoor					Outdoor				
	I <sub>ave</sub> (Amper, A)	V <sub>ave</sub> (Volt, V)	P <sub>ave</sub> (W)	T <sub>s</sub> (°C)	T <sub>amb</sub> (°C)	I <sub>ave</sub> (Amper, A)	V <sub>ave</sub> (Volt, V)	P <sub>ave</sub> (W)	T <sub>s</sub> (°C)	T <sub>amb</sub> (°C)
39°	0.10	9.31	0.93	30.47	24.45	0.44	21.59	9.51	30.45	14.55
	0.13	9.35	1.18	28.45	23.88	0.44	21.65	9.53	30.27	12.29
45°	0.10	9.31	0.93	30.47	24.45	0.44	21.59	9.51	30.45	14.55
	0.13	9.35	1.18	28.45	23.88	0.44	21.65	9.53	30.27	12.29

It was observed that the current was generally constant at 0.44 A at the panel inclination angles of 39° and 45° during the noon hours when the experiments were carried out in outdoor conditions. It has been observed that the voltage varies between 21.5 and 22 V when the panel inclination angle is set to 45°, and between 21.3 and 21.7 when the panel inclination angle is set to 39°. The electrical power was obtained as maximum 9.68 W at 45° inclination angle and 9.59 W at 39° inclination

angle. At the time of the experiments, the average outdoor temperature was measured as 13.42 °C.

Since the maximum electrical power of 9.68 W is obtained in the 25 W panel we use, the efficiency of the panel we use is around 38% as calculated in Equation (5) in outdoor winter conditions.

$$\text{Panel efficiency (\%)} = (100 \times 9.86) / 25 = 38 \quad (5)$$

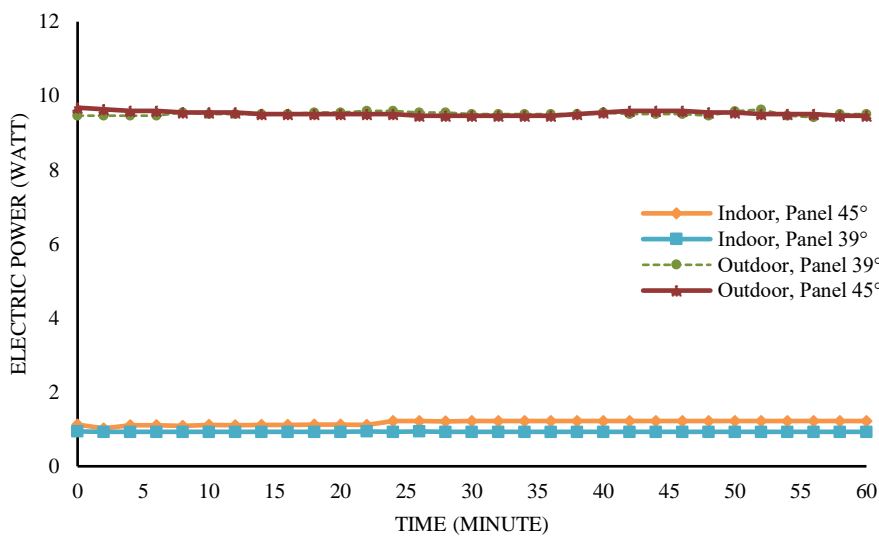


Figure 11. Electricity generation by angle in different conditions.



#### 4. DISCUSSION AND CONCLUSION

In our study, it has been observed that a maximum hourly 1.22 W indoor and 9.68 W outdoor electric power can be obtained from a 25 W monocrystalline panel in the winter in the province of Bingöl at an angle of inclination of 45 °C. It is understood that the best results are obtained for the 45 degree angle in the outdoor environment. The panel surface temperature increased up to 35 °C in the outdoor environment. However, no significant change in electric power was observed.

According to the regulation made in 2018 in our country, it is allowed to install a maximum of 10 kW solar panels on the roof of a house. This means meeting the electricity needs of a house with an average monthly electricity consumption of 1400 kWh and an average daily electricity consumption of 4.6 kWh. According to the cost analyzes made by solar energy installation companies, an average of 24 monocrystalline panels with a power of 455 W should be used to meet this capacity. According to today's conditions, the totality of the panels, other necessary equipment, and installation costs is 206000 TL including KDV [28]. If such a system is off-grid, the payback period will undoubtedly be very long, thus incurring unnecessary expense to the home owner. As it is known, electrical energy cannot be stored and meets the needs of the house as soon as it is produced. However, the electricity produced is given to the grid when the house does not need it. In this respect, if such a system is grid-connected (On Grid), the electricity produced more than the house's needs can be given to the grid, and the repayment period can be reduced to an average of 6 years with the settlement method [28]. This will start the income generation process for the home owner after the first six years, and will make significant contributions to the country's economy, and reduction of emissions.

#### REFERENCES

- [1] Anonymous [Internet]. TEİAŞ 2022 Yılı Aylık Elektrik Üretim-Tüketim Raporları; 2023 [cited 2023 January 23]. Available from: <https://www.teias.gov.tr/aylik-elektrik-uretim-tuketim-raporlari>. Carlson BM. Human embryology and developmental biology. 4th ed. St. Louis: Mosby; 2009.
- [2] Işık, S., Yavuz, S. Investigation of biogas production potential from livestock manure by anaerobic digestion in Bingöl Province. *Türk Doğa ve Fen Dergisi*, 2022;11(1), 116-122.
- [3] Şenpınar, A., Gençoğlu, M. T. Yenilenebilir Enerji Kaynaklarının Çevresel Etkileri Açısından Karşılaştırılması. *Fırat Üniversitesi Doğu Araştırmaları Dergisi*, 2006;4(2), 49-54.
- [4] Koç, E., Kaya, K. Enerji Kaynakları-Yenilenebilir Enerji Durumu. *Mühendis ve Makina*, 2015;56(668), 36-47.
- [5] Pamir, A. N. Dünyada ve Türkiye’de Enerji, Türkiye’nin Enerji Kaynakları ve Enerji Politikaları. *Metalurji Dergisi*, 2003;134(23).

- [6] Yılmaz, M. Türkiye’nin enerji potansiyeli ve yenilenebilir enerji kaynaklarının elektrik enerjisi üretimi açısından önemi. *Ankara Üniversitesi Çevre Bilimleri Dergisi*, 2012;4(2), 33-54.
- [7] Sağlam, M., Uyar, T. S., Göztepe, İ. Dalga enerjisi ve Türkiye’nin dalga enerjisi teknik potansiyeli. *Elektrik Mühendisleri Odası*, 2005;19, 2020.
- [8] Işık, S., Yıldız, C. Improving thermal energy storage efficiency of solar collector tanks by placing phase change materials in novel finned-type cells. *Thermal Science and Engineering Progress*, 2020;19, 100618.
- [9] Midilli, A., Ay, M., Dincer, I., Rosen, M. A. On hydrogen and hydrogen energy strategies: I: current status and needs. *Renewable and sustainable energy reviews*, 2005;9(3), 255-271.
- [10] Abe, J. O., Popoola, A. P. I., Ajenifuja, E., Popoola, O. M. Hydrogen energy, economy and storage: Review and recommendation. *International journal of hydrogen energy*, 2019;44(29), 15072-15086.
- [11] Anonymous [Internet]. T.C. Enerji ve Tabii Kaynaklar Bakanlığı Türkiye güneş enerjisi potansiyeli; 2023 [cited 2023 January 25]. Available from: <https://enerji.gov.tr/bilgi-merkezi-enerji-gunes>, Erişim tarihi: 25.01.2023.
- [12] Anonymous [Internet]. Enerji Atlası; 2023 [cited 2021 January 27]. Available from: <https://www.enerjiatlası.com/sehir/bingol/>, Erişim tarihi : 27.01.2023
- [13] Anonymous [Internet]. AA gündem, Türkiye'nin ilk, Avrupa'nın en büyük hibrit enerji santrali; 2023 [cited 2023 January 27]. Available from: <https://www.aa.com.tr/tr/gundem/turkiyenin-ilk-avrupanın-en-buyuk-hibrit-enerji-santrali-bingol-de-hizmete-girdi/2416097>, Erişim Tarihi: 27.01.2023.
- [14] Anonymous [Internet]. Solhan Belediyesi'nden Güneş Enerjisi Santrali (GES) projesi; 2023 [cited 2023 February 1]. Available from: <https://www.yeniakit.com.tr/haber/solhan-belediyesinden-gunes-enerjisi-santrali-ges-projesi-cevre-dostu-yatirim-1633422.html>
- [15] Keskin, A., Martin, K., Boran, K. Niğde İli Güneş Enerji Santrali Modellemesi ve Performans Parametreleri Değerlendirmesi. In 3rd International Symposium on Innovative Approaches in Scientific Studies, 2019;213-216.
- [16] Atlım, F., Bayram, E., Demirtaş, M. Balıkesir ilinde farklı iki GES tesisinin panel yerleşimi açısından verimliliklerinin karşılaştırılması. *Balıkesir Üniversitesi Fen Bilimleri Enstitüsü Dergisi*, 2019;21(2), 679-696.
- [17] Güven, Ş. Fotovoltaik Panel Yüzey Sıcaklığının Denizli İli için Çıkış Gücü ve Verim Üzerindeki Etkisinin İncelenmesi. *Mühendis ve Makina*, 2022;63(707), 429-442.
- [18] Yıldırım, E., Aktacir, M. A. Çatı üstü PV elektrik üretim potansiyelinin belirlenmesi: Şanlıurfa örneği. *Dicle Üniversitesi Mühendislik Fakültesi Mühendislik Dergisi*, 2021;12(1), 69-77.
- [19] Kabul, A., Duran, F. Isparta ilinde fotovoltaik/termal (PV/T) hibrit sistemin performans

- analizi. *Uluslararası Teknolojik Bilimler Dergisi*, 2014;6(1), 31-43.
- [20] Kerem, A., Atik, M., Bayram, A. Fotovoltaik (PV) panel sisteminde yüzey soğutma işleminin elektrik üretimine etkisinin deneysel incelenmesi. *International Journal of Engineering Research and Development*, 2020;12(2), 565-578.
- [21] Anonymous [Internet]. Wikipedia, Bingöl; 2023 [cited 2023 January 24]. Available from: [https://tr.wikipedia.org/wiki/Bing%C3%B6l\\_\(il\)](https://tr.wikipedia.org/wiki/Bing%C3%B6l_(il)).
- [22] Anonymous [Internet]. GNS solar, Türkiye Güneş Haritası; 2023 [cited 2023 January 25]. Available from: <https://www.gnssolar.com/icerik/860/turkiye-gunes-haritasi> Erişim Tarihi: 25 Ocak 2023
- [23] Anonymous [Internet]. Enerji İşleri Genel Müdürlüğü, Güneş enerjisi potansiyel atlası (GEPA); 2023 [cited 2023 January 25]. Available from: <https://gepa.enerji.gov.tr/MyCalculator/pages/12.aspx>
- [24] Nogueira, C. E. C., Bedin, J., Niedzialkoski, R. K., de Souza, S. N. M., Das Neves, J. C. M. Performance of monocrystalline and polycrystalline solar panels in a water pumping system in Brazil. *Renewable and Sustainable Energy Reviews*, 2015;51, 1610-1616.
- [25] Taşçıoğlu, A., Taşkın, O., Vardar, A. A power case study for monocrystalline and polycrystalline solar panels in Bursa City, Turkey. *International Journal of Photoenergy*, 2016.
- [26] Altaş, İ.H., Fotovoltaik Güneş Pilleri:Yapısal Özellikleri ve Karakteristikleri. Enerji, Elektrik, Elektromekanik-3e, Bileşim yayıncılık A.Ş., İstanbul: 1998;47, 66-71.
- [27] Kutlu, N. Isparta İlinde Bir Evin Elektrik İhtiyacını Karşılacak Panel Sayısı, Verimi ve Ekonomik Analizinin Hesabı. *Yalvaç Akademi Dergisi*, 2016;1(1), 41-52.
- [28] Anonymous [Internet]. Power Enerji GES kurulum mağazası; 2023 [cited 2023 February 1]. Available from: <https://satis.powerenerji.com/cati-uzeri-10-kw-gunes-enerjisi-elektrik-uretimi-maliyeti>

## Investigation of The Effect of Creamed Honey Production Process on The Sugar Profile of Honey

Davut KARAHAN<sup>1\*</sup>, Bayram YURT<sup>2</sup>, Esra ÇAPANOĞLU GÜVEN<sup>3</sup>

<sup>1</sup>Bingöl University, Honey Bee and Natural Products R&D and P&D Center, Bingöl, Türkiye

<sup>2</sup>Bingöl University, Faculty of Engineering and Architecture, Department of Food Engineering, Bingöl, Türkiye

<sup>3</sup>Istanbul Technical University, Faculty of Chemical and Metallurgical Engineering, Department of Food Engineering, Istanbul, Türkiye

Davut KARAHAN ORCID No: 0000-0003-4571-1095

Bayram YURT ORCID No: 0000-0001-5447-1586

Esra ÇAPANOĞLU GÜVEN ORCID No: 0000-0003-0335-9433

\*Corresponding author: [dkarahan@bingol.edu.tr](mailto:dkarahan@bingol.edu.tr)

(Received: 03.12.2022, Accepted: 24.05.2023, Online Publication: 22.06.2023)

### Keywords

Honey,  
Crystallization,  
Creamed  
Honey,  
Sugar Profile,  
HPLC-RID

**Abstract:** Honey is a supersaturated solution with more than 70% sugar and less than 20% water content. Crystallization of supersaturated solutions is expected from a physicochemical point of view. However, since the reasons for the crystallization of honey are not known by the consumers, crystallized honey is generally not liked. Beekeepers and/or marketers of bee products, liquefy crystallized honey by applying high degrees of heat treatment to convert it into the form preferred by consumers. Honey has been used for both healing and nutritional purposes from past to present. Unfortunately, some processes applied to honey, consciously or unconsciously, can make honey harmful for health, although it may lose its healing value. The new product, which is formed as a result of controlled crystallization to improve some sensory and physical characteristics of honey, is called creamed honey. Creamed honey is an alternative product to crystallization and its effects. In this study, creamed honey was produced from filtered honey and the effect of creamed honey production process on the sugar profile of honey was investigated by High Performance Liquid Chromatography- Refractive Index Detection (HPLC-RID) method. In the analyzes made, it was determined that the creamed honey production process did not have a significant effect on the sugar profile of honey ( $p>0.05$ ).

## Krem Bal Üretim Prosesinin Balın Şeker Profili Üzerindeki Etkisinin Araştırılması

### Anahtar

### Kelimeler

Bal,  
Kristalizasyon,  
Krem Bal,  
Şeker Profili,  
HPLC-RID

**Öz:** Balda bulunan baskın bileşikler esas olarak fruktoz ve glukozdan oluşan karbonhidratlardır. Bal % 70'den fazla şeker, % 20'den az su içeriği itibarıyla aşırı doymuş bir çözüldür. Aşırı doymuş çözeltilerin kristalizasyonu, fizikokimyasal açıdan beklenen bir durumdur. Ancak balın kristalleşmesinin sebepleri tüketiciler tarafından bilinmediği için kristalize bal genel olarak beğenilmemektedir. Arı yetiştiricileri ve/veya arı ürünleri pazarlamacıları, kristalize balı tüketicilerin tercih ettiği forma dönüştürmek için yüksek derecelerde ısı işlem uygulayarak sıvılaştırmaktadır. Bal, geçmişten günümüze hem şifa hem de beslenme amacıyla kullanılmaktadır. Ne yazık ki bala bilinçli veya bilinçsiz olarak uygulanan bazı işlemler, balın şifa değerini kaybettirmekle birlikte, balı sağlık için zararlı hale dönüştürebilmektedir. Balın duyu ve fiziksel özelliklerinin geliştirilmesi için yapılan kontrollü kristalizasyon sonucu oluşan yeni ürüne krem bal adı verilmektedir. Krem bal, kristalizasyon olayına ve etkilerine alternatif bir üründür. Bu çalışmada süzme baldan krem bal üretilmiş ve krem bal üretim prosesinin balın şeker profili üzerindeki etkisi HPLC-RID metodu ile incelenmiştir. Yapılan analizlerde krem bal üretim prosesinin, balın şeker profili üzerinde anlamlı bir etki göstermediği ( $p>0,05$ ) tespit edilmiştir.

## 1. INTRODUCTION

Codex Alimentarius [1] defines honey as follows; It is a viscous, naturally crystallable natural sweet product obtained by the honey bee (*Apis mellifera L.*) from the nectar of plants, the secretions of living parts or the secretions of plant-sucking insects living in the living parts of plants, which the bees transform by treating with their own substances, accumulate and leave in the honeycombs for maturation. Honey has been used for both healing and nutritional purposes throughout history. For example, the Ancient Egyptians, Assyrians, Greeks, Romans and Chinese used honey both for nutritional purposes and for the treatment of wounds [2]. Although the structure of honey varies depending on its botanical source, it contains more than 200 bioactive components. Honey is composed of vitamins, minerals, organic acids, flavonoids, phenolic compounds, amino acids, enzymes and other bioactive substances thus, it is not difficult to digest, nutritious and has many biological activities [3].

Due to its geographical location, Türkiye is known as a country rich in biodiversity and ecological differences. This ecological difference and biodiversity can be considered an important factor for other bee products, especially the richness and quality of honey production [4, 5]. In the literature, studies have shown that bioactive components in honey generally have antibacterial, antioxidant, anticarcinogenic, antiviral, antifungal, antitumoral, anti-inflammatory and anti-insecticidal effects. [6, 7]. The main sugars of honey are known as glucose and fructose. In addition, disaccharides such as sucrose, maltose, lactose, and some oligosaccharides are other sugars found in honey, albeit in small amounts. Honey is a supersaturated solution with more than 70% carbohydrates and less than 20% water content.

Crystallization of supersaturated solutions is expected from a physicochemical point of view. Honey is a supersaturated food with glucose molecules, which are usually less soluble than fructose. Therefore glucose tends to crystallize in the monohydrate form at certain temperatures [8, 9]. Honey crystallizes fastest in the temperature range of 10-15°C [8].

The water in honey binds carbohydrates with hydrogen bonds. Fructose gives weak energy to the hydrogen bonds between water molecules, and the water molecules move around them to hydrate the fructose molecules. Crystallization occurs as a result of the release of glucose by water molecules. In other words, crystallization is caused by the change of glucose and fructose ratio in honey due to this instability of fructose [10]. Since honey is a saturated solution in terms of carbohydrates, crystallization under certain conditions is a very natural phenomenon. However, since some consumers do not know exactly what crystallization is, crystallized honey is often not liked. Beekeepers and/or marketers of bee products bring the honey into liquid form and market it by applying a high degree of heat treatment to the crystallized honey in order to meet the preferences of the consumers. Although applying heat treatment to honey seems to improve some physical

properties of honey, it creates various negative effects. The most important of these risks is the increase in the 5-hydroxymethylfurfural (HMF) content of honey. HMF is formed as a result of hexoses losing water molecules at low pH and suitable temperature (usually high temperatures) or Maillard (non-enzymatic browning) reaction. As a result of the reactions in which acids act as catalysts, water is separated from the monosaccharide molecule; furfural pentoses, HMF consists of hexoses [11]. The reaction rate varies depending on pH, water activity ( $a_w$ ), reducing sugar and amino acid content and ambient temperature. It is reported that every approximately 10°C increase in temperature increases the reaction kinetics by approximately four times [12]. The results of studies on the effects of HMF compound on human health show that HMF has mutagenic, genotoxic, cytotoxic and tumor formation effects [13]. Another negative effect of heat treatment applied to honey is that it reduces the activity of enzymes in honey. In honey, high levels of  $\alpha$ -amylase, glucose oxidase,  $\beta$ -amylase  $\alpha$ -glucosidase; low levels of catalase and acid come from bees' pharyngeal secretions, salivary fluids, and nectar source [14]. Diastase enzyme provides hydrolysis of starch. Since the diastase enzyme denatures depending on the storage time and temperature of the honey, it can be considered as a freshness indicator of honey [15]. Unfortunately, some processes applied to honey consciously or unconsciously can have the opposite effect, although they lose the healing value of honey. Controlled crystallization is a good alternative in order to prevent the undesired crystallization phenomenon in honey and the application of heat treatment to honey, which is seen as a solution to improve this phenomenon.

Creamed honey is a new product formed as a result of controlled crystallization made to develop the some sensory and physical characteristics of honey (e.g. giving natural honey a spreadable feature), with crystals in very small sizes that cannot be perceived by the palate. In short, it is the controlled crystallization process to ensure that the honey is spread on the bread like butter and to prevent it from dripping [16]. The chemical content of Creamed honey is almost indistinguishable from the chemical content of raw honey. Creamed honey contains many small crystals that prevent the formation of larger crystals that would normally occur in raw honey. The main difference is physical and sensory differences. Many factors determine the crystal size formed in the product. However, fructose/glucose ratio and storage temperature are reported as the most important among these determining factors [16]. Creamed honey provides various advantages in consumption as it is more spreadable than strained honey. It is expected that the negative factors such as the appearance and dripping of strained honey, which is very important in the balanced diet of people, especially for children in development, disappear with the production of Creamed honey, and it is expected to have a soft taste, spread like butter at normal room temperature, and encourage people to consume honey. It is expected to contribute to the consumption of other bee products (royal jelly, propolis, perga, and pollen) during the production phase of

creamed honey, by mixing them with creamed honey in a homogeneous manner and presenting them to the consumer. In many countries, the Creamed form of honey is more common and preferred than the liquid form [17]. Although the production and consumption of creamed honey is popular in other countries, it is not very common in Türkiye yet. There is a lot of research in the literature investigating honey crystallization, creamed honey production and production optimization.

Karasu et al. (2015) carried out a study on determining the structural changes and thermal stability of creamed honey. For this, they studied the thermal stability of the test at a certain temperature range, that is, its rheological characterization [16]. In another study, different parameters were optimized to produce creamed honey from blossom, canola and honeydew honey [18]. D'arcy (2007) conducted research on the development of an alternative process based on the use of ultrasound technology to the current heating method used in the honey industry to liquefy crystallized honey [15]. Chen et al. (2009) transformed liquid honey into crystallized honey by adding a new nuclei material to give honey good spreadability. Moreover; they carried out a study to test the rheological properties and spreadability of the product they developed [17].

However, did not encounter studies investigating the effect of the creamed honey production process on the sugar profile of honey. It has been shown that in studies, various processes applied to honey caused changes in its physical and chemical properties. It is possible that these changes can also be seen in the Creamed honey production process. Therefore, it is important to detect these changes in the production process of creamed honey, which will be produced from honey with high sugar content. In this study, it was aimed to produce creamed honey and to determine the effect of this production process on the sugar profile of honey by HPLC.

## 2. MATERIAL AND METHOD

### 2.1. Sample

Raw honey sample were obtained from local beekeepers at Bingöl, Türkiye, in 2021. The sample was stored at room temperature to the time of next process.

### 2.2. Chemicals and Reagents

The fructose, glucose, maltose and sucrose standards were of high purity and were obtained from Sigma Aldrich (Darmstadt, Germany). All reagents used were analytical grade, Acetonitrile and methanol were HPLC grade Sigma Aldrich (Darmstadt, Germany).

### 2.3 HPLC System

The HPLC system; an auto sampler, pump, sample loop and a Refractive Index Detector (RID), all from Agilent (Santa Clara, United States).

Analyses were performed on an  $\text{NH}_2$  column (250mm×4.6mm, 5 $\mu\text{m}$  particle size-Zorbax). Data were analyzed using Agilent ChemStation Software (Agilent, Santa Clara, United States). All samples were prepared and injected in triplicate.

### 2.4. Creamed Honey Production Process

Creamed honey production was successfully carried out in the Food Analysis and Research Laboratory in the Food Engineering Department of the Faculty of Engineering and Architecture of Bingöl University-Türkiye. Raw flower honey produced in Bingöl province was used. Creamed honey production was carried out by modifying according to the methods in the literature [18-21]. Room temperature honey was filled into the creamed honey making machine. Then, creamed honey was produced in a creamed honey making machine with a constant mixing speed of 60 rpm, at a temperature of 14°C, and a mixing time and number of 4 minutes and 5 times, respectively, by adding 10% of the creamed honey purchased from a local company to act as a seed crystal. Figure 1 shows the creamed honey produced in our laboratory.



Figure 1. Creamed honey produced in our laboratory

### 2.5. Honey Sugar Profile Analysis by HPLC

For sugar profile analysis of honey, both raw honey and creamed honey samples were analysed according to the Turkish Standardization Institute method [22]. Standard solutions of glucose, fructose, sucrose, maltose at different concentrations were prepared for calibration. After the prepared standard solutions were transferred to vials, they were read in the HPLC device. The calibration curve was drawn by peak areas obtained from the read standard solutions were drawn with Agilent ChemStation Software. 5 g honey was weighed with 0.001 g precision and dissolved in approximately 40 mL ultrapure water. Then, 25 mL of methanol was added to it, and it was taken into a metered balloon and the volume was adjusted to 100 mL with adding ultrapure water. Approximately 1.5 mL of this solution was transferred to the HPLC vials with a sterile disposable syringe and a 0.45  $\mu\text{m}$  syringe filter. Then analyzed by the HPLC device. Sugar concentrations were calculated as % by using the formulas in the obtained peak area

calibration curves. An example of a chromatogram of the sugar standards solution is shown in Figure 2. During HPLC analysis ultrapure water: acetonitrile (20:80, v/v) mixture was the mobile phase, flow rate 1.3 mL/min, injection volume 10  $\mu$ L, and detection temperature 30°C.

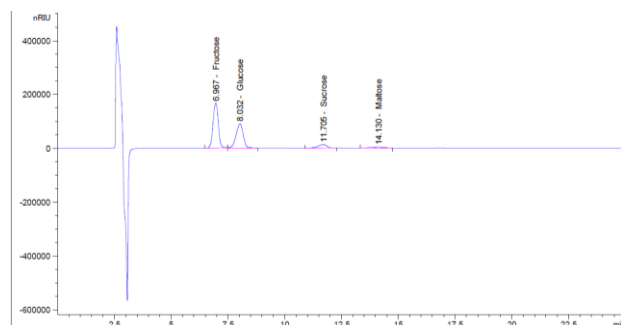


Figure 2. Chromatogram of the sugar standards solution

## 2.6. Statistical Analysis

In order to examine the effect of the creamed honey production process on the sugar profile of honey, the differences between them were analysed with the Mann-Whitney U Test, which is a non-parametric test in the IBM SPSS Statistics (Chicago, USA) program.

## 3. RESULTS and DISCUSSION

Sugar profile analysis is one of the important parameters like other parameters used to determine the quality of honey. Generally, the amount of fructose contained in honey is higher than glucose. The fructose content of honey is about 38-40%, and the glucose content is around 30-32%. However, this ratio may vary depending on storage time and temperature, as well as other factors such as the nectar source.

Fructose (F), glucose (G), sucrose, maltose, fructose/glucose (F/G) and fructose+glucose (F+G) results of raw honey and creamed honey samples are given in Table 1 and Table 2 respectively.

Table 1. Sugar amount of raw honey

Parameters	Descriptive Statistics			
	Minimum	Maximum	Mean	Std. Deviation
Fructose	39.998	40.322	40.171	0.164
Glucose	33.790	33.864	33.819	0.039
Sucrose	0.040	0.041	0.040	0.000
Maltose	1.460	1.486	1.472	0.013
F/G	1.184	1.191	1.188	0.004
F+G	73.787	74.186	73.990	0.200

The fructose amount of raw honey used in making creamed honey is between 39.998-40.322  $100\text{g}^{-1}$  and the average is 40.171  $100\text{g}^{-1}$ . The amount of glucose is between 33.790-33.864  $100\text{g}^{-1}$  and the average is 33.819  $100\text{g}^{-1}$ . This is expected because in general, the fructose ratio of honey is higher than glucose. The fructose content of honey is about 38-40%, and the glucose content is around 30-32% [23]. The lowest amount of sucrose is 0.040  $100\text{g}^{-1}$ , the highest amount is 0.041  $100\text{g}^{-1}$ , and the average is 0.040  $100\text{g}^{-1}$ . The amount of maltose is between 1.460-1.486  $100\text{g}^{-1}$  and on

average 1.472  $100\text{g}^{-1}$ . The average of F/G and F+G is 1.188  $100\text{g}^{-1}$  and 73.990  $100\text{g}^{-1}$ , respectively.

Table 2. Sugar amount of creamed honey

Parameters	Descriptive Statistics			
	Minimum	Maximum	Mean	Std. Deviation
Fructose	39.579	39.616	39.599	0.019
Glucose	33.659	33.701	33.686	0.024
Sucrose	0.030	0.037	0.033	0.004
Maltose	1.042	1.052	1.048	0.005
F/G	1.175	1.176	1.176	0.000
F+G	73.238	73.317	73.285	0.042

The fructose amount of creamed honey is between 39.579-39.616  $100\text{g}^{-1}$  and the average is 39.599  $100\text{g}^{-1}$ . The amount of glucose is between 33.659-33.701  $100\text{g}^{-1}$  and the average is 33.686  $100\text{g}^{-1}$ . This is expected because in general, the fructose ratio of honey is higher than glucose. The lowest amount of sucrose is 0.030  $100\text{g}^{-1}$ , the highest amount is 0.037  $100\text{g}^{-1}$ , and the average is 0.033  $100\text{g}^{-1}$ . Sucrose is generally present in honey in low amounts, ideally no more than 5%. Because pure honey contains a low amount of sucrose due to the presence of the enzyme invertase, which breaks down sucrose. For this reason, the high rate of sucrose in honey may raise suspicion of adulteration [24]. The amount of maltose is between 1.042-1.052  $100\text{g}^{-1}$  and on average 1.048  $100\text{g}^{-1}$ . The average of F/G and F+G is 1.176  $100\text{g}^{-1}$  and 73.285  $100\text{g}^{-1}$ , respectively. According to the obtained analysis results, fructose and glucose are present in all honey samples. Moreover; as expected in natural honey, the amount of fructose was found to be higher than the amount of glucose in all samples [23].

According to the Turkish Food Codex [25], the limits that honey should carry are shown in Table 3.

Table 3. Turkish Food Codex limits of sugar in honey

Parameters	Limits
Humidity (% , Max.)	% 20
Sucrose (Max.)	5 $100\text{g}^{-1}$
Fructose+ Glucose (Min.)	60 $100\text{g}^{-1}$
Fructose / Glucose	0.9 – 1.4
Maltose (% , Max.)	4

All sugar parameters of both the raw honey used and the creamed honey are in compliance with the Turkish Food Codex limits.

The sugar results found in a study [16] on the determination of the rheological properties of creamed honey are in a similar range with the results of our study. Kamal et al. [26] conducted a study on the determination of sugars in honey by liquid chromatography. The findings of our study are in the range of the findings of their study. Alghamdi et al. [23] determined the sugar composition in honey samples collected from Saudi Arabian markets using HPLC technique. The results they found are very close to the results of our study.

The results found in the study [24] on the determination of the physical and chemical properties of different honey samples are similar to the results we found. The differences between the findings were analysed with the Mann-Whitney U Test, which is a non-parametric

test in the SPSS (IBM, Chicago, USA) program. As a result of the analysis, it was observed that the creamed honey production process did not affect the sugar profile of the raw honey used in production significantly ( $p>0.05$ ). The reason for this is that, as mentioned above, the creamed honey production process is not a chemical process, but a physical process.

#### 4. CONCLUSION

In general, honey can be consumed directly for healing purposes as well as being used as a food supplement. With the recent studies, honey processing processes are developed and new functional products are tried to be produced. Creamed honey has an important place among these new products. Sugar content is very important in the selection of honey to be creamed. Because the sugar content is directly effective in the controlled crystallization of natural honey, which also affects the creamed honey production process. Therefore, determining the sugar profile of honey is of great importance for the honey industry in terms of both quality parameter and processing. The study in question is an original study to determine the effect of the Creamed honey production process on the sugar profile of honey. It is expected that the results of creamed honey production process does not affect the sugar profile, which is one of the important quality parameters of honey will contribute to both the food industry and the literature. Moreover; it is expected that will contribute to breaking the prejudices and drawbacks of both consumers and the industry against creamed honey.

#### Acknowledgement

The authors are greatly thankful to Bingöl University "Pilot University Coordination Central Unit" and "Bee and Natural Products R&D and Product Development Application and Research Center" for analyses support.

#### REFERENCES

- [1] Codex Alimentarius [Internet]. Codex Standard for Honey; 1987. Available from: <https://www.fao.org/3/w0076e/w0076e30.htm> [cited 2022 Oct 28].
- [2] Zumla A, Lulat A. Honey - a remedy rediscovered. *Journal of the Royal Society of Medicine*. 1989; (82):384-385.
- [3] Mutlu C, Erbaş M, Arslan Tontul, S. Bal ve diğer arı ürünlerinin bazı özellikleri ve insan sağlığı üzerine etkileri. *Akademik Gıda*. 2017; 15(1):75-75.
- [4] Silici S. Honeybee products and apitherapy. *Turkish Journal of Agriculture-Food Science and Technology*. 2019; 7(9):1249-1262.
- [5] Terrab A, Dı ez MJ, Heredia FJ. Characterisation of Moroccan unifloral honeys by their physicochemical characteristics. *Food chemistry*. 2002; 79(3):373-379.
- [6] Bakkali F, Averbeck S, Averbeck D, Idaomar M. Biological effects of essential oils- a Review. *Food and Chemical Toxicology*. 2008;46:446-475.
- [7] Balouiri M, Sadiki M, Ibensouda SK. Methods for in vitro evaluating antimicrobial activity: A review. *Journal of pharmaceutical analysis*. 2016; 6(2):71-79.
- [8] Conforti PA, Lupano CE, Malacalza NH, Arias V, Castells CB. Crystallization of honey at  $-20^{\circ}\text{C}$ . *International Journal of Food Properties*. 2006; 9(1): 99-107.
- [9] Anand S, Pang E, Livanos G, Mantri N. Characterization of physico-chemical properties and antioxidant capacities of bioactive honey produced from Australian grown *Agastache rugosa* and its correlation with colour and poly-phenol content. *Molecules*. 2018; 23(1):108.
- [10] Belitz HD, Grosch W. *Food Chemistry*. 2nd ed. Berlin Heidelberg: Springer-Verlag; 1999. P. 821-828.
- [11] Burdurlu HS, Karadeniz F. Gıdalarda maillard reaksiyonu. *Gıda*. 2002; 27 (2):77-82.
- [12] Durling L. JK. Busk L. Hellman BE. Evaluation of the DNA damaging effect of the heat induced food toxicant 5-hydroxymethylfurfural (HMF) in various cell lines with different activities of sulfotransferases. *Food and Chemical Toxicology*. 2009; 45:880-884.
- [13] Carabasa Giribet M. Ibarz-Ribas A. Kinetics of colour development in aqueous glucose systems at high temperatures. *Journal of food Engineering*. 2000; 44:181-189.
- [14] D'arcy B [Internet]. High-Power Ultrasound to Control of Honey Crystallisation. Rural Industries Research and Development Corporation, Australian Government; 2022. [cited 2022 Oct 20].
- [15] Karasu S, Toker ÖS, Yılmaz MT, Karaman S, Dertli E. Thermal loop test to determine structural changes and thermal stability of creamed honey: Rheological characterization. *Journal of Food Engineering*. 2015; 150:90-98.
- [16] Chen YW, Lin CH, Wu FY, Chen HH. Rheological properties of crystallized honey prepared by a new type of nuclei. *J. Food Process Eng*. 2009; 32: 512-527.
- [17] Mortaş M. Krem bal üretim parametrelerinin optimizasyonu [dissertation]. Samsun: Ondokuz Mayıs Üniversitesi; 2016.
- [18] Sunay AE, Basdogan G, Boyacıoğlu D, Suzme S. Mixing time affects consumer acceptance of creamed honey. 4th International Congress on Food and Nutrition 2011. Singapore.
- [19] Abd Elhamid Abeer M, Hossam F Abou-Shaara. Producing clover and cotton creamed honey under cooling conditions and potential use as feeding to honey bee colonies. *Journal of Apiculture*. 2016; 31(1): 59-64.
- [20] Sereti V, Lazaridou A, Tananaki C, Biliaderis CG. Development of a cotton honey-based spread by controlling compositional and processing parameters. *Food Biophysics*. 2021; 16(3): 365-380.
- [21] Türk Standardları Enstitüsü [Internet]. TS 13359 Bal-Fruktoz, glukoz, sakaroz, turanoz ve maltoz muhtevası tayini - Yüksek performanslı sıvı kromatografisi (hplc) metodu; 2008

Available from: <https://intweb.tse.org.tr/standard/standard/Standard.aspx?081118051115108051104119110104055047105102120088111043113104073097106122089121097102053048082055> [cited 2022 Oct 30].

- [22] Alghamdi BA, Alshumrani ES, Saeed MSB, Rawas GM, Alharthi NT, Baeshen MN, et al. Analysis of sugar composition and pesticides using HPLC and GC-MS techniques in honey samples collected from Saudi Arabian markets. *Saudi Journal of Biological Sciences*. 2020; 27(12):3720-3726.
- [23] Aljohar HI, Maher HM, Albaqami J, Al-Mehaizie M, Orfali R, Orfali R, Alrubia S. Physical and chemical screening of honey samples available in the Saudi market: An important aspect in the authentication process and quality assessment. *Saudi Pharmaceut. J*. 2018; 26: 932-942.
- [24] T.C. Tarım ve Orman Bakanlığı [Internet]. Türk Gıda Kodeksi Bal Tebliği; 2020 [cited 2022 Oct 28].
- [25] Chen YW, Lin CH, Wu FY, Chen HH. Rheological properties of crystallized honey prepared by a new type of nuclei. *J. Food Process Eng*. 2009; 32: 512-527.
- [26] Kamal Mohammad A, Klein Peter. Determination of sugars in honey by liquid chromatography. *Saudi journal of biological sciences*. 2011; 18(1): 17-21.



## The Effects of Water/Cement Ratio and Cement Dosage Variables on the Performance of Shotcrete: Compressive Strength and Drying Shrinkage Perspective

Hasan POLAT<sup>1\*</sup> , Cengiz ÖZEL<sup>2</sup> 

<sup>1</sup> Bingöl University, Vocational School of Technical Sciences, Department of Architecture and Urban Planning, 12000, Bingöl, Turkey

<sup>2</sup> Isparta University of Applied Sciences, Faculty of Technology, Department of Civil Engineering, 32260, Isparta, Turkey

Hasan POLAT ORCID No: 0000-0003-1521-0695

Cengiz ÖZEL ORCID No: 0000-0002-2715-1680

\*Corresponding author: [hpolat@bingol.edu.tr](mailto:hpolat@bingol.edu.tr)

(Received: 02.05.2023, Accepted: 02.06.2023, Online Publication: 22.06.2023)

### Keywords

Shotcrete,  
Cement  
dosage,  
Water/cement  
ratio,  
Compressive  
strength,  
Drying shrinkage

**Abstract:** Shotcrete is a construction material that is applied by spraying under high pressure, and there are many factors that affect its properties. In this study, the effect of cement dosage and water-to-cement ratio on the compressive strength and drying shrinkage performance of shotcrete was investigated. For this purpose, shotcrete specimens were produced using three different water-to-cement ratios (0.40, 0.45, 0.50) and three different cement dosages (400 dsg, 450 dsg, 500 dsg). The unit weight, ultrasonic pulse velocity (UPV), compressive strength, splitting tensile strength, and drying shrinkage performance of the produced specimens were examined. As a result of the experimental studies, an increase in cement dosage resulted in an increase in unit weight values, with the amount of increase ranging from approximately 1% to 3%. When the UPV value was examined, an increase in cement dosage resulted in an increase in UPV values, with an increase of approximately 1% to 5%. An increase in cement dosage also resulted in an increase in compressive strength and splitting tensile strength values, with the increase ranging from approximately 12%-16%, 5%-9%, and 10%-12% for the 500, 450, and 400 dosage groups, respectively. The drying shrinkage values increased with increasing cement dosage, the highest shrinkage values occurred in the groups with 0.50 water/cement ratio and 500 dosage, and it was observed that 85-95% of the total shrinkage of the shotcrete specimens was completed within the first 1 hour. Furthermore, the data obtained can be used to determine the optimum water/cement ratio and cement dosage for the construction of shotcrete.

## Püskürtme Betonlarında Su/Çimento Oranı ve Çimento Dozajı Değişkenlerinin Performansa Etkileri: Basınç Dayanımı ve Kuruma Rötresi Perspektifi

### Anahtar Kelimeler

Püskürtme  
beton,  
Çimento dozajı,  
Su/çimento  
oranı,  
Basınç dayanımı,  
Kuruma rötresi

**Öz:** Püskürtme beton, yüksek basınç altında püskürtülerek uygulanan bir yapı malzemesidir ve özelliklerini etkileyen birçok faktör vardır. Yapılan bu çalışmada püskürtme betonda kullanılan çimento dozajının ve su/çimento oranının basınç dayanımı ve kuruma rötresi performansına etkisini incelenmiştir. Bu amaç kapsamında üç farklı su/çimento oranı (0.40, 0.45, 0.50) ve üç farklı çimento dozajı (400 dzj, 450 dzj, 500 dzj) kullanılarak püskürtme beton numuneleri üretilmiştir. Üretilen numuneler üzerinde birim hacim ağırlık, ultrases geçiş hızı (UPV), basınç dayanımı, yarmada çekme ve kuruma rötresi performansları incelenmiştir. Deneysel çalışmalar sonucunda, çimento dozajının artmasıyla birim hacim ağırlık değerlerinde artış meydana gelmiş olup meydana gelen artış miktarı yaklaşık olarak %1 ve %3 arasında değişmektedir. UPV değeri incelendiğinde ise, çimento dozajının artmasıyla UPV değerlerinde yaklaşık olarak %1 ve %5 değerlerinde artış elde edilmiştir. Basınç dayanımı ve yarmada çekme dayanımı değerlerinde de çimento dozajının artmasıyla artış meydana gelmiş olup, artış miktarı 500 dzj, 450 dzj ve 400 dzj için sırasıyla yaklaşık %12-16, %5-9 ve %10-12 arasında meydana gelmiştir. Çimento dozajının

artmasıyla kuruma rötresi değerlerinde artış meydana gelmiş olup, en yüksek rötre değerleri 0.50 su/çimento oranı ve 500 dozlu gruplarda meydana geldiği, püskürtme beton numunelerinin toplam büzülmesinin %85-95'inin ilk 1 saat içerisinde tamamlandığı gözlemlenmiştir. Ayrıca, elde edilen veriler, püskürtme betonunun yapılandırılması için optimum su/çimento oranı ve çimento dozajını belirlemek için kullanılabilir.

## 1. INTRODUCTION

Shotcrete is a construction technique used in underground construction worldwide due to its technical and economic advantages over conventional concrete [1-2]. Today, shotcrete is widely used in construction, mining and tunnel construction [3-4-5-6]. Since the introduction of shotcrete, great progress has been made in terms of improving the performance of materials, mix ratio, and concrete and dust control of the spraying process [7-8-9]. While shotcrete technology has recently made great progress in terms of equipment, ease of use and capacity, many basic principles remain unchanged [10]. The main components that affect the rheological properties of fresh concrete include: (1) binder formulations, including the type and content of chemical and mineral additives; (2) type, shape and gradation of aggregates; (3) water-cement ratio (w/c); and (4) are the properties of cement materials. Even similar mixtures can show quite different flow properties with small changes in these components [11]. Main components of shotcrete (1) properties and dosage of cement; (2) type, shape and gradation of aggregates; (3) water/cement (w/c) ratio and (4) type and content of chemical and mineral additives [12].

In this study, the effects of cement dosage and water/cement ratio, which are important main components affecting shotcrete properties, were investigated. The main objective of the study was to determine the mechanical properties and drying shrinkage characteristics of shotcrete produced using three different water/cement ratios (0.40, 0.45, 0.50) and three different cement dosages (400, 450, 500) considering the water/cement ratio and cement dosage limits specified in EFNARC standard.

## 2. MATERIAL AND METHOD

### 2.1. Materials

#### 2.1.1. Cement

In the production of concrete mixtures, CEM I 42.5R Portland cement which conforms to the ASTM C 150 [13] and EN 197-1 [14] standard, was used for all concrete mixtures as a binder. Portland cement has the specific surface area and specific gravity of 4130 cm<sup>2</sup>/g and 3.13 respectively. Characteristic properties of Portland cement are tabulated in Table 1.

**Table-1.** Physical and chemical properties of cement (CEM I 42,5 R)

Chemical Composition (%)		Physical Properties of Cement	
SiO <sub>2</sub> (%)	19,16	Specific Gravity (g/cm <sup>3</sup> )	3,13
Al <sub>2</sub> O <sub>3</sub> (%)	4,87	Bleine (cm <sup>2</sup> /G)	4130
Fe <sub>2</sub> O <sub>3</sub> (%)	3,76	Fineness (μ)	2,8
CaO (%)	63,03	İnitial Setting min	125
MgO (%)	1,65	Final Setting min.	210
SO <sub>3</sub> (%)	3,26	Le Chatelier min.	1
K <sub>2</sub> O (%)	0,58	Compressive Strength (N/mm <sup>2</sup> )	
Na <sub>2</sub> O (%)	0,17	2 days	28,1
Cl (%)	0,0102	7 days	40,4
loss on ignition	3,43	28 days	54,2
Insoluble residue	0,61		

#### 2.1.2. Chemical Additives

Alkali containing, setting accelerator additive was used in the study. The setting accelerator additive was obtained from AKKİM Kimya A.Ş. and its properties are given in Table 2.

**Table 2.** Properties of Chemical Additives

COD	Solids content (%)	Density (gr/cm <sup>3</sup> )	pH	Chloride Content	Alkali Amount (Na <sub>2</sub> O equivalent, %)
AK SHOT 150	35	1,47	13,0	<0,1	<25

#### 2.2.3. Aggregates

In the study, crushed stone aggregate with a size between 0-7 mm was used and sieve analysis of the aggregates to be used was performed. As a result of the sieve analysis, granulometry curves of crushed stone aggregate were drawn and shown in Figure 1. The curve boundaries are based on EFNARC (1996) [15] limit values for shotcrete.

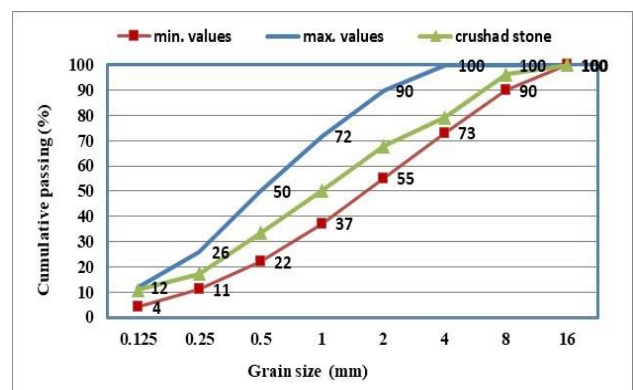


**Figure 1.** Granuometry curve of crushed stone aggregate

## 2.2 Methods

### 2.2.1. Production of mixtures

In this study, shotcrete specimens were produced to investigate the effect of water/cement ratio and cement dosage on the compressive strength and drying shrinkage performance of wet mix shotcrete. Three different water/cement ratios (0.40, 0.45, 0.50) and three different cement dosages (400, 450, 500) were used during the production of the specimens, considering the water/cement ratio and cement dosage limits specified in the EFNARC standard. The amount of setting accelerator admixture used in shotcrete production was kept constant at 4% by weight of cement. The mixture ratios used in shotcrete are given in Figure 2.

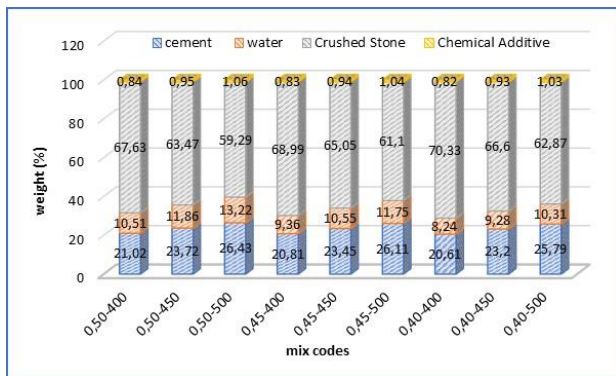


Figure 2. Shotcrete mixing ratios (%)

During the spraying process, 45x45x10 cm wooden molds placed at a 45o angle were used. After the spraying process was completed, the molds were kept for 24 hours and then the concrete blocks were cured for seven days under suitable conditions. After the curing process was completed, 10x10 cm core samples were produced from the concrete blocks and 4x4x16 cm rectangular samples were produced during the spraying process to determine the drying shrinkage performance. Shotcrete production stages are given in Figure 3.

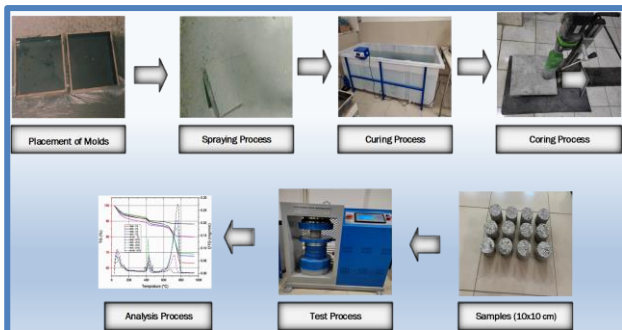


Figure 3. Shotcrete production stages

## 3. RESEARCH FINDINGS

Unit volume weight, ultrasonic transmission rate, compressive strength and tensile strength at splitting properties of the

specimens produced as a result of the study were analyzed. The data obtained are given below.

### 3.1. Density and UPV values

The unit weight test was performed according to TS EN 1015- 10 (2001) [16] The ultrasound transmission rate test was determined according to ASTM C 597, (1997) [17]. Test results are given in Table 4.

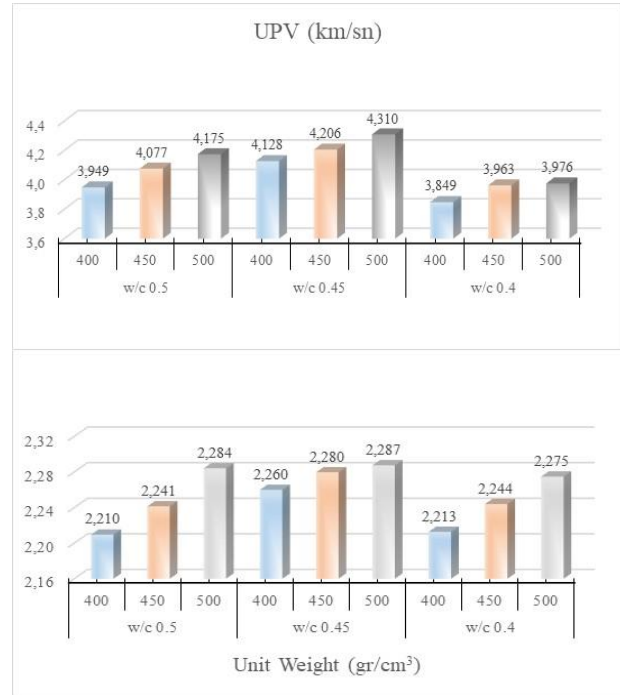


Figure 4. UPV and Unit weight values

When the unit volume weight values were analyzed, no significant change was observed in the unit volume weight values with increasing water/cement ratio. However, there was an increase in the unit weight values with the increase in cement dosage. The amount of increase varies between approximately 1% and 3%. When the UPV value was analyzed, UPV values increased by approximately 1% and 5% with increasing cement dosage, while compressive strength values decreased with increasing water/cement ratio. The lowest values were obtained from the specimens produced at a water/cement ratio of 0.40 and were due to the workability problem that occurred during placement.

### 3.2. Compressive strength values

The compressive strengths of the produced shotcrete concrete groups have been determined according to TS EN 12390-3 (2010) [18], and the compressive strength values are given in Figure 5. When the compressive strength values given in Figure 5 are analyzed, compressive strength values increased with the increase in cement dosage in all groups. The amount of increase was between 12%-16%, 5%-9% and 10%-12% for 500

dsg, 450 dsg and 400 dsg, respectively. Although compressive strength values increased up to a certain point with decreasing water/cement ratio, compressive strength values decreased due to the decrease in workability at 0.40 water/cement ratio. When all groups were analyzed, the highest values were obtained from the 0.45 water/cement group. The relationship between water/cement ratio and compressive strength is given in Figure 6. When the relationship is analyzed, the highest coefficient of determination ( $R^2=0,9786$ ) was obtained from 0.45 water/cement ratio.

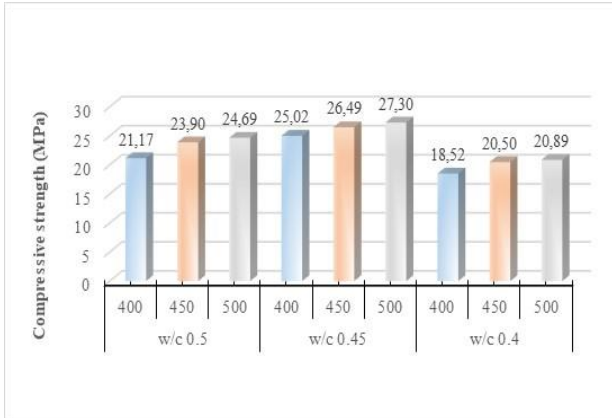


Figure 5. Compressive Strength Values (MPa)

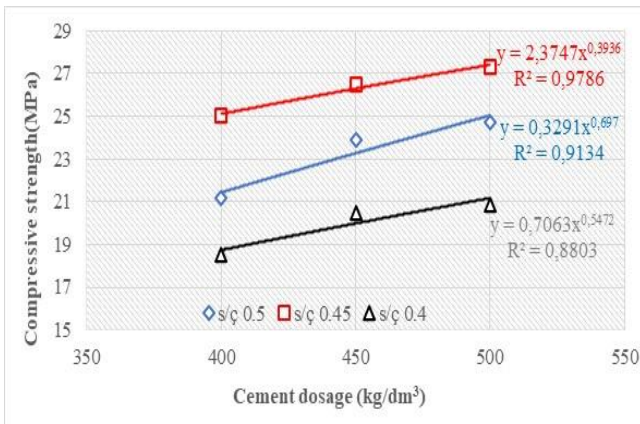


Figure 6. Compressive Strength and cement dosage relationship (MPa)

### 3.3. Splitting tensile strenght values

The splitting tensile strength of the shotcrete groups was determined according to TS EN 12390 -6 (2010) [19] and the splitting tensile strength values are given in Figure 7. When the splitting tensile strength values are examined, it is observed that it shows a similar behavior to the compressive strength. The tensile strength values increased with the increase in cement dosage.

The highest values in all groups were obtained from shotcrete groups where 0.45 water/cement ratio was used, similar to the compressive strength. The relationship between the tensile strength at splitting and the increasing cement dosage ratio for each increasing water/cement

ratio is given in Figure 8. When the relationship is analyzed, the highest coefficient of determination ( $R^2=0,999$ ) was obtained for the increasing cement dosage of 0.45 water/cement ratio.

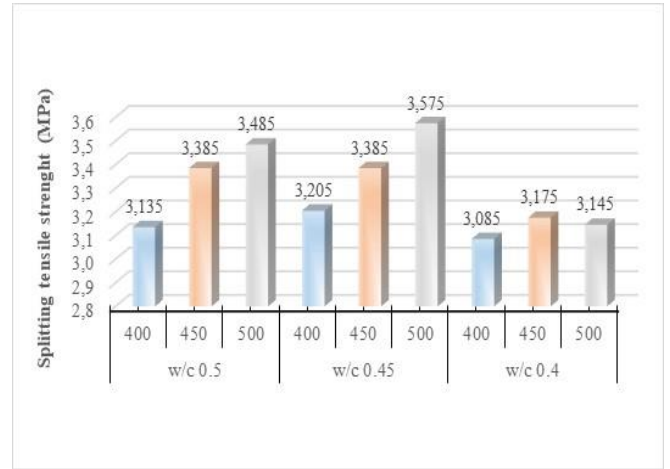


Figure 7. Splitting Tensile Strength Values (MPa)

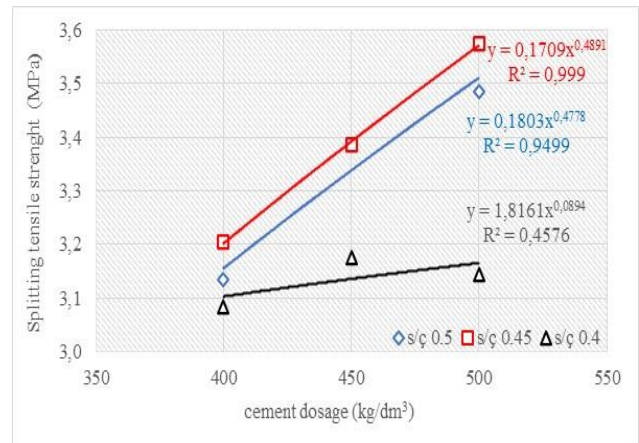


Figure 8. Splitting Tensile Strength Values (MPa)

### 3.4. Drying shrinkage values

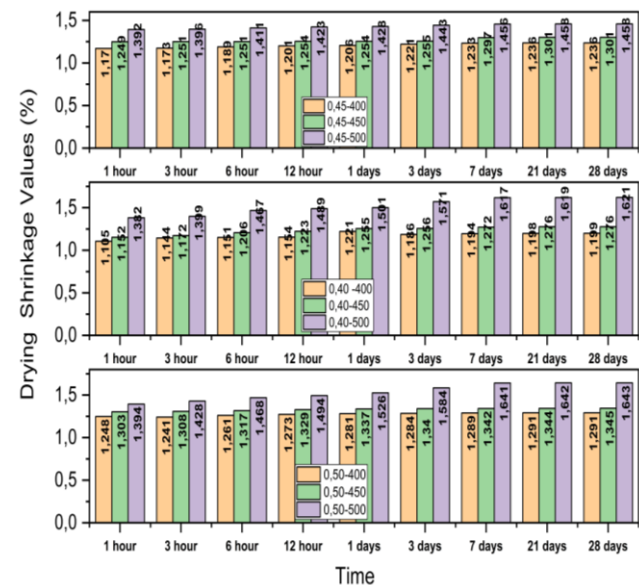


Figure 9. Drying Shrinkage Values

When the drying shrinkage performance values given in Figure 7 are analyzed, it is observed that the drying shrinkage values increased with the increase in curing time during the three-day curing period, while they remained approximately constant for the other curing periods. The shrinkage values increased with increasing water/cement ratio and cement dosage, and the highest shrinkage values were observed in the groups with 0.50 water/cement ratio and 500 dosage. It was observed that 85-95% of the total shrinkage of the shotcrete samples, whose drying shrinkage time-dependent percentage changes are given in Figure 10, was completed in the first 1 hour.

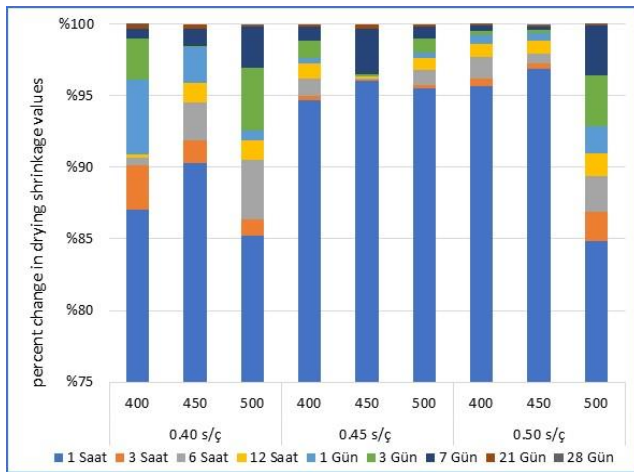


Figure 10. Percent change in drying shrinkage

#### 4. RESULTS

In this study, the effect of cement dosage and water/cement ratio used with shotcrete on compressive strength and drying shrinkage performance was investigated. The results obtained as a result of the above investigations are listed below.

Unit volume weight values increased with increasing cement dosage. The amount of increase varies between approximately 1% and 3%. The UPV values increased by approximately 1% and 5% with increasing cement dosage, while the compressive strength values decreased with increasing water/cement ratio.

Although there was an increase in compressive strength values up to a certain point with the decrease in water/cement ratio, compressive strength values decreased due to the decrease in workability at 0.40 water/cement ratio. When all groups were analyzed, the highest values were obtained from 0.45 water/cement groups.

The values of splitting tensile strength increased with the increase in cement dosage. When all groups were analyzed, the highest values were obtained from the shotcrete groups where 0.45 water/cement ratio was used, similar to the compressive strength.

The shrinkage values increased with increasing water/cement ratio and cement dosage, and the highest shrinkage values were observed in the groups with 0.50 water/cement ratio and 500 dosage. When the drying shrinkage percentage changes were analyzed, it was observed that the shotcrete samples completed 85-95% of the total shrinkage in the first 1 hour.

Furthermore, the data obtained can be used to determine the optimum water/cement ratio and cement dosage for the construction of shotcrete. The results of this study can help to make shotcrete more reliable and durable.

#### REFERENCES

- [1] Salvador, R. P., Cavalaro, S. H., Segura, I., Figueiredo, A. D., & Pérez, J. Early age hydration of cement pastes with alkaline and alkali-free accelerators for sprayed concrete. *Construction and Building Materials*, 2016; 111, 386-398.
- [2] Jolin, M., Beaupre, D. Understanding wet-mix shotcrete: mix design, specifications, and placement. *Shotcrete*, 2013; 1, 6-12.
- [3] Cengiz, O., Turanlı, L. Comparative evaluation of steel mesh, steel fiber and high-performance polypropylene fiber reinforced shotcrete in panel test. *Cement and concrete research*, 2004; 34(8), 1357-1364.
- [4] Franzen, T., Garshol, K. F., Tomisawa, N. Sprayed concrete for final linings: ITA working 4. group report. *Tunnelling and Underground Space Technology incorporating Trenchless Technology Research*, 2001; 4(16), 295-309.
- [5] Melbye, T. A., Dimmock, R. H. Modern advances and applications of sprayed concrete. *Shotcrete: Engineering Developments*, 2020; 7-29.
- [6] Wyatt, C. L., Prival'skiĭ, V. E., Datla, R. U. Recommended practice; symbols, terms, units and uncertainty analysis for radiometric sensor calibration. *US Department of Commerce*, 1998.
- [7] Chen, L., Liu, G. Airflow-dust migration law and control technology under the simultaneous operations of shotcreting and drilling in roadways. *Arabian Journal for Science and Engineering*, 2019; 44, 4961-4969.
- [8] Chen, L., Li, P., Liu, G., Cheng, W., & Liu, Z. Development of cement dust suppression technology during shotcrete in mine of China-A review. *Journal of Loss Prevention in the Process Industries*, 2018; 55, 232-242.
- [9] Zhou, W., Nie, W., Liu, C., Liu, Q., Hetang, W., Wei, C., Xu, C. Modelling of ventilation and dust control effects during tunnel construction. *International Journal of Mechanical Sciences*, 2019; 160, 358-371.
- [10] Nie, W., Liu, Y., Wang, H., Wei, W., Peng, H., Cai, P., Jin, H. The development and testing of a novel external-spraying injection dedusting device for the heading machine in a fully-mechanized excavation face. *Process Safety and Environmental Protection*, 2017; 109, 716-731.
- [11] Çakıroğlu, M. A., Kaplan, A. N., Süzen, A. A. Experimental and DBN-Based neural network

extraction of radiation attenuation coefficient of dry mixture shotcrete produced using different additives. *Radiation Physics and Chemistry*, 2021; 188, 109636.

- [12] Türkmen, İ. I. M., Gül, R., Çel [idot] k, C., Dem [idot] rboğa, R. Determination by the Taguchi method of optimum conditions for mechanical properties of high strength concrete with admixtures of silica fume and blast furnace slag. *Civil Engineering and Environmental Systems*, 2003; 20(2), 105-118.
- [13] ASTM C 150-07, "Standard Specification for Portland Cement," Annual Book of ASTM Standards, Vol. 4.01, ASTM International, 2009.
- [14] EN, TS, 197-1, "Çimento-Bölüm 1: Genel çimentolar-Bileşim, özellikler ve uygunluk kriterleri". Türk Standartları Enstitüsü, 2002, Ankara.
- [15] EFNARC, European Specification for Sprayed Concrete, UK, 1996.
- [16] EN, TS. "1015-10. Kâgir harcı-Deney metotları-Bölüm 10: Sertleşmiş harcın boşluklu kuru birim hacim kütesinin tayini." TSE, Ankara, 2001.
- [17] ASTM C 597. Standard Test Method for Pulse Velocity through Concrete. Annual Book of ASTM Standards, Pennsylvania. 1979; USA.
- [18] TS EN 12390-3. Sertleşmiş Beton Deneyleri Bölüm 3: Deney Numunelerinin Basınç Dayanımını Tayini. Türk Standartları Enstitüsü. 2010; Ankara.
- [19] TS EN 12390-6. Testing hardened concrete- Part 6: Tensile splitting strength of test specimens. Turkish Standards Institution, 2010; Ankara.

## Rough Groups Over Rough Sets

Ramazan YAŞAR<sup>1\*</sup> 

<sup>1</sup> Hacettepe University, Hacettepe-ASO 1.OSB Vocational School, Sincan, Ankara, Türkiye  
Ramazan YAŞAR ORCID No: 0000-0001-6775-1069

\*Corresponding author: [ryasar@hacettepe.edu.tr](mailto:ryasar@hacettepe.edu.tr)

(Received: 30.01.2023, Accepted: 02.02.2023, Online Publication: 22.06.2023)

### Keywords

Rough Set,  
Approximation  
Space,  
Rough Group,  
Rough  
Subgroup

**Abstract:** In this paper, the author focuses on the algebraic structure of the rough groups, especially those based on the rough sets. The author proposes a new definition of the rough group, based on Pawlak's rough sets. This new definition addresses some shortcomings of previous definitions. The author then provides a detailed description of the structure of the rough groups.

## Rough Kümeler Üzerinde Rough Gruplar

### Anahtar

### Kelimeler

Rough Set,  
Approximation  
Space,  
Rough Group,  
Rough  
Subgroup

**Öz:** Bu makalede yazar, kaba grupların, özellikle kaba kümelere dayalı olanların cebirsel yapısına odaklanmaktadır. Yazar, Pawlak'ın kaba kümelerine dayanan yeni bir kaba grup tanımı öneriyor. Bu yeni tanım, önceki tanımların bazı eksikliklerini gidermektedir. Yazar daha sonra kaba grupların yapısını ayrıntılı ele almaktadır.

## 1. INTRODUCTION

The theory of rough sets, an extension of the classical set theory, was introduced first by Pawlak [6]. The theory deals with the approximations of any subsets of the given universal set by traceable subsets which are called upper and lower approximation subsets of the addicted rough sets. Useful details of the rough set theory used in the further sections are given in this section with a new extended definition. Successful applications of the theory in a wide range of problems including basic algebraic notions, quasi-Boolean algebras, Boolean algebras of the topological spaces, rough algebraic structures, topological rough algebras, quasi-Boolean algebras of the topological spaces, etc., have properly demonstrated its versatility and practicality [1, 3].

In order to have the deep mathematical meanings for further developments, rough sets theory needed to contain universal algebraic structures. For this purpose, some investigations have been made by Biswas and

Nanda in 1994 [2]. They give the first definitions of rough group, rough subgroup and some properties of them. Subsequently Miao and colleagues in their paper [5] renew the definition of rough group given by Biswas and Nanda. The main work of Miao and et al. was to improve some deficiencies in the definition of rough group given by Biswas and Nanda such as the lack of associativity property, the trivial rough subgroups of a rough group, and the intersection of any two rough subgroups of a rough group should satisfy the rough subgroup property too.

In order to have the deep mathematical meanings for further developments, rough sets theory needed to contain universal algebraic structures. For this purpose, some investigations have been made by Biswas and Nanda in 1994 [2]. They give the first definitions of rough group, rough subgroup and some properties of them. Subsequently Miao and colleagues in their paper [5] renew the definition of rough group given by Biswas and Nanda. The main work of Miao and et al. was to improve some deficiencies in the definition of rough

group given by Biswas and Nanda such as the lack of associativity property, the trivial rough subgroups of a rough group, and the intersection of any two rough subgroups of a rough group should satisfy the rough subgroup property too.

## 2. APPROXIMATION SPACES

In the theory of rough sets, approximation spaces are the main concepts. In this section, the structure of Pawlak's approximation space is restated (see in [7]) which is used in the next sections.

Let  $U$  be a non-empty finite set and  $R$  be an equivalence relation over the set  $U$  ( $R \subseteq U \times U$ ). Then the pair  $(U, R)$  is called as an *approximation space*. In an approximation space  $(U, R)$ ,  $U$  is called the *universe* and  $R$  is called the *underlying relation* of the approximation space  $(U, R)$ . Since  $R$  is an equivalence relation on  $U$ , it separates  $U$  into disjoint subsets of its own. It is a quotient set of the universe  $U$  and denoted by  $U/R$ . Elements of  $U/R$  is called the equivalence classes. For every  $x \in U$  the equivalence class containing  $x$  is denoted by  $[x]_R$  and equals to  $\{y \in U \mid xRy\}$ . The set of all equivalence classes is also called a *classification* of  $U$  induced by underlying relation  $R$ . Further, if a classification  $\{E_1, E_2, \dots, E_n\}$  of  $U$  is given then it is not needed to construct corresponding underlying equivalence relation  $R$  any more.

Every union of equivalence classes of the underlying equivalence relation for an approximation space is called *definable* (or *exact*) set [6, 2]. In general, the empty set is considered to be a definable set. For an arbitrary subset  $A$  of  $U$ , if it is not a definable set then  $A$  could not be described precisely by using the underlying relation of the approximation space  $(U, R)$ . In this case, there are some characterization of  $A$  to give idea of its structure. They are lower and upper approximations:

$$\begin{aligned}\underline{apr}_R(A) &= \{x \in U \mid [x]_R \subseteq A\} \\ &= \cup\{[x]_R \mid [x]_R \subseteq A\}\end{aligned}$$

and

$$\begin{aligned}\overline{apr}_R(A) &= \{x \in U \mid [x]_R \cap A \neq \emptyset\} \\ &= \cup\{[x]_R \mid [x]_R \cap A \neq \emptyset\}.\end{aligned}$$

Here, the lower approximation  $\underline{apr}_R(A)$  is the greatest definable set which is contained in  $A$ , and the upper approximation  $\overline{apr}_R(A)$  is the least definable set which contains  $A$  in the approximation space  $(U, R)$ .

Considering lower and upper approximations as two operators from the power set of universes  $U$  to itself then they are duals of each other which means one of them can be found from the other by using the following formulas:

$$\begin{aligned}\sim \underline{apr}_R(A) &= \underline{apr}_R(\sim A) \\ \sim \overline{apr}_R(A) &= \overline{apr}_R(\sim A)\end{aligned}$$

where  $\sim A$  denotes the set of complement of  $A$  in the universe  $U$ .

Now for any subsets  $A, B$  of the universe  $U$ , it can be given the list of some properties satisfied dually by  $\underline{apr}_R$  and  $\overline{apr}_R$  together:

$$(LU1) \quad \begin{aligned}\underline{apr}_R(U) &= U, \\ \overline{apr}_R(\emptyset) &= \emptyset,\end{aligned}$$

$$(LU2) \quad \begin{aligned}\underline{apr}_R(A \cap B) &= \underline{apr}_R(A) \cap \underline{apr}_R(B), \\ \overline{apr}_R(A \cup B) &= \overline{apr}_R(A) \cup \overline{apr}_R(B),\end{aligned}$$

$$(LU3) \quad \begin{aligned}\underline{apr}_R(A \cup B) &\supseteq \underline{apr}_R(A) \cup \underline{apr}_R(B), \\ \overline{apr}_R(A \cap B) &\subseteq \overline{apr}_R(A) \cap \overline{apr}_R(B),\end{aligned}$$

$$(LU4) \quad A \subseteq B \text{ implies } \underline{apr}_R(A) \subseteq \underline{apr}_R(B) \text{ and } \overline{apr}_R(A) \subseteq \overline{apr}_R(B)$$

$$(LU5) \quad \begin{aligned}\underline{apr}_R(\emptyset) &= \emptyset, \\ \overline{apr}_R(U) &= U,\end{aligned}$$

$$(LU6) \quad \underline{apr}_R(A) \subseteq A \subseteq \overline{apr}_R(A)$$

$$(LU7) \quad \overline{apr}_R(\underline{apr}_R(A)) \subseteq A \subseteq \underline{apr}_R(\overline{apr}_R(A)),$$

$$(LU8)$$

$$\begin{aligned}\underline{apr}_R(A) &\subseteq \underline{apr}_R(\underline{apr}_R(A)), \\ \overline{apr}_R(\overline{apr}_R(A)) &= \overline{apr}_R(A),\end{aligned}$$

$$(LU9) \quad \begin{aligned}\overline{apr}_R(A) &\subseteq \underline{apr}_R(\overline{apr}_R(A)), \\ \overline{apr}_R(\underline{apr}_R(A)) &\subseteq \underline{apr}_R(A),\end{aligned}$$

$$(LU10) \quad \underline{apr}_R(\sim A \cup B) \subseteq \sim \underline{apr}_R(A) \cup \underline{apr}_R(B),$$

$$(LU11) \quad \underline{apr}_R(A) \subseteq \overline{apr}_R(A).$$



In an approximation space  $(U, R)$ , for any two definable subsets  $A$  and  $B$  of  $U$  with  $A \subseteq B$ , the pair  $(A, B)$  is called a *rough set* [4]. On the set of all rough sets of the approximation space  $(U, R)$ , the set-theoretic operators can be defined component wise by using the standard set operators. For any rough sets  $(A_1, B_1)$  and  $(A_2, B_2)$ , the following definitions can be stated

*union of rough sets:*

$$(A_1, B_1) \cup (A_2, B_2) = (A_1 \cup A_2, B_1 \cup B_2)$$

*intersection of rough sets:*

$$(A_1, B_1) \cap (A_2, B_2) = (A_1 \cap A_2, B_1 \cap B_2)$$

*set inclusion of rough sets:*

$$(A_1, B_1) \subseteq (A_2, B_2) \text{ iff } A_1 \subseteq A_2 \text{ and } B_1 \subseteq B_2$$

*difference of rough sets:*

$$(A_1, B_1) \setminus (A_2, B_2) = (A_1 \setminus A_2, B_1 \setminus B_2)$$

*set complement of a rough set:*

$$\sim (A_1, B_1) = (U, U) \setminus (A_1, B_1) = (\sim B_1, \sim A_1)$$

The set of all rough sets with the above set-theoretic operators is called a *rough set algebra*.

Now for any rough set  $(A', A'')$ , there is a subset  $A$  of the universe  $U$  such that  $\underline{apr}_R(A) = A'$  and  $\overline{apr}_R(A) = A''$ .

### 2.1. Definition

Let  $(U, R)$  be an approximation space and  $A$  be a subset of the universe  $U$ . Then the triple  $(A, \underline{apr}_R(A), \overline{apr}_R(A))$  is called the *rough set of A* and denoted by  $\mathcal{R}(A)$ .

It is obvious that if  $A$  is a definable subset of  $U$  then so  $A'$  and  $A''$ . Furthermore  $A = A' = A''$ . In this case, it can be considered that any definable subset  $A$  of  $U$  as a rough set of  $A$ ,  $\mathcal{R}(A) = (A, A, A)$ . The operations  $\cup$ ,  $\cap$ , and  $\setminus$  given above can be defined similarly over the set  $\mathcal{U} = \{\mathcal{R}(A) | A \in \mathcal{P}(U)\}$  of all rough sets of subsets in the approximation space  $(U, R)$ .

For two rough sets  $\mathcal{R}(A)$  and  $\mathcal{R}(B)$ , the rough inclusion could be defined as follows  $\mathcal{R}(A) \subseteq \mathcal{R}(B)$  iff  $A \subseteq B$ . If  $\mathcal{R}(A) \subseteq \mathcal{R}(B)$  then it can be said  $A$  is a rough subset of  $B$ . For  $A$  and  $B$ ,  $A$  is rough equal to  $B$  if and only if  $A$  is a rough subset of  $B$  and vice versa.

It is clear that with rough inclusion and the operations  $\cup$ ,  $\cap$ ,  $\setminus$ , and  $\sim$  defined above, the set  $\mathcal{U}$  can be considered as a rough set algebra.

## 3. ROUGH GROUPS

According to the given structural knowledges in former section, basic algebraic rough group structure can be introduced with the following definition over rough sets of subsets in an approximation space.

### 3.1. Definition

Let  $(U, R)$  be an approximation space and  $*$  be a binary operation defined on  $U$ . Let  $G$  be a subset of the universe  $U$ . If the following properties are satisfied then  $\mathcal{R}(G)$  is called a *rough group*:

- (i) for every  $x, y, z \in \overline{apr}_R(G)$ ,  

$$x * (y * z) = (x * y) * z,$$
- (ii)  $a_1 * a_2 * \dots * a_n \in \overline{apr}_R(G)$ ,  
 where  $a_1, a_2, \dots, a_n \in G$ ,
- (iii) there exists an element  $e \in \overline{apr}_R(G)$ , called *rough identity*, for all  $a \in G$ ,  $a * e = e * a = a$ ,
- (iv) for all  $a \in G$  there exists an element  $b \in G$ , called *rough inverse*, such that  $a * b = b * a = e$ .

A rough group  $\mathcal{R}(G)$  with the binary operation  $*$  is sometimes denoted by  $(\mathcal{R}(G), *)$ .  $(\mathcal{R}(G), *)$  is called *Abelian* if  $a * b = b * a$  for all  $a, b \in G$ . Further, the element  $a_1 * a_2 * \dots * a_n$  for  $a_1, a_2, \dots, a_n \in G$  is denoted by  $\prod_{j=1}^n a_j$ .

### 3.2. Proposition

Let  $(U, R)$  be an approximation space,  $\mathcal{R}(G)$  be a rough group and  $e$  be the rough identity of  $\mathcal{R}(G)$ . Then  $G \cap \overline{apr}_R(\{e\}) \neq \emptyset$ .

*Proof.* Since  $e \in \overline{apr}_R(G)$ ,  $[e]_R \cap G \neq \emptyset$  and  $[e]_R = \overline{apr}_R(\{e\})$  then the result is obvious.

### 3.3. Proposition

Let  $\mathcal{R}(G)$  be a rough group, then the following properties hold;

- (i)  $G$  has a unique rough identity element,

- (ii) every element of  $G$  has a unique rough inverse,
- (iii) for any  $a, b, x, y \in G$ ,  
 $x * a = x * b$  implies  $a = b$   
 $a * y = b * y$  implies  $a = b$ .

### 3.4. Definition

Let  $G$  be a rough group and  $H$  be a nonempty subset of  $G$ . If  $\mathcal{R}(H)$  is a rough group with the same binary operation on  $U$ , then  $\mathcal{R}(H)$  is called a *rough subgroup* of  $\mathcal{R}(G)$ .

### 3.5. Definition

Let  $G$  be a subset of the universe  $U$ , then the set  $\{a_1 * a_2 * \dots * a_n \mid a_1, a_2, \dots, a_n \in G\}$  is called *exact set* of  $G$  and denoted by  $\tilde{G}$ .

### 3.6. Example

Let  $S_3$  be the symmetric group on  $X = \{1, 2, 3\}$  and  $\alpha_i$  be functions on  $X$  with restrictions  $\alpha_i(1) \neq \alpha_i(2)$  and  $\alpha_i(1) \neq \alpha_i(3)$  where  $i = 1, \dots, 6$ . These functions are all given below,

$$\alpha_1(x) = \begin{cases} 1 & \text{if } x = 1 \\ 2 & \text{if } x = 2, 3 \end{cases},$$

$$\alpha_2(x) = \begin{cases} 1 & \text{if } x = 1 \\ 3 & \text{if } x = 2, 3 \end{cases},$$

$$\alpha_3(x) = \begin{cases} 2 & \text{if } x = 1 \\ 1 & \text{if } x = 2, 3 \end{cases},$$

$$\alpha_4(x) = \begin{cases} 2 & \text{if } x = 1 \\ 3 & \text{if } x = 2, 3 \end{cases},$$

$$\alpha_5(x) = \begin{cases} 3 & \text{if } x = 1 \\ 2 & \text{if } x = 2, 3 \end{cases},$$

$$\alpha_6(x) = \begin{cases} 3 & \text{if } x = 1 \\ 1 & \text{if } x = 2, 3 \end{cases},$$

Let  $U$  be the set of functions  $\{\alpha: X \rightarrow X \mid \alpha(1) \neq \alpha(2), \alpha(1) \neq \alpha(3)\}$ , using above notation  $U = S_3 \cup \{\alpha_i \mid i = 1, \dots, 6\}$ , and  $\{E_1, E_2, E_3, E_4\}$  be a classification of the universe  $U$  where  $E_1 = \{\alpha_1, \alpha_2, \alpha_3\}$ ,  $E_2 = \{(1), (13), \alpha_4\}$ ,  $E_3 = \{(23), (12), \alpha_5\}$ , and  $E_4 = \{(123), (132), \alpha_6\}$ . Function composition can be considered as an operation on  $U$ .

Therefore, for the subset  $G = \{(13), (12), (123), (132)\}$  of  $U$ ,  $(\mathcal{R}(G), o)$  is a rough group with  $\overline{\text{apr}}(G) = E_2 \cup E_3 \cup E_4$ ,  $\underline{\text{apr}}(G) = \emptyset$  and  $\tilde{G} = S_3$ . For the subset  $H = \{(13)\}$  of  $G$ ,  $\mathcal{R}(H)$  is a rough subgroup of  $\mathcal{R}(G)$  with  $\overline{\text{apr}}(H) = E_2$ ,  $\underline{\text{apr}}(H) = \emptyset$  and  $\tilde{H} = \{(1), (13)\}$ .

### 3.7. Definition

Let  $\mathcal{R}(G)$  be a rough group and  $\mathcal{R}(H)$  be a rough subgroup of  $\mathcal{R}(G)$ . Then  $\mathcal{R}(H)$  is called *rough cyclic subgroup* of  $\mathcal{R}(G)$  if there exists an element  $x \in G$  such that  $H \subseteq \langle x \rangle$ . In particular, if  $\mathcal{R}(G)$  is a rough cyclic subgroup of itself then it is called *rough cyclic group* of  $U$ .

### 3.8. Proposition

Let  $\mathcal{R}(G)$  be a rough group and  $\mathcal{R}(H), \mathcal{R}(K)$  be rough subgroups of  $\mathcal{R}(G)$ , then the following properties hold;

- (i)  $\tilde{\tilde{G}} = \tilde{G}$ ,
- (ii)  $G \subseteq \tilde{G} \subseteq \overline{\text{apr}}(G)$ ,
- (iii)  $\overline{\text{apr}}(\tilde{G}) = \overline{\text{apr}}(G)$ ,
- (iv) if  $H \subseteq K$  then  $\tilde{H} \subseteq \tilde{K}$ . In particular, if  $H = K$  then  $\tilde{H} = \tilde{K}$ .

Note that the converse of Proposition 3.8 (iv) is not true in general as in the following example.

### 3.9. Example

Let the universe  $U$  be as in Example 3.6 and  $G = S_3$ . If  $H = \{(1), (123)\}$  and  $K = \{(1), (132)\}$  are taken, then  $\overline{\text{apr}}(H) = \overline{\text{apr}}(K) = E_2 \cup E_4$  and  $\tilde{H} = \tilde{K} = \{(1), (123), (132)\}$ .  $\tilde{H} \subseteq \tilde{K}$  but  $H \not\subseteq K$ .

For a rough group  $(\mathcal{R}(G), *)$  of the universe  $U$ , the exact set of  $G$ ,  $\tilde{G}$  is called *exact group* of the rough group  $\mathcal{R}(G)$ . For any two subsets  $H, K$  of  $U$  the set  $\{a * b \mid a \in H, b \in K\}$  is denoted by  $H * K$ .

### 3.10. Proposition

Let  $\mathcal{R}(G)$  be a rough group and  $\mathcal{R}(H), \mathcal{R}(K)$  are rough subgroups of  $\mathcal{R}(G)$ . Then the following are satisfied:

- (i)  $\widetilde{H \cap K} \subseteq \tilde{H} \cap \tilde{K}$ ,
- (ii) if  $G$  is abelian then  $\widetilde{H * K} \subseteq \tilde{H} * \tilde{K}$ .

*Proof.* (i) Let  $x \in \widetilde{H \cap K}$ , then there exist  $a_1, a_2, \dots, a_n \in H \cap K$  such that  $x = a_1 * a_2 * \dots * a_n$ . Since  $a_1, a_2, \dots, a_n \in H$  and  $a_1, a_2, \dots, a_n \in K$  then  $x \in \tilde{H}$  and  $x \in \tilde{K}$ . And so  $x \in \tilde{H} \cap \tilde{K}$ .

(ii) Let  $x \in \widetilde{H * K}$ , then there exist  $x_j = a_j * b_j$  and  $a_j \in H, b_j \in K$  for  $j = 1, 2, \dots, n$  such that  $x = x_1 * \dots * x_n$ . Since  $G$  is abelian,  $x = (a_1 * a_2 * \dots * a_n) * (b_1 * b_2 * \dots * b_n) \in \tilde{H} * \tilde{K}$ .

### 3.11. Theorem

Let  $H$  be a nonempty subset of  $G$ .  $\mathcal{R}(H)$  is a rough subgroup of  $\mathcal{R}(G)$  if and only if for all  $a \in H$ ,  $a^{-1} \in H$  and  $\tilde{H} \subseteq \overline{\text{apr}}(H)$ .

*Proof.* If  $H$  is a rough subgroup then the condition holds. For the converse suppose that for all  $a \in H$ ,  $a^{-1} \in H$  and  $\tilde{H} \subseteq \overline{\text{apr}}(H)$ . Since associativity holds in  $\overline{\text{apr}}(G)$  for  $*$ , so in  $\overline{\text{apr}}(H)$ . It is clear that by our assumption, for all  $a_1, a_2, \dots, a_n \in H$ ,  $a_1 * a_2 * \dots * a_n \in \tilde{H} \subseteq \overline{\text{apr}}(H)$ . And so for  $a \in H$  and  $a^{-1} \in H$ , thus  $a * a^{-1} = e \in \tilde{H}$ . Hence  $\mathcal{R}(H)$  is a rough subgroup of  $\mathcal{R}(G)$ .

### 3.12. Proposition

Let  $\mathcal{R}(G)$  be a rough group and  $\mathcal{R}(H)$ ,  $\mathcal{R}(K)$  are rough groups of  $\mathcal{R}(G)$ . If  $\overline{\text{apr}}(H) \cap \overline{\text{apr}}(K) = \overline{\text{apr}}(H \cap K)$  then  $\mathcal{R}(H \cap K)$  is a rough subgroup.

*Proof.* Suppose that  $\overline{\text{apr}}(H) \cap \overline{\text{apr}}(K) = \overline{\text{apr}}(H \cap K)$  and let  $a_1, a_2, \dots, a_n \in H \cap K$ , then  $a_1 * a_2 * \dots * a_n \in \overline{\text{apr}}(H \cap K) \subseteq \overline{\text{apr}}(H) \cap \overline{\text{apr}}(K) = \overline{\text{apr}}(H \cap K)$ . The rest of proof follows easily.

### 3.13. Theorem

Let  $\mathcal{R}(G)$  be an abelian rough group and  $\mathcal{R}(H)$ ,  $\mathcal{R}(K)$  are rough subgroups of  $\mathcal{R}(G)$ . If  $\overline{\text{apr}}(H) * \overline{\text{apr}}(K) = \overline{\text{apr}}(H * K)$  then  $\mathcal{R}(H * K)$  is a rough subgroup of  $\mathcal{R}(G)$ .

*Proof.* Suppose that  $\overline{\text{apr}}(H) * \overline{\text{apr}}(K) = \overline{\text{apr}}(H * K)$  and let  $a_1, a_2, \dots, a_n \in H * K$ , then  $a_1 * a_2 * \dots * a_n \in \overline{\text{apr}}(H * K) \subseteq \overline{\text{apr}}(H) * \overline{\text{apr}}(K) = \overline{\text{apr}}(H * K)$ . Now take  $x \in H * K$ . Then there exists  $h \in H$ ,  $k \in K$  such that  $x = h * k$ . Since  $h^{-1} \in H$ ,  $k^{-1} \in K$ ,  $x^{-1} = h^{-1} * k^{-1} \in H * K$ . Hence,  $\mathcal{R}(H * K)$  is a rough subgroup of  $\mathcal{R}(G)$  by Theorem 3.11.

Note that for a rough group  $(\mathcal{R}(G), *)$  of the universe  $U$ , an element  $x \in G$  and a natural number  $n$ ,  $x^n$  is defined as  $x * x * \dots * x$  ( $n$  times). Similarly  $(x^{-1})^n = x^{-n}$  is defined as  $x^{-1} * x^{-1} * \dots * x^{-1}$  ( $n$  times). Then the set  $\langle x \rangle = \{x^n \mid n \in \mathbb{Z}\}$  can be defined. It is clear that  $\mathcal{R}(\langle x \rangle)$  is a rough group contained in  $\overline{\text{apr}}(G)$ . Furthermore,  $\langle x \rangle = \overline{\langle x \rangle} \subseteq \overline{\text{apr}}(\langle x \rangle)$ .

### 3.14. Theorem

Let  $\mathcal{R}(G)$  be a rough group and  $\mathcal{R}(H)$  be a rough subgroup of  $\mathcal{R}(G)$ . Then  $\mathcal{R}(H)$  is a rough cyclic subgroup of  $\mathcal{R}(G)$  if and only if  $\tilde{H} = \langle x \rangle$  for an element  $x$  of  $G$ .

*Proof.* Suppose that  $\tilde{H} = \langle x \rangle$  for an element  $x$  of  $G$ , then it is clear that  $H \subseteq \tilde{H} = \langle x \rangle$ . So  $\mathcal{R}(H)$  is a rough cyclic subgroup of  $\mathcal{R}(G)$ . Now suppose that  $\mathcal{R}(H)$  is a

rough cyclic subgroup. If  $H = \{e\}$  then  $\tilde{H} = \langle e \rangle$ . If  $H \neq \{e\}$  then there exists an element  $y \in G$  such that  $H \subseteq \langle y \rangle$ . Now let  $e \neq z \in H$ , then there exists  $n \in \mathbb{N}$  such that  $z = y^n$ . Let  $k \in \mathbb{N}$  be the least positive integer such that  $y^k \in H$ . Then if taken  $x = y^k$  then  $\tilde{H} = \langle x \rangle$ .

### 3.15. Corollary

Every rough subgroup of a rough cyclic group is a rough cyclic subgroup.

In summary, there are many possibilities for further research involving rough groups and rough sets. One can explore the structure of cosets of rough groups, the homomorphisms between rough groups, and even the construction of rough rings or rough fields over rough sets.

## REFERENCES

- [1] Banerjee MH, Chakraborty MK. Rough sets through algebraic logic. *Fundam. Inform.* 1996;28(3-4):211-221.
- [2] Biswas R, Nanda S. Rough Groups and Rough Subgroups. *Bull. Pol. AC. Math.* 1994;42:251-254.
- [3] Duentzsch I, Orłowska E, Wang H. Algebras of approximating regions. *Fundam. Inform.* 2001;46(1-2):78-82.
- [4] Iwinski TB. Algebraic approach to rough sets. *Bull. Polish Acad. Sci. Math.* 1987;35:673-683.
- [5] Miao D, Han S, Li D, Sun L. Rough group, rough subgroup and their properties. *Rough Sets, Fuzzy Sets, Data Mining, and Granular Computing.* 2005:104-113.
- [6] Pawlak Z. Rough Sets. *International Journal of Computer and Information Sciences.* 1982;11:341-356.
- [7] Yao, YY. Generalized rough set models. *Rough sets in knowledge discovery 1.* 1998:286-318.

## Geotechnical Inspections and Applications in Underground Rail System Constructions: Halkalı - İstanbul Airport Metro Line Example

Rabia KELEŞ<sup>1\*</sup> , İsa VURAL<sup>2</sup> 

<sup>1</sup> Sakarya University of Applied Sciences, Faculty of Technology, Department of Civil Engineering, Sakarya, Türkiye

<sup>2</sup> Sakarya University of Applied Sciences, Faculty of Technology, Department of Civil Engineering, Sakarya, Türkiye

Rabia KELEŞ ORCID No: 0000-0002-6689-4217

İsa VURAL ORCID No: 0000-0003-2370-7597

\*Corresponding author: [y18007009@subu.edu.tr](mailto:y18007009@subu.edu.tr)

(Received: 15.11.2022, Accepted: 08.06.2023, Online Publication: 22.06.2023)

### Keywords

İstanbul  
Airport  
Metro Line,  
Electrical  
Resistance  
Tomography,  
Electrical  
Resistivity

**Abstract:** In this study, geological researches carried out before the construction of underground rail systems and geotechnical application methods preferred during the construction were examined within the scope of Halkalı-İstanbul Airport metro project. The metro line consists of a total of 66.2 km long underground tunnels, 31.3×2 km main line and 1.8×2 km repertorium connection line. 1006 soil and 1230 rock samples were collected for the main line whose geological research was carried out with 198 core drillings with a total length of 9588.5 m. The results of the laboratory tests on the samples and the field tests carried out in the boreholes were obtained. In addition, a total of four two-dimensional inverse resistivity model were obtained by using the Multi-electrode Electrical Resistance Tomography measurement method in the middle of two lines (Line-1 Km: 61+440 – 61+660 /Line-2 Km: 61+400 - 61+620), in the Olympic Stadium station (Km: 62+215 – 62+490) and in the TBM route (Line-2 Km: 62+835 – 63+050). The geological sections obtained from the drillings and the geophysical sections obtained by the electrical resistivity method were compared.

## Yeraltı Raylı Sistem İnşaatlarında Jeoteknik İncelemeler ve Uygulamalar: Halkalı - İstanbul Havalimanı Metro Hattı Örneği

### Anahtar Kelimeler

İstanbul  
Havalimanı  
Metro Hattı,  
Elektriksel  
Direnç  
Tomografisi,  
Elektrik  
Direnci

**Öz:** Bu çalışmada yeraltı raylı sistemleri inşası öncesinde gerçekleştirilen jeolojik araştırmalar ve inşası sırasında tercih edilen jeoteknik uygulama yöntemleri Halkalı-Yeni Havalimanı metro projesi kapsamında incelenmiştir. Metro hattı 31,3×2 km ana hat, 1,8×2 km depo bağlantı hattı olmak üzere toplam 66,2 km uzunluğundaki yeraltı tünellerinden oluşmaktadır. Jeolojik araştırması toplam 9588,5 m uzunluğunda 198 adet karotlu sondaj ile gerçekleştirilen ana hat için 1006 adet zemin, 1230 adet kaya numunesi toplanmıştır. Numuneler üzerinde yapılan laboratuvar deneylerinin ve sondaj kuyularında gerçekleştirilen arazi deneylerinin sonuçları elde edilmiştir. Ayrıca TBM (Tünel Açma Makinesi) güzergahı iki hattın ortasında (Hat-1 Km: 61+440 – 61+660 / Hat-2 Km: 61+400 – 61+620), Olimpiyatköy Stadı istasyonunda (Km: 62+215 – 62+490) iki adet ve TBM güzergahında (Hat-2 Km: 62+835 – 63+050) olmak üzere Çoklu Elektrotlu Elektrik Özdirenç Tomografi ölçüm yöntemi kullanılarak toplam dört adet iki boyutlu ters çözüm özdirenç yeraltı kesiti elde edilmiştir. Sondajlardan elde edilen jeolojik kesitler ile elektrik özdirenç yöntemi ile elde edilen jeofizik kesitler karşılaştırılmıştır.

### 1. INTRODUCTION

Transportation problems occur due to the current urbanization in areas where circulation is concentrated such as new city centers, airports and touristic places in the rural areas of the city due to the increasing population and construction. For this reason, institutions

turn to rail system public transportation, which is fast, permanent and ecological, to solve transportation problems in metropolitan areas. With the invention of the elevator, a jump similar to that seen in high-rise construction productions were observed with the invention of TBM (Tunnel Boring Machine) in underground rail systems and the use of NATM (New Austria Tunneling Method) in manufacturing.

Underground rail system projects are generally stations, route line, warehouse area, switches, emergency escape shafts, etc. It contains structures of very different sizes, each serving separate purposes. Along the route, geological mapping been made in the zone up to a distance of roughly 150 meters (300 m in total width) on both sides of the tunnel lines. In order to obtain accurate data in problematic areas with karstic cavities where the created geological section is not sufficient, geophysical studies using Multi-electrode Electrical Resistance Tomography method in four different locations have obtained 2-dimensional underground resistivity reverse solution sections. There are even 1 HST (High Speed Train) station and 7 metro stations, 11 switch structures, 8 service stations, 2 emergency escape shafts, 12 construction shafts and 106 cross-passage tunnels. The length of the tunnels in which TBM is used in the project is approximately 55.7 km, and the total length of the tunnels in which the NATM is applied is approximately 15.8 km.

## 2. LITERATURE RESEARCH

Electrical resistivity method, one of the geophysical research methods, has been used for many years in determining the parameters of the underground. The resistivity method which was first applied by Wenner in 1915, was developed by Schlumberger in 1920 and positive results were reached. With the development of computer and geophysical device technology, the electrical resistivity method allows the examination of underground resistivity changes in one, two and three dimensions. [1, 2]

The main purpose in the application of electrical resistivity methods is to reveal the geological structure by taking advantage of the horizontal or vertical electrical conductivity differences of the rocks. The electrical resistivity method is defined as sending electricity underground with two current electrodes and determining the potential distribution of this current by two potential electrodes through measurements made from the surface. [3] Based on this, some usage areas can be listed as determination of salt water inlets, determination of weathering zone boundary, determination of faults and fractures, karstic cavity and cave research, determination of underground structures for archaeological purposes, determination of mineral deposits and determination of contact places of geological units. [4]

Under what conditions and depending on which circumstances the electrical properties will vary in underground, the resistance of the measured environment depends on the different physical parameters of the rock (such as mineral or liquid content, porosity and degree of water saturation) and these parameters are important factors in the transmission of the current given into the underground. [1]

The transport of electrical load takes place according to two main transmission modes as electronic and electrolytic transmission. In electronic transmission,

current flow occurs through free electrons as in a metal, while in electrolytic transmission, current flow occurs through ions. These types of transmission constitute a concept of self-conductivity for each environment. The movement of the electrical charge is a distinguishing feature for self-conductivity substances due to the presence of different physical parameters in each item and is used to distinguish the underground environments from each other. [1]

**Table 2.1: Resistivity of some materials. [5]**

Material	Resistivity( $\Omega$ m)	Material	Resistivity( $\Omega$ m)
Chalcopyrite	$1,5 \times 10^{-5} - 3 \times 10^{-1}$	Soil (upper)	250-1700
Pyrite	$2,9 \times 10^{-5} - 1,5$	Dry sandy soil	80-1050
Pyrotite	$7,5 \times 10^{-6} - 5 \times 10^{-2}$	Sand clay/clay sand	30-215
Galena	$3 \times 10^{-3} - 3 \times 10^2$	Sand and gravel	30-225
Sphalerite	$1,5 \times 10^7$	Gravel (dry)	1400
Hematit	$3,5 \times 10^{-3} - 10^7$	Gravel (saturated)	100
Limonite	$10^3 - 10^7$	Schist (limestone and mica)	20-104
Magnetite	$5 \times 10^{-5} - 5,7 \times 10^3$	Schist (graphite)	$10 - 10^2$
Ilmenitis	$10^{-3} - 5 \times 10$	Marble	$10^2 - 2,5 \times 10^8$
Quartz	$3 \times 10^2 - 10^6$	Conglomerate	$2 \times 10^3 - 10^4$
Rock Salt	$3 \times 10^2 - 10^{13}$	Sandstone	$1 - 7,4 \times 10^8$
Anthracite	$10^{-3} - 2 \times 10^5$	Limestone	$5 \times 10 - 10^7$
Lignite	$9 - 2 \times 10^2$	Dolomite	$3,5 \times 10^2 - 5 \times 10^3$
Granite	$3 \times 10^2 - 10^6$	Clay	$1 - 10^2$
Soil (40% clayey)	8	Alluvium and sand	$10 - 8 \times 10^2$
Gabro	$10^3 - 10^6$	Basalt	$10 - 1,3 \times 10^7$
Sea water	$3 \times 10^{-1}$	Clean underground water	10-100

Land consisting of easily meltable rocks that cannot resist abrasion is defined as karstic lands. Karstic regions are formed as a result of dissolution of soluble rocks such as gypsum, salt and limestone by external factors (for example, stream enriched with CO<sub>2</sub> in the soil and gaining acidic property, rainwater enriched with CO<sub>2</sub> in the air and gaining acidic property). Since the formation and expansion of these gaps depend on the flow of groundwater and surface waters and generally show an irregular spread, they pose a great danger in terms of construction and infrastructure works. Karstic cavities become interconnected during the dissolution process and allow surface water to reach the aquifer. For this reason, the melting process continues continuously and the karstic cavities expand over time. [6]

## 3. HALKALI-İSTANBUL AIRPORT METRO LINE GEOTECHNICAL EXAMINATIONS

This part of the metro line consists of approximately 31 km of tunnels, seven stations and storage areas in roughly double tubes. The parts of the route within Arnavutköy district center and Küçükçekmece district remain in the densely built area and the remaining parts remain in the areas that are not yet built or sparsely built. The line, which travels roughly north-south between Arnavutköy, Başakşehir and Küçükçekmece districts, ends in Halkalı district of Küçükçekmece District (Figure 3.1). In the project design, there are 104 passage tunnels, 11 switch tunnels, 8 service stations and 13 emergency escape shafts + construction shafts.



**Figure 3.1:** Halkalı – İstanbul Airport metro line satellite image and integration points.

Geological section of the line is formed by experiments conducted on 1006 soils and 1230 rock samples obtained from 198 cored research drillings with a total length of 9588.5 m. Drilling drills were carried out under the tunnel excavation base to obtain information up to a depth of 5 - 6 m. SPT (Standard Penetration Test) was performed at 1.5 m intervals in ground-like parts including completely weathered rock and disturbed soil samples were taken during the tests. Samples of undisturbed samples (UD) were also taken at appropriate clayey levels of consistency.

Key	Formation	Member	Definition
Yd	Artificial Filling		Off-white, beige colored rock fragments and blocks as well as gravel, sand, clay size intermediate material.
Qal	Alluvium		Gravel, sand, mile, clay.
Tik	İstanbul	Kıraç	Reddish, light brown, gray, mostly gravel and lesser sand-clay unattached material.
Tdg	Danişmen	Güngören	Greenish, dark gray, purple mottled, claystone-shale, sandstone, tuff, tuffite and fine lignite interbedded.
Tda	Danişmen	Ağaçlı	Gravel, sand, clay, coal intermediate level.
Tc	Ceylan		Unallocated; marl, claystone dominant, clayey limestone, calcareous claystone interbedded; calenite and sparse tuff interbedded.
Tso	Soğucak Limestone		White, cream, ash gray colored reefal limestone, abundant algae, coral, nummulit, micrite-biomicrite.
Tk	Koyunbaba		Sandstone; conglomerate, clayey-sandy-gravelous limestone, limy claystone, marl; coal intermediate level.
Ksgb	Garipe	Boğazköy	Grey, purplish ash color. Andesitic with mica and feldspar phenocrysts, porphyritic texture.
Tr	Trakya		Black, dark gray, degraded light brown, olive green; thin medium bedded claystone-siltstone-sandstone alternation.
Tçb	Çekmece	Bakırköy	White, beige, thin-medium bedded limestone dominant, clayey limestone, claystone and marl intercalated.
Tçç - Tçg	Çekmece	Güngören Çukurçeşme	Tçç: Yellowish gray, gray mica flakes, medium-sized, cross-bedded, unconsolidated coarse sand and gravel. Tçg: Sand, mile intercalated, green gray clay; interlayer at higher levels.

**Figure 3.2:** Halkalı – İstanbul Airport metro line stratigraphic columnar section [7, 8, 9 and 10].

In a significant part of the soil samples, only physical and index experiments such as sieve, hydrometer, specific gravity, consistency (Atterberg) limits, water content, unit volume weight were carried out, while in some of these experiments, mechanical experiments such as free pressure and cutting box were carried out. On rock samples, mechanical-elastic tests such as physical and point loading index, poison ratio, uniaxial pressure, and elasticity module was performed. In addition, the geological formations seen in the drillings along the line are listed in Figure 3.2.

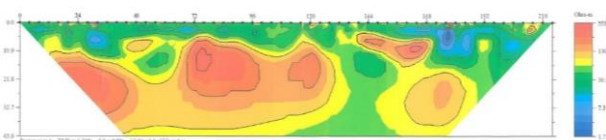


**Figure 3.3:** Two-dimensional (2D) inverse resistivity model of ERT-1 measurement profile calculated as a result of evaluations [11].

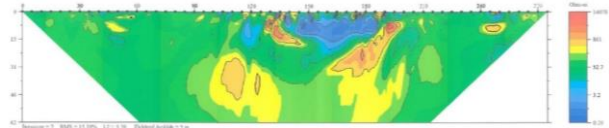


**Figure 3.4:** Two-dimensional (2D) inverse resistivity model of ERT-2 measurement profile calculated as a result of evaluations [12].

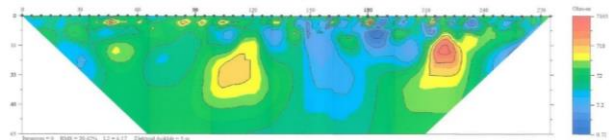


**Figure 3.5:** Two-dimensional (2D) inverse resistivity model of ERT-3 measurement profile calculated as a result of evaluations [12].

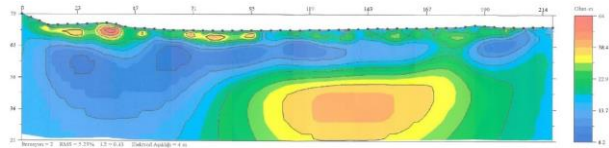


**Figure 3.6:** Two-dimensional (2D) inverse resistivity model of ERT-4 measurement profile calculated as a result of evaluations [13].

Within the scope of the Halkalı-İstanbul Airport metro line project; a total of four Two-dimensional (2D) inverse resistivity model (Figure 3.3, Figure 3.4, Figure 3.5, Figure 3.6) were obtained by using the Multi-electrode Electrical Resistance Tomography measurement method, two of which were in the middle of lines (Line-1 Km. 61+440 – 61+660 /Line-2 Km: 61+400 - 61+620), two of which were in the Olympic Stadium station and in the route of TBM (Line-2 Km: 62+835 – 63+050).

With the Multi-electrode Electrical Resistance Tomography measurement method applied to determine the lateral and vertical changes of the geological units underground in the study area, the resistivity changes depending on the conductivity of the geological units underground can be mapped in two dimensions.

In the measurements, 56-channel AGI brand Superstring R1 model multi-electrode resistance measuring device and equipment been used and dipole-dipole sequencing method was applied. Electrode range (a) was measured with a total 56 electrodes by selecting a =4 m for ERT-1 and ERT-4 and a=5 for ERT-3. In the measurements, the parameters for each sequence and point were automatically recorded as voltage (millivolts), given current (amperes), calculated resistivity (ohms-m) and error rate (%).

#### 4. COMPARISON OF GEOTECHNICAL AND GEOPHYSICAL SECTIONS OBTAINED IN THE HALKALI-İSTANBUL AIRPORT METRO LINE

Under this heading, the four resistivity reverse solution sections obtained as a result of the multi-electrode electrical resistance tomography measurement method on the line will be compared and interpreted by

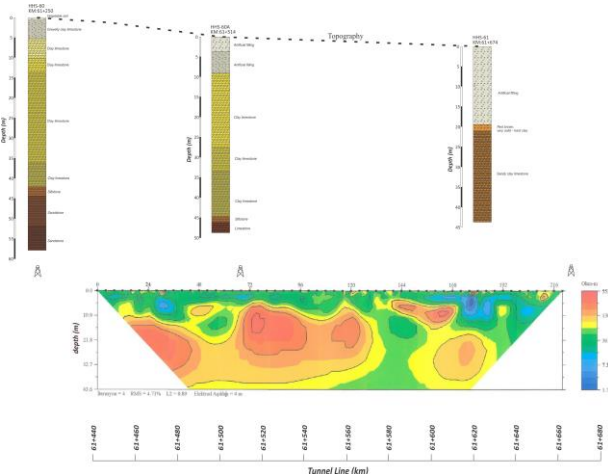
comparing the geological sections formed with the help of the drillings corresponding to these sections.

Figure 4.1 shows the ERT-1 section formed by geophysical examination at the location of Line-1 Km: 61+440 – 61+660 /Line-2 Km: 61+400 – 61+620 in the middle of two lines on the TBM route and the geological section obtained from HHS-60, HHS-60A and HHS-61 drillings corresponding to this section.

In the HHS-60A drilling at the Km: 61 +514 location, the electrical resistivity value was measured as 30 ohms on average in the artificial filling consisting of gravel units without water for 10 meters. In the continuation of the drilling, it is seen that the electrical resistivity values for water-free, fractured cracked limestone units with a depth of approximately 35 meters increase up to 553 ohms. In the last 5 meters of the drilling, the increase in the fracture crack rate and the presence of groundwater caused the resistivity values to decrease.

In the region where the HHS-61 (Km: 61 +674) drilling of the same resistivity reverse solution section coincides, the electrical resistivity method cannot be displayed after the first 20 meters due to horizontal data loss. The electrical resistivity values measured in the first 20-meter unit analyzed and the unit represented by artificial filling observed in the HHS-60A drilling show parallelism. Another indication of this parallelism is the characterization of approximately the first 20 meters in the HHS-61 drilling log as artificial filling.

The zone with low electrical resistance values between Km: 61+570 - 61+590 can be explained by the possible increase in clay or underground water level and the filling of limestone cracks with water.



**Figure 4.1:** ERT-1 reverse solution section and geological section obtained from drillings in the same location.

Figure 4.3 shows the ERT-2, ERT-3 sections formed as a result of the geophysical examination made in Olimpiyatköy station and the geological section obtained from the YHH-81, YHH-81A, YHH-81C and YHH-81E drillings corresponding to these sections.

In ERT-2 and ERT-3 section, there is no difference in electrical resistivity values in the analyzes corresponding

to YHH-81A and YHH-81E drillings. This situation is related to the continuity of the fractured cracked structure at a very high rate, as can be seen in the drilling crate photo in Figure 4.2.

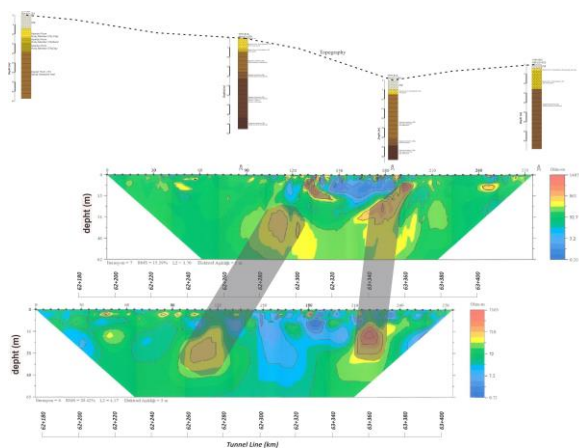
In ERT-2 and ERT-3 section, there is no difference in electrical resistivity values in the analyzes corresponding to YHH-81A and YHH-81E drillings. This situation is related to the continuity of the fractured cracked structure at a very high rate, as can be seen in the drilling crate photo in Figure 4.2.



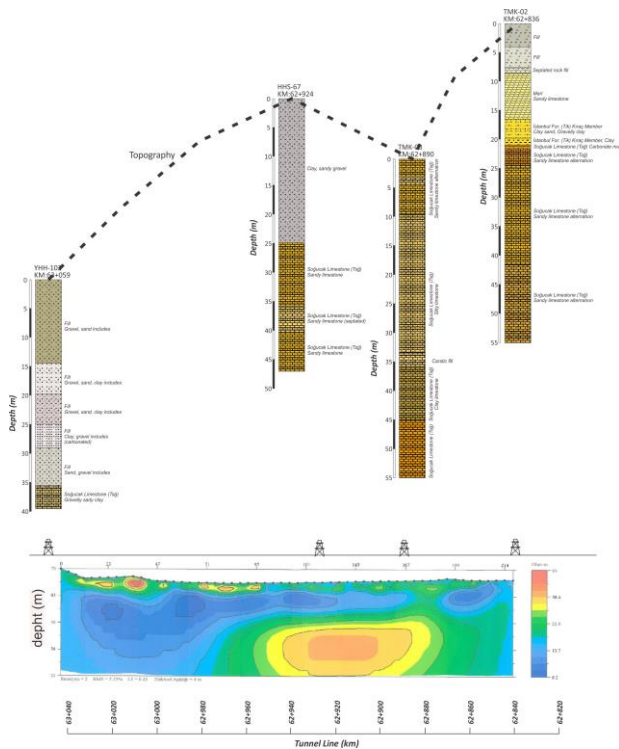
**Figure 4.2:** YHH-81C drill 24.30 m – 30.40 m caisson image (Soğucak limestone formation) [9].

On the other hand, the distinction between filler and limestone is clear in the regions corresponding to YHH-81C drilling in resistivity reverse solution sections. The electrical resistivity values in the filling part were 10 – 15 ohm.m due to the fact that the filling consisted of clayey silty units, while it was 50 – 70 ohm.m due to the cracked structure in the limestone.

The remarkable in these two sections are the inclusions with relatively high electrical resistivity values at the levels of 7000 ohm.m and 14000 ohm.m, which emerge close to the surface and at a depth of 30-30 meters from the surface. The high electrical resistance values that occur suddenly in limestone can be explained by the decrease in conductivity due to the possible karstic gaps. The karstic gaps observed during the production of Olimpiyatköy station support this interpretation. By scaling the positions of ERT-2 and ERT-3 measurements performed in parallel with each other, the horizontal extensions of the possible karstic spaces are approximately shown in Figure 4.4.



**Figure 4.4:** ERT-2/ERT-3 reverse solution sections and geological section obtained from drillings in the same location.



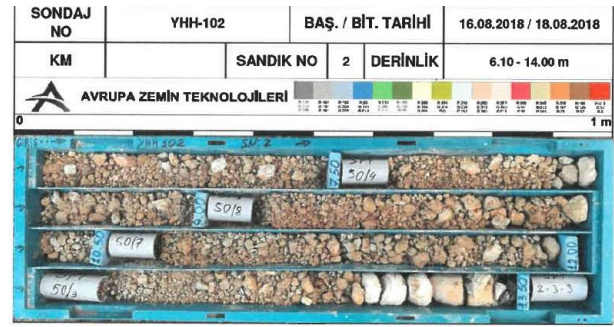
**Figure 4.5:** ERT-4 reverse solution section and geological section obtained from drillings in the same location.

Figure 4.5 shows the ERT-4 cross-section created as a result of the geophysical examination performed on Line-2 Km: 62 +835 – 63+050 on the TBM route and the geological cross-section obtained from TMK-02, TMK-03, HHS-67 and YHH-102 drillings corresponding to this cross-section.

In HHS-67 drilling in Km: 62 +924 location, the electrical resistivity value of the first 25 meters corresponding to the clayey sandy gravel unit been represented in the range of 8 – 20 ohms in the resistivity reverse solution section. The electrical resistivity value, which is observed to increase up to 64 ohms in the continuation, is represented by the different degrees of decomposed structure of the soğuçak limestone.

The electrical resistivity values corresponding to the TMK-03 drilling 35 m behind the HHS-67 drilling are similar for the ongoing units. In addition, the karstic gap observed in the drilling log at a depth of approximately 35 meters corresponds to the area where the maximum resistivity values at the same depth are measured in the resistivity reverse solution section.

Filling ground seen in YHH-102 drilling gives electrical resistivity values of 8 – 13 ohms at the end of ERT-4 section. Relatively low resistivity values can be explained by the highly hollow structure of the ground seen in Figure 4.6.



**Figure 4.6:** YHH-102 drilling 6.10 m – 14.00 m caisson image (Artificial filling) [10].

## 5. RESULTS

In this study, geotechnical studies conducted within the scope of Halkalı-İstanbul Airport metro line project been examined with the help of geological and geophysical survey reports. Geophysical sections and the geological sections obtained with the help of the drillings corresponding to the regions where these sections been formed were compared with each other.

As a result of this comparison, it was seen that karstic gaps could not be detected in the drillings made at Olimpiyatköy station. In addition, it is clear that the use of geophysical methods will provide effective time use and savings in order to predict and prevent possible problems in the manufacturing phase. Because it will be very costly and time-consuming to determine areas that are quite small compared to the project area, such as karst voids, by means of drilling in projects that require production in kilometers of different depths and sizes, such as underground rail systems.

In rail system projects where the production is concentrated on a line, the drilling plan mostly follows this line. Geophysical methods can be resorted to because the data obtained from the drillings in the regions where the production is intense in the second dimension, such as station structures, may be insufficient. In addition, data can be obtained by geophysical methods in regions where drilling cannot be performed due to topography or dense construction. On the other hand, it is a fact that geophysical methods performed indirectly should be supported by drilling or different methods. In order for the interpretation of electrical resistivity values to approach the truth, basic data that can be obtained by drilling such as presence of groundwater level, stratification of soils, rock quality are needed.

Accurate, fast and clear sharing of the necessary data in underground rail system constructions, which require many different disciplines to work together, is of great importance under the headings of time and cost.

## REFERENCES

- [1] Berge, M. A. (2005). Two-dimensional resistivity inversion-solution modeling. (Master's Thesis). Dokuz Eylül University Institute of Science,



- Bozkurt, M. (1987). Tunnels, lecture notes. İstanbul: ITU construction faculty printing house.
- [2] Drahor, M., G., Göktürkler, G., Berge, M. A., & Kurtuluş, Ö. T. (2004). Visible resistivity modeling of some three-dimensional shallow underground structures according to four different electrode arrays. *Earth sciences*, 115-128.
- [3] Şahinoğlu, A. (2018). Applications of geophysical methods in groundwater pollution research. *Academic Studies in Engineering*, 88-89.
- [4] Bernard, J., & Leite, O. (2004). Multi-electrode resistance imaging for environmental applications. *Progress in Environmental and Engineering Geophysics*, 317-322. Retrieved from <Go to ISI>://WOS:000223170000055
- [5] Reynolds, JM (1997). *An Introduction to Applied and Environmental Geophysics*: Wiley. Roland, G., Claudine, B. (1997). *The Canal du Midi* (English translation): MSM.
- [6] Uçar, F. (2014). Determination of karstic activity using 2-dimensional resistivity method (Master's Degree). Akdeniz Üniversitesi, Antalya.
- [7] Artson Geotechnical Engineering and Consultancy (2018). Geological-Geotechnical Survey Report of the Route between Km: 38 +077-Km: 44+700. İstanbul.
- [8] Artson Geotechnical Engineering and Consultancy (2018). Geological-Geotechnical Survey Report of the Route between Km: 44 +700-Km: 57+700. İstanbul.
- [9] Artson Geotechnical Engineering and Consultancy (2018). Geological-Geotechnical Survey Report of the Route between Km: 57 +700-Km: 62+500. İstanbul.
- [10] Artson Geotechnical Engineering and Consultancy (2018). Km: 62 +500-Km: 69+359 (End of Line) Route Geological-Geotechnical Survey Report. İstanbul.
- [11] Geometric Engineering Consultancy Underground Research (2020). İstanbul New Airport-Halkalı Metro Line Project Two Dimensional (2D) Electrical Resistivity Tomography Geophysical Research between TBM Route Line-1/Line-2. İstanbul.
- [12] Geometric Engineering Consultancy Underground Research (2020). İstanbul New Airport-Halkalı Metro Line Project Olimpiyatköy Station Two Dimensional (2D) Dimensional Electrical Resistivity Tomography Geophysical Research. İstanbul.
- [13] Geometric Engineering Consultancy Underground Research (2020). İstanbul New Airport-Halkalı Metro Line Project TBM Route Two-Dimensional (2D) Dimensional Electrical Resistivity Tomography Geophysical Research. İstanbul.

## Investigation of Arginine Deiminase Activity in *Bacillus cereus* and *Ralstonia eutropha* Under Minimal Conditions

Cennet Canan KARADERİ<sup>1\*</sup> , Hüseyin KAHRAMAN<sup>2</sup> 

<sup>1</sup> İnönü Üniversitesi, Fen Bilimleri Enstitüsü, Biyoloji Bölümü, Malatya, Türkiye

<sup>2</sup> İnönü Üniversitesi, Fen Edebiyat Fakültesi, Biyoloji Bölümü, Malatya, Türkiye

Cennet Canan KARADERİ ORCID No: 0000-0002-4841-4435

Hüseyin KAHRAMAN ORCID No: 0000-0001-6235-5497

\*Corresponding author: ckaraderi@gmail.com

(Received: 18.01.2023, Accepted: 12.06.2023, Online Publication: 22.06.2023)

### Keywords

*Bacillus cereus*,  
*Ralstonia eutropha*,  
Arginine deiminase

**Abstract:** Prokaryotes form an important part of our lives. These microorganisms, which we can not see with the naked eye, are used in medicine, biotechnology, microbiology and many other fields. They can produce many anti-cancer enzymes (Arginine deiminase, Asparaginase, Methionine gamma lyase etc.). In this study, an important bacterial anti-tumor enzyme of *B. cereus* and *R. eutropha* in the presence of different minimal sources (Dextrose, Fructose, Glucose, Xylose, Maltose, Nutrient Broth, Rhamnose, Ribose, Sucrose) under static and shaking (150 rpm) conditions.

Arginine deiminase activity was searched. In accordance with results of our study, these microorganisms showed the highest ADI activity in the disaccharide medium, maltose and sucrose, and in the aldose group, in the ribose medium. It has been shown that this enzyme, which is used in cancer treatment, can be produced more cheaply and easily in minimal environments.

99

## Minimal Koşullar Altında *Bacillus cereus* ve *Ralstonia eutropha*' da Arjinin deiminaz (ADI) Aktivitesinin Araştırılması

### Anahtar Kelimeler

*Bacillus cereus*,  
*Ralstonia eutropha*,  
Arjinin deiminaz

**Öz:** Prokaryotlar, hayatımızın önemli bir parçasını oluşturmaktadır. Çıplak göz ile göremediğimiz bu mikroorganizmalar tıp, biyoteknoloji, mikrobiyoloji ve daha pek çok alanda kullanılmaktadır. Pek çok anti kanser enzimlerini (Arjinin deiminaz, Asparaginaz, Metiyonin gama liyaz vb) üretebilmektedirler. Bu çalışmada *B. cereus* ve *R. eutropha*'nın statik ve çalkalamalı (150 rpm) koşullarda, farklı minimal kaynakları (Dekstroz, Fruktöz, Glukoz, Ksiloz, Maltoz, Nutrient Broth Ramnoz, Riboz, Sükroz) varlığında önemli bir bakteriyel anti-tümör enzimi olan ADI aktivitesi araştırılmıştır. Çalışmanın sonuçlarına göre bu mikroorganizmalar, disakkarit ortamlarında maltoz ve sükroz, aldoz grubunda ise riboz ortamında en yüksek ADI aktivitesi göstermiştir. Kanser tedavisinde kullanılan bu enzimin minimal ortamlarda, daha ucuz, kolay bir şekilde üretilebileceği gösterilmiştir.

### 1. INTRODUCTION

Cancer is an important metabolic syndrome and causes serious deaths. It is associated with high mortality rates though important progresses have been made in early discovery and treatment. Cancer is an important metabolic syndrome and causes serious deaths [1]. It is associated with high mortality rates though important progresses have been made in early discovery and treatment. Hence many methods such as chemotherapy

and radiotherapy are being developed to detect cancer early and to stop its progression [2].

Cancer cells; They are deadly cells that lose their functional properties, mutate due to external factors, and can multiply rapidly. These cells require large amounts of proteins to reproduce. Tumor cells can't perform their functions and reproduce because they can't perform protein synthesis without amino acids [3]. Therefore, in the medical world, a single amino acid starvation is seen as an effective strategy in cancer treatment [4]. Recent

scientific research has targeted amino acid metabolic enzymes that reduce specific enzyme metabolism required for cancer cell proliferation. With the degradation of amino acids, both DNA replication in cancer cells is prevented and the progression of cancer is stopped [3]. Enzymes are used as chemotherapeutic agents because of their high affinity and specificity towards their substrates and their rapid reaction [5].

Arginine deiminase (EC: 3.5.3.6), a bacterial arginine-catabolizing enzyme, has because of its antitumor activity in arginine auxotrophic cancers, particularly hepatocellular carcinomas and melanomas through consuming plasma arginine and causing cell deficiency [6]. Arginine deiminase catalyzes the hydrolysis of arginine to citrulline and ammonia by deamination of the guanidino group. In widespread, the hydrolysis of arginine with ADI is thought about the first step of the Arginine deiminase system consisting of two reactions: conversion of citrulline to ornithine and reduction of carboamyl phosphate to ammonia and CO<sub>2</sub> by carbamyl phosphate and carbamate kinase catalyzed by ornithine transcarbamylase [7]. Arginine deiminase is a medicinal protein for cancer therapy of arginine auxotrophic tumors [8]. Curiously, several researches demonstrated that cancer cell migration has been influenced by the exhausting of arginine. Though motility is a normal physiological process associated with injury healing, embryonic development and immune responses, it is a process used by cancer cells to metastasize to other organs [2]. L-Arginine homeostasis depends on catabolism and transport efficiency of L-arginine through cell membranes. Approximately 80% of L-arginine comes from recycled amino acids released by protein breakdown. The significant impact on the performance of endogenous L-arginine synthesis is the availability of cytokines produced by the enterocytes. It is the pioneer of many substances substantial for the organism [9].

Arginine deiminase, a metabolizing enzyme extracted from *Mycoplasma*, catalyzes arginine to its pioneer citrulline [10]. Besides, *Lactobacillus plantarum* is a Gram-positive widespread probiotic beneficial bacterium, and it can produce arginine deiminase enzyme in the presence of arginine [11]. ADI activity is reported in many lactic acid bacteria including *Leuconostoc*, *Oenococcus*, *Streptococcus* and *Weissella* [12]. Production of ADI enzyme is used as routinely to identify many species of *Enterococcus* like *E. faecium* and *E. faecalis* but *E. pseudoavium*, *E. raffinosus* and *E. avium* can not produce this enzyme [13].

*Bacillus cereus*; It is a facultative aerobic Gr (+) bacterium that is plenty in air, soil and water. It's strains are psychrotrophic and mesophilic. Moreover psychrotrophic strains are found in frozen foods and in some cases fresh nourishments. Mesophilic ones can grow at 37 °C and alive at temperatures below 10 °C. One of the most important features of these bacteria is that they can form endospores and biofilms under stress conditions (low temperature, pH, drought, diverse radiations etc.) [14].

*Ralstonia eutropha* (also *Alcaligenes eutrophus* or *Cupriavidus necator*) is rod-shaped microorganism with wideness of 0.5-1.0 µm and a long of 1.8-2.6 µm. It can use unlike organic synthesis as carbon sources. Optimum reproduction temperatures are about 30 °C. It can degrade nitrates to nitrogen gas. Besides, it is one of the non-pathogenic proteobacteria belonging to the Gr (-) and facultative chemolithotrophic β- class [14]. It is model organism for PHB (Polyhydroxybutyrate) production and commercially can be used for dissimilar goals [15]. When growing heterotrophically, it can use a various organic compounds as the sources of carbon and energy [16]. This study was carried out to investigate the production of Arginine deiminase enzyme in static and shaking (150 rpm) environments in the presence of minimal carbon sources of Gram (-) and Gram (+) some microorganisms.

## 2. MATERIAL AND METHOD

### 2.1. Microorganism and Growth conditions

In this study; *Bacillus cereus* (ATCC 10876) and *Ralstonia eutropha* (ATCC17699) were used. They were produced in an oven at 37 °C for 24 hours by passing them into Nutrient Agar media with loops at intervals of 20 days. The next day, the plates were removed from the oven and stored at +4 °C. Experimental stages were continued by producing bacteria in Nutrient Broth medium by using solid-to-liquid sowing method from these solid nutrient cultures that we prepared in the first stage of the experiment. In addition, Microorganisms were grown in static and shaking (150 rpm) conditions [17].

### 2.2. Carbon sources

1% Dextrose, 1% Glucose, 1% Fructose, 1% Maltose, 1% Nutrient Broth, 1% Rhamnose, 1% Ribose, 1% Sucrose, 1% Xylose.

### 2.3. Chemicals

Tris HCl, CaCl<sub>2</sub>, Dithiothreitol, Bovine Serum Albumin, Benzoyl Arginine Ethyl Ester, Perchloric acid, Iron Ammonium Sulphate Hexahydrate, Ammonium Iron (III) Sulphate Dodecahydrate, Phosphoric acid, H<sub>2</sub>SO<sub>4</sub>, Butanedione Monoxime, Nutrient Agar

### 2.4. Method

100 µl of bacterial cultures were inoculated into NB (Nutrient Broth), PBS and PBS, and nutrient media containing different carbon sources (1% Dextrose, 1% Glucose, 1% Fructose, 1% Xylose, 1% Maltose, 1% NB, 1% Rhamnose, 1% Ribose, 1% Sucrose) 200 µL Tris HCl (pH=7.2) + 100 µL CaCl<sub>2</sub> + 100 µL Dithiothreitol solution + 200 µL culture samples + 200 µL Bovine Serum Albumin solution was added.

It was kept on incubator at 55 °C for min. 100 µL of Benzoyl Arginine Ethyl Ester solution was added. It was kept statically on incubator at 55 °C for 30 minutes. 100

$\mu\text{L}$  of Perchloric acid was added to the samples and the blank. Centrifugation (13.500 rpm) was performed for 5 minutes at room temperature.

400  $\mu\text{L}$  of the prepared mixture was put into new glass tubes. 100  $\mu\text{L}$  of Redox solution (Iron Ammonium Sulphate Hexahydrate + Ammonium Iron (III) Sulphate Dodecahydrate) was added. It was vortexed for 1 second and kept in boiling water for 10 minutes. This solution, which was kept in boiling water, was then cooled in tap water.

500  $\mu\text{L}$  of the acid mixture (3 units of Phosphoric acid + 2 units of  $\text{dH}_2\text{O}$  and 1 unit of  $\text{H}_2\text{SO}_4$ ) was added. 200  $\mu\text{L}$  of Butanedione Monoxime solution was added to it.

The final mixture was vortexed, kept in boiling water for 20 minutes and then cooled in tap water.

The samples were measured at 490 nm against the blank (other mixtures except the enzyme solution and Bovine serum albumin solution) [18]. Arginine deiminase activity (U/mL) were found with the Citrulline Standard graph of the obtained data.

## 2.5. Preparation of Arginine deiminase standard graph

By taking different concentrations (5, 10, 20, 25  $\mu\text{g}/\text{mL}$ ) from commercially available pure citrulline and adding 200  $\mu\text{L}$  Butanedione Monoxime solution + 500  $\mu\text{L}$  Acid mixture (3 units of Phosphoric acid + 2 units of  $\text{dH}_2\text{O}$  and 1 units of  $\text{H}_2\text{SO}_4$ ) on them. It was kept in boiling water for 20 minutes,

Cooled in tap water,

The prepared solutions were measured at a wavelength of 490 nm and a standard graph was obtained with the values obtained.

The amount of Arginine deiminase production of bacteria was compared with the standard graph and the amount was calculated as  $\mu\text{g}/\text{mL}$  [18].

## 3. RESULTS

In a static, stable environment, the microorganism has more oxygen and nutrients, but as the ambient conditions change, when agitation conditions such as 100, 150, 200 rpm are passed, the amount of oxygen and nutrients in the environment begins to decrease. Therefore, in this study, static and shaking culture media were preferred comparatively in order to understand whether microorganisms would react in these environments.

Nutrient Broth is a nutrient medium with a rich content (peptone, yeast extract, salt, water) in which microorganisms can grow. *Bacillus cereus* and *Ralstonia eutropha* showed high Arginine deiminase activity in this medium. *B. cereus* 14.799 (U/mL) under static conditions, *R. eutropha* 17.169; Under shaking conditions (150 rpm), *B. cereus* showed 9.08 (U/mL), *R. eutropha* 7.984 (U/mL).

Looking at minimal environments; The highest ADI activity in *B. cereus* under static conditions was 4.917 U/ml in Ribose medium and 4.265 U/mL in Dextrose medium in the aldose group; showed 3.747 U/mL in maltose medium among disaccharides. *B. cereus* showed ADI activity of 3.895 U/mL in fructose medium. It showed the lowest ADI activity in glucose medium at 2.221 U/mL. In agitated conditions (150 rpm), the highest ADI activity was 4.695 U/mL in Sucrose medium in disaccharides; In the aldose group, it showed 3.302 U/mL in Ribose medium. In agitated conditions, the lowest ADI activity was 2.813 U/mL in dextrose medium (Fig.1).

In *R. eutropha*, the highest ADI activity under static conditions was 3.776 U/mL in Ribose medium in the aldose group; 5.658 U/mL in the Fructose medium in the ketose group; showed 3.761 U/mL in Maltose medium among disaccharides. It showed the lowest ADI activity at 2.132 U/mL in rhamnose medium. In agitated conditions (150 rpm), the highest ADI activity was 4.813 U/mL in sucrose medium in disaccharides; showed 3.436 U/mL in Ribose medium in the aldose group. It showed 3.924 U/mL ADI activity in fructose medium, which is in the ketose group. In agitated conditions, the lowest ADI activity was 2.102 U/mL in rhamnose medium (Fig. 2).

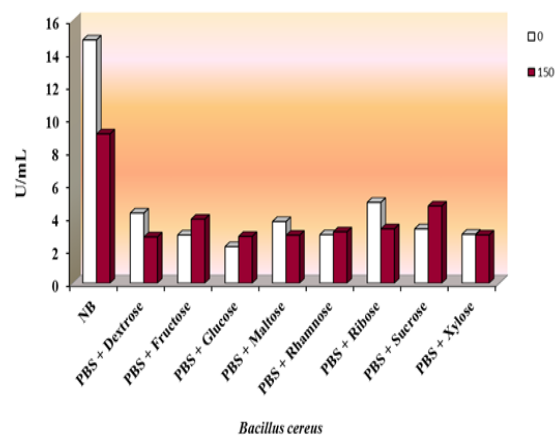


**Figure 1.** Arginine deiminase activity (U/mL) at 0 and 150 rpm under minimal conditions in *Bacillus cereus*

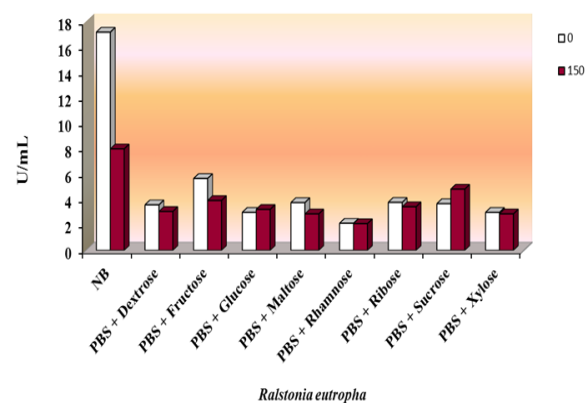


**Figure 2.** Arginine deiminase activity (U/mL) at 0 and 150 rpm under minimal conditions in *Ralstonia eutropha*

#### 4. DISCUSSION AND CONCLUSION

Biologically structured molecules (for example, enzymes, proteins) provide the continuity of life by performing biochemical reactions in the living system. It is also used as therapeutic agents in cancer, coronary heart diseases, neurological disorders and many other diseases that cause fatal diseases. [19]. Arginine deiminase, is an important anti-cancer enzyme produced by many microorganisms. It is catalyzed by many microorganisms such as *Mycoplasma arginini*, *Pseudomonas aeruginosa* and some species of *Enterococcus* [13]. In the experiments of Sharma et al., *Pseudomonas aeruginosa* PS2 strain showed 3.12 IU/mL ADI activity in minimal medium + 0.5 % galactose medium [19]. In our study, in static conditions, the highest ADI activity was found in *B. cereus* PBS + 1 % Ribose medium at 4,917 U/mL (Fig.1); in agitated conditions, *R. eutropha* showed 4,813 U/mL in PBS + 1 % Sucrose medium (Fig. 2).

In the research of Dhankhar et al., *Pseudomonas furukawaii* RS3 strain showed the highest ADI activity at 0.222  $\mu\text{mol/mL}$  in Super Broth medium + 1.5 % Fructose medium [20]. In our study, *B. cereus* was 3.895 U/mL (Fig. 1); *R. eutropha* showed 5,658 U/mL in PBS + 1% Fructose medium (Fig. 2). When we look at the results; *B. cereus* and *R. eutropha* showed the highest ADI activity in the disaccharide media, maltose and sucrose, and ribose in the aldose group.

Mahdy et al. (2014) conducted a study on ADI activity by adding different carbon sources to the Mineral Salt Broth medium under different conditions (1% Glucose, 1% Fructose, 1% Maltose, 1% Sucrose, 1% Arabinose, 1% Rhamnose, 1% Xylose, 1% Sorbitol and 1% Mannitol) with *Enterococcus faecium* M1 strain. *Enterococcus faecium* M1 showed the highest ADI activity in 1% Sucrose medium (3.9 U/mg) [21]. In our study; *R. eutropha* showed the highest ADI activity at 3.673 U/mL in PBS + 1% Sucrose medium under static conditions. *R. eutropha* showed the highest ADI activity at 4.813 U/mL under shaking conditions (Fig.2).

Ibrahim et al. (2019) conducted a study on ADI activity by adding 0.5% (glucose, galactose, lactose, maltose) different carbon sources to the minimal nutrient medium under different conditions with *Pseudomonas aeruginosa*. It showed the highest ADI activity in 0.5% maltose medium (1.2 U/mg) [22]. In our study; In PBS + 1% Maltose medium, *R. eutropha* showed the highest ADI activity of 3.761 U/mL under static conditions (Fig.2). In shaking conditions, *B. cereus* showed the highest ADI activity at 2.917 U/mL (Fig.1).

Khaleed Shaikh and Khobragade (2019); The Screening made a study on ADI activity by adding 0.2% (fructose, galactose, glucose, maltose, sucrose) different carbon sources to the medium with 11 bacterial isolates. These bacterial isolates showed the highest ADI activity in 0.2 % glucose medium (0.3-0.35 U/mL) [23]. In our study; *R. eutropha* showed the highest ADI activity at 2.991 U/mL in PBS + 1% Glucose medium under static

conditions. *R. eutropha* showed the highest ADI activity at 3.228 U/mL under shaking conditions (Fig.2).

Unissa et al. (2015) investigated ADI activity by adding various carbon sources (glucose, glycerol, maltose, mannitol, sucrose) to a nutrient medium containing 2% sea water with *Vibrio alginolyticus* 1374 strain. It showed the highest ADI activity in the presence of 2% sea water + 2% Maltose (192 IU/mL) [24].

With this study, it has been shown that Arginine deiminase, an important anti-cancer enzyme, can be produced with Gram (+) (*B. cereus*) and Gram (-) (*R. eutropha*) bacteria in less costly minimal environments. In addition, it is thought that this study will contribute to the literature.

#### Acknowledgement

This research study was supported by a Grant (APYB 2020/2145) from Research Fund Unit of Inonu University, Turkey.

#### REFERENCES

- [1] Iqbal J., Abbasi B.A., Mahmood T., Kanwal S., Ali B., Shah S.A., Khalil A.T. Plant-derived anticancer agents: A green anticancer approach, Asian Pac J Trop Biomed. 2017; 7(12): 1129–1150.
- [2] Al-Koussa H., El Mais N., Maalouf H., Abi-Habib R., El-Sibai M. Arginine deprivation: a potential therapeutic for cancer cell metastasis? A review, Cancer Cell Inter. 2020; 20(150): 1-7.
- [3] Prajapati B., Supriya N. R. Review on anticancer enzymes and their targeted amino acids, World J Pharm Res, 2017; 6(12), 268-284.
- [4] Zolfaghar M., Amoozegar M. A., Khajeh K., Babavalian H., Tebyanian H. Isolation and screening of extracellular anticancer enzymes from halophilic and halotolerant bacteria from different saline environments in Iran, Mol Biol Rep, 2019; 46: 3275–3286.
- [5] Özalp Erenler Ş. L-asparaginaz geninin (ansB) farklı gram-negatif bakterilere klonlanması, izolasyonu ve ekspresyonu (Doktora tezi). 2007; İnönü Üniversitesi, Fen Bilimleri Enstitüsü, Malatya
- [6] Zarei M., Nezafat N., Rahbar M.R., Negahdaripour M., Sabetian S., Morowvat M.H., Ghasemi Y. Decreasing the immunogenicity of arginine deiminase enzyme via structure-based computational analysis, J Biomol Structure and Dynamics. 2019; 37(2): 523-536.
- [7] Kahraman H., Karaderi C.C., The Importance of Arginine deiminase, Arch Chem and Chem Eng. 2019; 1(1): 1-3.
- [8] Cheng F., Yang J., Schwaneberg U., Zhu L. Rational surface engineering of an arginine deiminase (an antitumor enzyme) for increased PEGylation efficiency, Biotechnol Bioeng. 2019;116: 2156–2166.

- [9] Szeffel J., Danielak A., Kruszewski W.J. Metabolic pathways of L-arginine and therapeutic consequences in tumors, *Adv in Med Sci.* 2019; 64:104-110.
- [10] Zou S., Wang X., Liu P., Ke C., Xu S. Arginine metabolism and deprivation in cancer therapy, *Biomed Pharm.* 2019; 118:1-11.
- [11] Zaki Mahdi N. Investigation of the lethal effect of purified Arginine deiminase purified from *Lactobacillus plantarum* p5 on murine mammary adenocarcinoma and vero cell lines, *Archives of Razi Institu.* 2022; 77(1): 223-229.
- [12] Kaur B., Kaur R. Application of Response Surface Methodology for Optimizing Arginine deiminase Production Medium for *Enterococcus faecium* sp. GR7, *The Sci World J.* 2013; 1-12.
- [13] Mahdy N.Z., Al-Tahan S.S., Yaseen N.Y., Optimization of Arginine deiminase production from a local higher productive isolate *Enterococcus faecium* M1, *Iraqi J Cancer and Med Genet*, 2014; 7(1):36-43.
- [14] Karaderi C.C., Kahraman H. Trehalose Production at Different Mediums in *Bacillus cereus* and *Ralstonia eutropha*, *Acta Sci Agricul.* 2021; 5(10): 2-4.
- [15] Juengert J.R., Borisova M., Mayer C., Wolz C., Brigham C.J., Sinskey A.J., Jendrossek D. Absence of ppGpp leads to increased mobilization of intermediately accumulated Poly (3-Hydroxybutyrate) in *Ralstonia eutropha* H16, *Appl Environ Microbiol.* 2017; 83(13): 1-17.
- [16] Arenas-López, C., Locker, J., Orol, D., Walter, F., Busche, T., Kalinowski, J., Minton, N.P., Kovács, K., Winzer, K., The genetic basis of 3-hydroxypropanoate metabolism in *Cupriavidus necator* H16, *Biotechnol for Biofuels.* 2019; 12(150): 1-16.
- [17] Karaderi, C.C., Bakterilerin Farklı Karbon Kaynaklarının Varlığında Arjinin deiminaz, Trehalaz ve Poli Hidroksi Bütirat Üretiminin Araştırılması (Doktora Tezi), İnönü Üniversitesi, Malatya. 2022.
- [18] Takahara H., Okamoto H., Sugawara K. Enzymatic assay of peptidyl Arginine deiminase, *J Biochem.* 1986; 99:1417- 1424.
- [19] Sharma A., Bala K., Husain I. Optimization of Arginine Deaminase production from Indigenous bacterium *Pseudomonas aeruginosa* PS2, *Int J Curr Microbiol Appl Sci.* 2017; 6(11): 3621-3632.
- [20] Dhankhar R., Kumar A., Kumar S., Chhabra D., Shukla P., Gulati P. Multilevel algorithms and evolutionary hybrid tools for enhanced production of arginine deiminase from *Pseudomonas furukawaii* RS3, *Bioresour Technol.* 2019; 290: 1-9.
- [21] Mahdy N.Z., Al-Tahan S.S., Yaseen N.Y. Optimization of arginine deiminase production from a local higher productive isolate *Enterococcus faecium* M1, *Iraqi J Cancer Med Genet*, 2014; 7(1): 36-43.
- [22] Ibrahim R.A., Hussein A.A., Abdulwahed S. Optimizing arginine deiminase production from *Pseudomonas aeruginosa* clinical isolate, *J Pharm Sci Res*, 2019; 11(2): 656-660.
- [23] Khaleed Shaikh A.N., Khobragade R.M. Production and partial purification of arginine deiminase isolated from bacteria, *J Emerg Technol Innov Res*, 2019; 6(3): 241-248.
- [24] Unissa R., Sudhakar M., Kumar Reddy A.S. Condition optimization and production of extracellular l-Arginine deiminase from *Vibrio alginolyticus* 1374, *Curr Biotechnol*, 2015; 4: 254-260

## Amoebicidal Effect of Fluconazole and Verapamil Together Against Trophozoites and Cysts of *Acanthamoeba castellanii*

Mehmet AYKUR<sup>1\*</sup> 

<sup>1</sup> Tokat Gaziosmanpaşa University, Medicine Faculty, Parasitology Department, Tokat, Türkiye  
 Mehmet AYKUR ORCID No: 0000-0002-6100-1037

\*Corresponding author: [mehmetaykur@gmail.com](mailto:mehmetaykur@gmail.com)

(Received: 02.03.2023, Accepted: 12.06.2023, Online Publication: 22.06.2023)

### Keywords

*Acanthamoeba castellanii*,  
 Fluconazole,  
 Verapamil,  
 Combination,  
 Amoebicidal effect,  
 Growth inhibition

**Abstract:** *Acanthamoeba* species are important pathogens that causes *Acanthamoeba* keratitis, which causes a visual loss, as well as central nervous system infection and death by causing encephalitis. Due to the limited available options to successfully treat *Acanthamoeba* infections, new therapeutic approaches must be developed, and especially combination drug therapy may be a successful and effective strategy. The aim of this study was to assess the combination efficacy of verapamil and fluconazole against *Acanthamoeba* trophozoites and cysts. The effects of drugs on growth inhibition against *Acanthamoeba* were tested using amoebicidal assays. The viability of *Acanthamoeba* was assessed using Trypan blue and hemocytometer counts. The effect of three different concentrations of “fluconazole”, “verapamil” and “fluconazole + verapamil” combination on growth inhibition against *Acanthamoeba* trophozoites and cysts was significant compared to the control ( $p < 0.05$ ). While *Acanthamoeba* reduced the viability of 250 µg/ml fluconazole and verapamil on trophozoites to  $2.3 \times 10^4$  and  $3 \times 10^4$  numbers, fluconazole + verapamil combination showed 100% growth inhibition on trophozoites. Moreover, the combination of 250 µg/ml fluconazole + verapamil showed up to 90% growth inhibition on cysts. As a result, it was revealed that the combination of fluconazole and verapamil was more effective against the trophozoites and cysts of *Acanthamoeba*.

104

## *Acanthamoeba castellanii*'nin Trofozoitleri ve Kistlerine Karşı Flukonazole ve Verapamil'in Birlikte Amip Öldürücü Etkisi

### Anahtar Kelimeler

*Acanthamoeba castellanii*,  
 Flukonazol,  
 Verapamil,  
 Kombinasyonu,  
 Amip öldürücü etkisi,  
 Büyüme inhibisyonu

**Öz:** *Acanthamoeba* türleri, görme kaybına neden olan *Acanthamoeba* keratiti ve ayrıca merkezi sinir sistemi enfeksiyonuna ve ensefalite neden olarak ölüme yol açan önemli bir patojendir. *Acanthamoeba* enfeksiyonlarını başarılı bir şekilde tedavi etmek için mevcut seçeneklerin başarısı sınırlı olmasından dolayı yeni terapötik yaklaşımlar geliştirilmelidir ve özellikle kombinasyon ilaç tedavisi başarılı ve etkili bir strateji olabilir. Bu çalışmanın amacı, *Acanthamoeba* trofozoitleri ve kistlerine karşı verapamil ve flukonazol kombinasyonunun etkinliğini değerlendirmektir. İlaçların *Acanthamoeba*'ya karşı büyüme inhibisyonu üzerine etkileri amoebisidal yöntemler kullanılarak test edildi. *Acanthamoeba*'nın canlılığı, tripan mavisi ve hemositometre sayımları kullanılarak değerlendirildi. Flukonazol, verapamil ve flukonazol + verapamil kombinasyonunun üç farklı konsantrasyonunun *Acanthamoeba* trofozoitleri ve kistlerine karşı büyüme inhibisyonu üzerindeki etkisi, kontrol ile karşılaştırıldığında anlamlı bulundu ( $p < 0.05$ ). *Acanthamoeba*, 250 µg/ml flukonazol ve verapamilin trofozoitler üzerindeki canlılığını  $2,3 \times 10^4$  ve  $3 \times 10^4$ 'e düşürürken, flukonazol + verapamil kombinasyonu trofozoitler üzerinde % 100 büyüme inhibisyonu göstermiştir. Ayrıca, 250 µg/ml flukonazol + verapamil kombinasyonu, kistlerde % 90'a varan büyüme inhibisyonu göstermiştir. Sonuç olarak, *Acanthamoeba*'nın trofozoitlerine ve kistlerine karşı flukonazol ile verapamil'in kombinasyonunun daha etkili olduğu ortaya konuldu.

## 1. INTRODUCTION

The genus *Acanthamoeba* is widely found in the natural environment [1]. *Acanthamoeba* can also be found in many environmental specimens such as seawater, river water, lakes, swimming pools, soil, and contact lens and lens solutions [2]. Throughout its life cycle, *Acanthamoeba* has two forms: an active trophozoite form that may reproduce by binary fission and a latent cyst form under unfavorable environmental circumstances. The cyst stage is a defense mechanism for survival in adverse environmental conditions [1]. *Acanthamoeba* species are resistant to various antibiotics, chlorine and low temperatures in the cyst stage [3]. According to the sequence of study of the 18S rRNA gene, the molecular classification of *Acanthamoeba* species has been established, and 23 genotypes have been reported so far. [4, 5]. The *Acanthamoeba* genus can cause fatal brain infections known as granulomatous amebic encephalitis (GAE), as well as vision-threatening corneal ulcers called *Acanthamoeba* Keratitis (AK) [6].

The use of contact lenses is the biggest risk factor for AK in industrialized nations, whereas trauma (including contact with plant material) and corneal exposure to polluted soil and water are bigger risk factors in underdeveloped nations [7]. In addition to increasing the danger of corneal *Acanthamoeba* exposure, contact lens solutions also raise the possibility of being linked to ongoing AK outbreaks [8]. Even though there are an estimated 125 million contact lens wearers worldwide, that number is rising each year [9].

AK is not considered in the differential diagnosis since it is uncommon in comparison to other infections that cause keratitis [10]. For this reason, because the diagnosis cannot be made on time, empirical treatment with various drugs is started and long-term use is ensured [11]. Although there is no definitive treatment for the treatment of *Acanthamoeba* infection, long-term anti-amoebic treatment is required to entirely remove both the forms of the parasite. No selective drug has been developed for *Acanthamoeba* infections [4, 12, 13]. Polyhexamethylene biguanide (PHMB) and chlorhexidine digluconate are currently the most commonly used eye drops in the treatment of AK, and it is recommended to be used every 1-2 hours and then tapering off over time to achieve full recovery [14]. In addition, amphotericin B, voriconazole, itraconazole, azithromycin, rifampin, and miltefosine was used systemically to treat *Acanthamoeba* infections [15, 16]. Although some antifungals and antibiotics have been used in *Acanthamoeba* infections, the available anti-amoebic agents that will fully affect AK infection are still limited [10]. Hence, alternative strategies to the development of new anti-amebic drugs are urgently needed.

Fluconazole is important in preventing fungal keratitis infections in the azole group, with its low toxicity and cost even when used at high doses. However, new drugs available are limited due to increasing drug resistance [17]. The mechanism of action of fluconazole interacts with the cytochrome P-450 enzyme 14-demethylase,

fluconazole, which catalyzes the conversion of lanosterol to ergosterol. Ergosterol is a crucial component of the cell membranes of fungi and *Acanthamoeba*, and fluconazole prevents its formation from making cells more permeable [18, 19]. Various calcium channel-blocking agents, such as amlodipine and loperamide have been reported to have anti-amoebic effects against *Acanthamoeba* and FLA [20]. Therefore, calcium channel blockers suggest that they are effective on FLA.

It has been demonstrated that calcium channel blockers, which are medications frequently used to treat cardiovascular diseases, have a variety of anti-fungal, antibiotic, and antiparasitic properties [21, 22]. It is known that calcium channels are involved in crucial cellular processes including the development of parasitic protozoan diseases [20]. Recent studies have provided evidence for the presence of voltage-sensitive calcium channels in *Acanthamoeba* [20, 23]. Various calcium channel blockers have been shown to have an anti-amoebic effect on *Acanthamoeba* [24]. It has been reported that some known antifungal agents are more effective with combinations of calcium channel blockers [25, 26]. In this study, we aimed to test the synergistic effects of fluconazole and verapamil together for the treatment of *Acanthamoeba* keratitis on the clinical strain *Acanthamoeba castellanii* using growth inhibition and viability assays.

## 2. MATERIAL AND METHOD

### 2.1. Chemicals

The chemicals including Trypan blue (Gibco), Page's saline solution, proteose peptone (Sigma Aldrich), gentamicin, yeast extract (Merck, Germany), glucose (Sigma Aldrich), agar (Oxoid no.1), phosphate-buffered saline (PBS) (Invitrogen Corp., Carlsbad, Calif.) was used in the present study. Fluconazole topical solution (Fluzamed, 0,3%, 3 mg/ml, World Medicine Pharmaceuticals Industry), verapamil hydrochloride (Isoptin, 80 mg, tablet, Abbott Laboratories) was purchased commercially. To prepare the verapamil hydrochloride, 80 mg was added into sterile 10 ml of distilled water to obtain a concentration of 8 mg/ml. Verapamil hydrochloride was prepared separately at three different concentrations (50 µg/ml, 100 µg/ml, and 250 µg/ml), and stored at +4°C until use.

### 2.2. *Acanthamoeba* Isolate and Culture

The clinical isolate of *Acanthamoeba castellanii* (GenBank No: ON600792.1) identified as genotype T4 used in this study was isolated from a patient with keratitis in previously study [27]. The clinical isolate was cultured axenically in PYG medium in 25 cm<sup>2</sup> culture flasks at 37 °C. Briefly, PYG medium was included proteose peptone 0.75% (w/v), yeast extract 0.75% (w/v), glucose 1.5% (w/v), Page's saline solution (PAS; 0.12 g NaCl, 0.04 g MgSO<sub>4</sub>·7H<sub>2</sub>O, 0.04 g CaCl<sub>2</sub>·2H<sub>2</sub>O, 0.142 g Na<sub>2</sub>HPO<sub>4</sub>, 0.136 g KH<sub>2</sub>PO<sub>4</sub> per liter of distilled water) one liter distilled water containing 40 µg/mL gentamicin. The *Acanthamoeba* culture flask was incubated at 30 °C, and



the media in flask was refreshed after every 24 h of incubation. *Acanthamoeba* trophozoite forms that adhered on the bottom of the flasks were collected by incubating on ice for 20 minutes and gently shaking.

### 2.3. Amoebicidal Activity Assay

To determine the anti-*acanthamoeba* activities of each drug, *Acanthamoeba* trophozoites ( $2 \times 10^5$  amoeba/ml/tube) were incubated in PBS with different concentrations of fluconazole (50 µg/ml to 250 µg/ml) and verapamil hydrochloride (50 µg/ml to 250 µg/ml) in capped microcentrifuge tubes (1.5 ml) at 37 °C for 24 hours. Following this incubation, the number of *Acanthamoeba* trophozoites was determined by hemocytometer counting. The number of *Acanthamoeba* incubated with PBS alone was used as control 100%. The viability of *Acanthamoeba* was assessed by adding 0.1% Trypan blue to live (unstained) and dark blue for dead amoebae using a hemocytometer under a light microscope. The results are representative as the mean  $\pm$  standard error of three independent experiments performed in duplicate. The growth inhibition percentage was calculated according to the equation  $(A - B/A) \times 100$ , where A = the mean number of viable *Acanthamoeba* in the control group and B = the mean number of viable *Acanthamoeba* in the treatment groups [24].

### 2.4. Cysticidal Activity Assays

For cysticidal assay, *Acanthamoeba* cyst form was prepared using 1.5 % non-nutrient agar plates as described previously [24, 28]. Briefly, *Acanthamoeba* trophozoites ( $2 \times 10^5$  amoeba) were transferred from PYG medium to NNA plate and incubated at 37 °C for at least two weeks. Then, whether the trophozoites transformed into cysts was checked under an inverted microscope. After incubation, the cysts were removed from the NNA plates by adding PBS and using a cell scraper and transferred to 15 ml tubes. Tubes were centrifuged at 2000 x g for 10 minutes and cysts were counted using a hemocytometer. The *Acanthamoeba* cysts were transferred to microcentrifuge tubes as  $2 \times 10^5$  cysts/ml and incubated in PBS with different drug concentrations for 24 hours at 37 °C. After incubation, centrifugation was done at 2000 x g for 10 minutes to remove the effects of the drugs and the supernatant was discarded. This process was performed with three-times washes with PBS to remove the effect of the drug. After incubation, whether the cysts transformed into trophozoite form was counted under the light microscope using a hemocytometer. Each drug was evaluated in triplicate, and each experiment was performed in duplicate.

### 2.5. Statistical Analysis

The data are presented as mean values with standard error and calculated the average of the groups on Microsoft Excel sheet. Two sample *t*-test; two-tailed distribution were used for analysis of the data. The statistical analysis was carried out using Graph Pad Prism v.8.0 software. The significant value  $p < 0.05$  is used for all evaluations.

## 3. RESULTS AND DISCUSSION

### 3.1. Amoebicidal Effects Against *Acanthamoeba castellanii* Trophozoites

The anti-*acanthamoebic* effects of fluconazole and verapamil on *Acanthamoeba* trophozoites at various concentrations were evaluated. At 50 µg/ml fluconazole and verapamil caused a reduction in the number of *Acanthamoeba* trophozoites from  $9 \times 10^4$  and  $1 \times 10^5$  (from  $2 \times 10^5$ ), respectively, resulting in 50 % inhibition on growth of *Acanthamoeba* ( $p < 0.005$ ) (Figure 1). However, the combined effect of 50 µg/ml fluconazole + verapamil was significant compared to the control, in which it showed effects more than the effect of a single drug and showed 67 % growth inhibition on trophozoites of *Acanthamoeba castellanii* ( $p < 0.005$ ) (Figure 2). The effects of 100 µg/ml fluconazole and verapamil on *Acanthamoeba* trophozoites were decreased  $5 \times 10^4$  and  $6.6 \times 10^4$  numbers, respectively (Figure 1). Although fluconazole and verapamil (100 µg/ml) showed growth inhibition of 70 % on the viability of *Acanthamoeba* trophozoites, the combination of these two drugs (fluconazole + verapamil) had a growth inhibition effect of 87% (Figure 2). At 250 µg/ml concentration of fluconazole and verapamil exhibited significant effects against *Acanthamoeba castellanii* trophozoites ( $p < 0.001$ ) (Figure 1). At 250 µg/ml fluconazole + verapamil significantly reduced the number of viable *Acanthamoeba* trophozoites to  $6.6 \times 10^3$  as compared to the control ( $2 \times 10^5$ ) ( $p < 0.001$ ) (Figure 1). In particular, fluconazole + verapamil (250 µg/ml) showed approximately 100 % growth inhibition effects on trophozoites (Figure 2). The results showed that although the drugs had a dose-dependent lethal effect against the *Acanthamoeba* trophozoites, the combined effect of drug concentrations was much stronger on the trophozoites. *Acanthamoeba castellanii* trophozoites were found to be statistically significant with all drug concentrations as compared to the control ( $p < 0.001$ ,  $p < 0.005$ ,  $p < 0.05$ ) (Figure 1). The previous two studies, the minimum amoebicidal concentration on trophozoites of *Acanthamoeba* of fluconazole was reported to be  $>320$  µg/ml and  $> 1024$  µg/ml [29, 30]. In another study was observed that the effects of fluconazole on clinical isolates of *Acanthamoeba castellanii* were more susceptible to environmental isolates such as *Acanthamoeba lenticulate* and *Acanthamoeba hatchetti* and also, the minimal inhibition concentration ranged from 64 to 256 µg/ml [31]. Baig et al. reported the presence of calcium channels in *Acanthamoeba castellanii*. It also revealed the effect of various calcium channel blockers on *Acanthamoeba* [20]. In addition, Baig et al. showed that the effects of voltage-sensitive calcium channel blockers such as verapamil and nifedipine on *Acanthamoeba castellanii* trophozoites range from 50 to 100 µg/ml [32]. In another study, the effect of fluconazole alone was more than two-fold as effective against *Candida albicans* when combined with calcium channel blockers such as amlodipine, nifedipine, benidipine, and flunarizine [17].

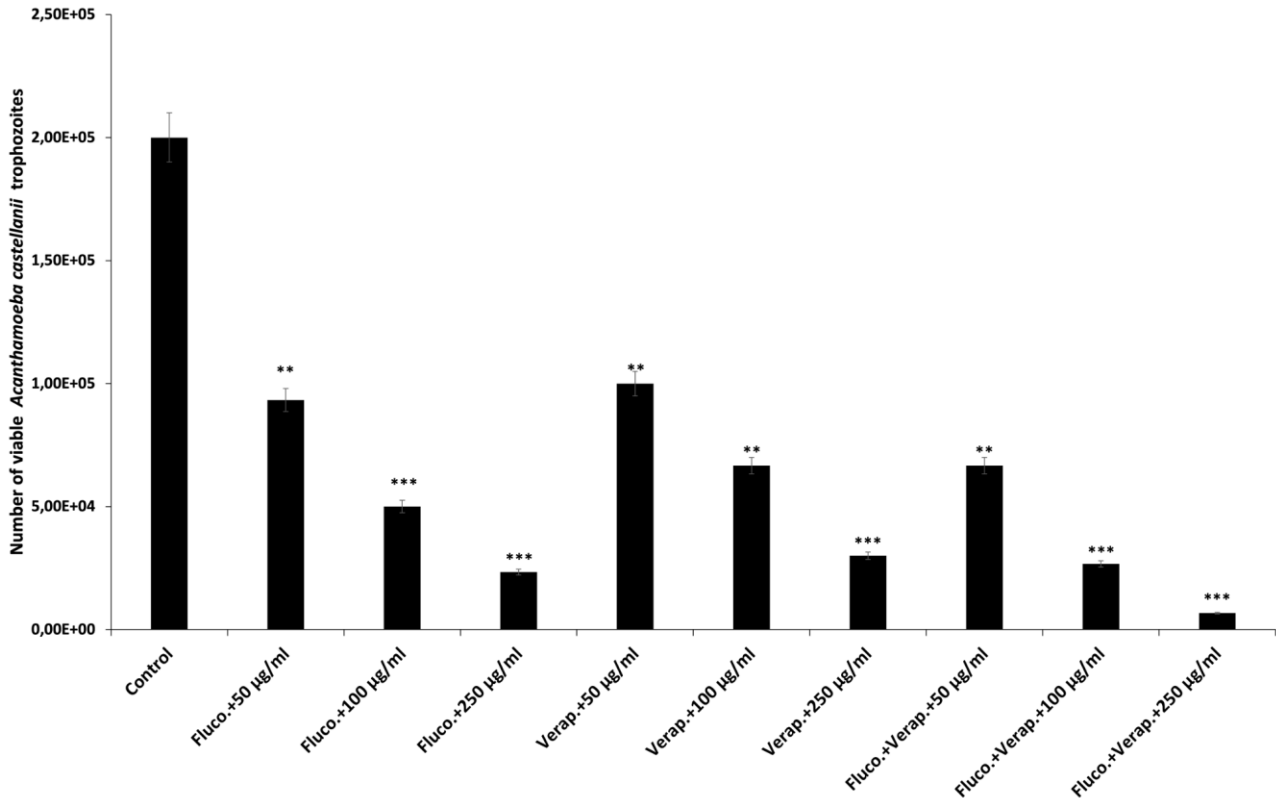


**Figure 1.** *Acanthamoeba castellanii* viability effects of various drugs were determined using Trypan blue staining. *Acanthamoeba castellanii* ( $2 \times 10^5$  trophozoites) was incubated with (50 µg/ml, 100 µg/ml and 250 µg/ml) fluconazole, verapamil and fluconazole + verapamil drugs at 37 °C for 24 h. The results show significant anti-*acanthamoebic* activity when compared to the control ( $***p < 0.001$ ,  $**p < 0.005$ ,  $*p < 0.05$ )

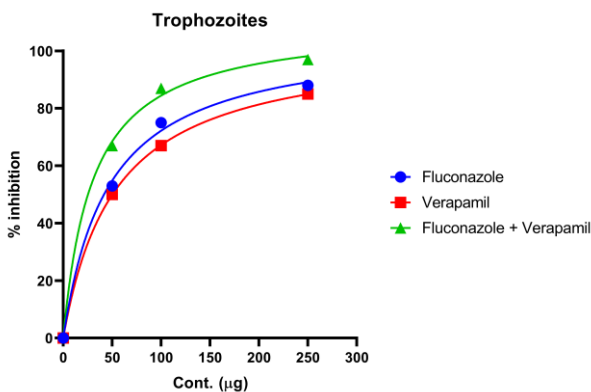


**Figure 2.** Growth inhibition curve of *Acanthamoeba castellanii* trophozoite at different concentrations. Growth inhibition curves of trophozoites treated with fluconazole, verapamil, and fluconazole + verapamil at 24 h.

### 3.2. Cysticidal Effects Against *Acanthamoeba castellanii* Cysts

Three different drug concentrations were evaluated by scraping *Acanthamoeba castellanii* cysts on non-nutrient agar plates after at least two weeks at 37 °C. It was observed that the drugs at 50, 100 and 250 µg/ml concentrations of fluconazole reduced the number of viable *Acanthamoeba castellanii* cysts by  $1.48 \times 10^5$ ,  $1.03 \times 10^5$  and  $8 \times 10^4$  as compared to the control ( $2 \times 10^5$  cysts) ( $*p < 0.05$ ,  $**p < 0.005$ ,  $***p < 0.001$ ) (Figure 3). At 50 µg/ml fluconazole showed 27 % growth inhibition on the viability of the cysts, while 250 µg/ml fluconazole had a growth inhibition of more than 50 % (Figure 4). Similar to the effect of fluconazole, 50, 100, and 250

µg/ml verapamil had a reduction effect of  $1.53 \times 10^5$ ,  $1.2 \times 10^5$  and  $7 \times 10^4$  in the number of viable *Acanthamoeba castellanii* cysts ( $*p < 0.05$ ,  $**p < 0.005$ ,  $***p < 0.001$ ) (Figure 3). While the 250 µg/ml concentration of fluconazole and verapamil showed growth inhibition of 61 % and 66 %, respectively, on the viability of *Acanthamoeba castellanii* cysts, 100 µg/ml Fluconazole + verapamil showed 60 % growth inhibition (Figure 4). At 250 µg per ml of fluconazole + verapamil showed up to 90 % growth inhibition (Figure 4).

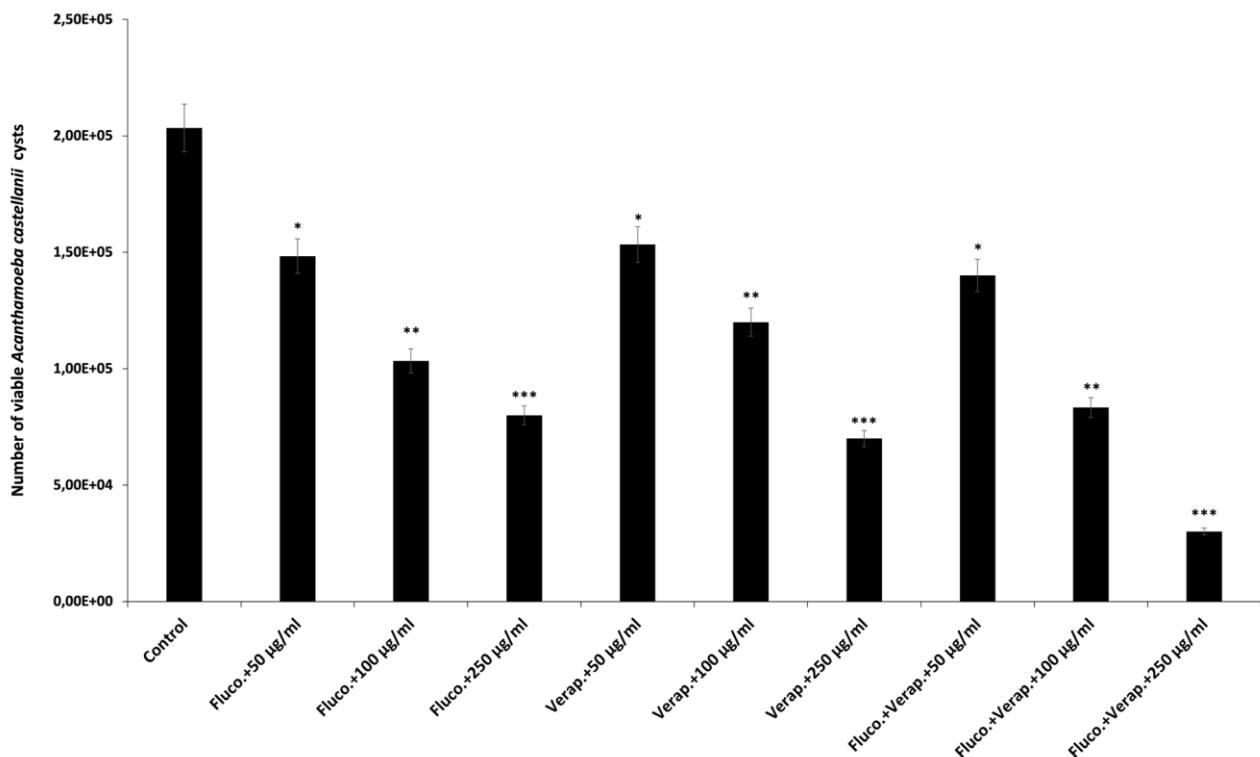


**Figure 3.** *Acanthamoeba castellanii* viability effects of various drugs were determined using Trypan blue staining. *Acanthamoeba castellanii* ( $2 \times 10^5$  cysts) was incubated with (50 µg/ml, 100 µg/ml and 250 µg/ml) fluconazole, verapamil and fluconazole + verapamil drugs at 37 °C for 24 h. The results show significant anti-acanthamoebic activity when compared to the control (\*\*\* $p < 0.001$ , \*\* $p < 0.005$ , \* $p < 0.05$ )

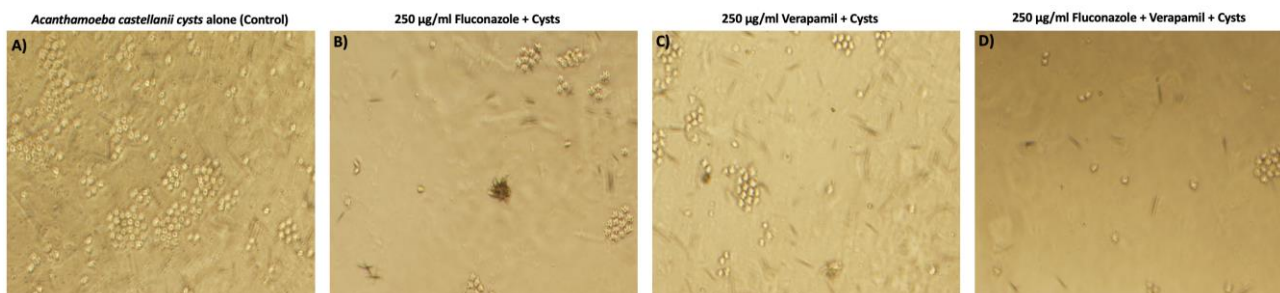


**Figure 5.** Representative effects of fluconazole, verapamil, and combination fluconazole + verapamil on inhibiting the viability of *Acanthamoeba castellanii* cysts. **A)** *Acanthamoeba castellanii* alone (control); **B)** Fluconazole +250 µg/ml; **C)** Verapamil +250 µg/ml; **D)** Fluconazole + Verapamil+250 µg/ml

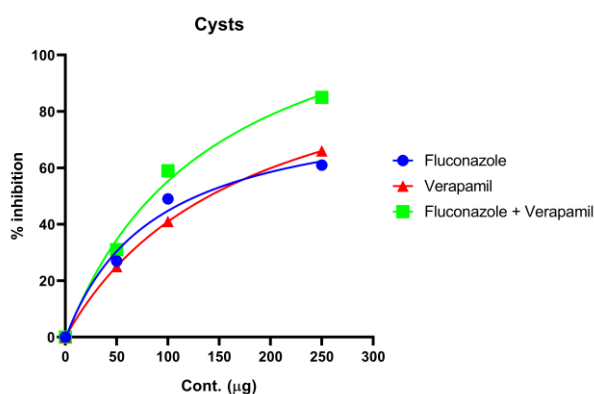


**Figure 4.** Growth inhibition curve of *Acanthamoeba castellanii* cysts at different concentrations. Growth inhibition curves of trophozoites treated with fluconazole, verapamil, and fluconazole + verapamil at 24 h.

The growth inhibition assay revealed that both fluconazole and verapamil alone and the combination of fluconazole + verapamil exhibited cysticidal effects on

the growth of *Acanthamoeba castellanii*. The cysticidal activity analysis results are supported by representative images recorded at x100 magnification (Figure 5). Therefore, the combination effect of fluconazole and verapamil was observed to increase growth inhibition with increasing dose. In the previous studies, cysticidal activity of fluconazole on *Acanthamoeba* was reported as >500 µg/ml and >128 µg/ml [30, 33]. Nakaminami et al. reported that the effect of fluconazole on *Acanthamoeba* cysts showed the minimum cystic concentration range from 256 to 512 µg/ml [9]. Anti-infective effects of calcium channel blocking agents such as amlodipine have been reported against *Candida* spp. and *Acinetobacter baumannii* [34, 35]. The effects of amlodipine on various *Candida* spp. at doses of 256 µg/mL and on *Acinetobacter baumannii* at dose ranges of 40 to 320 µg/ml demonstrated the antibiotic potential of these calcium channel blockers [34, 35].

#### 4. CONCLUSION

Recently, it was reported that the presence of calcium channels that are comparable to human calcium channels and the impact of calcium ions on *Acanthamoeba* viability and growth. Furthermore, calcium channel blockers (amlodipine, loperamide, nifedipine and verapamil) have been found to have amoebicidal effects on *Acanthamoeba*. In our study, although fluconazole and verapamil have influenced *Acanthamoeba* trophozoites and cysts, it was observed that the effect increased, especially with the increase in the dose of the drugs. Fluconazole alone had a minimal impact on the survivability of *Acanthamoeba* trophozoites, but when combined with verapamil, it completely inhibited proliferation. This study revealed that the combined effects of fluconazole and verapamil were very effective against *Acanthamoeba* trophozoites and cystic.

#### REFERENCES

- [1] Khan NA. *Acanthamoeba*: biology and increasing importance in human health. *FEMS microbiology reviews*. 2006;30(4):564-95.
- [2] Marciano-Cabral F, Cabral G. *Acanthamoeba* spp. as agents of disease in humans. *Clinical microbiology reviews*. 2003;16(2):273-307.
- [3] De Jonckheere JF. Ecology of *Acanthamoeba*. *Reviews of infectious diseases*. 1991;13 Suppl 5:S385-7.
- [4] de Lacerda AG, Lira M. *Acanthamoeba* keratitis: a review of biology, pathophysiology and epidemiology. *Ophthalmic Physiol Opt*. 2021;41(1):116-35.
- [5] Putaporntip C, Kuamsab N, Nuprasert W, Rojrung R, Pattanawong U, Tia T, et al. Analysis of *Acanthamoeba* genotypes from public freshwater sources in Thailand reveals a new genotype, T23 *Acanthamoeba bangkokensis* sp. nov. *Scientific reports*. 2021;11(1).
- [6] Visvesvara GS, Moura H, Schuster FL. Pathogenic and opportunistic free-living amoebae: *Acanthamoeba* spp., *Balamuthia mandrillaris*, *Naegleria fowleri*, and *Sappinia diploidea*. *FEMS immunology and medical microbiology*. 2007;50(1):1-26.
- [7] Radford CF, Bacon AS, Dart JK, Minassian DC. Risk factors for *acanthamoeba* keratitis in contact lens users: a case-control study. *Bmj*. 1995;310(6994):1567-70.
- [8] Carnt N, Hoffman JJ, Verma S, Hau S, Radford CF, Minassian DC, et al. *Acanthamoeba* keratitis: confirmation of the UK outbreak and a prospective case-control study identifying contributing risk factors. *British Journal of Ophthalmology*. 2018;102(12):1621-8.
- [9] Nakaminami H, Tanuma K, Enomoto K, Yoshimura Y, Onuki T, Nihonyanagi S, et al. Evaluation of In Vitro Antiamoebic Activity of Antimicrobial Agents Against Clinical *Acanthamoeba* Isolates. *Journal of ocular pharmacology and therapeutics : the official journal of the Association for Ocular Pharmacology and Therapeutics*. 2017.
- [10] Lorenzo-Morales J, Khan NA, Walochnik J. An update on *Acanthamoeba* keratitis: diagnosis, pathogenesis and treatment. *Parasite*. 2015;22:10.
- [11] Varacalli G, Di Zazzo A, Mori T, Dohlman TH, Spelta S, Coassin M, et al. Challenges in *Acanthamoeba* Keratitis: A Review. *Journal of Clinical Medicine*. 2021;10(5).
- [12] Fanselow N, Sirajuddin N, Yin X-T, Huang AJW, Stuart PM. *Acanthamoeba* Keratitis, Pathology, Diagnosis and Treatment. *Pathogens*. 2021;10(3).
- [13] Carrijo-Carvalho LC, Sant'ana VP, Foronda AS, de Freitas D, de Souza Carvalho FR. Therapeutic agents and biocides for ocular infections by free-living amoebae of *Acanthamoeba* genus. *Surv Ophthalmol*. 2017;62(2):203-18.
- [14] McCoy C, Patel S, Thulasi P. Update on the Management of *Acanthamoeba* Keratitis. *Current Ophthalmology Reports*. 2022.
- [15] Kalra SK, Sharma P, Shyam K, Tejan N, Ghoshal U. *Acanthamoeba* and its pathogenic role in granulomatous amebic encephalitis. *Experimental parasitology*. 2020;208.
- [16] Szentmary N, Daas L, Shi L, Laurik KL, Lepper S, Milioti G, et al. *Acanthamoeba* keratitis - Clinical signs, differential diagnosis and treatment. *J Curr Ophthalmol*. 2019;31(1):16-23.
- [17] Liu S, Yue L, Gu W, Li X, Zhang L, Sun S. Synergistic effect of fluconazole and calcium channel blockers against resistant *Candida albicans*. *PLoS one*. 2016;11(3):e0150859.
- [18] Spampinato C, Leonardi D. *Candida* infections, causes, targets, and resistance mechanisms: traditional and alternative antifungal agents. *BioMed research international*. 2013;2013.
- [19] Anwar A, Siddiqui R, Hussain MA, Ahmed D, Shah MR, Khan NA. Silver nanoparticle conjugation affects antiacanthamoebic activities of amphotericin B, nystatin, and fluconazole. *Parasitology research*. 2018;117(1):265-71.
- [20] Baig AM, Zohaib R, Nuzair W, Saiqa K, Mehdia N. Evidence of human-like Ca<sup>2+</sup> Channels and Effects of Ca<sup>2+</sup> Channel blockers in *Acanthamoeba castellanii*. *Chemical biology & drug design*. 2018.
- [21] Rodrigues AA, Pina-Vaz C, Mardh PA, Martinez-de-Oliveira J, Freitas-da-Fonseca A. Inhibition of germ tube formation by *Candida albicans* by local anesthetics: an effect related to ionic channel blockade. *Current microbiology*. 2000;40(3):145-8.
- [22] Baig AM, Khaleeq A, Nazim F. Targeting CNS Related Protist Pathogens: Calcium Ion Dependency in the Brain-Eating Amoebae. *ACS Chem Neurosci*. 2019.
- [23] Baig AM. Drug targeting in *Acanthamoeba* keratitis: rational of using drugs that are already approved for ocular use in non-keratitis indications. *Eye (London, England)*. 2018.
- [24] Baig AM, Iqbal J, Khan NA. In vitro efficacy of clinically available drugs against growth and viability of *Acanthamoeba castellanii* keratitis isolate belonging to the T4 genotype. *Antimicrobial agents and chemotherapy*. 2013;AAC. 00299-13.
- [25] Yu Q, Ding X, Zhang B, Xu N, Jia C, Mao J, et al. Inhibitory effect of verapamil on *Candida albicans*

- hyphal development, adhesion and gastrointestinal colonization. *FEMS Yeast Res.* 2014;14(4):633-41.
- [26] Yu Q, Xiao C, Zhang K, Jia C, Ding X, Zhang B, et al. The calcium channel blocker verapamil inhibits oxidative stress response in *Candida albicans*. *Mycopathologia.* 2014;177(3-4):167-77.
- [27] Dirim Erdogan D, Aykur M, Selvi Gunel N, Palamar M, Barut Selver O, Ozel B, et al. The Risk Factors and Clinical Features of *Acanthamoeba Keratitis*: First Time Detection of *Acanthamoeba T5* Genotype from Keratitis Patients in Turkey. *Acta Parasitologica.* 2022;67(3):1384-92.
- [28] Karakavuk M, Aykur M, Sahar EA, Karakus M, Aldemir D, Donduren O, et al. First time identification of *Acanthamoeba* genotypes in the cornea samples of wild birds; Is *Acanthamoeba keratitis* making the predatory birds a target? *Experimental parasitology.* 2017;183:137-42.
- [29] Nakaminami H, Tanuma K, Enomoto K, Yoshimura Y, Onuki T, Nihonyanagi S, et al. Evaluation of in vitro anti-amoebic activity of antimicrobial agents against clinical *Acanthamoeba* isolates. *Journal of Ocular Pharmacology and Therapeutics.* 2017;33(8):629-34.
- [30] Elder M, Kilvington S, Dart J. A clinicopathologic study of in vitro sensitivity testing and *Acanthamoeba keratitis*. *Investigative ophthalmology & visual science.* 1994;35(3):1059-64.
- [31] Megha K, Sharma M, Sharma C, Gupta A, Sehgal R, Khurana S. Evaluation of in vitro activity of five antimicrobial agents on *Acanthamoeba* isolates and their toxicity on human corneal epithelium. *Eye (Lond).* 2022;36(10):1911-7.
- [32] Mannan Baig A. Identification of chemotherapeutic agents for the treatment of *Acanthamoeba* infections: rationale for repurposing drugs via the discovery of novel cellular targets: University of Sunderland; 2020.
- [33] Osato MS, Robinson NM, Wilhelmus KR, Jones DB. In vitro evaluation of antimicrobial compounds for cysticidal activity against *Acanthamoeba*. *Reviews of infectious diseases.* 1991;13(Supplement\_5):S431-S5.
- [34] Gupta P, Chanda R, Rai N, Kataria VK, Kumar N. Antihypertensive, amlodipine besilate inhibits growth and biofilm of human fungal pathogen *Candida*. *Assay and Drug Development Technologies.* 2016;14(5):291-7.
- [35] Li Yj, Pan Cz, Zhao Zw, Zhao Zx, Chen Hl, Lu Wb. Effects of a combination of amlodipine and imipenem on 42 clinical isolates of *Acinetobacter baumannii* obtained from a teaching hospital in Guangzhou, China. *BMC infectious diseases.* 2013;13:1-9.

## Investigation of Vegetative High Temperature Tolerance of Some Cotton (*Gossypium hirsutum* L.) Varieties

Yusuf Güzel DEMİRAY<sup>1</sup> , Remzi EKİNCİ<sup>2\*</sup> , Adem BARDAK<sup>3</sup> 

<sup>1</sup> GAP International Agricultural Research and Training Center, 21200, Diyarbakir, Turkey

<sup>2</sup> Dicle University, Faculty of Agriculture, Department of Field Crops, 21280, Diyarbakir, Turkey

<sup>3</sup> Kahramanmaraş Sütcü Imam University, Faculty of Agriculture, Department of Agricultural Biotechnology, Kahramanmaraş, Turkey

Yusuf Güzel DEMİRAY ORCID No: 0000-0002-4113-5855

Remzi EKİNCİ ORCID No: 0000-0003-4165-6631

Adem BARDAK ORCID No: 0000-0002-5715-302X

\*Corresponding author: [remzi.ekinci@dicle.edu.tr](mailto:remzi.ekinci@dicle.edu.tr)

(Received: 26.04.2023, Accepted: 13.06.2023, Online Publication: 22.06.2023)

### Keywords

Cotton,  
Vegetatively  
High  
Temperature,  
Cell Membrane  
Thermostability  
(CMT),  
Leaf  
Temperature

**Abstract:** It was carried out to determine the harmful effects of high temperature stress on cotton plant during the vegetative development period in this study. The trial was established in the GAPUTAEM trial area in 2020, with 4 blocks according to the Augmented trial design. As standard; Tamcot Spnhix, SJU86, AGC208, STV468, ST474 and Carmen varieties and 88 cotton varieties registered in the National Variety List were used as trial material. In the study, the relative cell damage rate (RCI) and leaf high temperature stress index values (YYSSI) were investigated. Cell membrane damage (%RCI) varied between 41.81% and 74.84%; While the average of the standards was 68.15%, the general average was determined as 62.42%. Leaf high temperature stress index (YYSSI) values varied between 0.48 and 1.85, while the YYSSI average of the standards was 0.98, the overall YYSSI average of the experiment was found to be 1.02. It was determined that there was a wide variation among the genotypes screened for vegetatively high temperature stress. It has been concluded that YYSSI and RCI traits are important, effective, easy and applicable selection criteria for screening genotypes that are vegetatively tolerant and sensitive to high temperature stress in cotton plants. It is recommended to evaluate these two parameters together as it will provide more accurate results. It has been determined that Teksa 415 cotton variety is in the vegetatively tolerant group. Vegetatively, 31 genotypes were in the moderately tolerant group and 62 genotypes were in the susceptible group.

## Bazı Pamuk (*Gossypium hirsutum* L.) Çeşitlerinin Vejetatif Olarak Yüksek Sıcaklığa Karşı Tolerantlıklarının İncelenmesi

### Anahtar Kelimeler

Pamuk,  
Vejetatif Olarak  
Yüksek  
Sıcaklık,  
Hücre  
Membran  
Termostabilitesi  
(CMT),  
Yaprak  
Sıcaklığı

**Öz:** Bu çalışmada, vejetatif gelişim döneminde pamuk bitkisinde yüksek sıcaklık stresinin, zararlı etkilerinin belirlenmesi amacıyla yapılmıştır. Deneme, 2020 yılında GAPUTAEM deneme alanında, Augmented deneme desenine göre 4 bloklu olarak kurulmuştur. Standart olarak; Tamcot Spnhix, SJU86, AGC208, STV468, ST474 ve Carmen çeşitleri ve Milli Çeşit Listesinde kayıtlı 88 adet pamuk çeşidi deneme materyali olarak kullanılmıştır. Araştırmada, bağıl hücre zararlanma oranı (RCI) ile yaprak yüksek sıcaklık stres indeksi değerleri (YYSSI) incelenmiştir. Hücre membran hasarı (%RCI) %41.81 ile %74.84 arasında değişim göstermiş; standartların ortalaması %68.15 iken, genel ortalama %62.42 olarak saptanmıştır. Yaprak yüksek sıcaklık stres indeksi (YYSSI) değerleri 0.48 ile 1.85 arasında değişmiş olup, standartların YYSSI ortalaması 0.98 iken, denemenin genel YYSSI ortalaması 1.02 olarak saptanmıştır. Vejetatif olarak yüksek sıcaklık stresi için taranan genotipler arasında geniş bir varyasyon olduğu belirlenmiştir. YYSSI ve RCI özellikleri, pamuk bitkisinde vejetatif olarak yüksek sıcaklık stresine karşı toleran ve hassas genotiplerin taranması için önemli, etkili, kolay ve uygulanabilir seçim kriteri olduğu kanısına

varılmıştır. Bu iki parametrenin birlikte değerlendirilmesi daha doğru sonuçların elde edilmesini sağlayacağından tavsiye edilmektedir. Teksa 415 pamuk çeşidinin vejetatif olarak tolerant grubuna girdiği tespit edilmiştir. Vejetatif olarak, 31 genotip orta tolerant ve 62 genotip ise hassas grupta yer almıştır.

## 1. INTRODUCTION

The cotton plant is an important and strategic product that constitutes the raw material of approximately 50 different industrial industries, especially the textile, oil, and feed industry sectors. In the 2021 and 2022 cotton production seasons, the world's four largest cotton-producing countries are India (5.9 million tons), China (5.7 million tons), the USA (4 million tons), and Brazil 2.7 million tons, respectively. In Turkey, seed cotton production increased by 26.9% in 2021 and amounted to 2.25 million tons [1]. Considering the average data of the last 10 years in Turkey, the cotton cultivation area is 462 thousand hectares, the amount of fiber produced is 835 thousand tons, and the fiber yield is 19.3 kg.ha<sup>-1</sup> [2]. In our country, cotton is grown intensively, especially in the South eastern Anatolia Region, Aegean Region, Adana, and Antalya regions with the determining effect of climate factors [3]. Approximately 59.31% of the cotton produced in our country is produced in the south eastern Anatolia Region [4]. However, due to the fact that the climate conditions of the south eastern Anatolia Region are dry and hot in summer, high temperature has a negative and significant effect on the vegetative and generative periods of cotton. Cotton is frequently exposed to many biotic and abiotic stresses during its growth stages [5, 6, 45, 46]. According to the International Intergovernmental Panel on Climate Change report, air temperatures are expected to increase by 0.2 °C every 10 years, with global warming being the key factor of high temperature stress. And from 2020 to 2080, the world temperature is predicted to increase by 0.5–5.44 °C [7, 8]. Temperature trends display that the global average temperature may increase by 1–4 °C by the end of the 21st century [9]. Although the temperature requirement of the cotton plant varies according to the growth stage, in conditions where it does not fall below 15 °C, leaf, bud, flower, and boll development takes place and it tends to grow continuously, and temperatures of 25–32 °C are sufficient for optimum growth [10, 11, 12]. The optimum temperature values for the first development stages of cotton (main stem elongation, leaf area development, and biomass production) are 30/22 °C day/night. Heat stress can be defined as the emergence of morphological, physiological, and biochemical changes in the plant that exceeds the thermal capacity of the plant above the desired optimum temperature in its life cycle. Accordingly, since registered commercial cultivars with little resistance to high temperature stress have a narrow genetic base with limited genetic gain, these cultivars may increase their susceptibility in a stressful environment [13, 14, 15, 45, 46]. While the cotton plant produces four times more fruit branches at 30/22 °C than at 20/12 °C, it produces fewer monopodial branches [16]. Going on of the daily maximum temperature affects the germination of cotton plants in the vegetative period, root and tiller growth, sympodial and monopodial branches, internode distance, photosynthesis, respiration, and ATP formation.

In the generative period, it affects biomass, boll number per plant, boll size and weight, cellulose accumulation and fiber yield, fiber quality, fiber length, strength and micronaire value [17, 18, 18, 19, 20, 45, 46, 47]. In addition, high temperature affects the morpho-physiological properties of the cotton plant. Therefore, by discovering high temperature tolerant cultivars or genes, various techniques have been used to develop temperature tolerant genotypes. Among the many screening techniques that have been used for cotton plants, relative cell damage (%RCI) using Cell Membrane Thermostability (CMT) is a popular and rapid physiological technique for screening cotton germplasm for resistance to heat stress [21]. This method is widely used in many plants such as paddy, soybean, tomato, and cotton [22]. In cotton, the %RCI technique is widely used to screen for temperature tolerant genotypes. Because % RCI is a true indicator of cell membrane thermostability (CMT) and is simpler, more effective, and more cost-effective than other scanning techniques [23, 24, 25]. The use of canopy and leaf temperature is an important technique that has been used more and more recently in terms of germplasm temperature tolerance [22]. This technique has been used by various researchers for temperature tolerance of cotton and corn varieties [25, 26]. Our main aim in this study is to determine the response and tolerance status of some domestic and foreign origin cotton (*Gossypium hirsutum* L.) genotypes in our inventory, especially originating and registered cotton varieties in our country, to high temperatures in the vegetative period. At the same time, determining the parents with special characteristics and including them in the breeding program [27] is to facilitate the researchers in breeding studies and to minimize the environmental effects in selection.

## 2. MATERIAL AND METHOD

**2.1. Material:** In this study, 94 cotton (*Gossypium hirsutum* L.) genotypes registered in the national variety list of domestic and foreign origin, cotton varieties originating from especially our country and registered were used as plant material (Table 1).

**2.2. Experimental Design:** The field experiment was established in the trial area of the GAP International Agricultural Research and Training Center, in the cotton growing season of 2020, with 4 blocks according to the Augmented Design. Stonville474, Tamcot Sphinx, SJU86, Stonville468, AGC208, and Carmen genotypes were included as standard in the experiment. In the experiment, each of the parcels consisting of two rows is 4.0 m long and 1.4 m wide.

**Table 1.** Information on Cotton Genotypes Used as Material

Origin of Material	Cotton Varieties
USA	Tamcot Sphinx, SJU86, AGC208
BASF Turkish Chem. Inds. and Trade Ltd. Comp.	Fiona, Carla, ST498, STV468, Carmen
Bayer Turkish Chem. Inds. Ltd. Comp.	Claudia, Gloria, Candia, Flora
Birlik Seed. Inds. and Trade. Ltd. Comp.	Bir781, Bir949, Cosmos, Bir138
Caso Seed. Inds. and Trade Ltd. Comp.	Caso9048
EMTZARI	Furkan
EMARI	TYA193, Ceykot340, TYA366, ADN701, MAY355, MAY455, MAY505, TMK122, TMN18, MAY344, Nihal, ADN413, ADN710, ADN712, ADN123, ADN811, Gelincik, Sargelin, Çukurova 1518, Bossa 159, Teksa415, Yıldırım63, Ayzek 595, Gapkot 732, Ceykot 92
GAP ARI	ZN 243
GAP IARTC	Kartanesi
Golden West Seed Trade Ltd. Comp.	Optasia, Esperia, Bomba, GW2345, Babylon, Famosa, Fantom, Penta (Golda), Primera
Livagro Agr. Seed. Ltd. Comp.	Zara
May-Agro Seed Inds. and Trade Incorp. Comp.	Gaia, ST474, MAY404
Monsanto Nutr. and Agr. Trade. Ltd. Comp.	DP332, ST478, DP396, DP499, SG125
Özaltın Agr. Bus. Inds. and Trade Incorp. Comp.	Lodos, Özaltın404, Özaltın112
Özbuğday Agr. Bus. and Seed Incorp. Comp.	Lider (Mig119), Diva (Teks)
CRI	SC2009, SC2079, Efe, Ergüven, Harem1, Harem2, ES1, ES2, Sezener76, Özbek105, İpek607, Gürelbey, Aydın110, Şahin2000
Progen Seed Incorp. Comp.	Kaira, Lima, Astoria, Edessa, BA440, Carisma, PG2018, BA525, Flash
Tiriyo Seed. Ltd. Comp.	Zena1010, Zena1040, Zena1018

EMTZARI (East Mediterranean Transitional Zone Agricultural Research Institute), EMARI (East Mediterranean Agricultural Research Institute), GAPARI (GAP Agricultural Research Institute), GAP IARTC (GAP International Agricultural Research and Training Center), CRI (Cotton Research Institute)

### 2.3. Examined Features

**Leaf Temperature:** In the experimental area created under field conditions, the cotton plant was subjected to high temperature shock practice (HTSP) by being placed in a low tunnel for an uninterrupted 96 hours during the peak flowering period. With the help of the thermometer placed in the low tunnel, during the hot hours of the day (13:00-16:00), when the temperature is above 50 °C, the low tunnel was opened from the sides to reduce the temperature. Observations were taken before high temperature shock application was recorded as Control. Observations taken at the end of the high temperature shock application period were recorded as Stress. Control and Stress observations were taken separately from 3 of

the same plants, which were previously coded and selected in each parcel, and the average of the observations was taken. Leaf temperature was taken separately with an Infrared device (Multifunction InfraRed Thermometer CEM DT-8811H) before and after HTSP. It was evaluated statistically over the averages of the observations taken. Leaf High Temperature Stress Index (LHTSI) was calculated according to the formula specified by Fischer and Maurer [28] and evaluated by modifying it according to Ekinçi [29].

$$LHTSI: ((G_N - G_S) / G_N) / ((A_N - A_S) / A_N) \quad (1)$$

LHTSI: Leaf high temperature stress index

G<sub>S</sub>: Leaf temperature value of the genotype under stress conditions

G<sub>N</sub>: Leaf temperature value of the genotype under normal conditions

A<sub>S</sub>: Average of leaf temperature values of all genotypes under stress conditions

A<sub>N</sub>: The average of leaf temperature values of all genotypes under normal conditions

Regarding the evaluation of genotypes after calculating LHTSI values; If LHTSI ≤ 0.5 it was evaluated as “Tolerant”, if 0.5 < LHTSI ≤ 1 as “Medium Tolerant” and if LHTSI > 1 as “Sensitive” [30].

The data obtained after control and stress were analyzed according to Augmented Design and calculated and analyzed over corrected values [31].

**Cell Membrane Injury/Damage Rate %:** Cell damage percentage is based on the measurement of electrolyte leakage from leaf discs in distilled water after heat treatment [32]. The cell membrane damage feature was calculated by utilizing the cell membrane thermostability feature. Samples were taken from 3 randomly selected and coded plants from each plot. Two sets of five 10 mm diameter leaf discs were taken from the same leaf. One of these sets was used for control and the other for stress. Leaf discs were placed in test tubes containing 15 ml of distilled water. One set was exposed to a digital water bath at 50 °C and the other set was exposed to room conditions at 25 °C for 1 hour. At the end of this period, 30 ml of distilled water was added to the test tubes and incubated at 10 °C for 24 hours. Then, the test tubes were mixed in a rinser until they reached 25 °C, and C<sub>1</sub> - C<sub>2</sub> values were measured. Both the samples were again heat treated at a temperature of 121 °C for a period of 10 minutes under a pressure of 15 lbs. Then, the test tubes were mixed in a rinser until they reached 25 °C, and T<sub>1</sub> - T<sub>2</sub> values were measured. Cell membrane injury/damage ratio (%RCI) values were obtained by formula 2 (Figure 1).



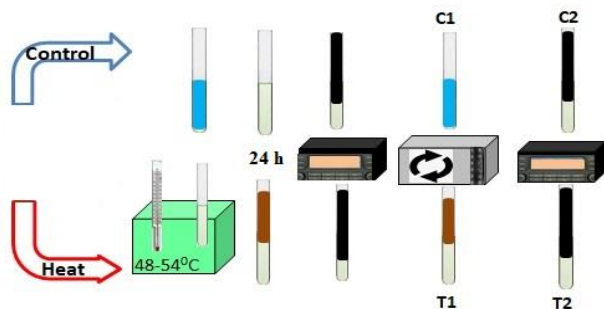


Figure 1. Cell Membrane Thermostability Practice Method

$$\%RCI: [1 - (1 - (T1/T2)) / (1 - (C1/C2))] \times 100 \quad (2)$$

%RCI= Cell membrane injury/damage ratio

T<sub>1</sub> = EC value after high temperature application

T<sub>2</sub> = EC value after autoclave

C<sub>1</sub> = EC value before control autoclave

C<sub>2</sub> = EC value after control autoclave

YGDR value was calculated with Formula 3 for the classification of RCI values.

$$YGDR = (RCIMax - RCIMin) / 3 \quad (3)$$

Regarding the evaluation of genotypes after calculating the RCI values;  $RCI \leq RCIMin + YGRD$  is "Tolerant",  $RCIMin + YGRD < RCI \leq RCIMin + 2 * YGRD$  "Medium Tolerant" and  $RCI > RCIMin + 2 * YGRD$  "Sensitive".

### 3. RESULTS

#### 3.1. Cell Membrane Injury/Damage Ratio (RCI)

The histogram of the %RCI feature is given in Figure 2a. The %RCI feature values were determined as the lowest at 41.81%, the highest at 74.84%, the genotype average at 62.78%, the standard average of 68.15%, and the YGDR value at 11.01%. The number of cotton genotypes included in the sensitive group ( $RCI > 63.82\%$ ) in terms of RCI feature is 51 (values are in the range of 64.15-74.83%); The number of cotton genotypes in the medium tolerant group (RCI values are in the range 52.82-63.82%) is 30 (values are in the range of 53.45-63.56%) and the number of cotton genotypes in the tolerant group (RCI value  $< 52.82\%$ ) is 13 (values are 41.80-49.84%). Cotton varieties that are in the tolerant group in terms of their %RCI values; Caso9048 (41.81%), Flora (41.98%), Primera (42.65%), Lider (Mig119) (43.71%), Ceykot92 (43.77%), Bir138 (44.22%), Zara (46.03%), Teksa415 (46.73%), BA525 (47.23%), Flash (47.88%), TYA193 (49.32%), Gürelbey (49.42%) and Diva (Teks) (49.84%) (Table 2).

#### 3.2. Leaf High Temperature Stress Index (LHTSI)

The histogram of the leaf high temperature stress index (LHTSI) feature is given in Figure 2b. In the control conditions, the average leaf temperature of the genotypes varied between 26.28 °C and 33.77 °C, while the average leaf temperature of the genotypes changed between 33.31 °C and 41.55 °C after HTSP. While the mean of the standard genotype was 30.62 °C in the control conditions,

the mean of the standard genotypes was 38.73 °C after HTSP. While the average leaf temperature of all genotypes was 30.45 °C in the control conditions, it was determined that the average leaf temperature of all genotypes was 38.64 °C after HTSP. LHTSI value is greater than one, and 39 cotton varieties (LHTSI: 1.01-1.85) were found to be in the sensitive group. It has been determined that 52 cotton genotypes (LHTSI: 0.54-0.995) have an LHTSI value between  $0.5 < LHTSI \leq 1$  and are in the middle tolerant group. In addition, it was determined that the LHTSI value was greater than 0.5, and 3 cotton genotypes (LHTSI: 0.48-0.495) were included in the tolerance group. It was determined that cotton genotypes in the tolerant group in terms of their LHTSI values were TMK122 (LHTSI: 0.483), ADN811 (LHTSI: 0.495), and Teksa415 (LHTSI: 0.492) (Table 2). The change of genotypes to %RCI and LHTSI values are given in Figure 3.

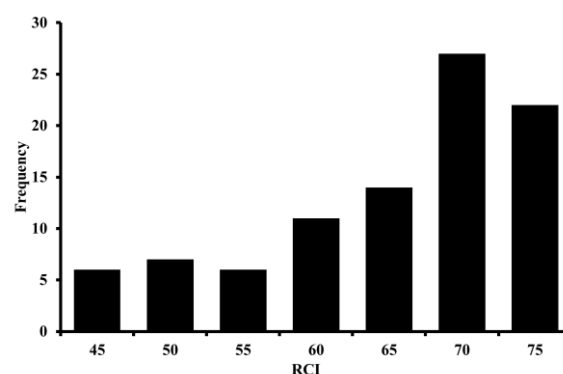


Figure 2a. Histogram for the %RCI

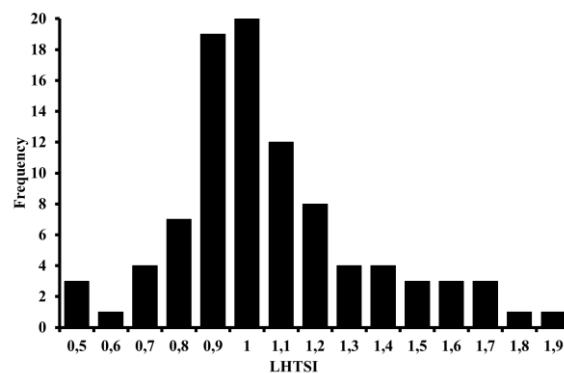


Figure 2b. Histogram for the LHTSI

Table 2. Numbers and Names of Cotton Genotypes in Sensitive, Medium Tolerant and Tolerant Groups According to %RCI and LHTSI

Groups	In terms of %RCI	In terms of LHTSI	Joint
Sensitive	51	39	
Medium Tolerant	30	52	
Tolerant	13 Caso9048, Flora, Primera, Lider (Mig119), Ceykot92, Bir138, Zara, Teksa415, BA525, Flash, TYA193, Gürelbey ve Diva (Teks)	3 TMK122, ADN811, Teksa415	Teksa415

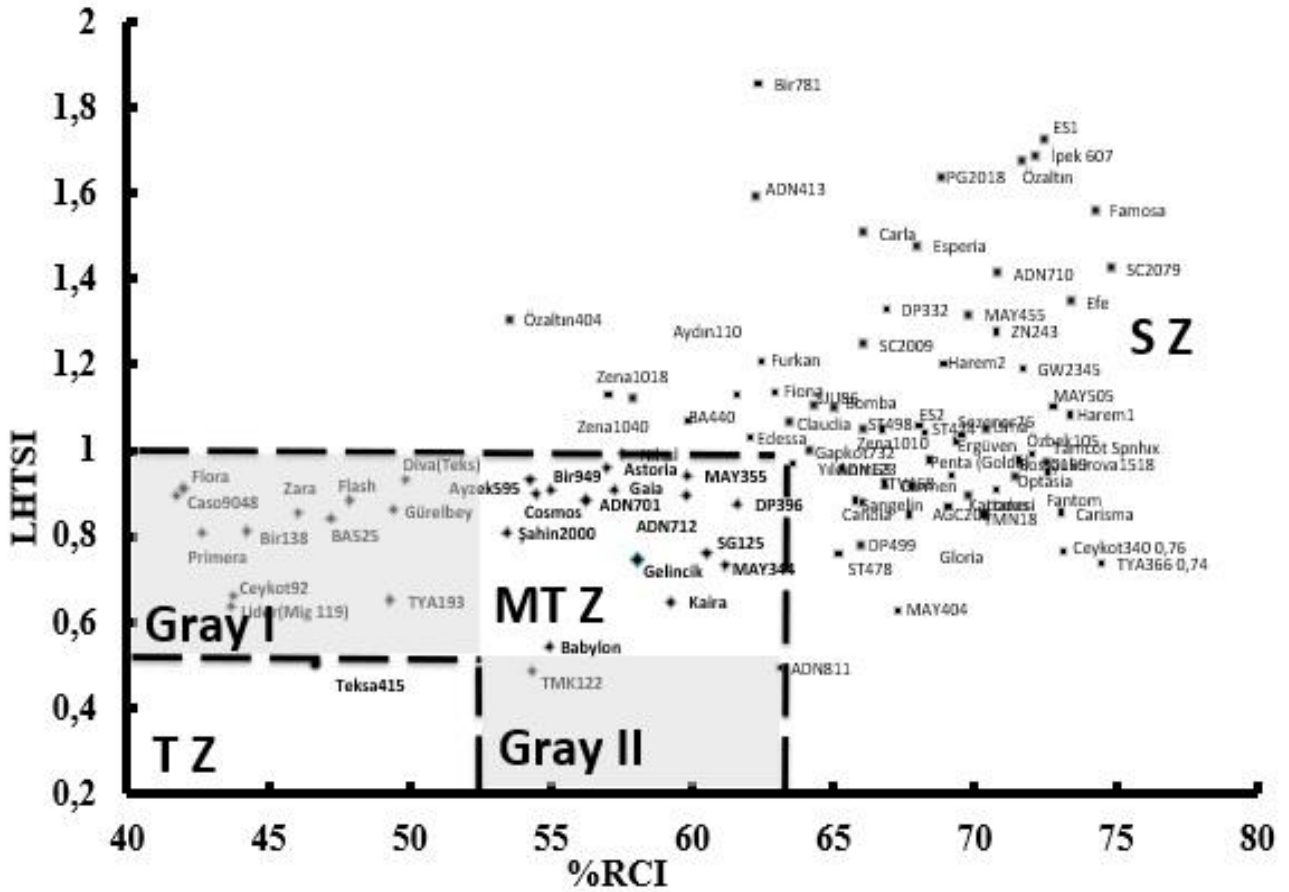


Figure 3. LHTSI and %RCI Graph

As the genotypes get closer to the origin, vegetative tolerance increases in terms of both traits (Figure 3). In terms of RCI and LHTSI characteristics examined, the Tolerance Zone ( $\%RCI \leq 52.82$  and  $LHTSI \leq 0.5$ ) was marked as TZ. It attracts attention that the Medium Tolerance Zone ( $52.82\% < RCI < 63.82\%$  or  $0.5 < LHTSI \leq 1$ ) consists of 3 parts (MTZ, Gray I, and Gray II). Although the Gray I region is tolerant in terms of the RCI feature, it is seen to be in the Medium Tolerant group in terms of the LHTSI feature. Similarly, although the Gray II region is tolerant in terms of the LHTSI feature, it is noticed that it is in the Medium Tolerant group in terms of the RCI feature. Therefore, Gray I and Gray II zones were included in the Medium Tolerant Zone. The Sensitivity Zone ( $RCI > 63.82\%$  or  $LHTSI > 1.0$ ) has been named SZ for both traits examined vegetatively. ADN123, ADN413, ADN710, AGC208, Aydın110, BA440, Bir781, Bomba, Bossa159, Candia, Carisma, Carla, Carmen, Ceykot340, Claudia, Çukurova1518, DP332, DP499, Edessa, Efe, Ergüven, ES1, ES2, Esperia, Fantom, Fiona, Furkan, Gloria, GW2345, Harem1, Harem2, İpek607, Kartanesi, Lima, Lodos, MAY404, MAY455, MAY505, Optasia, Özalın112, Özalın404, Özbek105, Penta (Golda), PG2018, Sarigelin, SC2009, SC2079, Sezener76, SJU86, ST474, ST478, ST498, STV468, Tamcot Sphix, TMN18, TYA366, Yıldırım63, Zena1010, Zena1018, Zena1040 and ZN243 cotton genotypes (62 pieces) were determined to have in the sensitive region (SZ). In our study, our findings obtained by measuring different values as a result of screening genotypes in terms of vegetative tolerance or sensitivity

under control and stress conditions in terms of CMT or %RCI characteristics were similar to the findings of Sajid [33], Azhar [24], Rahman [23], Farooq [34], Zafar [35], Jamil [36]. It was determined that there was a wide variation among the genotypes screened for vegetatively high temperature stress. High temperature stress reduced the vegetative growth of the cotton plant, causing the yellowing of young leaves and drying of young tillers. A high CMT value, namely a low %RCI ratio, indicates that genotypes are less vegetatively affected by high temperature. Therefore, it has been understood that genotypes with low %RCI are an important criterion for cotton breeding programs. It has been understood that plant characteristics such as plant type, leaf woolly, and cell wall thickness affect the %RCI rate depending on the severity of the temperature, the period in which the heat is experienced, and the duration of exposure to the heat. It has been concluded that the investigated RCI and LHTSI properties are two important, effective, easy, and applicable properties in revealing the vegetative performance of cotton against high temperature stress, and it is concluded that more accurate results will be obtained by examining these two properties together [18, 23, 24, 25, 33, 35, 37, 38, 39, 40, 41, 42, 43, 44].

#### 4. DISCUSSION AND CONCLUSION

In this study, it was passed judgment that using CMT and LHTSI characteristics, it is an important, effective, easy and applicable selection criterion for the screening of genotypes in terms of tolerance or sensitivity to high

temperature stress vegetatively in cotton plants. It is recommended that more accurate and reliable data can be obtained as a result of applying these two parameters together. As a result of examining the LHTSI and RCI characteristics together, it was determined that only the Teksa415 cotton variety was vegetatively tolerant. It was determined that 31 cotton genotypes were included in the medium tolerant group vegetatively and 62 cotton genotypes were included in the sensitive group.

### Acknowledgement

This study was produced from the Ph.D. thesis titled "Determination of DNA Markers Associated with High Temperature Stress Tolerant / Strength in Cotton (*G. hirsutum* L.)" conducted by Yusuf Güzel DEMİRAY in the Department of Field Crops, Institute of Science and Technology, Dicle University. It was supported by Dicle University Scientific Research Projects Coordination Unit with project number ZİRAAT.20.007 and by the General Directorate of Agricultural Research and Policies with project number TAGEM/TBAD/A/20/A7/P5/1536. We thank the Scientific Research Coordination Unit and the General Directorate of Agricultural Research and Policies for their support.

### REFERENCES

- [1] Anonymous. Bitkisel Üretim Genel Müdürlüğü Tarla ve Bahçe Bitkileri Daire Başkanlığı Ürün Masalları- Pamuk Bülteni, Ocak 2022, sayı, 19 s4. Erişim Linki: [https://www.istib.org.tr/resim/siteici/files/916\\_Pamuk%20B%C3%BClteni%20-%20C3%9Cr%C3%BCn%20Masalar%C4%B1%20\(Ocak%202022\).pdf](https://www.istib.org.tr/resim/siteici/files/916_Pamuk%20B%C3%BClteni%20-%20C3%9Cr%C3%BCn%20Masalar%C4%B1%20(Ocak%202022).pdf) Erişim Tarihi: 14.02.2023, (in Turkish).
- [2] TUIK. 2022. Türkiye Cotton Statistics. Access link: <https://biruni.tuik.gov.tr/medas/?kn=92&locale=tr>, Access date: 14.02.2023.
- [3] Yaşar, M. & Yalınkılıç, N. Main Problems and Solutions of Cotton Agriculture in Turkey. ISPEC 8th International Conference on Agriculture, Animal Sciences and Rural Development, Proceeding Book p: 620-630. ISBN: 978-625-7720-68-7. 24-25 December 2021 Bingöl, Turkey.
- [4] Aytaç, S., Başbağ, S., Arslanoğlu, F., Ekinci, R., Ayan, A.K. Lif Bitkileri Üretiminde Mevcut Durum ve Gelecek, Türkiye Ziraat Mühendisliği IX. Teknik Kongresi, 13-17 Ocak 2020, Ankara, TMMOB Ziraat Mühendisleri Odası, Bildiri Kitabı-1, ISBN-978-605-01-1321-1, Ankara Üniversitesi Basın Yayın Müdürlüğü, S: 463-491, [http://www.zmo.org.tr/resimler/ekler/37c782b9ce7a76f\\_ek.pdf](http://www.zmo.org.tr/resimler/ekler/37c782b9ce7a76f_ek.pdf), (in Turkish).
- [5] Li, Z. K., Chen, B., Li, X. X., Wang, J. P., Zhang, Y., Wang, X. F., ... & Ma, Z. Y. A newly identified cluster of glutathione S-transferase genes provides Verticillium wilt resistance in cotton. *The Plant Journal*, 2019; 98(2), 213-227.
- [6] Yaşar, M. Evaluation of Some New Cotton Genotypes Against Verticillium Disease (*Verticillium dahliae* Kled.). *ISPEC Journal of Agricultural Sciences*, 2022; 6(1), 110-117.
- [7] IPCC. Intergovernmental Panel on Climate Change, Climate Change 2007: Working Group I: The Physical science basis (online) [http://www.ipcc.ch/publications\\_and\\_data/publications\\_ipcc\\_fourth\\_assessment\\_report\\_wg1\\_report\\_the\\_physical\\_science\\_basis.htm](http://www.ipcc.ch/publications_and_data/publications_ipcc_fourth_assessment_report_wg1_report_the_physical_science_basis.htm) (verified 26 June. 2015).
- [8] IPCC. Intergovernmental Panel on Climate Change, Climate change 2018. Synthesis report. Version ingles. Page Climate Change 2018: Synthesis Report. Contribution of Working Groups I, II and III to the Fifth Assessment Report of the Intergovernmental Panel on Climate Change.
- [9] Driedonks N, Rieu I, Riezen WH. Breeding for plant heat tolerance at vegetative and reproductive stages. *Plant reprod.* 2016;29(1):67-79. <https://doi.org/10.1007/s00497-016-0275-9>.
- [10] Reddy KR, Hodges HF, McKinion J.M. Modeling temperature effects on cotton internode and leaf growth. *Crop Sci.* 1997;37: 503-509.
- [11] Burke JJ, Wanjura D.F. Plant responses to temperature extremes. In: *Physiology of cotton*. Springer, 2010; pp. 123-128.
- [12] Yaşar, M., Başbağ, S., Ekinci, R. Determination effects of topping at different times on yield and yield components in cotton. *Harran Journal of Agricultural and Food Science.* 2019, 23(1): 52-59, DOI: 10.29050/harranziraat.422916.
- [13] McCarty JC, Wu J, Jenkins J.N. Genetic association of cotton yield with its component traits in derived primitive accessions crossed by elite upland cultivars using the conditional ADAA genetic model. *Euphytica.* 2008;161(3):337-52. <https://doi.org/10.1007/s10681-007-9562-8>.
- [14] Wang M, Tu L, Lin M, et al. Asymmetric subgenome selection and cis-regulatory divergence during cotton domestication. *Nat gen.* 2017;49(4):579-87. <https://doi.org/10.1038/ng.3807>.
- [15] Ma Z, He S, Wang X, et al. Resequencing a core collection of upland cotton identifies genomic variation and loci influencing fiber quality and yield. *Nat Genet.* 2018;50(6):803-13. <https://doi.org/10.1038/s41588-018-0119-7>.
- [16] Reddy, K.R., Hodges, H.F., McKinnon, J.M., and Wall, G.A. Temperature effect on Pima cotton growth and development. *Agron. J.* 1992;84:237-243.
- [17] Wahid A, Gelani S, Ashraf M, Foolad M.R. Heat tolerance in plants: an overview. *Environ. Exp. Bot.* 2007;61:199-223.
- [18] Bibi A, Oosterhuis D, Gonias E. Photosynthesis, the quantum yield of photosystem II and membrane leakage as affected by high temperatures in cotton genotypes. *J. Cotton Sci.* 2008;12: 150-159.
- [19] Pettigrew W. The effect of higher temperatures on cotton lint yield production and fiber quality. *Crop Sci.* 2008;48: 278-285.
- [20] Loka DA, Oosterhuis D.M. Effect of high night temperatures during anthesis on cotton (*G. hirsutum*

- L.) pistil and leaf physiology and biochemistry. *Aust. J. Crop Sci.* 2016;10(5): 741-748.
- [21] Baker NR, Rosenqvist E. Applications of chlorophyll fluorescence can improve crop production strategies: an examination of future possibilities. *J. Exp. Bot.* 2004; 55:1607-1621.
- [22] Singh RP, Prasad PV, Sunita K, Giri S, Reddy K.R. Influence of high temperature and breeding for heat tolerance in cotton: A review. *Adv. Agron.* 2007;93: 313-385.
- [23] Rahman H., Malik S.A., Saleem M. Heat tolerance of upland cotton during the fruiting stage was evaluated using cellular membrane thermostability. *Field Crops Res.* 2004;85: 149-158.
- [24] Azhar FM, Ali Z, Akhtar MM, Khan AA, Trethowan R. Genetic variability of heat tolerance, and its effect on yield and fiber quality traits in upland cotton (*G. hirsutum* L.). *Plant Breed.* 2009;128: 356-362.
- [25] Karademir E. Screening cotton varieties (*G. hirsutum* L.) for heat tolerance under field conditions. *Afr. J. Agric. Res.* 2012;7: 6335-6342.
- [26] Wanjura, D. F., Maas, S. J., Winslow, J. C., & Upchurch, D.R. Scanned and spot measured canopy temperatures of cotton and corn. *Computers and Electronics in Agriculture*, 2004;44(1), 33-48.
- [27] Demiray, YG., Ekinçi, R., and Yaşar, M. Characterization of F6 Generation Cotton Genotypes Developed by Double Cross Hybrid Method. *International Agricultural Congress of Muş Plain, Proceeding Book Sayfa: 89-94. ISBN: 978-605-51370-69. 24-27. September 2019 Muş, Türkiye.*
- [28] Fischer, R. A., & Maurer, R. Drought resistance in spring wheat cultivars. I. Grain yield responses. *Australian Journal of Agricultural Research*, 1978;29(5), 897-912.
- [29] Ekinçi R, Başbağ S, Karademir E, Karademir Ç. Determination of Heat Tolerance Levels of some Cotton Varieties and Lines Exist in Genetic Stock within Turkey. TUBITAK TOVAG Project p:156, Projec Number: 109O339, Diyarbakır, 2012
- [30] Khanna-Chopra, R., and Viswanathan C. Evaluation of heat stress tolerance in an irrigated environment of *T.aestivum* and related species. I. Stability in yield and yield components. *Euphytica* 1999;106:169-180
- [31] Roger G.P. Augmented Designs for Preliminary Yield Trials (Revised) Oregon State University, Corvallis, USA, RACHIS Vol. 4, No:1 Jan 1985 p:27-32
- [32] Sullivan C.Y. Mechanisms of heat and drought resistance in grain sorghum and methods of measurement. *Sorghum in Seventies.* Oxford and IBH Pub. Co. Heat shock protein expression in the thermotolerant and thermosensitive lines of cotton, 1972.
- [33] Sajid M., Saddique M.A.B, Tahir M.H.N, Matloob A., Ali Z., Ahmad F., Shakil Q., Nisa Z.U., Kifayat M. Physiological and molecular response of cotton (*Gossypium hirsutum* L.) to heat stress at the seedling stage. *March 2022 SABRAO journal of breeding and genetics* 2022;54(1):44-52 DOI: 10.54910/sabrao2022.54.1.5.
- [34] Farooq A., Shakeel A., Saeed A., Farooq J., Rizwan M., Chattha W.S., Sarwar G., Ramzan Y. Genetic variability predicting breeding potential of upland cotton (*Gossypium hirsutum* L.) for high temperature tolerance. Preprint from Research Square, 26 Aug 2022, DOI:10.21203/rs.3.rs-1957883/v1.
- [35] Zafar S.A., Noor M.A., Waqas M.A., Wang X., Shaheen T., Raza M., Rahman M.U. Temperature Extremes in Cotton Production and Mitigation Strategies. Additional information is available at the end of the chapter, 2018. <http://dx.doi.org/10.5772/intechopen.74648>
- [36] Jamil, A., Khan, S. J., & Ullah, K. Genetic diversity for cell membrane thermostability, yield and quality attributes in cotton (*Gossypium hirsutum* L.). *Genetic Resources and Crop Evolution*, 2020;67, 1405-1414.
- [37] Singh K, Wijewardana C, Gajanayake B, Lokhande S, Wallace T, Jones D. Genotypic variability among cotton cultivars for heat and drought tolerance using reproductive and physiological traits. *Euphytica* 2018;214: 1-22.
- [38] Malik MN, Chaudhry FI, Makhdum M.I. Cell membrane thermostability as a measure of heat-tolerance in cotton. *Pak. J. Sci. Ind. Res.* 1999;42:44-46.
- [39] Rahman H.U. Genetic analysis of stomatal conductance in upland cotton (*Gossypium hirsutum* L.) under contrasting temperature regimes. *J. Agric. Sci.* 2005;143:161-168.
- [40] Cottee N.S., Tan D.K.Y., Cothren T, Bange M P, Campbell L.C. Screening Cotton Cultivars for Thermotolerance under Field Conditions, 2007. [http://www.icac.org/meetings/wcrc/wcrc4/presentations/data/papers/P\\_aper2234.pdf](http://www.icac.org/meetings/wcrc/wcrc4/presentations/data/papers/P_aper2234.pdf).
- [41] Khan AI, Khan IA, Sadaqat H.A. Heat tolerance is variable in cotton (*Gossypium hirsutum* L.) and can be exploited for breeding of better yielding cultivars under high temperature regimes. *Pak. J. Bot.* 2008;40(5):2053-2058
- [42] Oosterhuis DM, Bourland FM, Bibi AC, Gonias ED, Loka D, Storch D. Screening for Temperature Tolerance in Cotton. *Summaries of Arkansas Cotton Research in 2008, AAES Research Series 573, 2009.* <http://arkansasagnews.uark.edu/573-5.pdf>
- [43] Abro S., Rizwan M., Deho Z.A., Abro S.A., Sial M.A. Identification of Heat Tolerant Cotton Lines Showing Genetic Variation in Cell Membrane Thermostability, Stomata, and Trichome Size and Its Effect on Yield and Fiber Quality Traits, 1 Plant Breeding and Genetics Division, Nuclear Institute of Agriculture (NIA), Tando Jam, Pakistan, 2 Technical Services Division, Nuclear Institute of Agriculture (NIA), 2022, Tando Jam, Pakistan. doi: 10.3389/fpls.2021.804315.
- [44] Asha R., Ahamed L.M. Screening of cotton genotypes for heat tolerance. *Int J Bioresour Stress Manag* 2016;4(4):599-604.
- [45] Majeed, S.; Rana, I.A.; Mubarak, M.S.; Atif, R.M.; Yang, S.-H.; Chung, G.; Jia, Y.; Du, X.; Hinze, L.; Azhar, M.T. Heat Stress in Cotton: A Review on Predicted and Unpredicted Growth-Yield

- Anomalies and Mitigating Breeding Strategies. *Agronomy* 2021, 11, 1825. <https://doi.org/10.3390/agronomy11091825>.
- [46] Khan, A.H., Min, L., Ma1, Y., Zeeshan, M., Jin, S., Zhang, X. High-temperature stress in crops: male sterility, yield loss and potential remedy approaches. *Plant Biotechnology Journal* (2023) 21, pp. 680–697. doi: 10.1111/pbi.13946.
- [47] Yousaf, M.I., Hussain, Q., Alwahibi, M.S., Aslam, M.Z., Khalid, M.Z., Hussain, S., Zafar, A., Shah, S.A.S., Abbasi, A.M., Mehboob, A., Riaz, M.W., Elshikh, M.S. Impact of heat stress on agromorphological, physio-chemical and fiber related paramters in upland cotton (*Gossypium hirsutum* L.) genotypes. *Journal of King Saud University – Science*, 35 (2023) 102379, <https://doi.org/10.1016/j.jksus.2022.102379>.

## Determination of Ground-Based Structural Problems in the Historical Four-Legged Minaret with Ground Penetration Radar

Süleyman İPEK<sup>1\*</sup>, Nursen IŞIK<sup>2</sup>, Fatma Meral HALİFEOĞLU<sup>3</sup>

<sup>1</sup> Bingöl University, Engineering and Architecture Faculty, Architecture Department, Bingöl, Türkiye

<sup>2</sup> Dicle University, Architecture Faculty, Architecture Department, Diyarbakır, Türkiye

<sup>3</sup> Dicle University, Architecture Faculty, Architecture Department, Diyarbakır, Türkiye

Süleyman İPEK ORCID No: 0000-0001-8891-949X

Nursen IŞIK ORCID No: 0000-0002-6125-1896

Fatma Meral HALİFEOĞLU ORCID No: 0000-0003-2032-3774

\*Corresponding author: [sipek@bingol.edu.tr](mailto:sipek@bingol.edu.tr)

(Received: 25.12.2022, Accepted: 14.06.2023, Online Publication: 22.06.2023)

### Keywords

Historical structure, Ground-penetrating radar, Masonry structure, Minaret, Nondestructive testing method

**Abstract:** The Four-Legged Minaret, which has an important place thanks to its building period and unique architecture, is located in the southeastern part of the historical Suriçi region of Diyarbakır. This structure located outside the courtyard of Sheikh Mutahhar Mosque and inside the Dört Ayaklı Minare Street was built on a monolithic stone column from basalt stone in a tetragon plan and is carried by four columns that are in cylindrical form. After 2015, partial damages occurred to the minaret. During the restoration works carried out between 2016-2019, these partial damages were tried to be repaired. But the condition of the ground was not instrumentally detected and investigated in these restoration works. In the present study, observational geological and instrumental geophysical studies were carried out on the Four-Legged Minaret and its surrounding area. The ground condition of the Four-Legged Minaret and the situation of its construction materials were determined by scannings achieved from the ground penetration radar and whether the damages in the structure were related to the ground condition was analyzed. As a consequence of the study, fractures and cracks were detected in the wall, and fractures, cracks, and water leakage-dependent collapses were detected on the floor. Besides, finally, repair recommendations for these damages are also presented in this study.

## Tarihi Dört Ayaklı Minare’de Zemine Dayalı Strüktürel Sorunların Yer Radarı ile Belirlenmesi

### Anahtar

**Kelimeler**  
Tarihi yapı,  
Yer radarı,  
Yığılma yapı,  
Minare,  
Tahribatsız  
deney yöntemi

**Öz:** Hem inşa edildiği dönem hem de sahip olduğu eşsiz mimariyle önemli bir yere sahip olan Dört Ayaklı Minare, Diyarbakır’ın tarihi Suriçi Bölgesinin güneydoğu diliminde yer almaktadır. Şeyh Mutahhar Cami avlusu dışında ve Dört Ayaklı Minare Sokak içinde bulunan bu yapı, yekpare taş sütun üzerinde bazalt malzemeden dört köşeli olarak inşa edilmiş olup, dört adet silindirik formlu sütunla taşınmaktadır. 2015 yılından sonra minarede kısmi hasarlar meydana gelmiştir. 2016-2019 yılları arasında yapılan restorasyon çalışmalarında bu kısmi hasarlar giderilmeye çalışılmıştır. Ancak yapılan bu restorasyon çalışmalarında zemine yönelik herhangi bir aletsel tespit ve inceleme yapılmamıştır. Bu çalışmada, Dört Ayaklı Minare ve çevresinde gözlemsel olarak jeolojik ve aletsel olarak jeofizik etütler yapılmıştır. Dört Ayaklı Minare’nin zemin durumu ve yapı malzemelerinin durumu, yer radarından yapılan taramalarla tespit edilmiş ve yapıda meydana gelen hasarların zemin durumu ile ilgili olup olmadığı analiz edilmiştir. Yapılan çalışma neticesinde, duvarda kırık ve çatlaklar, zeminde kırık, çatlak ve su sızıntılarına bağlı çökmeler olduğu tespit edilmiştir. Son olarak, bu hasarlara yönelik onarım önerileri de bu çalışmada sunulmuştur.

## 1. INTRODUCTION

The United Nations Educational, Scientific and Cultural Organization (UNESCO) describes the term ‘cultural heritage’ as the legacy, inherited from past generations, reaching today, and endowing for the benefit of future generations, that is associated with intangible attributes and physical science artifacts of a society or group [1,2]. But this term has been applied to tangible cultural heritages such as monuments, historical places, buildings, works of art, artifacts, and books, as well as intangible cultural heritages such as beliefs, traditions, language, folklore, knowledge, and customs, and natural heritages such as culturally significant marine ecosystems, landscapes, and biodiversity [1]. However, not all legacies passed down through the centuries qualify as legacy; rather, the item is designated as heritage by society [3]. In this manner, the preservation of historical buildings in all their physical forms makes this an important issue as it is a special component of the collective identity [4]. Human involvement and natural disasters like earthquakes, landslides, floods, etc. are typical causes of the deterioration of such buildings as time passes. Therefore, finding a route that combines and safeguards such historical structures should be created and followed to boost the efficiency of the fortification, conservation, and restoration method [4,5].

In this context, historical mosques, which are centers of worship and belief that have an important place in the social and cultural life of cities from past to present, can be regarded as tangible cultural heritage, implicitly also intangible cultural heritage. After the acceptance and spread of Islam, mosques were built in different forms and plans, reflecting the characteristics of the period in which they were built and used as places of worship. In many periods from the past to the present, minarets have been built in mosques for the purpose of reciting the azan and making reciting the azan heard. In this context, the first minaret example in the mosque was built in the Mosque of ‘Amr ibn al-‘As in Egypt in 673 AD, and it was built with a balcony to announce the azan [6].

Minarets, which were built from stones, bricks, and wood, did not have a certain shape in the beginning and there are two styles of minarets that might be described in general: the first style is inspired by ancient lighthouses and/or bell towers having a square/rectangular cross-section in-plane and the second style that originated in Asia constructed in a cylindrical slender body [7]. Minarets can be considered one of the distinctive and essential structural components of the Islamic cityscape [8]. Throughout history, countless majestic minarets have been built in various parts of the world adapting structural approaches and utilizing various materials [6]. Similar to many other ancient structures, the historical minarets are made of brick/stone and mortar and they are regarded as tower-like structures [9].

Diyarbakır which has hosted many civilizations and still has born traces of these civilizations is located in southeast Turkey. In the course of these periods, the social, cultural, religious, and interaction of communities

from different cultures and traditions with the local resident increased over time. With the spread of Islam, the majority of the city community perpetuated living according to Islamic traditions and rules. In this manner, mosques have become the buildings where the people of the city performed their religious worship and have been actively used in many parts of the city [10].

In the yearbooks of Diyarbakır, it is stated that there were 24 mosques and 21 masjids in the city center in the 1900s. In the Suriçi region, a limited number of the mosques that were constructed during the early Islamic period have survived to the present day, and a majority of the structures have been destroyed. Besides, there are no mosques or masjids that have survived to the present day from the Umayyad period, while information about the mosques belonging to the Abbasid period is learned from the inscriptions and reliefs on the city walls. The oldest mosque in the city is the Diyarbakır Ulu Mosque, which was built in the 7th century with the characteristics of Arabic architecture. Many of the other mosques were built during and after the Akkoyunlu period.

Khoja Ahmet (Ayn Minaret) Mosque (in 1489) was built in the southwest of the Suriçi region, Sheikh Mutahhar and the Four-Legged Minaret (in 1500) and Lala Kasım Bey Mosque in the southeast of the Suriçi region, Nebi Mosque (in 1503) and some masjids (such as İbrahim Bey, Hacı Büzruk, Tacettin masjids) were built in the northwest of the Suriçi region. Fatih Pasha (Kurşunlu) Mosque (in 1516-1520) and Nasuh Pasha Mosque (in 1601) in the northeast of the Suriçi region, Hüsrev Pasha Mosque and its madrasa (in 1521-1528) in the southeast of the Suriçi region, Ali Pasha Mosque (in 1534-1537) and Defterdar Mosque (in 1594) in the south of the Suriçi region, İskender Pasha Mosque (in 1551) and Melik Ahmet Pasha Mosque (in 1587-1591) in the northwest of the Suriçi region, Behram Pasha Mosque (in 1564-1567) in the southwest of the Suriçi region are among the Ottoman period mosques [11]. In Diyarbakır mosques, the minarets are built in either square (or nearly square) form or cylindrical form, while the minaret of the Khoja Ahmet (Ayn Minaret) Mosque has an octagonal form. The minarets of the Ulu Mosque, Nebi Mosque, Hz. Süleyman Mosque, Hüsrev Pasha Mosque, and Sheikh Mutahhar Mosque are in a square plan order. However, there are cylindrical annexes in most of these minarets. Figures 1a-n exhibit the mosques and their minarets in the Suriçi region in Diyarbakır.

Among the aforementioned minarets, the Four-Legged Minaret has an important status from the point of cultural heritage, due to its building period and peerless architecture, and the historical events it has witnessed. During the repair and restoration works carried out on the minaret, drilling works and compression tests were carried out in 2011 by the Regional Directorate of Foundations to determine the soil condition of this area. However, after this date, there is no convenient and useful examination of the soil condition of this building and its surrounding area. For this reason, the present study has importance since it is aimed to examine the

structural status of the building in regard to its soil condition. Because of that, the investigation of cracks, fractures, and partial axis slippage problems in the minaret depending on the soil structure was carried out with a non-destructive measurement method called ground-penetrating radar, and thereby, the structure was evaluated in this context. Here, it can be stated that nondestructive testing (NDT) is the examination of a system and its components and materials, in terms of situations and features using a number of analytical procedures [12]. Though fast progress in NDT technology has been witnessed due to increasing performance expectations from current buildings and engineering materials, the process of adapting NDT technologies to historical buildings is still in its infancy [5]. However, Moropoulou et al. [13] have recently defined NDT methods as essential instruments for cultural heritage buildings. The capacity to use NDT methods in situ and the elimination of the necessity for disruptive sample taking are the two most important benefits of using them on ancient buildings. They can be used not only to determine material situations and

characteristics like density, moisture content, strength, dimension, stiffness, etc., but also to detect discontinuities, anomalies, internal cracks, and voids in structure and/or its components. Additionally, they can be employed in displaying the architectural detailing and layouts, evaluating frame and structural performances of the building, and monitoring anomalies underground. Examining the qualities of historical materials, studying the origins of these materials, analyzing the environmental consequences, considering prior interferences, and, most importantly, searching the historical records may all be done as part of extensive studies on historical structures [4,13,14]. NDT methods which can be grouped into four major groups: electromagnetic, penetrating radiation, sound, and optical, can be particularly considered a valuable diagnostic tool for determining material qualities, environmental influences, and prior interferences [5]. In this way, using NDT methods on historical buildings prior to attempting any conservation or restoration may reveal specific scientific knowledge of the structure.



**Figure 1.** The photographic view of mosques and their minarets in the Suriçi region in Diyarbakır (taken in 2021): (a) Ulu Mosque, (b) Hz. Süleyman Mosque, (c) Safa (Parlı) Mosque, (d) Khoja Ahmet Mosque, (e) Sheikh Mutahhar Mosque (Four-Legged Minaret), (f) Nebi Mosque, (g) Fatih Pasha Mosque, (h) Hüsrev Pasha Mosque, (i) Ali Pasha Mosque, (j) İskender Pasha Mosque, (k) Behram Pasha Mosque, (l) Lala Kasım Bey Mosque, (m) Melik Ahmet Mosque, and (n) Nasuh Pasha Mosque



The GPR technique, which is one of the significant NTD methods, has been used frequently in the literature to assess and monitor the condition of historic buildings. By incorporating another nondestructive testing method, Alani et al. [15], for example, employed GPR to monitor the state of the stone arch bridges. Imposa [16], on the other hand, used the GPR technique to examine the inside walls of the “Sala delle Nicchie” of Florence’s Pitti Palace. Similar to this, before the Collemaggio Basilica, a medieval church in L’Aquila (central Italy), was restored, Ranalli et al. [17] assessed the Collemaggio Basilica’s façade’s condition of conservation and determined the thickness of its walls using the GPR approach. In order to create a structural model based on finite elements, Lubowiecka et al. [18] also used the GPR technique to determine the homogeneity or heterogeneity of the interior construction of an old bridge. Masini et al. [19] also provided three instances of GPR prospecting to see historical monuments. Three distinct constructional components, including a wall, a masonry pillar, and a marble column, were chosen for this study to describe the masonry, detect and locate fractures, and document the metallic reinforcing bars. In another investigation, Pieraccini et al. [20] used the GPR method to find cracks in the stone walls of the famous “Salone dei 500” chamber in the Palazzo Vecchio (Firenze, Italy). In addition to the investigations stated above, Yağciner et al. [21] employed the GPR technique to find a new temple at the Nysa archaeological site in western Turkey.

In this context, the target of the study is to investigate the subject of geological formations, the sequence changes, geometric behavior patterns, underground cavity structures and dimensions of ground/sub-structure fractures. For that purpose, a GPR device having 100-MHz and 1.8-GHz antennas were used for measurements, and 3D analyzes were carried out using the data obtained. The working area was separated into distinct places, and GPR sections in the shape of lines/profiles were obtained at each of these places. Penetration depths differ in regard to the measurement location: for example, 2.00 m was designated for the scanning of the load-bearing elements whereas 10 m as the shallowest and 20 m as the deepest were chosen for the ground scanning.

## 2. ARCHITECTURAL PROPERTIES AND LOCATION OF THE FOUR-LEGGED MINARET

Diyarbakır which is also included in the UNESCO Cultural Heritage List owing to its historical city walls [22] is located in the southeast of Turkey, as shown in Figure 2. Sheikh Mutahhar Mosque and Four-Legged Minaret, located in the southeast part of the Suriçi region that is surrounded by city walls and 82 towers as shown in Figure 2, were constructed in 1500 during the Akkoyunlu’s period [23]. The Suriçi region is largely populated with historical buildings [24].

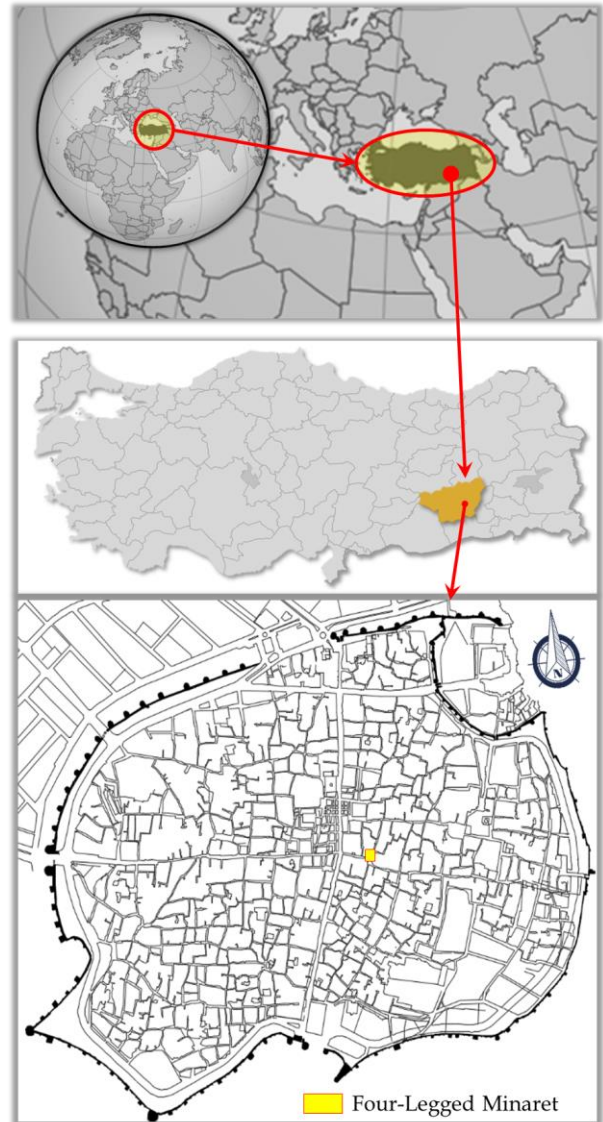
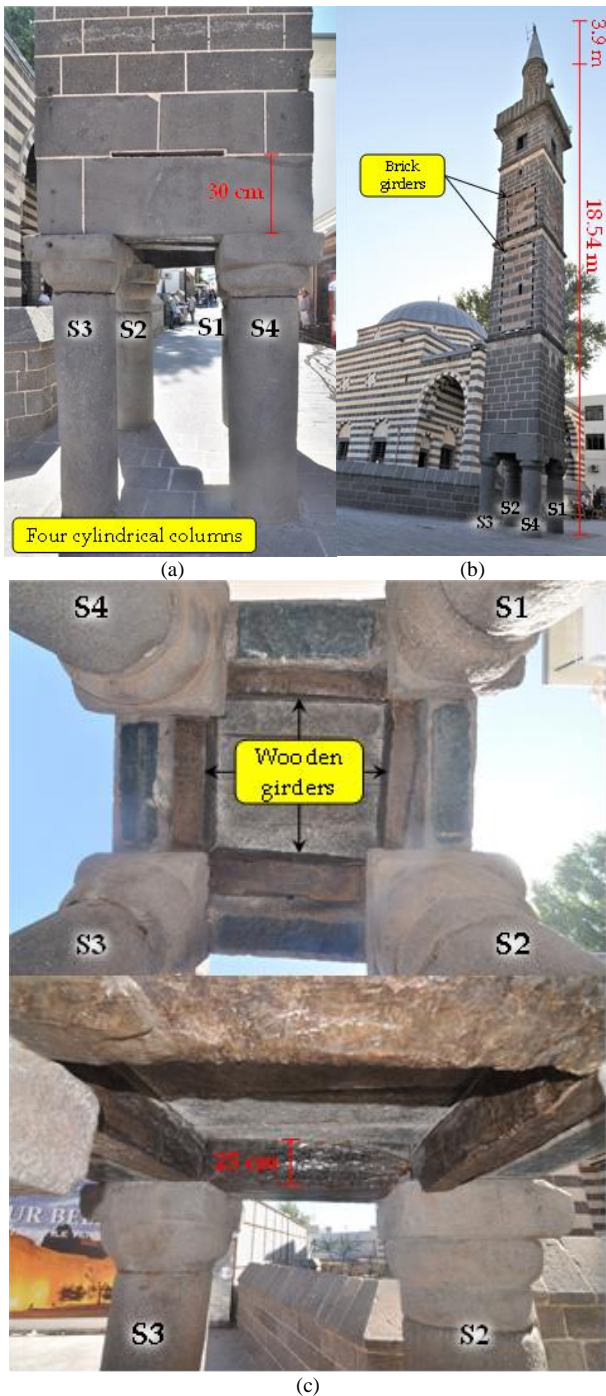


Figure 2. The location of Diyarbakır province on the map [25,26] and the Four-Legged Minaret in the Suriçi region

The Four-Legged Minaret is one of these historical buildings and it is located to the northeast of the Sheikh Mutahhar Mosque. The minaret has been repaired and restored many times from the time it was built to the present day in order to eliminate the existing problems in the minaret. However, nowadays, the minaret remained outside the borders of the mosque due to the widening of the street and the introduction of a wall boundary for the mosque, and hence, the minaret remained as an independent minaret in Yenikapı Street (known also as Four-Legged Minaret Street). The square-formed minaret is carried by four cylindrical columns as can be seen in Figure 3a. The minaret, which was built with the masonry technique, has a height of 18.54 m up to the spire and 22.44 m up to the top including the finial as marked in Figure 3b. The main building material used in the minaret is basalt; however, at certain intervals, brick was also used as a girder as indicated in Figure 3b. Besides, there are four wooden girders above the cylindrical columns and under the square minaret base as shown in Figure 3c.



**Figure 3.** Photographic view of: (a) four cylindrical columns (west view), (b) brick girders (west and north views), and (c) wooden girders (bottom view)

The diameter of each load-bearing column in the Four-Legged Minaret is different from the other: the diameters of the S1 (in the northwest direction) and S4 (in the northeast direction) labeled columns are about 51 and 55 cm, respectively, whereas that of the S2 (in the southwest direction) and S3 (in the southeast direction) named columns are 59 and 49 cm, respectively. For the array and labeling of the columns, see Figure 4a. There are wooden beams having a 25-cm height on these columns as shown in Figure 3c and a basalt lintel with a height of approximately 30 cm above these beams as can be seen in Figure 3a. A spiral staircase that can be also seen in Figure 4b starts after the level of +1.00 m in the minaret.

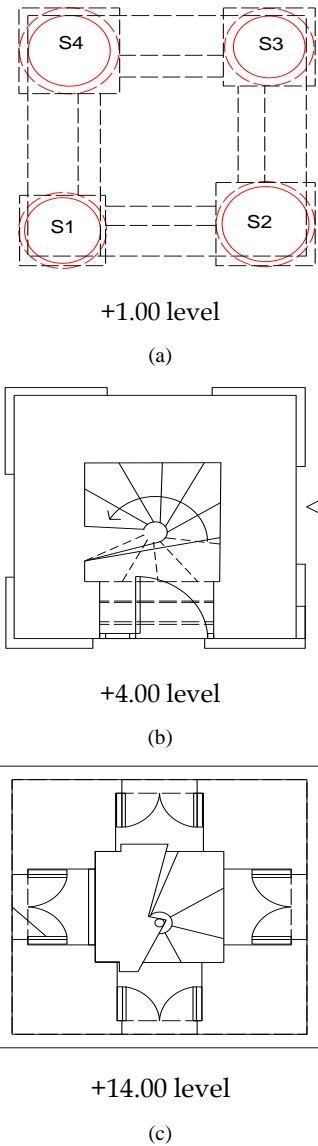


**Figure 4.** Plans of Four-Legged Minaret at: (a) +1.00, (b) +4.00, and (c) +14 levels

There are basalt cornices as three horizontal bands on the body. Between these cornices on the surfaces of the body, there is brickwork as partial stripes. The upper body section of the square planned minaret is located after a height of 15.37 m. This body in the basalt cylindrical form was completed with a lead spire as shown in Figure 3b. Besides, in the last section of the body, there is a window on each surface of the minaret, as can be seen in Figure 3b and shown in the plan view presented in Figure 4c.

During the restoration work of the Four-Legged Minaret carried out between 2011-2012, the cracks in the north and east directions were reinforced by injection. In addition, steel clamps were added to the lintels as part of this restoration as shown in Figure 5a. However, in 2015, the clamp added around the minaret was removed. Besides, the lintels on the columns of the minaret were strengthened using carbon fiber strips as can be seen in Figure 5b.

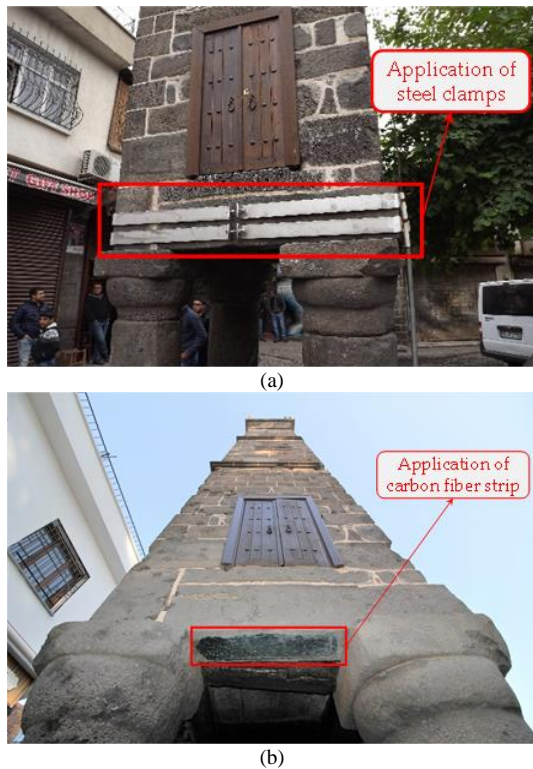


**Figure 5.** Photographic view of strengthening work on the Four-Legged Minaret: (a) application of steel clamps (taken in 2015) and (b) application of carbon fiber strip (taken in 2021)

### 3. MEASUREMENT METHOD

The GPR measuring technique consists of a simple system involving a recording device (computer) and two antennas named receiving and transmitting, as schematically exhibited in Figure 6.

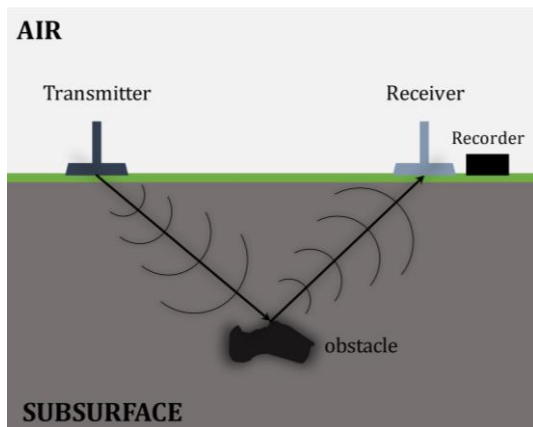


**Figure 6.** Schematic demonstration of the working principle of a typical GPR system

The transmitting antenna generates multi-nanosecond electromagnetic waves in the horizontal direction, parallel to the electric field vector. During the measurement progress, any anomaly, obstacle, disturbances, and/or negativity leads to the reflection and scattering of the waves under the ground and on the surface. In such conditions, waves are reflected and start to move through the upstream direction, and thereby, they are captured by the receiving antenna, and then the receiving antenna transfers these waves to the computer. In broad, this method is based on the difference between

electromagnetic signals produced by the transmitting antenna and captured by the receiving antenna, during its underground travel [27]. The most important components of these signals are the electrical and magnetic constants of the energy transfer process. The resulting data and fluctuations are therefore called “radar traces”. These nanosecond measurements and radar traces are concatenated into a time unit, and the resulting portions are called “radargrams” [28].

GPR signals arrive at the objective by determining their speed according to the physical and chemical characteristics of the environment it is traveling to, thus collecting information about the target during this travel. In situations where the travel time is known and the speed of the medium is also known, the target depth can be determined with precision. Herein, the most important factors are the signal distribution and the environments in which the travel of electromagnetic signals can be affected. As previously stated, the receiving ( $R_x$ ) and transmitting ( $T_x$ ) antennas constitute the GPR system where the short high-frequency radio signals are emitted by transmitting antennas and the signals are picked up by the receiving antennas while being reflected by the obstacle or target, or by layers with different dielectric constant. Unlike seismic reflections, GPR produces reflections from both strata and buried objects. Objects with different electromagnetic properties such as water tables, sediment layers, foundation structures, buried tanks, and archaeological remains lead to reflections in the GPR. In other words, GPR reflections generally occur because objects have different dielectric constants. The dielectric constant reveals how much charge an object can store when an electromagnetic charge is applied to it. In this context, Conyers [27] graphically demonstrated an inverse relationship between radar travel speed and partial dielectric constant, as shown in Figure 7.

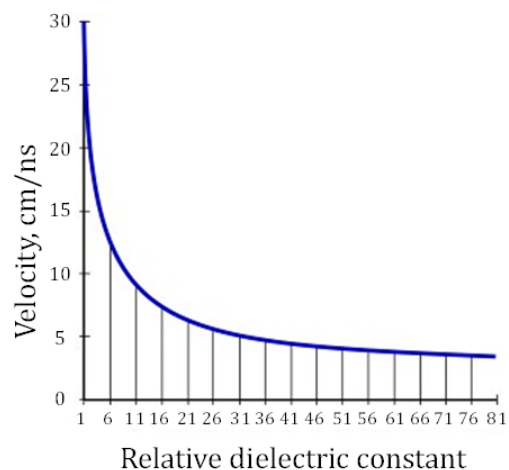


**Figure 7.** The inverse relationship between radar travel speed and partial dielectric constant [27]

There are just a few studies in the literature that look at the dielectric constants of various materials [29-31]. In radar frequencies, the dielectric constant of dry rocks usually ranges from 3 to 5, while water has dielectric values of 80-81. In general, dielectric constants of rocks,

which contain water, vary between 6 and 30, depending on the amount of water they retain. In the present study, a device setup having a constant width between the transmitting and receiving antennas was used to examine the ground and structure-dependent damages of the Four-Legged Minaret. Sheltered antennas were used in the measurements and both the transmitting and receiving antennas were placed into a box then, it was moved on the ground, and thereby traces under the ground were collected in the course of this movement process. Subsequently, thousands of traces were collected, which form the profile when they are put together. After some measurements, anomaly situations on the surface were clarified with the help of three-dimensional images. In order to carry out the GPR scanning on both Four-Legged Minaret and its surrounding area, a Python-3 named GPR device having frequency values of 250/100/50/38/25 MHz and the antenna length changing between 1 to 4 m depending on the frequency value was employed [32] and besides, Prism 2 named software was used to manage the data processing steps in the GPR measurement works. The internal Wi-Fi system in the device provided the data transmission to the computer. The device may be used with both default and custom digital filters, and it can display 16-bit digital data. The device also features a user-selectable time range of 1 to 2500 ns with a 1 ns step, as well as a 28 and 1024x16-bit scan rate and samples per scan, respectively. 100 MHz and 1.6 GHz antennas were used for measurements in this study. In addition to these measurements, 3D analyzes were carried out using the data obtained.

The subject of geological formations, the sequence changes, geometric behavior patterns, underground cavity structures, and dimensions of ground/sub-structure fractures are included in this study. Besides, the conditions and changes of the formations and the classifications according to the characteristics of the host rocks and their electromagnetic permeability were also taken into consideration. In this case, the working area was separated into distinct places, and GPR sections in the shape of lines/profiles were obtained at each of these places. The exact depth capability of the GPR is highly dependent on the antenna frequency, the soil conditions and material properties, the quality and capability of the equipment, and the size of the target. The depth of radar penetration and the ability to identify the target object at any depth depends on the soil properties in that area. If the soil is highly conductive, the GPR method may be ineffective. In this regard, the maximum penetration depth of the GPR into the ground can be determined by the total propagation loss, which is determined by the electrical properties of the materials. Different penetration depths have been determined depending on the GPR equipment and antenna used in this study, the soil characteristics of the area being surveyed, and the size of the target. For example, 4.00 m was designated for scanning the structural elements, while 10 m was chosen as the shallowest and 20 m as the deepest for scanning the ground. Figure 8 shows some representative photographs taken during the GPR measurements.



**Figure 8.** A typical application of the GPR on: (a) the ground of the surrounding area of the minaret, (b) the basalt lintel of the minaret, and (c) the column of the minaret

For good data to be generated, it is necessary to perform proper filtering after careful measuring, which is suitable for interpreting [21]. Converting the obtained numerical data into understandable images is the basis of data processing in GPR measurements. The following filtering processes which are explained in detail by Işık et al. [14] are applied to obtain understandable images once the pure data is obtained from the site [33]:

- i. First-time filter
- ii. Current correction (Dewow)
- iii. Energy delay
- iv. Average value cleaning:
- v. Velocity analysis

#### 4. RESULTS AND DISCUSSION

As previously noted, the research location, which has a 5-degree slope and a 660 elevation, is located in Diyarbakır province's Sur district (called Suriçi region). The lithological sequence from the earth's surface to the subterranean in this study region, its near surrounds, and certain section cuts are detected as vegetable soil unit, clayey sandy unit, and clayey silty sand unit in accordance with the prior geological and geotechnical research. Despite these sequence alterations revealing local variances in areas, they generally follow the same pattern as the one described above.

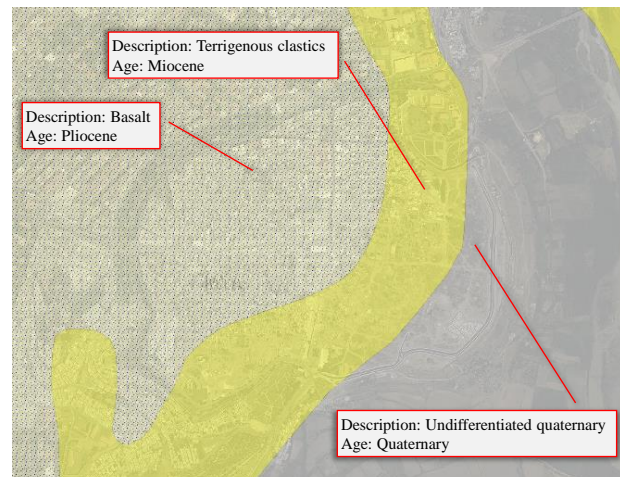


**Figure 9.** Possible geology map related to the immediate environment of the study area [34]

In regard to the General Directorate of Mineral Research and Exploration, as shown in Figure 9, the geology of the research region and its close surrounds comprises basalt, terrigenous clastics, and undifferentiated quaternary belonging to the Pliocene epoch, Miocene epoch, and quaternary period, respectively. Terrigenous clastics from the Miocene epoch, on the other hand, are widespread in this research region and its close surroundings.

#### 4.1. Observationally Detected Structural Problems in the Four-Legged Minaret

Due to the fact that the minaret was outside the courtyard of the mosque due to its location, partial material losses occurred due to vehicle hits. In addition, in 2015, damage such as fragmentation and abrasion due to firearms occurred on columns S1 and S2 in the northwest direction of the minaret, and bullet holes occurred in some places (see Figure 10).



**Figure 10.** Photographic views of damages caused by firearms on: (a) the body and (b) columns of the Four-Legged Minaret (taken in 2021)

During the restoration work carried out between 2016-2017, no comprehensive repairs were made to the minaret, except for cleaning and removing mortar losses. Especially, there has not been any attempt to complete the material losses in the minaret during the period of vehicle traffic. The existing crack in the lintel of the minaret in the northwest direction was filled with injection during the repair works. In addition, macro-sized (visible) cracks were detected on the lintels on the

columns in the northeast and southeast directions (see Figure 11).

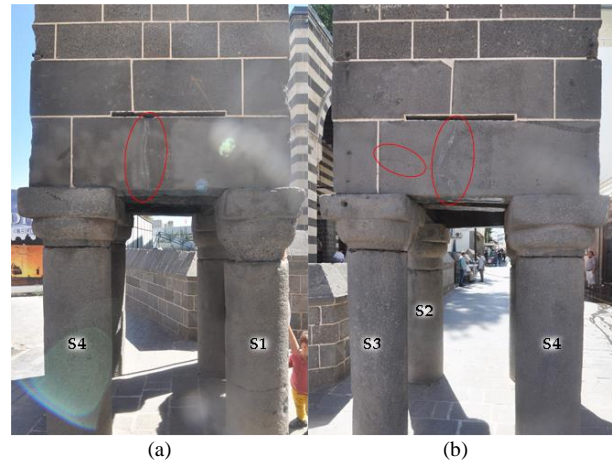
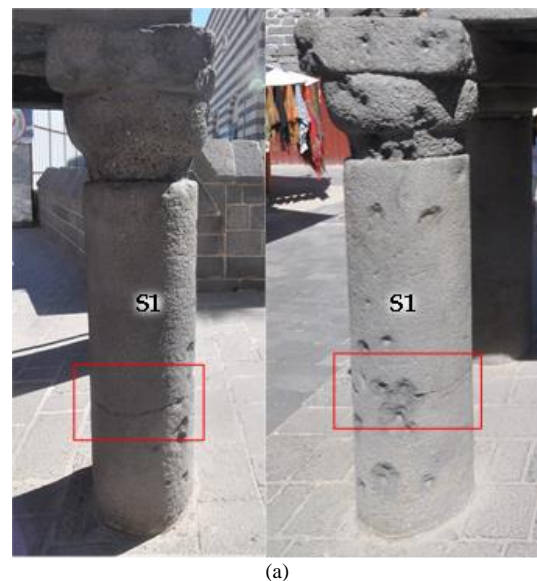


**Figure 11.** Photographic view of crack damage on lintels on: (a) S1-S4 columns in the northeast direction and (b) S3-S4 columns in the southeast direction (taken in 2021)

There are level irregularities on the street floor where the minaret is located. Although the street floor where the minaret is located was renewed with cut stone during the repair works, no detailed examination was done on the cause and correction of the level irregularities on the street floor. Besides, partial axis slippage due to vehicle hit, vibration, and level irregularity on the street floor has been observationally detected at the column heads. However, these irregularities and damages were not eliminated during the repairs. In addition, there is a horizontal crack in the middle part of the S1 column due to the loss of material because of the hit of a large number of bullets in that area and the impact of these bullets (see Figure 12). The wooden girders on the minaret columns are original but partially damaged. During the repair work, they were maintained by applying impregnation and protective paint for wood protection, and thereby, the current condition of the wooden girders was preserved.



(a)

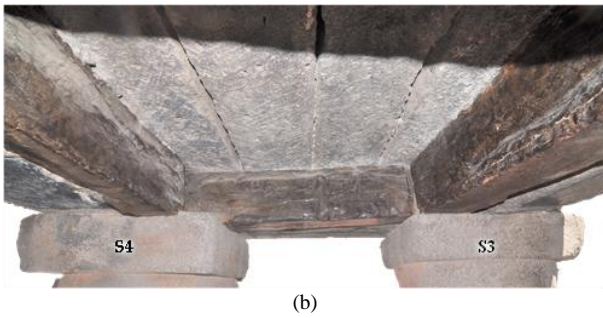


Figure 12. Photographic view of: (a) the horizontal crack on column S1 and its location and (b) the current condition of wooden girders

## 4.2. GPR Measurements and Evaluations on the Four-Legged Minaret

### 4.2.1. Ground scanning

GPR scanings on the ground of the Four-Legged Minaret were carried out by dividing the area into zones. Figure 13 indicates the location and border of each zone in which the GPR scanings were carried out. The GPR Z1 labeled zone had a profile length of 80.0 m while the GPR Z2 and GPR Z3 labeled zones had profile lengths of 50.0 m and 74.0 m, respectively. In all zones, the penetration depth was designated as 20.0 m.

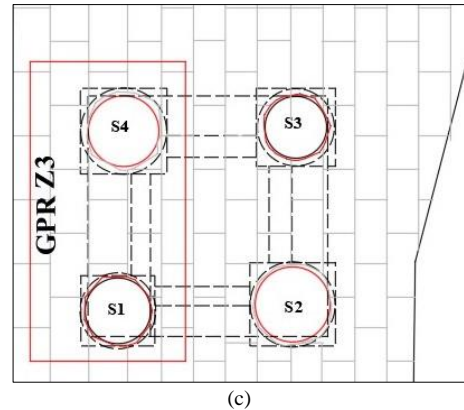
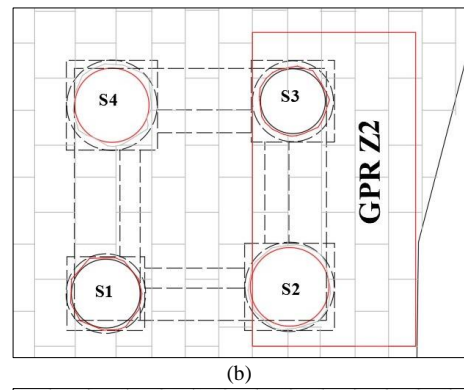
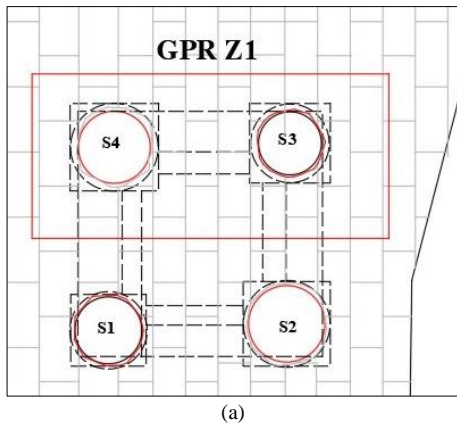
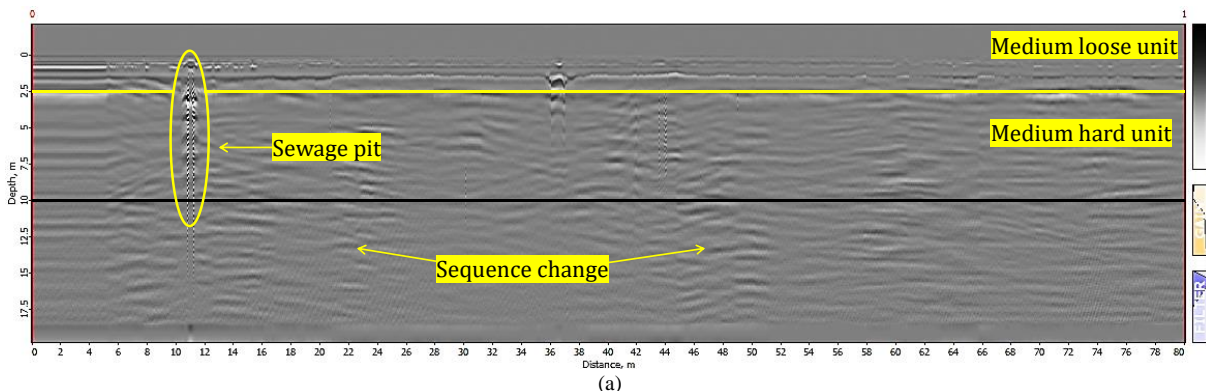


Figure 13. The locations and borders of the GPR scanning zones on the ground (each zone is shown by the box in red color)

Figures 14a-c demonstrate the 2-dimensional GPR sections taken at zones 1, 2, and 3, respectively. As marked in these figures, 2 different levels were observed from the radargram section of each zone. It is considered to be a medium loose unit of about 2.50 m in the upper part, and a medium hard unit between 2.50 and 10.00 m. As indicated in Figure 14a, there is a sewer pit starting at a depth of 2.50 m and lasting about 10.00-12.00 m throughout the profiling of zone 1. Additionally, in this zone, there is no anomaly formation on the ground, except for the sequence changes. On the other hand, subsidence anomaly formations were identified in the profiling of zone 2. As can be seen in Figure 14b, the regions starting at a depth of 7.50 m lasting through 10.00 and 26.00 m took in water, thus collapsed. In the profiling of zone 3, only subsidence deformations caused by taking in water were detected, as pointed out in Figure 14c. These anomalies are starting at the depth of 5.00 m and lasting through the 50.00 and 52.00 m.



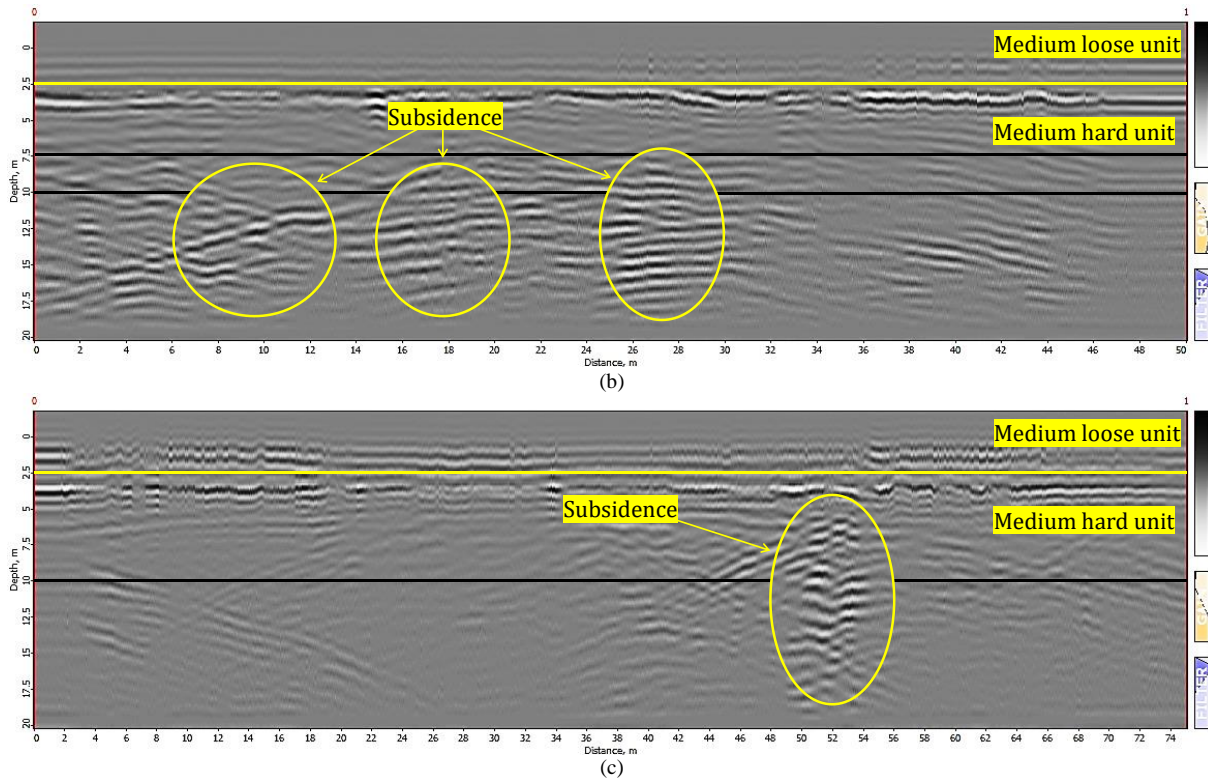


Figure 14. GPR sections: (a) taken at zone 1, (b) taken at zone 2, and (c) taken at zone 3

4.2.2. Lintel scanning

In addition to the GRP scanings on the ground, the lintels on the columns of the Four-Legged Minaret were also scanned by dividing the area into two regions named GPR 1 and GPR 2. Figure 15 indicates the border of each region in which the GPR scanings of lintels were carried out. In the scanning of the region named GPR 1, the profile length was designed as 10.0 m while in the GPR 2 labeled region, it was chosen as 15.0 m. In both regions, the 4.00-m penetration depth was designated. Region 1 involves the lintels on the S2-S3 columns and S3-S4 columns while region 2 includes the lintels on the S1-S2 columns and S1-S4 columns.

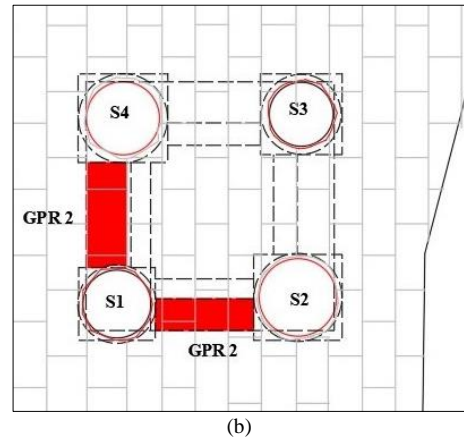
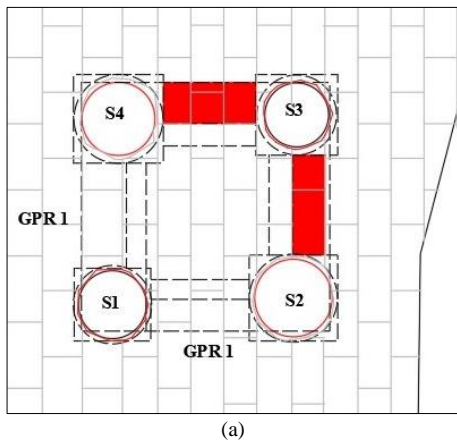


Figure 15. The indication of the GPR scanning regions on the lintels (each region is shown by the red color)



In regard to the radargram section obtained from region 1 (see Figure 16a), it can be stated that it has been observed that the cracks and fractures in the lintels are at a level that will affect the load-bearing system of the minarets. It is considered that cracks and fractures, the smallest 12.00 cm and the largest 20.00 cm, have been detected on the lintels in this area. On the other hand, broken V-type crack systems are at the maximum level in the lintels of region 2, as pointed out in Figure 16b. It is thought that the detected damages on the lintels may adversely influence the load-bearing system of the minaret.

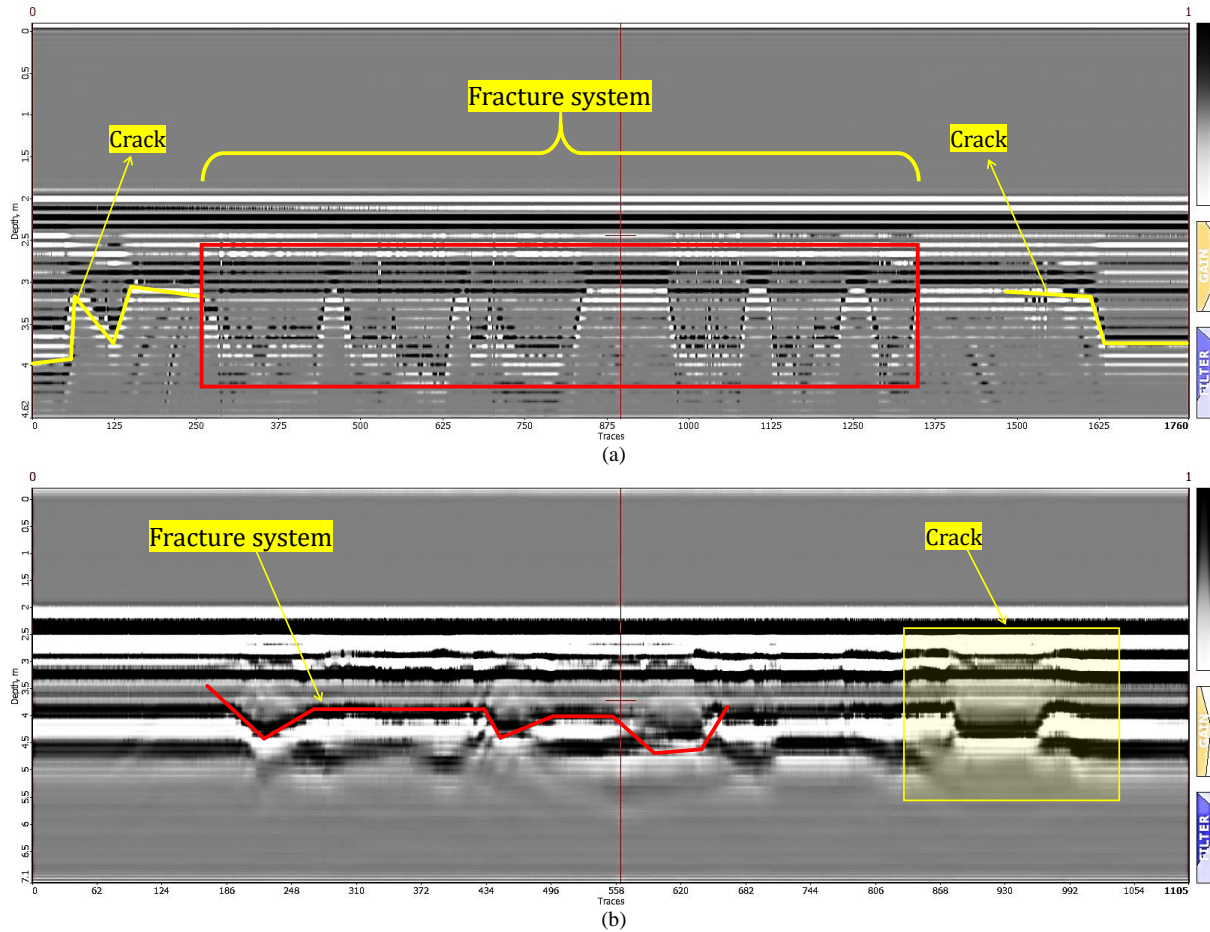


Figure 16. GPR sections: (a) taken at Region 1 and (b) taken at Region 2

### 4.2.3. Column scanning

Unlike the GPR scanings carried out on the ground and lintels of the Four-Legged Minaret, 3-dimensional GPR scanning was performed on the S2 named column. Crack-, fracture-, and corrosion-dependent deformations were detected in this scanning. In order to simulate the crack and fracture formations, spectral color was appointed in the radargram section of column 2, as shown in Figure 17. In the scanning, the areas and locations involving cracks and fractures are demonstrated by red color. In regard to the radargram sections, it can be stated that the cracks and fractures accumulated in the lower regions of the scanned column.

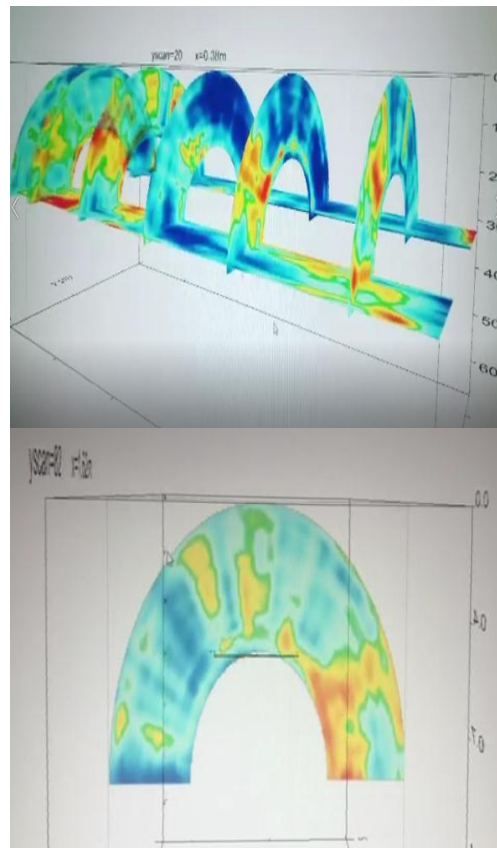
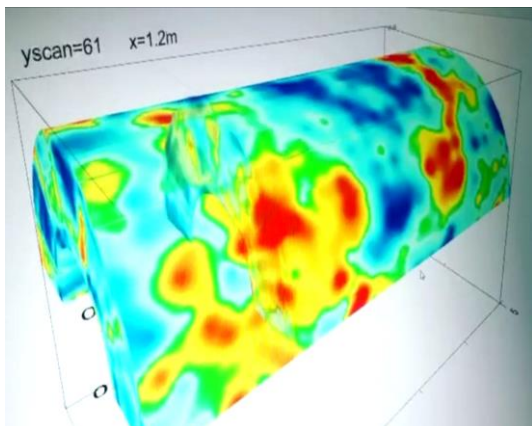


Figure 17. 3D GPR sections of S2 named column of the Four-Legged Minaret



## 5. CONCLUSIONS AND RECOMMENDATIONS

Based on the findings presented above, the following conclusions and recommendations can be drawn:

GPR scans and studies were carried out for the existing damages under the ground and on the load-bearing members of the Four-Legged Minaret in the Suriçi region of Diyarbakır province. In the studies carried out, the current condition of the ground and possible damages and deformations in the load-bearing members were determined and revealed by the radargram sections obtained from the GPR scannings. In the scannings carried out on the Four-Legged Minaret, the conditions of the deformations, their variations, the properties of the surrounding rocks, and their classification according to their electromagnetic permeability were taken into account. As a result of the ground scanning, it was observed that the sequence changes were differentiated at 2 different levels. A medium loose unit was detected from the ground to a depth of 2.50 m, and a medium-hard unit formation was detected between 2.50-10.00 m. It was detected that there was a sewage pit in the scanning zone named GPR Z1 to the east of the minaret. On the south of the minaret, in the scanning zone named GPR Z2, deformations caused by water leakage and related collapse were detected after the levels of 7.50-10.00 m. In the ground scans of the zone called GPR Z3 to the north of the minaret, voids due to collapse were detected in the soil. Some cracks and fractures can be visually seen on lintels in the north and east directions of the Four-Legged Minaret. During the restoration works carried out in 2012 and 2017, the existing cracks were filled with injections. However, in the GPR scans, it was detected that the existing cracks and fractures continued into the inside of the lintels. On the other hand, fragment losses caused by vehicle hits during the periods when the street was open to vehicle traffic were detected on the columns by observational investigation. In addition, by the time, axis slippages have occurred due to the absence of any tension ring or any protective application between the top caps of the columns and the column bodies. The column diameters of the minaret are close to each other. There are fragmentations and abrasions caused by firearms in 2015 in the columns (S1 and S2) in the northwest and southwest directions of the minaret. In the S2 named column, 3D GPR scannings were made and material losses, corrosion, and cracks were detected, and besides, it was observed that they accumulated in the lower regions of the column.

To repair the existing damages on the Four-Legged Minaret, comprehensive survey and restoration projects should be prepared under the leadership of the relevant experts, and reinforcement applications should be carried out immediately. In addition to the determination of the damages on the minaret with non-destructive methods, observation pits should be opened in the regions determined by the experts and the physical condition of the ground should be determined. Soil improvements should be carried out around the building, and also columns and walls having axis slippages should be suspended, and reinforcement work should be

conducted. In the past years, GPR scanning was not carried out during the restoration works carried out on the ground and load-bearing members of the Four-Legged Minaret. For this reason, it is very important because it is the first study to determine the problems in this cultural heritage using the GPR technique. In recent years, damage assessment studies using non-destructive methods employed for historical buildings continue increasingly. The GPR technique is an important non-destructive geophysical method used for historical buildings. For this reason, it is thought that this method, which will be used for historical buildings, will be an up-to-date guide for all historical buildings, specific to the Four-Legged Minaret.

## REFERENCES

- [1] Sullivan AM. Cultural Heritage & New Media: A Future for the Past. *John Marshall Rev Intel Prop Law*. 2016;15(3):604-46.
- [2] UNESCO [Internet]. Cultural Heritage; 2022 [cited 2022 November 19]. Available from: [https://en.unesco.org/creativity/sites/creativity/files/cdis/heritage\\_dimension.pdf](https://en.unesco.org/creativity/sites/creativity/files/cdis/heritage_dimension.pdf)
- [3] Logan WS. Closing Pandora's Box: Human rights conundrums in cultural heritage protection. In: Silverman H, Ruggless DF, editors. *Cultural Heritage and Human Rights*. Springer, New York-ABD, 2007; p. 33-52.
- [4] Ortega-Ramirez J, Bano M, Cordero-Arce MT, Villa-Alvarado LA, Frafa CC. Application of Non-invasive Geophysical Methods (GPR and ERT) to Locate the Ancient Foundations of the First Cathedral of Puebla, Mexico: A case study. *J Appl Geophy*. 2020;174:103958.
- [5] Işık N, Halifeoğlu FM, İpek S. Nondestructive testing techniques to evaluate the structural damage of historical city walls. *Constr Build Mater*. 2020;253:119228.
- [6] Bağbancı, MB, Bağbancı, ÖK. Structural health monitoring through vibration-based approaches. *Shock Vibr*. 2018;2018:9853896.
- [7] Usta, P. Assessment of seismic behavior of historic masonry minarets in Antalya, Turkey. *Case Stud Constr Mater*. 2021;15:e00665.
- [8] Günaydın, M, Tonyalı, Z. Dynamic response of a reinforced concrete minaret. *J Struct Eng App Mech*. 2018;1(2):62-72.
- [9] Ercan, E, Arısoy, B, Hökelekli, E, Nuhoğlu, A. Estimation of seismic damage propagation in a historical masonry minaret. *Sigma J Eng Nat Sci*. 2017;5(4):647-666.
- [10] Beysanoğlu Ş. Anıtları ve Kitabeleri ile Diyarbakır Tarihi 2, İrmak Matbaası, Ankara-Turkey; 1998.
- [11] Han Z. Diyarbakır kültür envanteri, Cilt 1, T.C. Diyarbakır Valiliği İl Kültür ve Turizm Müdürlüğü, Müze Müdürlüğü, Diyarbakır-Turkey; 2015.
- [12] Umar, MU, Hanafi, MH, Latip, NA. Analysis of non-destructive testing of historic building structures. *Australian J Basic App Sci*. 2015;9(7):326-330.
- [13] Moropoulou, A, Labropoulos KC, Delegou, ET, Karoglou, M, Bakolas, A. Non-destructive

- techniques as a tool for the protection of built cultural heritage. *Constr Build Mater.* 2013;48:1222-1239.
- [14] Işık N, Halifeoğlu FM, İpek S. Detecting the ground-dependent structural damages in a historic mosque by employing GPR. *J App Geophy.* 2022;199:104606.
- [15] Alani AM, Tosti F, Ciampoli LB, Gagliardi V, Benedetto A. An integrated investigative approach in health monitoring of masonry arch bridges using GPR and InSAR technologies. *NDT&E Inter.* 2020;115:102288.
- [16] Imposa S. Infrared Thermography and Georadar Techniques Applied to the “Sala delle Nicchie” (Niches Hall) of Palazzo Pitti, Florence (Italy). *J Cult Herit.* 2010;11:259-264.
- [17] Ranalli D, Scozzafava M, Tallini M. Ground penetrating radar investigations for the restoration of historic buildings: the case study of the Collemaggio Basilica (L’Aquila, Italy). *J Cult Herit.* 2004;5(1):91-99.
- [18] Lubowiecka I, Armesto J, Arias P, Lorenzo H. Historic bridge modelling using laser scanning, ground penetrating radar and finite element methods in the context of structural dynamics. *Eng Struct.* 2009;31(11):2667-2676.
- [19] Masini N, Persico R, Rizzo E. Some examples of GPR prospecting for monitoring of the monumental heritage. *J Geophy Eng.* 2010;7(2):190-199.
- [20] Pieraccini M, Noferini L, Mecatti D, Luzzi G, Atzeni C, Persico R, Soldovieri R. Advanced processing techniques for step-frequency continuous-wave penetrating radar: The case study of “Palazzo Vecchio” Walls (Firenze, Italy). *Res Nondestruct Eva.* 2006;17(2):71-83.
- [21] Yalçiner CÇ, Bano M, Kadioglu M, Karabacak V, Meghraoui M, Altunel E. New temple discovery at the Archaeological Site of Nysa (Western Turkey) using GPR method. *J Archaeol Sci.* 2009;36:1680-1689.
- [22] UNESCO [Internet]. United Nations Educational, Scientific and Cultural Organization – World Heritage in Turkey; 2016 [cited 2022 November 19]. Available from: [http://www.unesco.org.tr/Content\\_Files/Content/Ya\\_yinlar/wht\\_2016.pdf](http://www.unesco.org.tr/Content_Files/Content/Ya_yinlar/wht_2016.pdf)
- [23] Atılğan A [Internet]. Diyarbakır’da Dört Ayaklı Minare; 2015 [cited 2022 December 04]. Available from: <http://mimdap.org/2015/12/diyarbakyrdadort-ayakly-minare-arif-atylgan>
- [24] Işık N, Halifeoğlu FM, İpek S. A Proposal for the Conservation and Integration of Historic Diyarbakır City Walls: the Urfa Gate. Towers and City Walls, *Turkish J Nat Sci.* 2020;9(2):146-156.
- [25] Wikipedia [Internet]. Turkey; 2022 [cited 2022 November 20]. Available from: <https://commons.wikimedia.org/w/index.php?curid=7818230>
- [26] Wikipedia [Internet]. Diyarbakır; 2022 [cited 2022 November 20]. Available from: <https://commons.wikimedia.org/w/index.php?curid=7123114>
- [27] Conyers LB. *Ground-Penetrating Radar for Archaeology (Geophysical Methods for Archaeology)*, 3th Edition, Lanham, AltaMira Press, Rowman & Littlefield Publishers; 2013.
- [28] Kadioğlu S, Ulugergerli EU. Determination of cavities using ground penetrating radar in Dalaman-Akköprü Dam construction area. The 16th International Geophysical Congress and Exhibition of Turkey, 7-10 December, Ankara; 2004.
- [29] Davis JL, Annan, AP. Ground-penetrating radar for high-resolution mapping of soil and rock stratigraphy. *Geophysical Prospecting*, 1989;37:531-551.
- [30] Reynolds JM. *An Introduction to Applied and Environmental Geophysics*, John Wiley & Sons, New York-USA; 1997.
- [31] Daniels DJ. *Ground Penetrating Radar (Radar, Sonar and Navigation)*, 2nd Edition, The Institution of Electrical Engineers, London-England; 2004.
- [32] Phthon-3 GPR [Internet]. Radar Systems Inc. Products; 2022 [cited 2022 November 23]. Available from: <http://www.radsys.lv/en/products-soft/products/prod/6>
- [33] Leucci G, Negri S. Use of ground penetrating radar to map subsurface archaeological features in an urban area. *J Archaeol Sci.* 2006;33:502-512.
- [34] MTA [Internet]. Geoscience Mapviewer and Drawing Editor, General Directorate of Mineral Research and Exploration; 2022 [cited 2022 November 26]. Available from: <http://yerbilimleri.mta.gov.tr/anasayfa.aspx>

## Carvacrol Ameliorates Sodium Arsenite-Induced Intestinal Toxicity

Mustafa İLERİTÜRK<sup>1\*</sup> , Özge KANDEMİR<sup>2</sup> 

<sup>1</sup> Ataturk University, Horasan Vocational College, Department of Animal Science, Erzurum, Türkiye

<sup>2</sup> Aksaray University, Aksaray Technical Sciences Vocational School, Aksaray, Türkiye

Mustafa İLERİTÜRK ORCID No: 0000-0002-4581-4492

Özge KANDEMİR ORCID No: 0000-0001-8884-4168

\*Corresponding author: [m.ileriturk@atauni.edu.tr](mailto:m.ileriturk@atauni.edu.tr)

(Received: 10.05.2023, Accepted: 15.06.2023, Online Publication: 22.06.2023)

### Keywords

Apoptosis,  
Carvacrol,  
Inflammation,  
Intestinal  
toxicity,  
Oxidative  
stress,  
Sodium arsenite

**Abstract:** Arsenic is a very dangerous metal that is widely distributed in the environment as a result of anthropogenic and natural processes. On the other hand, it is thought that treatment with natural flavonoids may protect against arsenic toxicity. Carvacrol (CRV) is a naturally occurring phenolic compound with anti-inflammatory, anti-apoptotic, and antioxidant properties. This study aims to investigate the protective effects of CRV on sodium arsenite (SA)-induced intestinal toxicity. For this purpose, rats were randomly divided into five groups and administered SA and CRV orally for 14 days. The data indicate that when SA is administered, lipid peroxidation increase and antioxidant enzyme activities decrease. The administration of CRV ameliorated this impairment in the antioxidant defense system. Examining the expression levels of NF- $\kappa$ B and IL-1 $\beta$  revealed that inflammation increased with SA application but decreased with CRV administration. Moreover, the expression levels of Caspase-3 and Apaf1 increased in rats treated with SA, whereas the severity of apoptosis decreased when CRV was administered. In light of these findings, it is possible to state that CRV protects tissues from damage by presenting antioxidant, anti-inflammatory, and anti-apoptotic effects in SA-induced intestinal toxicity.

## Carvacrol, Sodyum Arsenit Kaynaklı İnce Bağırsak Toksisitesini İyileştirmektedir

### Anahtar Kelimeler

Apoptoz,  
Carvacrol,  
İnce bağırsak  
toksisitesi,  
İnflamasyon,  
Oksidatif stres,  
Sodyum arsenit

**Öz:** Arsenik, doğal ve antropojenik faaliyetler yoluyla çevrede bol miktarda bulunan son derece tehlikeli bir metaldir. Bununla beraber doğal flavonoidlerle tedavinin arsenik toksisitesine karşı koruyucu etkisi olabileceği öngörülmektedir. Carvacrol (CRV) antioksidan, anti-inflamatuvar ve antiapoptotik özellikleri bilinen doğal bir fenolik bileşiktir. Bu çalışmanın amacı sodyum arsenit (SA) ile oluşturulan ince bağırsak toksisitesinde CRV'nin koruyucu etkilerinin araştırılmasıdır. Bu amaçla ratlar rastgele 5 gruba ayrıldı ve 14 gün boyunca oral olarak SA ve CRV uygulaması gerçekleştirildi. Veriler SA uygulaması ile lipid peroksidasyonunun şekillendiğini antioksidan enzim aktivitelerinin ise azaldığını göstermektedir. Antioksidan savunma durumundaki bu bozukluk CRV uygulaması ile azaldı. NF- $\kappa$ B ve IL-1 $\beta$  ekspresyon düzeylerine bakıldığında SA uygulaması ile inflamasyonun şiddetlendiği CRV uygulaması ile bu şiddetin azaldığı tespit edildi. Buna ek olarak yine SA uygulanan ratlarda artan Caspase-3 ve Apaf1 ekspresyon düzeylerinin CRV uygulaması ile düştüğü ve apoptozun şiddetinin azaldığı belirlendi. Tüm bu veriler ışığında SA kaynaklı ince bağırsak toksisitesinde CRV'nin antioksidan, anti-inflamatuvar ve antiapoptotik etki göstererek dokuları hasarda koruduğu söylenebilir.

### 1. INTRODUCTION

The health effects of arsenic are becoming more serious worldwide [1]. The main source of arsenic exposure is drinking water that has more arsenic than is allowed. Drinking water may get contaminated with arsenic due to natural deposits, industrial processes, and excessive use of

agricultural pesticides and rodenticides [2]. Multiple organs, including intestine, are affected by arsenic [3]. Arsenic is also a well-known cancer-causing substance that results in a variety of malignant tumors in people [4]. The most extensively researched and recognized mechanism for arsenic poisoning is oxidative stress, despite the fact that it has not yet been fully understood.

Lipid peroxidation and reactive oxygen species (ROS) are both increased by arsenic, which leads to organ damage [5]. In addition, arsenic depletes antioxidants that are protective, including glutathione (GSH), superoxide dismutase (SOD), and glutathione peroxidase (GPx). Therefore, by reducing the impact of reactive oxygen metabolites on cellular components, increasing cellular antioxidant capacity may be useful in limiting the toxicity of arsenic.

Protein inactivation and an increase in ROS are caused by arsenic binding to the sulfhydryl groups of proteins and glutathione [6, 7]. Additionally, it has been shown that increased ROS may damage DNA and trigger pathways that result in cell death [8]. Due to this, antioxidant molecules are thought to be a potential therapy for arsenic poisoning, and interest in using naturally occurring phytochemicals is growing daily.

Carvacrol (CRV), also known as 5-isopropyl-2-methylphenol, is a phenolic monoterpene present in the essential oils of many Lamiaceae plants [9, 10]. This substance was shown to have antioxidant, anti-inflammatory, anticancer, antispasmodic, and chemoprotective properties in earlier in vitro and in vivo research [11, 12]. According to studies, CRV not only improves endogenous antioxidant levels but also defends against inflammation, which is the underlying cause of many diseases, by controlling the expression of genes that are essential for inflammation [13].

The purpose of this study was to determine whether CRV has protective effects against sodium arsenite-induced intestinal toxicity.

## 2. MATERIAL AND METHOD

### 2.1. Supply, Care and Ethics Committee Approval of Experimental Animals

35 male Sprague-Dawley rats weighing between 220 and 250 g and aged 10 to 12 weeks were used in the experiment. Ataturk University Medical Experimental Application and Research Center provided the animals. They had free access to water and standard laboratory pellet feeds. They were kept in an environment with a temperature of  $24 \pm 1$  °C, humidity of  $45 \pm 5$  %, and a light/dark cycle of 12 hours. Before administering the compounds, the animals were observed for one week to corroborate that they had adapted to the environment. All animal investigations were conducted at the Medical Experimental Research Center of Ataturk University. The Ataturk University Animal Experiments Local Ethics Committee approved the investigation (Protocol Number: 2022-11-226) with ethics committee approval.

### 2.2. Experimental Procedure

Rats were randomly divided into 5 groups, with 7 animals in each group.

- *Control Group*: For 14 days, physiological saline was administered orally.

- *CRV Group*: For 14 days, 50 mg/kg CRV was orally administered to rats.
- *SA Group*: The rats received 10 mg/kg sodium arsenite (SA) orally for 14 days.
- *SA + CRV 25 Group*: The rats received 10 mg/kg SA for 14 days, followed by 25 mg/kg CRV administered 30 minutes later.
- *SA + CRV 50 Group*: The rats received 10 mg/kg SA for 14 days, followed by 50 mg/kg CRV administered 30 minutes later.

24 hours after the last sodium arsenide administration, animals were decapitated under mild sevoflurane anesthesia. Intestine tissue was stored at  $-80$  °C for biochemical and Real-Time PCR studies.

### 2.3. Preparation of Tissue Homogenates

To generate the intestine tissue homogenate, the tissues were diluted 1:20 with phosphate-buffered saline (PBS; pH 7.4). With a tissue lysate device (TissueLyser II, Qiagen), the resulting mixture was quickly homogenized. 30 minutes at  $+4$  °C and 3000 rpm were spent centrifuging the homogenate. Analysis was conducted using the supernatant.

### 2.4. Determination of Oxidative Stress Status

Using the method established by Placer et al.[14], the level of lipid peroxidation was determined by quantifying the amount of malondialdehyde (MDA). SOD activity was determined using a method developed by Sun et al.[15]. The catalase (CAT) activity was measured using a method established by Aebi [16], and the data were expressed as catal/g protein. GPx activity was assessed using a technique created by Lawrence and Burk [17]. GSH levels were determined using the method described by Sedlak and Lindsay [18]. The Lowry et al.[19] technique was used to analyze total protein, with bovine serum albumin serving as the reference.

### 2.5. Real -Time PCR Analysis

After collecting intestinal tissues from animals treated with sodium arsenide and carvacrol, the expression levels of the genes Nrf2, HO-1, NF- $\kappa$ B, IL-1 $\beta$ , Caspase-3, and Apaf-1 were examined using the RT-PCR technique. In accordance with the manufacturer's instructions, tissues were treated with QIAzol Lysis Reagent (79306; Qiagen) to obtain total RNAs. Concentrations of RNAs were measured in NanoDrop (BioTek Epoch). The obtained RNAs were then transformed into double-stranded cDNAs using the iScript cDNA Synthesis Kit (Bio-Rad). This procedure was carried out in accordance with the manufacturer's instructions, and the following reaction conditions were established:

1. Priming: 5 minutes at 25 °C
2. Reverse transcription: 20 minutes at 46 °C
3. RT inactivation: 1 minute at 95 °C

In the final phase of the analysis, cDNAs, primers of the pertinent genes, and the mixture prepared with iTaq

Universal SYBR Green Supermix (BIORAD) were reacted in the Rotor-Gene Q (Qiagen) device using the time and temperature cycles indicated by the manufacturer. Following the completion of the cycles, the CT values provided by the device were normalized according to  $\beta$ -Actin. This process was performed according to the  $2^{-\Delta\Delta CT}$  method [20]. Primer sequences have been presented in Table 1.

**Table 1.** Primer sequences

Gene	Sequences (5'-3')	Length (bp)
NF- $\kappa$ B	F: AGTCCCGCCCTTCTAAAAC R: CAATGGCCTCTGTGTAGCC	106
IL-1 $\beta$	F: ATGGCAACTGTCCTGAACT R: AGTGACACTGCCTTCTGAA	197
Apaf-1	F: ACCTGAGGTGTCAGGACC R: CCGTCGAGCATGAGCCAA	192
Caspase-3	F: ACTGGAATGTCAGCTCGCAA R: GCAGTAGTCGCCTCTGAAGA	270
Nrf2	F: TTTGTAGATGACCATGAGTCGC R: TCCTGCCAACTTGCTCCAT	161
HO-1	F: ATGTCCCAGGATTTGTCCGA R: ATGGTACAAGGAGGCCATCA	144
$\beta$ -Actin	F: CAGCCTTCCTTCTTGGGTATG R: AGCTCAGTAACAGTCCGCCT	360

## 2.6. Statistical Analysis

One-way analysis of variance (One-way ANOVA) was used to perform a statistical analysis of the biochemical and Real-Time PCR data. Tukey's multiple comparison test was employed to determine whether there was a significant difference between the groups. Results were shown as mean  $\pm$  standard deviation. Statistical significance was defined as a p value  $<0.05$ .

## 3. RESULTS

### 3.1. Effect of CRV on Lipid Peroxidation in SA-Induced Intestine Toxicity

Table 2 shows the effects of CRV against SA-induced lipid peroxidation in intestine tissue. Compared with the control group, SA increased MDA levels, an essential biomarker of lipid peroxidation, by approximately 1.7-fold. The levels of SA-induced lipid peroxidation reduced with CRV and approached those of the control group. The therapeutic efficacy of the CRV doses of 25 mg/kg and 50 mg/kg was also statistically significantly different ( $p < 0.01$ ).

**Table 2.** Effect of CRV on oxidative stress biomarkers in SA-induced intestinal toxicity

	Control	CRV	SA	SA+CRV 25	SA+CRV 50
MDA (nmol/g tissue)	75,3 $\pm$ 5,6 <sup>###</sup>	73,2 $\pm$ 4,3 <sup>###</sup>	126,1 $\pm$ 8,7 <sup>***</sup>	110,0 $\pm$ 6,6 <sup>**</sup>	83,8 $\pm$ 6,3 <sup>###/ΔΔ</sup>
GSH (nmol/g tissue)	6,2 $\pm$ 0,5 <sup>###</sup>	7,0 $\pm$ 0,5 <sup>###</sup>	3,9 $\pm$ 0,4 <sup>***</sup>	4,4 $\pm$ 0,3 <sup>**</sup>	5,3 $\pm$ 0,5 <sup>#</sup>
CAT (katal/g protein)	25,1 $\pm$ 1,6 <sup>###</sup>	23,7 $\pm$ 1,4 <sup>###</sup>	12,9 $\pm$ 0,9 <sup>***</sup>	15,2 $\pm$ 1,0 <sup>***</sup>	21,2 $\pm$ 1,2 <sup>**/###/ΔΔΔ</sup>
SOD (U/g tissue)	11,0 $\pm$ 0,9 <sup>###</sup>	11,3 $\pm$ 0,8 <sup>###</sup>	5,7 $\pm$ 0,5 <sup>***</sup>	7,4 $\pm$ 0,7 <sup>***</sup>	9,2 $\pm$ 0,7 <sup>###</sup>
GPx (U/g tissue)	28,9 $\pm$ 1,6 <sup>###</sup>	27,6 $\pm$ 1,7 <sup>###</sup>	13,4 $\pm$ 1,0 <sup>***</sup>	18,5 $\pm$ 1,3 <sup>###/***</sup>	24,5 $\pm$ 1,2 <sup>**/###/ΔΔ</sup>

Statistical significance (Control vs others: \* $p < 0.05$ , \*\* $p < 0.01$ , \*\*\* $p < 0.001$ , SA vs others: # $p < 0.05$ , ## $p < 0.01$ , ### $p < 0.001$ , SA + CRV 25 vs SA + CRV 50:  $\Delta p < 0.05$ ,  $\Delta\Delta p < 0.01$ ,  $\Delta\Delta\Delta p < 0.001$ ) was analyzed using One Way ANOVA.

### 3.2. Effect of CRV on Enzymatic and Non-Enzymatic Antioxidant Markers in SA-Induced Intestine Toxicity

In the study, it was determined that SA reduced the activity of antioxidant enzymes relative to the control group ( $p < 0.001$ ). In addition, GSH stores, an essential antioxidant in the body, were found to decrease by approximately 37% in response to SA treatment. This indicates that SA causes oxidative stress in intestine tissue. As contrast to the SA group, the CRV-treated groups showed higher GSH levels and SOD, CAT, and GPx activities that were closer to those of the control group ( $p < 0.001$ ). In addition, there was a statistically significant difference between the 25 mg/kg and 50 mg/kg doses of CRV for CAT and GPx ( $p < 0.001$ ,  $p < 0.01$ , respectively). Table 2 presents the data for enzymatic and non-enzymatic indicators in intestine tissue.

### 3.3. Effect of CRV on Nrf2 and HO-1 in SA-Induced Intestine Toxicity

In addition to biochemical analyses, the mRNA expression levels of Nrf-2 and HO-1 were measured to further clarify the oxidative stress state. According to the obtained results, the expression levels of Nrf-2 and HO-1 in rats administered SA were lower than those in the control group ( $p < 0.001$ ). It was found that CRV co-administration reversed this expression decrease and regulated the antioxidant defense mechanism. There was a significant difference between low-dose and high-dose CRV administration ( $p < 0.05$  and  $p < 0.001$ , respectively). Figure 1 shows the mRNA transcription levels on Nrf2 and HO-1.

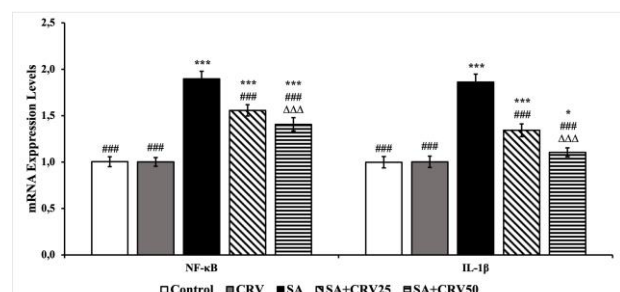


**Figure 1.** The mRNA transcript level of Nrf2 and HO-1 in the intestine of rats. All data were expressed as mean  $\pm$  SD. Statistical significance (Control vs others: \* $p < 0.05$ , \*\* $p < 0.01$ , \*\*\* $p < 0.001$ , SA vs others: # $p < 0.05$ , ## $p < 0.01$ , ### $p < 0.001$ , SA + CRV 25 vs SA + CRV 50:  $\Delta p < 0.05$ ,  $\Delta\Delta p < 0.01$ ,  $\Delta\Delta\Delta p < 0.001$ ) was analyzed using One Way ANOVA.

### 3.4. Effect of CRV on Inflammation in SA-Induced Intestine Toxicity

Real-time PCR was used to determine the NF- $\kappa$ B and IL-1 $\beta$  mRNA transcript levels in intestine tissue to determine the inflammation. Analysis of mRNA transcripts revealed that NF- $\kappa$ B and IL-1 $\beta$  increased considerably in the SA group compared to the control group ( $p < 0.001$  for both). The levels of NF- $\kappa$ B and IL-1 $\beta$  were decreased in the CRV-treated group compared to the SA-treated group ( $p < 0.001$  for both dosages). Figure 2 shows the mRNA transcript levels of NF- $\kappa$ B and IL-1 $\beta$ .

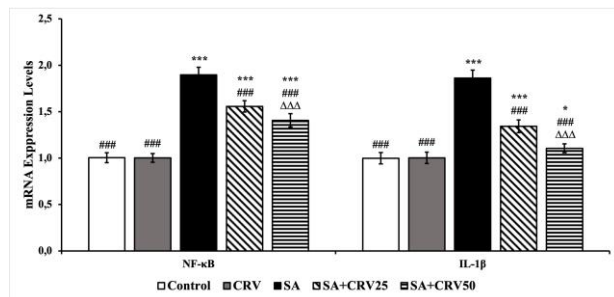


**Figure 2.** The mRNA transcript level of NF- $\kappa$ B and IL-1 $\beta$  in the intestine of rats. All data were expressed as mean  $\pm$  SD. Statistical significance (Control vs others: \* $p < 0.05$ , \*\* $p < 0.01$ , \*\*\* $p < 0.001$ , SA vs others: # $p < 0.05$ , ## $p < 0.01$ , ### $p < 0.001$ , SA + CRV 25 vs SA + CRV 50:  $\Delta p < 0.05$ ,  $\Delta\Delta p < 0.01$ ,  $\Delta\Delta\Delta p < 0.001$ ) was analyzed using One Way ANOVA.

### 3.5. Effect of CRV on Apoptosis in SA-Induced Intestine Toxicity

The degree of apoptosis in intestine tissue was determined by analyzing mRNA transcript levels of Caspase-3 and Apaf1. According to the findings of mRNA transcripts, Caspase-3 and Apaf1 levels in the SA group were 2.21 and 2.25 times higher, respectively, than in the control group (Figure 3). With CRV co-administration, Caspase-3 and Apaf1 transcript levels decreased compared to SA alone ( $p < 0.001$ ). Evaluating the difference between the two groups revealed that the 50 mg/kg dosage was more effective than the 25 mg/kg dose ( $p < 0.001$ ).

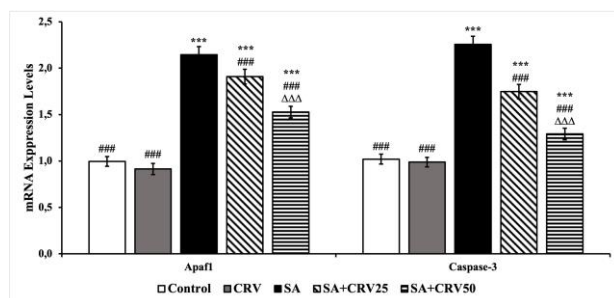


**Figure 3.** The mRNA transcript level of Caspase-3 and Apaf1 in the intestine of rats. All data were expressed as mean  $\pm$  SD. Statistical significance (Control vs others: \* $p < 0.05$ , \*\* $p < 0.01$ , \*\*\* $p < 0.001$ , SA vs others: # $p < 0.05$ , ## $p < 0.01$ , ### $p < 0.001$ , SA + CRV 25 vs SA + CRV 50:  $\Delta p < 0.05$ ,  $\Delta\Delta p < 0.01$ ,  $\Delta\Delta\Delta p < 0.001$ ) was analyzed using One Way ANOVA.

## 4. DISCUSSION AND CONCLUSION

Arsenite is prevalent in the environment and is harmful to virtually all body tissues; therefore, it is essential to focus on alternative therapies to mitigate and avoid its effects

[21, 22]. Recent research on the efficacy of natural flavonoids against the toxicity of heavy metals suggests that these compounds may be useful in mitigating and avoiding the effects of arsenite. Arsenite exposure is damaging to tissues in a variety of ways, some of the most widely acknowledged of which include an increase in ROS that leads to oxidative stress. Because ROS contribute to the pathogenesis of arsenite toxicity, their elimination should be one of the protective targets [23, 24]. A natural herb, CRV contains anti-inflammatory and antioxidant properties [25]. However, it has not yet been investigated for its possible protective effect against arsenite-induced intestinal damage. This study investigated the anti-inflammatory, antioxidant, and antiapoptotic effects of CRV on the SA-induced intestinal toxicity of rats.

The initial line of defense against reactive oxygen species damage is provided by enzymes like SOD, CAT, and GPx. CAT and GPx break down hydrogen peroxide into water and molecular oxygen, whereas SOD catalyzes the transformation of superoxide radical into extremely dangerous hydrogen peroxide and normal molecular oxygen, which can cause persistent cell damage [26, 27]. Free radicals, peroxides, and heavy metals are just a few examples of the ROS that may harm cells, and GSH is a nonenzymatic antioxidant that protects against these effects. GSH can become oxidized (GSSG) when it binds free radicals, and the GSSG/GSH ratio is a significant indicator of oxidative stress [28, 29]. MDA is an indicator that membrane lipids have been damaged by oxidation, which is strongly linked to the amount of lipid peroxidation [30, 31]. It has been demonstrated that SA inhibits the activity of antioxidant enzymes and causes oxidative stress and lipid peroxidation [32]. This study investigated the protective and beneficial effects of CRV on SA-induced intestinal toxicity. It was found that SA increased oxidative stress and decreased the antioxidant system in intestinal tissue. On the other hand, it was discovered that CRV reduced intestinal injury by reducing the effectiveness of free radicals and activating the antioxidant system. It was discovered that SA caused oxidative damage by inducing an inverse relationship between SOD, CAT, and GPx enzyme activity and MDA concentrations in intestinal tissues. Alternatively, it was discovered that CRV inhibits the deterioration of the oxidant-antioxidant balance by scavenging free radicals, resulting in a decrease in MDA levels by restoring antioxidant enzyme activity and replenishing GSH reserves.

The transcription factor NF- $\kappa$ B plays a crucial role in the production of inflammatory cytokines and the onset of the immune response in a variety of tissues [33-35]. In a previous study, it was discovered that SA promotes inflammation in tissues via triggering NF- $\kappa$ B activation [36]. In the present study, it was shown that SA increased NF- $\kappa$ B transcript levels in intestinal tissues, leading to oxidative stress and tissue damage; CRV treatment given in combination with SA decreased NF- $\kappa$ B transcript levels and intestinal toxicity. The secretion of the proinflammatory mediator IL-1 $\beta$  is decreased by preventing the translocation of NF- $\kappa$ B to the nucleus. In

the present study, an increase in IL-1 $\beta$  transcript levels was found, and it was hypothesized that this was due to an increase in NF- $\kappa$ B gene expressions resulting from SA-induced ROS production.

Cell death occurs naturally via a process called apoptosis [37, 38]. However, tissue function becomes disrupted when it develops excessively [39]. Apoptotic factors Caspase-3 and Apaf1 play crucial roles in the apoptotic process and are commonly used biomarkers for determining apoptotic state. In our research, SA treatment increased Caspase-3 and Apaf1 expressions. On the other hand, it has been discovered that CRV may inhibit Caspase-3 and Apaf1 expressions, thereby reducing apoptosis. Similarly, a recent study showed that Caspase-3 expression increased significantly after CRV administration [6].

As a result, it was found that CRV had anti-oxidant, anti-inflammatory, and anti-apoptotic effects in intestinal toxicity induced by SA, decreasing ROS formation and healing tissue and organ damage. It was therefore determined that utilizing CRV as a supportive treatment in SA toxicity would be beneficial.

## REFERENCES

- [1] Nikraves M, Mahdavinia M, Neisi N, Khorsandi L, Khodayar MJ. Citicoline ameliorates arsenic-induced hepatotoxicity and diabetes in mice by overexpression of VAMP2, PPAR- $\gamma$ , As3MT, and SIRT3. *Pestic Biochem Physiol.* 2023;192:105391.
- [2] Anetor JJ, Wanibuchi H, Fukushima S. Arsenic exposure and its health effects and risk of cancer in developing countries: Micronutrients as host defence. *Asian Pac J Cancer P.* 2007;8(1):13-23.
- [3] Liu RQ, Kong SQ, Shao YX, Cai DW, Bai B, Wei XG, et al. Chorover, Mechanisms and health implications of toxicity increment from arsenate-containing iron minerals through in vitro gastrointestinal digestion. *Geoderma.* 2023;432:116377.
- [4] Brown KG, Ross GL. Arsenic, drinking water, and health: A position paper of the American Council on Science and Health. *Regul Toxicol Pharm.* 2002;36(2):162-174.
- [5] Caglayan C, Demir Y, Kucukler S, Taslimi P, Kandemir FM, Gulcin I. The effects of hesperidin on sodium arsenite-induced different organ toxicity in rats on metabolic enzymes as antidiabetic and anticholinergics potentials: A biochemical approach. *J Food Biochem.* 2019;43(2): e12720.
- [6] Akaras N, Gur C, Kucukler S, Kandemir FM. Zingerone reduces sodium arsenite-induced nephrotoxicity by regulating oxidative stress, inflammation, apoptosis and histopathological changes. *Chem Biol Interact.* 2023;374:110410.
- [7] Kuzu M, Kandemir FM, Yildirim S, Caglayan C, Kucukler S. Attenuation of sodium arsenite-induced cardiotoxicity and neurotoxicity with the antioxidant, anti-inflammatory, and antiapoptotic effects of hesperidin. *Environ Sci Pollut Res Int.* 2021;28(9):10818-10831.
- [8] Turk E, Kandemir FM, Yildirim S, Caglayan C, Kucukler S, Kuzu M. Protective Effect of Hesperidin on Sodium Arsenite-Induced Nephrotoxicity and Hepatotoxicity in Rats. *Biol Trace Elem Res.* 2019;189(1):95-108.
- [9] Yesildag K, Gur C, Ileriturk M, Kandemir FM. Evaluation of oxidative stress, inflammation, apoptosis, oxidative DNA damage and metalloproteinases in the lungs of rats treated with cadmium and carvacrol. *Molecular Biology Reports.* 2022;49(2):1201-1211.
- [10] Nouri A, Izak-Shirian F, Fanaei V, Dastan M, Abolfathi M, Moradi A, Khaledi M, Mirshekari-Jahangiri H. Carvacrol exerts nephroprotective effect in rat model of diclofenac-induced renal injury through regulation of oxidative stress and suppression of inflammatory response. *Heliyon.* 2021;7(11): e08358.
- [11] Kandemir FM, Caglayan C, Darendelioglu E, Kucukler S, Izol E, Kandemir O. Modulatory effects of carvacrol against cadmium-induced hepatotoxicity and nephrotoxicity by molecular targeting regulation. *Life Sciences.* 2021;277:119610.
- [12] Gur C, Akarsu SA, Akaras N, Tuncer SC, Kandemir FM. Carvacrol reduces abnormal and dead sperm counts by attenuating sodium arsenite-induced oxidative stress, inflammation, apoptosis, and autophagy in the testicular tissues of rats. *Environ Toxicol.* 2023;38: 1265-1276.
- [13] Riaz M, Al Kury LT, Atzaz N, Alattar A, Alshaman R, Shah FA, et al. Carvacrol Alleviates Hyperuricemia-Induced Oxidative Stress and Inflammation by Modulating the NLRP3/NF- $\kappa$ B. *Drug Des Dev Ther.* 2022;16:1159-1170.
- [14] Placer ZA, Cushman LL, Johnson BC. Estimation of product of lipid peroxidation (malonyl dialdehyde) in biochemical systems. *Anal Biochem.* 1966;16(2):359-364.
- [15] Sun Y, Oberley LW, Li Y. A simple method for clinical assay of superoxide dismutase. *Clin Chem.* 1988;34(3):497-500.
- [16] Aebi H. Catalase in vitro. *Methods Enzymol.* 1984;105:121-126.
- [17] Lawrence RA, Burk RF. Glutathione peroxidase activity in selenium-deficient rat liver. *Biochem Biophys Res Commun.* 1976;71(4):952-958.
- [18] Sedlak J, Lindsay RH. Estimation of total, protein-bound, and nonprotein sulfhydryl groups in tissue with Ellman's reagent. *Anal Biochem.* 1968;25(1):192-205.
- [19] Lowry OH, Rosebrough NJ, Farr AL, Randall RJ. Protein measurement with the Folin phenol reagent. *J Biol Chem.* 1951;193(1):265-275.
- [20] Livak KJ, Schmittgen TD. Analysis of relative gene expression data using real-time quantitative PCR and the 2(-Delta Delta C(T)) Method. *Methods.* 2001;25(4):402-408.
- [21] Oyagbemi AA, Omobowale TO, Asenuga ER, Ochigbo GO, Adejumbi AO, Adedapo AA, et al. Sodium arsenite-induced cardiovascular and renal

- dysfunction in rat via oxidative stress and protein kinase B (Akt/PKB) signaling pathway. *Redox Report.* 2017;22(6):467-477.
- [22] Oyibo A, Gbadegesin MA, Odunola OA. Ethanol extract of *Vitellaria paradoxa* (Gaertn, F) leaves protects against sodium arsenite - induced toxicity in male wistar rats. *Toxicol Rep.* 2021;8:774-784.
- [23] Mehrzadi S, Goudarzi M, Fatemi I, Basir Z, Malayeri A, Khalili H. Chrysin attenuates sodium arsenite-induced nephrotoxicity in rats by suppressing oxidative stress and inflammation. *Tissue Cell.* 2021;73:101657.
- [24] Panghal A, Sathua KB, Flora SJS. Gallic acid and MiADMSA reversed arsenic induced oxidative/nitrosative damage in rat red blood cells. *Heliyon.* 2020;6(2):e03431.
- [25] Bashir N, Ahmad SB, Rehman MU, Muzamil S, Bhat RR, Mir MUR, et al. Zingerone (4-(4-hydroxy-3-methylphenyl) butane-2-ol) modulates adjuvant-induced rheumatoid arthritis by regulating inflammatory cytokines and antioxidants. *Redox Rep.* 2021;26(1):62-70.
- [26] İleritürk M, Doğan T, Kandemir Ö. Investigation of the Effect of Berberine with Arginase Activity and Oxidant-Antioxidant Parameters on Bortezomib-Induced Spleen Injury in Rats. *Kocatepe Vet J.* 2021;14:6-15.
- [27] İleritürk M, Doğan T, Statıcı E, Rutin'in Deltamethrin ile Mide Toksikitesi Geliştirilen Ratlarda Oksidatif Stres, Apoptoz ve İnflamasyon Parametreleri Üzerine Etkisinin Araştırılması. *Fırat Üniversitesi Sağlık Bilimleri Veteriner Dergisi* 2021;35(3): 158-165.
- [28] Kandemir FM, İleritürk M, Gur C. Rutin protects rat liver and kidney from sodium valproate-induced damage by attenuating oxidative stress, ER stress, inflammation, apoptosis and autophagy. *Mol Biol Rep.* 2022;49(7):6063-6074.
- [29] Gur C, Kandemir FM. Evaluation of the Levels of Metalloproteinases as well as Markers of Oxidative Stress and Apoptosis in Lung Tissues After Malathion and Rutin Administrations to Rats. *Turkish Journal of Nature and Science.* 2022;11(3):51-57.
- [30] Semis HS, Gur C, İleritürk M, Kaynar O, Kandemir FM. Investigation of the anti-inflammatory effects of caffeic acid phenethyl ester in a model of lambda-Carrageenan-induced paw edema in rats. *Hum Exp Toxicol.* 2021;40(12\_suppl):S721-S738.
- [31] Gür C, Kandemir Ö, Kandemir FM. Evaluation of the Effects of Chrysin on Diclofenac-Induced Cardiotoxicity in Rats by the Markers of Oxidative Stress, Endoplasmic Reticulum Stress and Apoptosis. *Kocatepe Vet J.* 2022;15(2):151-160.
- [32] Mirzaei M, Moosavi M, Mansouri E, Mohtadi S, Khodayar MJ. Diosmin exerts hepatoprotective and antihyperglycemic effects against sodium arsenite-induced toxicity through the modulation of oxidative stress and inflammation in mice. *J Trace Elem Med Bio.* 2023;78:127154.
- [33] Semis HS, Gur C, İleritürk M, Kandemir FM, Kaynar O. Evaluation of Therapeutic Effects of Quercetin Against Achilles Tendinopathy in Rats via Oxidative Stress, Inflammation, Apoptosis, Autophagy, and Metalloproteinases. *Am J Sport Med.* 2022;50(2):486-498.
- [34] İleritürk M, Benzer F, Aksu EH, Yildirim S, Kandemir FM, Dogan T, et al. Chrysin protects against testicular toxicity caused by lead acetate in rats with its antioxidant, anti-inflammatory, and antiapoptotic properties. *J Food Biochem.* 2021;45(2): e13593.
- [35] Çomaklı S, İleritürk M, Manavoğlu Kirman E. Protective Effects of Rutin on Oxidative DNA Damage, NF-κB-Mediated Inflammation, and Apoptosis in Colistin-Induced Testicular Damage of Rats. *Turkish Journal of Nature and Science.* 2020;9(2):83-90.
- [36] Akbari S, Amiri FT, Naderi M, Shaki F, Seyedabadi M. Sodium arsenite accelerates D-galactose-induced aging in the testis of the rat: Evidence for mitochondrial oxidative damage, NF-κB, JNK, and apoptosis pathways. *Toxicology.* 2022;470:153148.
- [37] Gur C, Kandemir FM, Darendelioglu E, Caglayan C, Kucukler S, Kandemir O, et al. Morin protects against acrylamide-induced neurotoxicity in rats: an investigation into different signal pathways. *Environ Sci Pollut R.* 2021;28(36):49808-49819.
- [38] Buyuklu M, Kandemir FM, Ozkaraca M, Set T, Bakirci EM, Topal E, et al. Beneficial effects of lycopene against contrast medium-induced oxidative stress, inflammation, autophagy, and apoptosis in rat kidney. *Hum Exp Toxicol.* 2015;34(5):487-496.
- [39] İleritürk M, Kandemir O, Akaras N, Simsek H, Genc A, Kandemir FM. Hesperidin has a protective effect on paclitaxel-induced testicular toxicity through regulating oxidative stress, apoptosis, inflammation and endoplasmic reticulum stress. *Reprod Toxicol.* 2023;118:108369.



## Anti-oxidant, Anti-inflammatory, and Anti-apoptotic Effects of Rutin in Spleen Toxicity Induced by Sodium Valproate in Rats

Nurhan AKARAS<sup>1\*</sup>, Fatih Mehmet KANDEMİR<sup>2</sup>, Hasan ŞİMŞEK<sup>3</sup>, Cihan GÜR<sup>4</sup>, Serpil AYGÖRMEZ<sup>5</sup>

<sup>1</sup> Aksaray University, Faculty of Medicine, Department of Histology and Embryology, Aksaray, Türkiye

<sup>2</sup> Aksaray University, Faculty of Medicine, Department of Medical Biochemistry, Aksaray, Türkiye

<sup>3</sup> Aksaray University, Faculty of Medicine, Department of Physiology, Aksaray, Türkiye

<sup>4</sup> Atatürk University, Faculty of Veterinary, Department of Veterinary Biochemistry, Erzurum, Türkiye

<sup>5</sup> Kafkas University, Faculty of Veterinary, Department of Veterinary Biochemistry, Kars, Türkiye

Nurhan AKARAS ORCID No: 0000-0002-8457-9448

Fatih Mehmet KANDEMİR ORCID No: 0000-0002-8490-2479

Hasan ŞİMŞEK ORCID No: 0000-0001-5573-4923

Cihan GÜR ORCID No: 0000-0001-6775-7858

Serpil AYGÖRMEZ ORCID No: 0000-0002-5675-5096

\*Corresponding author: [nurakaras@hotmail.com](mailto:nurakaras@hotmail.com)

(Received: 20.05.2023, Accepted: 15.06.2023, Online Publication: 22.06.2023)

### Keywords

Sodium  
Valproate,  
Rutin,  
Oxidative  
stress,  
Inflammation,  
Apoptosis,  
Spleen Toxicity

**Abstract:** Long-term exposure to sodium valproate, an anti-epileptic drug, causes toxic effects in tissues, especially by increasing oxidative stress and inflammation. Rutin is a flavanoid with anti-oxidant, anti-inflammatory and anti-apoptotic effects found naturally in many plants. In this study, we aimed to investigate the effects of rutin, a natural anti-oxidant, on sodium valproate-induced spleen tissue damage. 35 male rats were divided into 5 groups as control, sodium valproate, rutin, sodium valproate+Rutin 50 and sodium valproate+Rutin 100 groups. For 14 days, 500 mg/kg dose of sodium valproate and 50 or 100 mg/kg of rutin were administered by oral gavage. On day 15, spleen tissues were removed and biochemical methods, oxidative stress, inflammation and apoptotic parameters were analyzed and histologic analysis was performed. The levels of sodium valproate-induced oxidative stress, inflammation and apoptosis parameters increased in spleen tissues compared to the control group ( $p<0.05$ ). With routine administration, all of these sodium valproate-induced increases were decreased ( $p<0.05$ ). It was concluded that rutin has potential protective properties against the toxic effect caused by sodium valproate exposure in spleen tissues.

## Sıçanlarda Sodyum Valproat ile İndüklenen Dalak Toksisitesinde Rutinin Anti-oksidan, Anti-inflamatuvar ve Anti-apoptotik Etkileri

### Anahtar Kelimeler

Sodyum  
Valproat,  
Rutin,  
Oksidatif  
stres,  
İnflamasyon,  
Apoptoz,  
Dalak  
Toksisitesi

**Öz:** Anti-epileptik bir ilaç olan sodyum valproatın uzun süreli maruziyeti, dokularda özellikle oksidatif stres ve inflamasyon artışına neden olarak toksik etki oluşturur. Rutin, birçok bitkide doğal olarak bulunan anti-oksidan, anti-inflamatuvar ve anti-apoptotik etkilere sahip bir flavanoiddir. Bu çalışmada, sodyum valproat kaynaklı dalak doku hasarı üzerine doğal bir anti-oksidan olan rutin etkilerinin araştırılması amaçlanmıştır. 35 adet erkek sıçan kontrol, sodyum valproat, rutin, sodyum valproat+Rutin 50 ve sodyum valproat+Rutin 100 grupları olmak üzere 5 gruba ayrıldı. 14 gün boyunca 500 mg/kg dozda sodyum valproat uygulamasıyla birlikte 50 veya 100 mg/kg rutin uygulaması oral gavaj yolla yapıldı. 15. günde dalak dokuları alındı ve biyokimyasal yöntemler ile oksidatif stres, inflamasyon ve apoptotik parametrelerin analizi ve histolojik analizler yapıldı. Dalak dokularında sodyum valproat kaynaklı oksidatif stres, inflamasyon ve apoptoz parametrelerin düzeyleri kontrol grubuna göre artmıştır ( $p<0,05$ ). Rutin uygulamasıyla birlikte sodyum valproata bağlı tüm bu artış miktarlarında azalmalar meydana gelmiştir ( $p<0,05$ ). Dalak dokularında sodyum valproat maruziyetinin neden olduğu toksik etkiye karşı rutin potansiyel koruyucu özelliklere sahip olduğu sonucuna varıldı.

## 1. INTRODUCTION

Sodium valproate (VPA) is an significant fatty acid (2-propylpentenoic acid) that has been used for more than 30 years to treat epilepsy, which affects more than 70 million people [1,2]. VPA is also used in the treatment of migraine and is an FDA-approved medicine [3]. Among the main reasons for the use of VPA in the treatment of seizure disorders is its GABA transaminase inhibitory action [4].

Despite the proven efficacy of VPA, it has varying side effects [5]. VPA toxicity can occur with dose adjustments to reach therapeutic levels in patients with metabolic disorders, drug-drug interactions, or self-harm attempts [6]. Its toxic effects are seen in multiple organ systems such as the hematological, nervous, and digestive systems [7]. Long-term use of VPA may cause nausea, vomiting, anorexia, sedation, weight gain, hair loss, hepatotoxicity, encephalopathy, and myopathy [8]. For all these reasons, the off-target toxicity of VPA, one of the drugs used against neurological diseases, remains a significant concern for some patients undergoing treatment [9]. Among the various mechanisms underlying the toxic effect of VPA, induction of oxidative stress and inflammation are among the most well-known. Therefore, research on natural active ingredients that regulate these mechanisms against VPA toxicity continues intensively [1].

Oxidative stress results from a disturbance in the balance between the anti-oxidant system and the production of reactive oxygen species (ROS) in the body in favor of ROS [10,11]. Lipid peroxidation produces MDA as a breakdown by-product. Superoxide dismutase (SOD), Catalase (CAT), and Glutathione peroxidase (GPx) are anti-oxidant enzymes that provide anti-oxidant defense in the body [12,10].

Flavonoids are secondary metabolites found naturally in plants [13]. Flavonoids are a popular research area due to their anti-oxidant, anti-inflammation, anti-allergic, anti-viral, anti-bacterial, and anti-tumor properties [14]. Rutin (3,3',4',5,7-pentahydroxyflavone-3-rhamnoglucoside - RUT) is a flavonoid glycoside found naturally in buckwheat, spinach, tomato leaves, apples, onions, and tea [15]. In studies, it has been reported that RUT has protective effects against many diseases, especially against diseases caused by oxidative stress and lipid peroxidation, due to its anti-inflammatory, anti-oxidant, anti-hypertensive, anti-apoptotic, anti-autophagic, and neuroprotective properties [16]. RUT can be considered a non-toxic and non-oxidizing molecule [17].

This study aimed to investigate the anti-oxidant, anti-inflammatory, and anti-apoptotic effects of RUT on VPA-induced splenic toxicity in rats by biochemical and histological methods.

## 2. MATERIAL AND METHOD

### 2.1. Drug and Chemicals

VPA (Depakin, Sanofi, Turkey) and RUT ( $\geq 94\%$ , Sigma, USA) and other chemicals (analytical purity, Sigma, USA) were used.

### 2.2. Groups and Experiment Protocol

In the experiment, 220-250 g, 10-12 weeks old, 35 male Sprague dawley rats were used. Rats were housed in standard cages with a constant temperature of 24-25°C and a 12-hour dark-light cycle. Rats were fed ad libitum with normal drinking water and standard rat chow. Ethics committee approval was obtained from Atatürk University Animal Experiments Local Ethics Committee (12.04.2021 - 2021/3-106). All animal experiments were performed at Atatürk University Animal Experiment Center. Experimental animals were randomly divided into 5 groups with 7 rats in each group. Doses were determined by using the literature [1].

1. Control Group: Saline was given by oral gavage for 14 days.
2. Rutin Group (RUT): 100 mg/kg rutin was given by oral gavage for 14 days.
3. Sodium Valproate Group (VPA): 500 mg/kg sodium valproate was given by oral gavage for 14 days.
4. Sodium Valproate+Rutin 50 Group (VPA+RUT50): 500 mg/kg sodium valproate was given by oral gavage for 14 days and 30 minutes later 50 mg/kg rutin was given by oral gavage for 14 days.
5. Sodium Valproate+Rutin 100 Group (VPA+RUT100): 500 mg/kg sodium valproate was given by oral gavage for 14 days and 30 minutes later 100 mg/kg oral gavage rutin was given for 14 days.

### 2.3. Tissue Collection

24 hours after the last administration of RUT (day 15), rats were decapitated under mild sevoflurane anesthesia, and spleen tissues were removed. Some of the spleen tissues were placed in 10% formalin solution for histopathologic analyses while the other part was stored at -20 °C until biochemical analyses were performed.

### 2.4. Lipid Peroxidation Analysis

MDA level was analyzed for lipid peroxidation. For the analysis, the spleen tissues of rats were homogenized in 1.15% potassium chloride (KCl) solution, and the homogenates were centrifuged at 3,500 RPM for 15 min. The supernatant obtained was used for analysis. MDA levels were determined spectrophotometrically (Bio-Tek, USA) using the method developed by Placer et al. [18].

## 2.5. Analysis of Anti-oxidant Markers

SOD, CAT and GPx activities, and Glutathione (GSH) levels were measured in rat spleen tissues for anti-oxidant status analysis. For the SOD and CAT activity, supernatants were obtained as in lipid peroxidation. The supernatants used for the determination of GPx activity and GSH levels were obtained after centrifugation at 10,000 RPM for 20 minutes. Previous methods were used for SOD [19], CAT [20], GPx [21] activity, and GSH [22] level analysis. Lowry et al. method was used for spleen tissue protein content analysis, which is necessary for the calculation of enzyme activities [23]. The spectrophotometric method (Bio-Tek, U.S.A.) was used in the analysis.

## 2.6. Analysis of Inflammatory Cytokines

Nuclear Factor Kappa B (NF- $\kappa$ B) and Tumor Necrosis Factor- $\alpha$  (TNF- $\alpha$ ) levels and P38 mitogen-activated protein kinases (P38 MAPK) activity were determined from spleen tissues using a commercial rat ELISA kit (Sunred, China).

## 2.7. Apoptosis Markers Analysis

Apoptotic factor Bax and anti-apoptotic factor Bcl-2 levels were determined using a commercial rat ELISA kit (Sunred, China) according to the manufacturer's instructions.

## 2.8. Histopathological Analysis

Spleen tissues were removed from anesthetized rats and fixed in 10% formalin solution for 48 hours. Spleen tissues were washed under running water overnight in accordance with the routine tissue monitoring procedure and then subjected to dehydration by passing through an ascending alcohol series (70% (1 hour), 80% (1 hour), 96% (1 hour) and 99% (1 hour)). Following alcohol, the tissues were placed in xylol in two stages for one hour and then treated with paraffin and infiltrated. The tissues were then embedded in paraffin in metal blocks and turned into hard blocks. The paraffin blocks were sectioned into 5-micrometer sections on slides using a semi-automatic microtone. Hematoxylin and Eosin staining was performed to examine the tissues in the sections. The stained sections were then examined using a binocular Olympus Cx43 light microscope (Olympus Inc., Tokyo, Japan) and photographed with an EP50 camera (Olympus Inc., Tokyo, Japan).

## 2.9. Statistical Analysis

Data obtained from all analyses were presented as mean  $\pm$  standard deviation using GraphPad Prism 5.0 software. Data were analyzed using one-way ANOVA with Tukey's post hoc tests for multiple comparisons. A value of  $p < 0.05$  was accepted for statistical significance.

## 3. RESULTS

### 3.1. Oxidative Stress Findings

MDA levels for lipid peroxidation and SOD, CAT, GPx activities, and GSH level for anti-oxidant level were analyzed in spleen tissue. In the VPA group, the activities of SOD, CAT, GPx, and GSH levels were decreased, and the MDA level was increased compared to the control ( $p < 0.05$ ). Compared to the VPA group, SOD and CAT activities were increased in the VPA+RUT50 group ( $p < 0.05$ ), while all of them were increased in the VPA+RUT100 group ( $p < 0.05$ ). The 100 mg/kg dose of RUT reversed the negative effect of VPA administration on MDA and GSH levels ( $p < 0.05$ ).

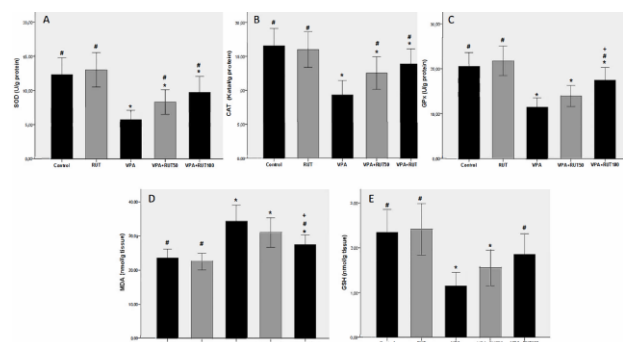


**Figure 1.** The level of anti-oxidants and oxidant in the spleen tissue of rats. All data were expressed as mean  $\pm$  SD. Statistical significance (Control vs others: \* $p < 0.05$ , VPA vs others: # $p < 0.05$ , VPA+RUT50 vs VPA+RUT100: + $p < 0.05$ ) was analyzed using One Way ANOVA.

### 3.2. Inflammatory Cytokines Findings

NF- $\kappa$ B, TNF- $\alpha$ , and P38 MAPK levels were measured in spleen tissue to show the inflammatory effect. P38 MAPK plays a significant role in the inflammatory response in many cell types [24]. NF- $\kappa$ B, TNF- $\alpha$ , and P38 MAPK levels increased in the VPA group compared to the control ( $p < 0.05$ ). When RUT was treated at 100 mg/kg dose, the parameters were decreased compared to the VPA group ( $p < 0.05$ ).

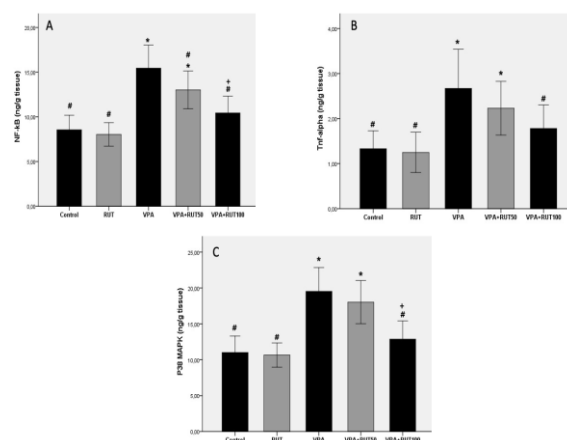


**Figure 2.** The level NF- $\kappa$ B, TNF- $\alpha$ , and P38 MAPK and in the spleen tissue of rats. All data were expressed as mean  $\pm$  SD. Statistical significance (Control vs others: \* $p < 0.05$ , VPA vs others: # $p < 0.05$ , VPA+RUT50 vs VPA+RUT100: + $p < 0.05$ ) was analyzed using One Way ANOVA.

### 3.3. Apoptosis Findings

To investigate the apoptotic pathway in spleen tissue, the Bax/Bcl-2 ratio, which shows the effect of pro-apoptotic and anti-apoptotic factors, was analyzed (Figure 3A-3B). Compared to the control group, the Bax/Bcl-2 ratio was increased in the VPA group with an increase in Bax and a decrease in Bcl-2 ( $p < 0.05$ ). At both doses (50mg and 100mg), RUT counteracted this deleterious effect of VPA and decreased the Bax/Bcl-2 ratio ( $p < 0.05$ ).

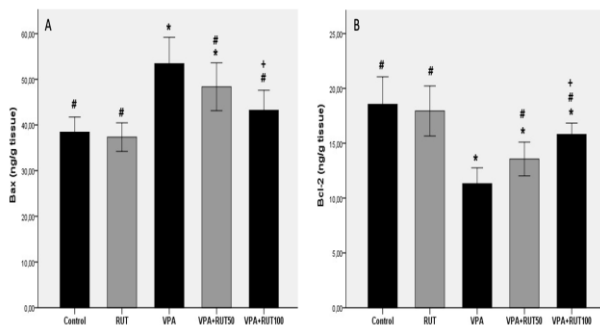


**Figure 3.** The level of Bax, and Bcl-2 in the spleen of rats. All data were expressed as mean  $\pm$  SD. Statistical significance (Control vs others: \* $p < 0.05$ , VPA vs others: # $p < 0.05$ , VPA+RUT50 vs VPA+RUT100: + $p < 0.05$ ) was analyzed using One Way ANOVA.

### 3.4. Histopathologic Findings

When the spleen sections of the control group rats were examined, it was observed that the red and white pulps were well differentiated. The borders of the pulps were clear, and marginal zones and periarterial lymphatic sheath (PALS) could be distinguished. Splenic cords, venous sinuses, and veins in the spleen showed normal structure (Figure 4A). RUT administration alone preserved the histomorphology of the spleen (Figure 4B). When the spleens in the VPA group were examined, it was noted that the red and white pulp structure was disrupted and the white pulp was depleted. Vacuolated cells, dilatation of sinusoids, and hemorrhage were observed especially in the VPA groups (Figure 4C). There was no obvious damage in VPA+RUT 50 and VPA+RUT 100 groups compared to VPA. The boundaries between white and red pulps were clear, morphology was largely normal and vacuolization was reduced (Figure 4D,4E).

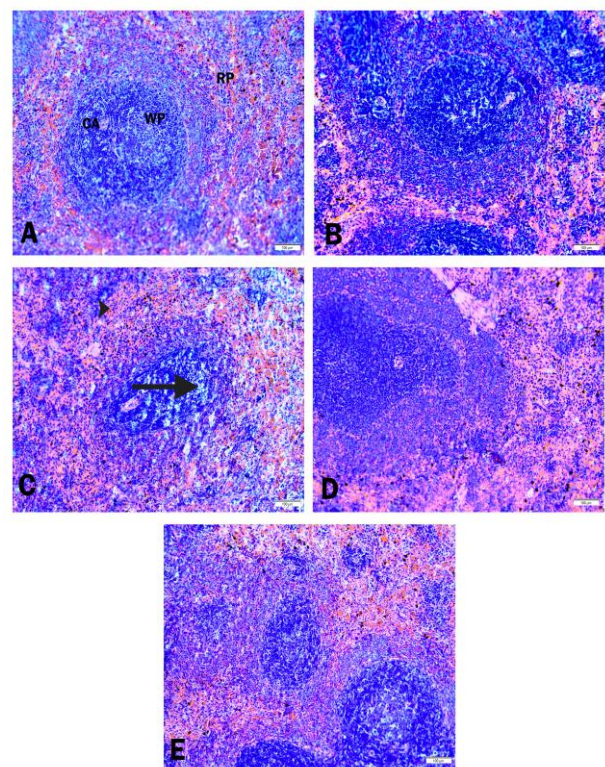


**Figure 4.** Photomicrographs of histological changes in spleen tissue (H&E staining, 100  $\mu$ m), (A) Control group, CA: central arteriole, WP: White pulp, RP: Red pulp, (B) RUT group, (C) VPA group, arrow: vacuolization, arrowhead: hemorrhage, (D) VPA+RUT 50, (E) VPA+RUT 100

## 4. DISCUSSION AND CONCLUSION

Epilepsy is one of the most common neurological disorders worldwide, and approximately 90% of patients with epilepsy live in developing regions [25]. Anti-epileptic drugs (AEDs) used in the treatment of epilepsy are widely used by patients [26]. Approximately one-third of patients given AEDs as treatment options do not achieve optimal seizure control. Patients adequately treated with AEDs and who do not become seizure-free are now considered to have drug-resistant epilepsy [27]. VPA is an AED used to treat various seizure disorders. However, serious side effects such as hepatotoxicity, pancreatitis, thrombocytopenia, and platelet aggregation are associated with VPA treatment [25]. After treatment with VPA, changes may occur in the number and characteristics of T lymphocytes in the spleen, a central organ of the immune system [28]. VPA has been reported to cause tissue damage mainly by causing oxidative stress followed by inflammation and apoptosis [16]. The discovery of anti-oxidant, anti-inflammatory, anti-autophagic, and anti-apoptotic properties in herbal medicines has led to renewed interest in these compounds [29]. RUT has different protective effects against oxidative stress-mediated diseases and lipid peroxidation in vitro and in vivo [1]. Metabolomic studies of VPA-induced toxicity have primarily focused on changes in serum and urine metabolites but have not evaluated changes in major organs or tissues [30]. Therefore, the present study was designed to determine the effect of RUT in preventing VPA-induced spleen toxicity in spleen tissue.

Since lipids are the most important component of the cell membrane, excessive production of free radicals causes lipid peroxidation in the cell [31]. Triglycerides play important roles in controlling interactions between lipoproteins. However, triglycerides have also been reported to play an active role in HDL remodeling and cholesterol esterification in human plasma. Oxidative stress reactions occur as a result of excessive ROS formation. Many diseases such as inflammation, liver diseases, atherosclerosis and neurodegenerative diseases are largely caused by oxidative stress [32,33]. Since MDA is the end product of polyunsaturated fatty acids, it is the strongest indicator of oxidative stress [31]. There are defense systems consisting of enzymatic and non-enzymatic anti-oxidant components to reduce the effect of oxidants in the cell. Some enzymes such as SOD, CAT, and GPx are some of the anti-oxidant enzymes involved in the removal of ROS from cells [34]. GSH removes radical species such as superoxide radicals and hydrogen peroxide from the cell and protects membrane protein thiols [35]. Glutathione-S-transferases (GSTs) are major enzymes of the phase II biotransformation system. GSTs can catalyze the conjugation of GSH to the electrophilic centers of many endogenous or exogenous toxic compounds including chemical carcinogens, oxidative stress products, insecticides, herbicides, and cancer chemotherapeutic agents [36,37]. The preferential reaction of GSTs with GSH through their enzymatic action results in the protection of cellular components [38].

In the present study, VPA administration in spleen tissue increased MDA levels and decreased GSH levels and SOD, CAT, and GPx activities. The decrease in GSH levels and the significant decrease in SOD, CAT, and GPx activities compared to control levels indicate that anti-oxidant capacity decreased and the increase in MDA levels indicates that oxidant capacity increased, in which case VPA increased oxidative stress in spleen tissue. On the other hand, RUT administration together with VPA reversed this situation and caused a decrease in oxidative stress. RUT showed this effect more prominently, especially at the dose of 100 mg/kg. Our in vivo findings are consistent with previous studies demonstrating the anti-oxidant and free radical scavenging properties of RUT in spleen tissue [17,39].

Inflammation is among the adaptive responses of the body to various damages, including biological and chemical factors [40]. Excessive ROS production is associated with the activation of inflammatory pathways. Among these pathways, the NF- $\kappa$ B signaling pathway is the main signal transduction pathway involved in gene regulation and activation of some proinflammatory cytokines including TNF- $\alpha$  [41]. TNF- $\alpha$  also regulates various signaling pathways such as inflammation and apoptosis. TNF- $\alpha$  has a vital function in the important innate immune response and cellular activation, followed by proliferation and programmed cell death or necrosis [42]. P38 MAPK promotes phosphorylation of I $\kappa$ B, leading to dissociation of NF- $\kappa$ B and I $\kappa$ B complexes [13]. In the present study, VPA administration increased the level of inflammation by significantly increasing NF-

$\kappa$ B and TNF- $\alpha$  levels and P38 MAPK activity reflecting inflammatory responses. On the other hand, RUT treatment showed anti-inflammatory properties by decreasing the levels and activity of these markers.

Apoptosis, known as programmed cell death, plays a critical role in both embryonic development and in the survival and function of developed tissues [43]. ROS are largely produced in mitochondria and have a significant impact on the development of apoptosis [44]. The mitochondrial pathway, which plays an important role in the apoptosis process, is controlled by members of the Bcl-2 protein family, which includes Bax and Bcl-2. An increase in the Bax/Bcl-2 ratio in favor of Bax leads to an increase in cytochrome c levels in the cytoplasm. This activates the caspase enzyme cascade, resulting in cell death [45,46]. In the current study, it was determined that VPA caused activation of the mitochondrial apoptotic pathway by increasing the Bax/Bcl-2 ratio together with oxidative damage in spleen tissue. On the other hand, RUT showed anti-apoptotic properties by acting in the opposite direction of VPA by decreasing both ROS formation and Bax/Bcl-2 ratio.

The findings of this study suggest that suppression of oxidative stress, inflammatory response, and apoptosis by RUT may be an effective strategic approach for the treatment of VPA-induced splenic toxicity.

## REFERENCES

- [1] Kandemir FM, Ileriturk M, Gur C. Rutin protects rat liver and kidney from sodium valproate-induced damage by attenuating oxidative stress, ER stress, inflammation, apoptosis and autophagy. *Mol Biol Rep.* 2022;49(7):6063-74.
- [2] Phillips A, Bullock T, Plant N. Sodium valproate induces apoptosis in the rat hepatoma cell line, FaO. *Toxicology.* 2003;192(2-3):219-27.
- [3] Parikh SK, Silberstein SD. Current status of antiepileptic drugs as preventive migraine therapy. *Curr Treat Options Neurol.* 2019;21(4):16.
- [4] de Campos Vidal B, Mello MLS. Sodium valproate (VPA) interactions with DNA and histones. *Int J Biol Macromol.* 2020;163, 219-231.
- [5] Khani S, Hejazi SA, Yaghoubi M, Sharifipour E. Comparative study of magnesium, sodium valproate, and concurrent magnesium-sodium valproate therapy in the prevention of migraine headaches: a randomized controlled double-blind trial. *J Headache Pain.* 2021;22(1), 1-10.
- [6] Patel AR, Nagalli S. Valproate toxicity. [Updated 2023 May 17]. In: StatPearls [Internet]. Treasure Island (FL): StatPearls Publishing; 2023 May-. Available from: <https://www.ncbi.nlm.nih.gov/books/NBK560898/>
- [7] Mei X, Wu HC, Ruan M, Cai LR. Acute liver failure with thrombotic microangiopathy due to sodium valproate toxicity: A case report. *World J Clin Cases.* 2021;9(17):4310-17.
- [8] Sharma A, Sinha S, Narang A, Chouhan DK, Gupta S. Waddling Gait: A complication of valproate

- therapy and a thought beyond vitamin d deficiency. Sultan Qaboos Univ Med J. 2020;20(1):e104-e108.
- [9] Ola OS, Adewole KE. Anticlastogenic and hepatoprotective effects of kolaviron on sodium valproate-induced oxidative toxicity in wistar rats. Egyptian Journal of Basic and Applied Sciences. 2021;8(1):167-79.
- [10] Ayna A, Darendelioğlu E. Evaluation of the biological activities of royal jelly on prostate and breast cancer cells. Türk Doğa ve Fen Dergisi. 2022;11(3):166-70.
- [11] Ayna A. Apoptotic effects of beta-carotene, alpha-tocopherol and ascorbic acid on PC-3 prostate cancer cells. Hacettepe Journal of Biology and Chemistry. 2020;48(3):211-18.
- [12] Varışlı B, Caglayan C, Kandemir FM, Gür C, Ayna A, Genç A, et al. Chrysin mitigates diclofenac-induced hepatotoxicity by modulating oxidative stress, apoptosis, autophagy and endoplasmic reticulum stress in rats. Mol Biol Rep. 2023;50(1):433-42.
- [13] Caglayan C, Kandemir FM, Darendelioğlu E, Yıldırım S, Kucukler S, Dortbudak MB. Rutin Ameliorates Mercuric Chloride-Induced Hepatotoxicity in Rats via Interfering with Oxidative Stress, Inflammation And Apoptosis. J Trace Elem Med Biol 2019;56:60-68
- [14] Kandemir FM, Caglayan C, Aksu EH, Yıldırım S, Kucukler S, Gur C, et al. Protective effect of rutin on mercuric chloride-induced reproductive damage in male rats. Andrologia 2020;52(3):e13524.
- [15] Caglayan C, Kandemir FM, Yıldırım S, Kucukler S, Eser G. Rutin protects mercuric chloride-induced nephrotoxicity via targeting of aquaporin 1 level, oxidative stress, apoptosis and inflammation in rats. J Trace Elem Med Biol. 2019;54:69-78.
- [16] Çelik H, Kandemir FM, Caglayan C, Özdemir S, Çomaklı S, Kucukler S, et al. Neuroprotective effect of rutin against colistin-induced oxidative stress, inflammation and apoptosis in rat brain associated with the CREB/BDNF expressions. Mol Biol Rep 2020;47(3):2023-34.
- [17] Kandemir FM, Ozkaraca M, Yıldırım BA, Hanedan B, Kirbas A, Kilic, et al. Rutin attenuates gentamicin-induced renal damage by reducing oxidative stress, inflammation, apoptosis, and autophagy in rats. Renal failure. 2015;37(3):518-525.
- [18] Placer ZA, Cushman LL, Johnson BC. Estimation of product of lipid peroxidation (malonyl dialdehyde) in biochemical systems. Anal Biochem 1966;16(2):359-64.
- [19] Sun Y, Oberley LW, Li Y. A simple method for clinical assay of superoxide dismutase. Clin Chem. 1988;34(3):497-500.
- [20] Aebi H. Catalase in vitro. Methods Enzymol 1984;105:121-26.
- [21] Lawrence RA, Burk RF. Glutathione peroxidase activity in selenium-deficient rat liver. Biochem Biophys Res Commun. 1976;71(4):952-58.
- [22] Sedlak J, Lindsay RH. Estimation of total, protein-bound, and nonprotein sulfhydryl groups in tissue with ellman's reagent. Anal Biochem. 1968;25(1):192-205.
- [23] Lowry OH, Rosebrough NJ, Farr AL, Randall RJ. Protein Measurement with the Folin Phenol Reagent. J Biol Chem. 1951;193(1):265-75.
- [24] Lo U, Selvaraj V, Plane JM, Chechneva OV, Otsu K, Deng W. p38 $\alpha$  (MAPK14) critically regulates the immunological response and the production of specific cytokines and chemokines in astrocytes. Scientific reports. 2014;4(1):7405.
- [25] Ardianto C, Wardani HA, Nurrahmi N, Rahmadi M, Khotib J. Alpha-lipoic acid ameliorates sodium valproate-induced liver injury in mice. Vet World. 2020;13(5):963-66.
- [26] Işık M, Demir Y, Kırıcı M, Demir R, Şimşek F, Beydemir Ş. Changes in the anti-oxidant system in adult epilepsy patients receiving anti-epileptic drugs. Arch Physiol Biochem 2015;121(3):97-102.
- [27] Beydemir Ş, Demir Y. Antiepileptic drugs: Impacts on human serum paraoxonase-1. J Biochem Mol Toxicol. 2017;31(6).
- [28] Mozūraitė R, Stakišaitis D, Didžiapetrienė J, Balnytė I, Matusevičius P, Valančiūtė A. Gender-related rat gl. thymus and spleen changes under the influence of Sodium valproate. In "Baltic Morphology VII Scientific Conference" Morphological Sciences in the Experimental and Clinical Medicine": November 7-9, 2013, Rīga, Latvia: abstract book/Rīga Stradiņš University (RSU). [Institute of Anatomy and Anthropology]; Committee: Māra Pilmane [et al.]. Rīga: Rīga Stradiņš University, 2013.
- [29] Yardım A, Gur C, Comaklı S, Ozdemir S, Kucukler S, Celik H, et al. Investigation of the effects of berberine on bortezomib-induced sciatic nerve and spinal cord damage in rats through pathways involved in oxidative stress and neuroinflammation. Neurotoxicology. 2022;89:127-39.
- [30] Gao Y, Jiang D, Wang C, An G, Zhu L, Cui C. Comprehensive analysis of metabolic changes in male mice exposed to sodium valproate based on GC-MS analysis. Drug Des Devel Ther. 2022:1915-30.
- [31] İleriturk M, Kandemir O, Akaras N, Simsek H, Genc A, Kandemir FM. Hesperidin has a protective effect on paclitaxel-induced testicular toxicity through regulating oxidative stress, apoptosis, inflammation and endoplasmic reticulum stress. Reprod Toxicol. 2023;118:108369.
- [32] Palabıyık E, Sulumer AN, Uguz H, Avcı B, Askın S, Askın H, et al. Assessment of hypolipidemic and anti-inflammatory properties of walnut (*Juglans regia*) seed coat extract and modulates some metabolic enzymes activity in triton WR-1339-induced hyperlipidemia in rat kidney, liver, and heart. J Mol Recognit. 2023;36(3):e3004.
- [33] Korkmaz IN, Türkeş C, Demir Y, Öztekin A, Özdemir H, Beydemir Ş. Biological evaluation and in silico study of benzohydrazide derivatives as paraoxonase 1 inhibitors. J Biochem Mol Toxicol. 2022;36(11):e23180.

- [34] Akaras N, Gur C, Kucukler S, Kandemir FM. Zingerone reduces sodium arsenite-induced nephrotoxicity by regulating oxidative stress, inflammation, apoptosis and histopathological changes. *Chem Biol Interact.* 2023;374:110410.
- [35] Ömür AD, Kandemir FM, Yıldırım BA. Protective effect of dandelion (*Taraxacum officinale*) extract Against gentamicin-induced reproductive damage in male rats. *Kafkas Univ. Vet. Fak.* 2016;22:929-36.
- [36] Özaslan MS, Demir Y, Aksoy M, Küfrevioğlu ÖI, Beydemir Ş. Inhibition effects of pesticides on glutathione-S-transferase enzyme activity of Van Lake fish liver. *J Biochem Mol Toxicol.* 2018;32(9):e22196.
- [37] Türkeş C, Kesebir AÖ, Demir Y, Küfrevioğlu ÖI, Beydemir Ş. Calcium channel blockers: The effect of glutathione S-Transferase enzyme activity and molecular docking studies. *ChemistrySelect.* 2021;6(40):11137-43.
- [38] Türkeş C, Demir Y, Beydemir Ş. Infection medications: Assessment in-vitro glutathione S-Transferase inhibition and molecular docking study. *ChemistrySelect.* 2021;6(43):11915-24.
- [39] Aksu EH, Kandemir FM, Özkaraca M, Ömür AD, Küçükler S, Çomaklı S. Rutin ameliorates cisplatin-induced reproductive damage via suppression of oxidative stress and apoptosis in adult male rats. *Andrologia.* 2017;49(1):e12593.
- [40] Caglayan C, Kandemir FM, Darendelioğlu E, Küçükler S, Ayna A. Hesperidin protects liver and kidney against sodium fluoride-induced toxicity through anti-apoptotic and anti-autophagic mechanisms. *Life Sciences.* 2021;281:119730.
- [41] Caglayan C, Kandemir FM, Ayna A, Gür C, Küçükler S, Darendelioğlu E. Neuroprotective effects of 18β-glycyrrhetic acid against bisphenol A-induced neurotoxicity in rats: involvement of neuronal apoptosis, endoplasmic reticulum stress and JAK1/STAT1 signaling pathway. *Metab Brain Dis.* 2022;37(6):1931-40.
- [42] Yardım A, Kandemir FM, Çomaklı S, Özdemir S, Caglayan C, Kucukler S, et al. Protective effects of curcumin against paclitaxel-induced spinal cord and sciatic nerve injuries in rats. *Neurochem Res.* 2021;46:379-95.
- [43] Şimşek H, Demiryürek Ş, Demir T, Atabay HD, Çeribasi AO, Bayraktar R, et al. Assessment of expressions of Bcl-XL, b-FGF, Bmp-2, Caspase-3, PDGFR-α, Smad1 and TGF-β1 genes in a rat model of lung ischemia/reperfusion. *Iran J Basic Med Sci.* 2016;19(2):209-14.
- [44] Simsek H, Akaras N. Acacetin ameliorates acetylsalicylic acid-induced gastric ulcer in rats by interfering with oxidative stress, inflammation, and apoptosis. *Int J Med Biochem.* 2023;6(2):96-103.
- [45] Kucukler S, Caglayan C, Darendelioğlu E, Kandemir FM. Morin attenuates acrylamide-induced testicular toxicity in rats by regulating the NF-κB, Bax/Bcl-2 and PI3K/Akt/mTOR signaling pathways. *Life Sciences.* 2020;261:118301.
- [46] Şimşek H, Akaras N, Gür C, Küçükler S, Kandemir FM. Beneficial effects of Chrysin on Cadmium-induced nephrotoxicity in rats: Modulating the levels of Nrf2/HO-1, RAGE/NLRP3, and Caspase-3/Bax/Bcl-2 signaling pathways. *Gene.* 2023;875:147502.

## A New Method for Obtaining Haploid Plant Shed-Microspore Culture

Mevlûde TATAR<sup>1\*</sup> 

<sup>1</sup> Alata Horticultural Research Institute, 33740, Mersin, Türkiye  
Mevlûde TATAR ORCID No: 0000-0002-3707-1721

\* Corresponding author e-mail: [mtatar65@hotmail.com](mailto:mtatar65@hotmail.com)

(Received: 22.06.2022, Accepted: 12.06.2023, Online Publication: 22.06.2023)

### Keywords

Pepper,  
Shed-microspore  
Culture,  
Androgenesis,  
Dihaploidisation

**Abstract:** In plant breeding studies, dihaploidisation method is used to obtain homozygous pure lines used to develop varieties in a shorter time. Dihaploidisation method is applied in most types of vegetables such as wheat and corn, as well as in vegetable species. Androgenesis methods (anther and microspore culture) and gynogenesis and parthenogenesis methods (ovula and ovary culture) are used to obtain haploid plants. One of the androgenetic methods, shed-microspore culture has been a new alternative technique to anther and microspore cultures, and successful results have been obtained. The most important feature of this technique is the presence of a double-layered nutrient medium in a single petri dish, and the culture of microspores in the anthers in solid and liquid nutrient mediums. In this study, the definition and application of microspore culture and shed-microspore cultures, studies conducted in the world and in our country and their developments in recent years were discussed.

## Haploid Bitki Elde Etmede Yeni Bir Yöntem Shed-Mikrospor Kültürü

### Anahtar Kelimeler

Biber,  
Shed-Mikrospor  
Kültürü,  
Androgenesis,  
Dihaploidizasyon

**Öz:** Bitki ıslah çalışmalarında çeşit geliştirmek için kullanılan homozigot saf hatların daha kısa zamanda elde etmede dihaploidizasyon yönteminden yararlanılmaktadır. Dihaploidizasyon yöntemiyle sebze türlerinde uygulandığı gibi buğday, mısır gibi çoğu türde de uygulanmaktadır. Haploid bitki eldesi için androgenesis yöntemleri (anter ve mikrospor kültürü) ile ginogenesis ve partenogenesis yöntemleri kullanılmaktadır. Androjenetik yöntemlerden shed-mikrospor kültürü ise anter ve mikrospor kültürlerine alternatif yeni bir teknik olmuş başarılı sonuçlar elde edilmiştir. Bu teknik en önemli özelliği tek bir petride çift katlı besin ortamının olması, anterlerin içindeki mikrosporların katı ve sıvı besin ortamına kültüre alınmasıdır. Bu çalışmada mikrospor kültürü ve shed-mikrospor kültürlerinin tanımı, uygulaması ile dünyada ve ülkemizde yapılan çalışmalar ile son yıllardaki gelişmeleri incelenmiştir.

### 1. INTRODUCTION

With the increase in the world population, the demand for food has increased due to the rapid development of urbanization, the decrease in agricultural lands and the changes in climatic conditions. They are among the leading important vegetables in our country and world production, especially in tomato, pepper, eggplant and potato species from the *Solanaceae* family. Increasing food production needs to be done in a reliable and healthy

way. This is not sufficient with traditional methods. Plant biotechnology offers alternative solutions to many problems that are difficult or unsolvable with classical breeding methods; It offers easier, faster, economical, efficient and quality methods for plant breeding.

All of the techniques that enable the plant's organs, tissues and cells to be isolated and cultured using artificial food sources in sterile conditions and to improve their genetic characteristics are all within plant biotechnology. Today,



rapid and technological developments in the fields of plant biochemistry, plant physiology and molecular biology help researchers to prevent some problems in plant breeding. Accordingly, with the development of new techniques and protocols, there are important developments in the field of breeding and development of the plants grown. Since researchers shorten the concept of time in breeding, the haploid method has an important place in its use in the field of vegetable breeding. Researchers shorten the concept of time in breeding, the haploid method has an important place in its use in the field of vegetable breeding. Anther culture and microspore culture, which are more preferred in obtaining haploid plants, are among the methods that have become common.

While much faster and shorter-term studies are needed in breeding studies due to reasons such as the increase in population, rapid development of urbanization and changes in climatic conditions with the decrease of agricultural lands, androgenesis methods (anther and microspore culture) and gynogenesis and parthenogenesis methods to obtain haploid plants. culture) is applied [1-8]. From methods of obtaining haploid plants to microspore culture and anther culture shed-microspore culture, which is an alternative new method, is different from anther and microspore culture. It is a method of culturing in a suitable liquid nutrient medium prepared as a whole, by removing the filaments of the appropriate anthers and without damaging the anthers. In microspore culture, embryogenesis is the method of creating embryos from gametophytic development by using anther culture or microspore culture methods of immature male gametophytes during in vitro culture. In microspore culture, haploid plants can be obtained directly from embryos obtained from microspores or by organogenesis from calli obtained from microspores [22]. Haploid embryos can be transformed into homozygous DH plants after being treated either by themselves or with chromosome folding agents and can be used in breeding programs. Haploid embryos can be transformed into homozygous double haploid plants either spontaneously or after treatment with chromosome folding agents and breeding used in their work.

The first study in microspore culture was performed by Kameya and Hinata in 1970 [9]. Researchers have done many studies on microspore culture [9-27] and have achieved successful results. It is reported that one of the most important factors affecting the success in microspore culture is the isolation of microspores. For isolation, buds or anthers are left in different environments according to the characteristics of the species, and it has been reported that the anthers are crushed in these environments, allowing microspores to be released [28-35]. In recent studies, the shed-microspore culture, which is a new method and continues to be developed, is being studied on hot pepper, and its studies are continuing in the sweet pepper group. It is thought that this technique will be further developed and made widespread, and it will shed light on the field of plant breeding and plant breeders. Shed-microspore culture, one of the androgenetic methods, is a new alternative technique to anther and

microspore cultures and successful results have been obtained. It was first applied and successful in Indonesia's local hot pepper. This method is called the shed microspore method. In the method, microspores in the anthers are cultured in solid and liquid nutrient medium in a double-layer nutrient medium.

The most important difference of the Shed-Microspore culture method is that it is completely separated from the filaments of the anthers isolated from the flower buds, by crushing or separating them, without isolating the microspores inside and without damaging the anthers, and they are cultured in a double-layered nutrient medium. Microspores within the anthers are cultured freely floating into the liquid layer of the bilayer nutrient medium. The microspores that develop inside the anthers benefit from the nutrient medium and are allowed to develop freely in the liquid medium. In the Shed-Microspore culture technique, embryoids and callus tissues do not form on the cultured anthers as in anther culture. All of the embryos are embryos consisting of haploid microspores by completing their formation and development in the liquid medium. Observing and examining embryos in liquid medium is much more functional than other methods.

When the shed-microspore culture is compared with other (anther and microspore culture) methods [36]; due to the double-layered nutrient medium, additional substances can be added to the nutrient medium in the next steps, and the liquid layer can be renewed when necessary. If a large number of embryos are formed in a single petri dish, the liquid nutrient medium is renewed without any intervention to the embryos, and their development continues. With the liquid layer, antibiotics can be added to the nutrient medium quickly and effectively, which will protect them from possible infections. Since the anthers are isolated as a whole and microspores develop easily during the developmental stage, the highest rate of embryo is formed. The researchers reported that the haploid plant percentage was higher when colchicine applications to plantlets obtained from the Shed-microspore culture technique had better results compared to other methods. The determination of ploidy levels of the plantlets obtained by this method is facilitated by flow cytometry and chloroplast counting technique.

In this study, the definition and application of microspore and shed-microspore cultures, their embryo production potential, studies conducted in the world and in our country and their recent developments were examined.

### 1.1. Microspore Culture Studies

Obtaining the first haploid plant by microspore culture method it was reported that Nitsch succeeded in 1974 and the first microspore culture studies were applied in 1989 by Pesticelli et al. in tobacco and corn plants [5]. One of the most important factors affecting androgenesis is the developmental stage of microspores, and researchers report that unless microspores at the appropriate stage are cultured, there will be no development in pollen embryogenesis even if other culture conditions are met

[37]. It is known that there are many factors affecting the number of androgenic microspores and the number of embryos obtained per microspore. Some of the factors that will affect the success of microspore culture are genetic and depend on the genotype of the donor plants from which the microspores are taken. Another part is the microspore culture technique. It is related to the environmental conditions during its implementation [38]. Yin and his colleagues reported that conducted a study of microspores isolated from pepper anther have developed a system for rapid progression by initiating embryoids in culture medium [39].

As a result of the study, it was determined that low temperature pretreatment, combinations of plant growth regulators, activated carbon concentrations and temperature pretreatments were the most important factors affecting the embryoid formation of pepper microspores isolated in vitro. In another study, it was reported that it was successful in increasing embryo formation with temperature applications [40]. Studies such as different nutrient media and pre-applications have been carried out to obtain haploid plants by anther culture method in local peppers originating from Turkey and successful results have been reported [41]. Examined all the factors affecting the androgenesis developmental stage in the culture medium of microspores isolated from Hungarian and Spanish local pepper genotypes [42]. As a result of the study, it was reported that the anthers with 80% mononuclear and 20% double-core microspores were successful and high yield was obtained. They stated the high frequency of embryo production and plant regeneration in the culture of microspores isolated from pepper [43].

## 1.2. Shed-Microspor Culture Studies

In Indonesia, six hot and four rolled local pepper genotypes and two bell pepper genotypes for comparison purposes, anthers at single seed stage were transferred to the nutrient media. The researcher, who opened the anthers one to two weeks after the medium and dispersed the microspores on the nutrient medium, named this method as the "Shed microspore" technique. It has been reported that all hot and curly pepper genotypes used were successful, and curly peppers were less successful than other hot peppers [44].

Aimed to create a new method and protocol to increase the DH (double haploid) rate by applying different additions by using anther and microspore culture methods in the local hot pepper genotypes of Indonesia [36]. In the experiment, anthers containing 50% single-core microspores were used. As preliminary applications before media transfer; After keeping the flower buds at 4°C for 24 hours, they were incubated at 9°C for a week and grown at 28°C in complete darkness. Unlike the nutrient media applied in the microspore and shed microspore culture method, NN media with solid first layer and liquid second layer were applied. In the study, it was reported that 0-2% activated charcoal added to the solid medium increased the number of embryos and decreased the number of embryos by 2%. It has been

reported that one hundred eight plants, one hundred four haploids, sixty-one diploids, two triploids and one tetraploid were obtained from 6 hot pepper genotypes.

The same researchers [45] used the material they used in their anther and microspore culture studies in another study they conducted. Success rates were investigated by using different antibiotic combinations with the shed microspore culture method in order to prevent infections assumed to originate from these donor plants, which used Indonesian local hot pepper genotypes, and to increase the phytotoxic efficiency of different antibiotics. In the study, it was reported that chloroplast count and ploidy levels were determined exactly and accurately in flow-cytometry and leaf stomata of plantlets obtained by applying shed microspore culture method and two-layer solid and liquid media. In addition, as a result of four different antibiotic combinations, it has been reported that the most appropriate antibiotic component against infections originating from donor plants is 20 mg/l Rifampicin + 100 mg/l Timentin. The following picture shows the stages of the shed microspore (Fig1).

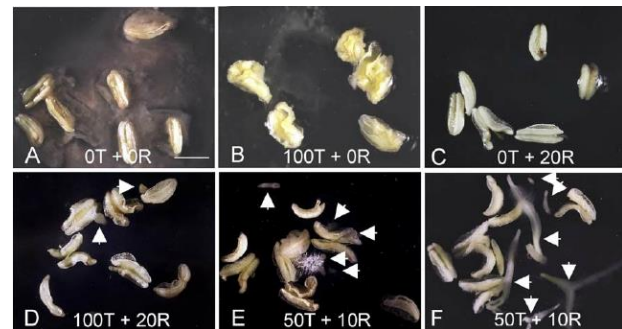


**Figure 1.** Shed-microspore culture of Indonesian hot pepper (*C. annuum* L.) 'Gada' after single and combination treatments of antibiotics. (A) Control without antibiotic treatment (0T+0R) showing contaminated culture; (B) culture treated with 100 mg/l timentin (100T+0R) showing contamination; (C) culture treated with 20 mg/l rifampicin (0T + 20R) showing no contamination, but without undergoing embryogenesis; (D) culture treated with 100 mg/l timentin + 20 mg/l rifampicin (100 + 20R) showing no contamination, where some embryos can be seen (arrows); (E and F) culture treated with 50 mg/l timentin + 10 mg/l rifampicin (50T + 10R) showing no contamination, where more embryos can be seen (arrows). The culture was with 0.5% activated charcoal in solid medium. Donor-plants for the anthers were grown in Indonesia. (A-E) After 5 weeks of culture; (F) after 6 weeks of culture. Bar = 4 mm.[36,45].

Aimed to achieve success by using the shed microspore culture method in order to increase the embryo number and embryo quality in hot pepper (*Capsicum annuum* L.) genotypes [46,47]. The protocol applied in Shed microspore culture; 1% activated charcoal was kept at 4°C for 1 day and exposed to 9°C for 1 week, then it was subjected to growth conditions at 4 different temperatures by applying 5 different growth nutrients in addition to 2.5 μM zeatin and 5 μM IAA to 28°C completely dark and liquid environments. As a result of the study, the number of embryos and quality of the petri dishes to which 50 and 100 μM were added in the 3rd week in liquid medium decreased, but in the petri dishes to which 2.5 μM zeatin + 5 μM IAA was added, 35.3 in 6 anthers, 24.7 in the medium with growth regulator, 27.3 in which 2.5 μM zeatin was added. There were 18.4 normal embryos with 5 μM. Within the scope of the study, in 6 anthers, 20.6

embryos were formed at 28°C, 20.2 at 25°C, 19.5 at 23°C, 17.1 at 21°C, and 7.5 at 18°C. According to the obtained data, it has been reported that the medium with 2.5 µM zeatin + 5 µM IAA addition and the environment with 28°C temperature are more successful than the other applied conditions for normal embryo formation.

In a study by [48], it was aimed to determine the response of commercial varieties of 3 different pepper genotypes by applying the shed microspore method. In the experiment, anther sizes, anthocyanin levels and developmental stages of microspores in anthers, embryo formation and plant transformation rate, embryo formation potential of liquid nutrient medium in shed microsporida method were investigated. [49], anther and shed microspore culture techniques were applied to 2 commercial pepper spikes (Lumbard RZ F1) and Cubanelle (Üçbuun F1) cultivars to observe haploid and dihaploid plant production and anther development stages. Anther culture was made in MS [50] medium, after collecting the pepper buds, which came to the stage of ingestion in the shed microspore technique, after 24 hours of pre-treatment at +4°C, the anthers were transferred to NN medium and covered with a liquid layer by adding +2% maltose to NN medium. The pH of the nutrient medium was 5.7-5.8 as semi-solid - semi-liquid. The findings obtained in the research; In anther culture, the rate of embryo development from Lumbard RZ F1 variety is 8.94% and the rate of embryos turning into plants is 23.63%, while the rate of embryo formation in Üçburun F1 is 22.18% and the rate of embryos turning into plants is 22.22%, while the rate of embryos turning into plants is 22.22% in shed microspore method. It has been reported that embryo development was detected only in Lumbard RZ F1 variety. In the study conducted by [51], the effect of the use of agitator on embryo yield in 29 ornamental pepper genotypes (commercial and local) shed microspore method was examined, while the bud morphologies and bud sizes of the genotypes at the culture stage of microspores were also examined. Before removing the anthers of the flower buds, pre-chilling was done at +4 °C and 24 hours in the dark, and the anthers shed microspore (semi-solid-semi-liquid medium) method was applied. It was determined that the success rate of the medium on the shaker was higher in terms of embryo formation, and the embryo formation performance was more successful in the medium on the shaker than the control group.

In this study, it was aimed to determine the morphological and molecular characterization of Gaziantep local pepper (GB) genotypes and the possibilities of obtaining double haploid (DH) lines by anther culture and shedmicrospore culture method. In the study, 96 pepper genotypes, including 81 different GB genotypes and 15 standard varieties, collected from the region were used. For the first time, the shed microspore method was applied to local pepper genotypes. As a result of the study, in shed microspore culture in GB local pepper genotype; While the total number of anthers was 920 and the number of developing anthers was 140 in total, the highest embryo formation rate; it has been reported that 5% was achieved [52].

## 2. CONCLUSION

In this study, the effectiveness of dihaploidization methods in obtaining homozygous pure lines used to develop varieties in breeding studies in a shorter time and the results obtained are summarized. Anther and microspore cultures, which provide haploid plant production among tissue culture techniques, have an important place in plant breeding studies. However, shed microspore, which is one of the new methods in tissue culture, is reported to be successful in literature studies. Studying new methods will increase the success rate in plant species that are difficult to study in breeding. The use of these new methods is limited in economically important plants, especially in our country, and there are few studies. However, it is very few and insufficient and it is very important to increase the studies on this subject. Studies with shed-microspore culture, which is an alternative method in anther and microspore culture methods, have shown in studies that the success rate has increased and it has become increasingly widespread in the world recently. At the same time, it has been shown in literature studies that it will be beneficial to many subjects that have not been studied yet in tissue culture. For this reason, it is necessary to carry out studies in this direction and to develop protocols for future studies or to create new protocols. Thus, when shed-microspore culture, which is an efficient and promising technique, is applied, an important gap in breeding studies will be filled. The improvement of this method will be able to offer more successful solutions in breeding studies.

## REFERENCES

- [1] Andrews, J. (1985). Peppers, The Domesticated Capsicum. University of Texas Press, Austin, Texas.
- [2] Bal, U., Abak, K., Büyükalaca, S., Çömlekçiöğlü, N. 2003. Development of Callus Colonies From the Isolated Microspore Culture of Capsicum annuum L. Biotechnol. & Biotechnol. Eq., 17(2): 28-43.
- [3] Khush, G. S. and Virmani, S. S., 1996. Somatic embriyogenesis in cultured unfertilized ovules of *Cucurbita moschata*. *Journal of the Japanese Society for Horticultural Science*, 57 (1):34-42.
- [4] Çömlekçiöğlü, N., Büyükalaca, S. ve Abak, K., 2001. Effect of Silver Nitrate on Haploid Embryo Induction by Anther Culture in Pepper (*Capsicum annuum L.*). *XI. th. Eucarpia Meeting on Genetics and Breeding of Capsicum and Eggplant*, April 9-13, Antalya.
- [5] Ellialtıoğlü, Ş. ve Tıprıdamaz, R. 2002. Soğuk uygulamaları ve aktif kömürün biberde (*Capsicum annuum L.*) Anter kültürü süresince absisik asit miktarındaki değişim üzerine etkisi. *Akdeniz Üniversitesi Ziraat Fakültesi Dergisi*, 15 (1): 9-18.
- [6] Ellialtıoğlü, S., Kaplan F., and Abak, K., 2001. The effect of carrot extract and activated charcoal on the androgenesis of pepper (K. Abak., S. Büyükalaca, Y. Daşgan editors). *Proc. of the XIth EUCARPIA Meeting on Genetics and Breeding of Capsicum & Eggplant*, 9-13 April 2001, Antalya, Turkey, pp. 142-145.

- [6] Popova, T., Grozeva, S., Todorova, V., Stankova, G., Anachkov, N. and Rodeva, V., 2016. Effects of low temperature, genotype and culture media on in vitro androgenic answer of pepper (*Capsicum annuum* L.). *Acta Physiologiae Plantarum*, 38, 273.
- [7] Parra-Vega V. and Seguí-Simarro J. M., 2016. *Anther Culture in Pepper (Capsicum annuum L.)*. Methods in Molecular Biology (pp. 1359). New York, NY.
- [8] Ozsan, T. and Onus, A. N., 2017. In vitro biber (*Capsicum annuum* L.) anter kültürü B vitaminleri ile etkilenebilir mi? *Uluslararası Biyoteknoloji Dergisi*, 20(1):1-13.
- [9] Bal, U., 2002. Domateste (*Lycopersicon esculentum* Mill.) İzole Edilmiş Mikrospor Kültürü, Ovaryum Kültürü ve *Solanum sisymbriifolium* Lam. ile Tozlanma Yöntemleri ile Haploid Embriyo Oluşumunun Uyartılması. T.Ü. Tekirdağ Ziraat Fakültesi BahçeBitkileri Anabilim Dalı, Doktora Tezi (basılmamış), 1-156 s., Tekirdağ.
- [10] Nitsch, C., Norreel, K., 1973. Effect d'un choc thermique sur le pouvoir embryogene du polende *Datura innoxia* cultivé dans l'anthere ou isolé de l'anthere. C.R. Acad. Sci., 276 D, 303-306.
- [11] Lichter, B., 1982. Induction of haploid plants from isolated pollen of *Brassica napus*. *Z.Pflanzenphysiol.* 105: 427-434.
- [12] Takahata, Y., Keller, W.A., 1991. High Frequency Embryo Genesis and Plant Regeneration in Isolated Microspore Culture of *Brassica oleracea* L. *Plant Science*, 74: 235-242.
- [13] Duijs, J.G., Voorrips, R.E., Visser, D.L., Custers, J.B.M., 1992. Microspore Culture is Successful In Most Crop Types of *Brassica oleracea* L. *Euphytica*, 60: 45-55.
- [14] Cao, M., Li, Y., Liu, F., Dore, C., 1994. Embryo Genesis and Plant Regeneration of Pakchoi (*B.rapa* L.ssp. *chinensis*) via in vitro Isolated Microspore Culture. *Plant Cell Reports*, 13: 447-450.
- [15] Holme, I.B., Olesen, A., Hansen N.J.P., Andersen, S.B., 1999. Anther and Isolated Microspore Culture Response of Wheat Lines from Northwestern and Eastern Europe. *Plant Breeding*, 118: 111-117.
- [16] Barro, F., Martin, A., 1999. Response of Different Genotype of *Brassica carinata* to Microspore culture. *Plant Breeding*, 118: 79-81.
- [17] Nageli, M., Schmid, J.E., Stamp, P., Büter, B., 1999. Improved Formation of Regenerable Callus in Isolated Microspore Culture of Maize: Impact of Carbohydrates, Plating Density and Time of Transfer. *Plant Cell Reports*, 19: 177-184.
- [18] Ferrie, A.M.R., Taylor, D.C., Mackenzie, S.L., Keller, W.A., 1999. Microspore embryo genesis of high sn-2 erucic acid *Brassica oleracea* germplasm. *Plant Cell, Tissue and Organ Culture*, 57: 79-84.
- [19] Lemonnier-Le Penhuizic, C., Chatelet, C., Kloareg, B., Potin, P., 2001. Carrageenan Oligosaccharides Enhance Stress-Induced Microspore Embryo Genesis in *Brassica oleracea* var. *italica*. *Plant Science*, 160: 1211-1220.
- [20] Kasha, K.J., Hu, T.C., Oro, R., Simion, E., Shim, Y.S., 2001. Nuclear Fusion Leads to Chromosome Doubling During Mannitol Pretreatment of Barley (*Hordeum vulgare* L.) Microspores. *Journal of Experimental Botany*, Vol. 52, No. 359, pp. 1227-1238.
- [21] Dias, J.S., Correia, M.C., 2002. Effect of Medium Renovation and Incubation Temperature Regimes on Tronchuda Cabbage Microspore Culture Embryo Genesis. *Scientia Horticulturae*, 93: 205-214.
- [22] Segui-Simarro, J.M., Testillano, P.S., Risueno, M.C., 2003. Hsp70 and Hsp90 Change Their Expression and Subcellular Localization After Microspore Embryo Genesis Induction in *Brassica napus* L. *Journal of Structural Biology*, 142: 379-381.
- [23] Bal, U., Abak, K., Büyükalaca, S., Çömekçiöglü, N., 2003. Development of Callus Colonies From the Isolated Microspore Culture of *Capsicum annuum* L. *Biotechnol. & Biotechnol. Eq.*, 17(2): 28-43.
- [24] Patel, M., Darvey, N.L., Marshall, D.R. and Berry, J. O., 2004. Optimization of culture conditions for improved plant regeneration efficiency from wheat microspore culture. *Euphytica*, 140: 197-204.
- [25] Weber, S., Ünker, F., Friedt, W., 2005. Improved Doubled Haploid Production Protocol for *Brassica napus* Using Microspore Colchicine Treatment in vitro and Ploidy Determination by Flow Cytometry. *Plant Breeding*, 124: 511-513.
- [26] Dunwell, J. M. 2010. Haploids in flowering plants: origins and exploitation. *Plant Biotechnology Journal*, 8: 377-424.
- [27] Lantos, C., Juhasz, A.G., Vagi, P., Mihaly, R., Kristof, Z., Pauk, J., 2012. Androgenesis induction in microspore culture of sweet pepper (*Capsicum annuum* L.). *Plant Biotechnology Rep*, 6: 123-132.
- [28] Nitsch, C., Nitsch, J.P., 1967. The Induction of Flowering in vitro in Stem Segments of *Plumbago indica* L. I. The Production of Vegetative Buds. *Planta*, 72, 355-370.
- [29] Gamborg, O.L., Miller, R.A., Ojima, K., 1968. Nutrient Requirements of Suspension Cultures of Soybean Root Cells. *Exp. Cell Res.*, 60: 151-158.
- [30] Lichter, B., 1981. Anther culture of *Brassica napus* in A Liquid Culture Medium. *Z.Pflanzenphysiol.* 103: 229-237.
- [31] Kyo, M., Harada, H., 1986. Control of the Developmental Pathway of Tobacco Pollen in vitro. *Planta*, 168: 427-432.
- [32] Duijs, J.G., Voorrips, R.E., Visser, D.L., Custers, J.B.M., 1992. Microspore Culture is Successful In Most Crop Types of *Brassica oleracea* L. *Euphytica*, 60: 45-55.
- [33] Carlos, J., Dias, S., 1999. Effect of Activated Charcoal on *Brassica oleracea* Microspore Culture Embryo Genesis. *Euphytica*, 108: 65-69.
- [34] Indrianto, A., Heberle-Bors, E., Touraev, A., 1999. Assessment of Various Stresses and Carbohydrates for Their Effect on the Induction of Embryo Genesis

- in Isolated Wheat  
Microspores. *Plant Science*, 143:71-79.
- [35] Jahne-Gartner, A., Lorz, H. 1999 Protocols for Anther and Microspore Culture of Barley. *Methods Mol. Biol.*, 111: 269-279.
- [36] Supena, E. D. J., Suharsono, S., Jacobsen E., Custers, J. B. M., 2006a. Successful development of a shed-microspore culture protocol for doubled haploid production in Indonesian hot pepper (*Capsicum annuum L.*) *Plant Cell Rep*, 25: 1-10 DOI 10.1007/s00299-005-0028-y.
- [37] Arı, E. 2006. Anemone coronaria var. in coccinea anther culture studies, PhD Thesis, Çukurova University, Science Institute, Department of Horticulture, Adana.
- [38] Coşkun, Y. 2011. Microspore culture and durum wheat plant (*Triticum status Desf.*) embryo production and plant regeneration, PhD Thesis, Süleyman Demirel University, Graduate School of Natural and Applied Sciences, Department of Biology Branch, Isparta.
- [39] Yin, T., Tian, S., Luo, S., Chen, X., Wang, Y., Shen, S. 2010. Studies on isolated microspore embryoid induction of *C. annuum L.* *Front. Agric. China*, 4(4): 438-442.
- [40] Dumas, De Vault, R., Chambonnet, D. & Pochard, E., 1981. *In vitro* culture of pepper (*Capsicum annuum L.*) anthers: high rate plant production from different genotypes by +35 °C treatments. *Agronomie*, 1(10):859-864.
- [41] Abak, K., 1983. Biberde (*Capsicum annuum L.*) Anther Kültürü Yoluyla Haploid Bitki Elde Etme Üzerinde Araştırma. Ankara Üniversitesi Ziraat Fakültesi Yıllığı. Cilt: 33, Fasikül 1-2-3-4'den ayrı basım, 155-163.
- [42] Lantos, C., Juhasz, A.G., Somogyi, G., Ötvös, K., Vagi, P., Mihaly, R., Kristof, Z., Somogyi, N., Pauk, J. 2009. Improvement of isolated microspore culture of pepper (*Capsicum annuum L.*) via co-culture with ovary tissues of pepper or wheat. *Plant Cell Tissue Organ Culture*, 97: 285-293.
- [43] Kim, M., Jang, I.C., Kim, J.A., Park, E.J., Yoon, M., Lee, Y. 2008. Embryogenesis and plant regeneration of hot pepper (*Capsicum annuum L.*) through isolated microspore culture. *Plant Cell Rep*, 27: 425-434.
- [44] Supena, E. D. J. ve Custers, J. B. M., 2002. Establishment of haploid technology to improve hot pepper breeding efficiency in Indonesia. *Proceedings of the International 7th Indonesian Student's Scientific Meeting*, ISSM 2002. Berlin, October 4-6, 69-72.
- [45] Supena, E.D.J., Muswita, W. and Suharsono, S., 2006b. Evaluation of crucial factors for implementing shed-microspore culture of Indonesian hot pepper (*Capsicum annuum L.*). *Scientia Horticulturae*, 107: 226-232.
- [46] Supena, E. D. J., Custers, J. B. M., 2011. Refinement of shed-microspore culture protocol to increase normal embryos production in hot pepper (*Capsicum annuum L.*). *Scientia Horticulturae*, 130 (2011) 769-774.
- [47] Supena, E. D. J., 2004. *Innovations in microspore embryogenesis in Indonesian hotpepper (Capsicum annuum L.) and Brassica napus L.* (phd thesis). Wageningen University, 131.
- [48] Erım, F. B., 2019. *Farklı Biber (Capsicum Annuum L.) Genotipleri Üzerinde Shedmikrospor Kültürü Tekniğinin Uygulanması ve Mikrospor Gelişim Aşamalarının Belirlenmesi* (yüksek lisans tezi). Akdeniz Üniversitesi Fen Bilimleri Enstitüsü Bahçe Bitkileri Anabilim Dalı, Antalya.
- [49] Benli, Y., 2019. A Study on the Response of Some Pepper (*Capsicum annuum L.*) Genotypes to Different Androgenesis Methods (master's thesis). Akdeniz University, Institute of Science, Department of Horticulture, Antalya.
- [50] Murashige, T. and Skoog, F., 1962. A revised medium for rapid growth and bio assays with tobacco tissue cultures. *Physiologia Plantarum*, 15 (3): 473-497.
- [51] Doğan, S., Arı, E., 2019. The effect of shaker use on embryo yield in shed-microspore cultures of ornamental peppers. *Uluslararası Tarım ve Yaban Hayatı Bilimleri Dergisi (UTYHBD)*, 5 (2): 299-307.
- [52] Tatar, M., 2022. Gaziantep yerel biber genotiplerinin morfolojik ve moleküler karakterizasyonu ve double haploid (DH) hatların elde edilme olanakları (Doktora tezi). Yüzüncü Yıl Üniversitesi Fen Bilimleri Enstitüsü Bahçe Bitkileri Anabilim Dalı, Van.